U.PORTO

DOUTORAMENTO EM PATOLOGIA E GENÉTICA MOLECULAR

Mesenchymal Stem / Stromal Cell Mobilization Following Immune Responses to 3D Biomaterials: A Road Towards in situ Regeneration

Hugo Ronaldo Freitas Caires

D

2016

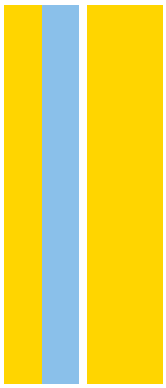

HUGO RONALDO FREITAS CAIRES

MESENCHYMAL STEM / STROMAL CELL MOBILIZATION FOLLOWING IMMUNE RESPONSES TO 3D BIOMATERIALS

A ROAD TOWARDS *IN SITU* REGENERATION

Tese de Candidatura ao grau de Doutor em Patologia e Genética Molecular submetida ao Instituto de Ciências Biomédicas Abel Salazar da Universidade do Porto.

Orientador – Doutora Catarina Rodrigues de Almeida
Categoria – Professor Auxiliar Convidado
Afiliação – I3S, Instituto de Investigação e Inovação em Saúde, INEB, Instituto de Engenharia Biomédica, Microenvironments for NEWTherapies Group,
Universidade do Porto

e

Department of Medical Sciences and Institute for Biomedicine - iBiMED,
Universidade de Aveiro

Co-orientadora – Doutora Melba Navarro
Categoria – Investigador Assistente
Afiliação – CIMME, International Center for Numerical Methods in Engineering and
IBEC, Institute for Bioengineering of Catalonia

PUBLICATIONS

Papers in peer-reviewed scientific journals

Caires HR, Lázaro MG, Oliveira C, Gomes D, Mateus DD, Oliveira C, Barrias CC, Barbosa MA, & Almeida CR. Finding and tracing human MSC in 3D microenvironments with the photoconvertible protein Dendra2. Sci. Rep. 5, 10079 **(2015)**;

Caires HR, Esteves T, Quelhas P, Barbosa MA, Navarro M, & Almeida CR. Macrophage interactions with PLA and chitosan scaffolds lead to improved recruitment of human MSC: a comprehensive study with different immune cells. J R Soc Interface 13, 122 **(2016)**;

Caires HR, Silva P, Barbosa MA, & Almeida CR. A co-culture system with three different primary human cell populations reveals that MSC diminish macrophage-driven fibroblast recruitment. *Manuscript in preparation*, **(2016)**;

Caires HR, & Almeida CR. MSC dynamics upon scaffold implantation: challenges and opportunities for improved *in situ* regeneration. *Manuscript in preparation*, **(2016)**;

Almeida CR, **Caires HR**, Vasconcelos DP & Barbosa MA. Neutrophil Activating Protein (NAP)-2 secreted by human NK cells can stimulate Mesenchymal Stem/Stromal Cell recruitment. Stem Cell Reports, 6(4), 466-73 **(2016)**;

Almeida M, Silva A, Vasconcelos D, Almeida C, **Caires HR**, Pinto M, Calin G, Santos S, & Barbosa M. miR-195 in human primary mesenchymal stromal/stem cells regulates proliferation, osteogenesis and paracrine effect on angiogenesis. Oncotarget, 7(1), 7-22 **(2015)**.

MESENCHYMAL STEM / STROMAL CELL MOBILIZATION FOLLOWING IMMUNE RESPONSES TO 3D BIOMATERIALS:

A ROAD TOWARDS *IN SITU* REGENERATION

Hugo R. Caires

This thesis was supervised by:

Catarina Rodrigues de Almeida, PhD

I3S, Instituto de Investigação e Inovação em Saúde

INEB, Instituto de Engenharia Biomédica

Microenvironments for NEWTherapies Group,

Universidade do Porto

Portugal

Department of Medical Sciences and Institute for Biomedicine - iBiMED,

Universidade de Aveiro

Portugal (*current address*)

and

Melba Navarro, PhD

CIMME, International Center for Numerical Methods in Engineering

IBEC, Institute for Bioengineering of Catalonia

Spain

As thesis advisor.

The research described in this thesis was conducted at:

I3S, Instituto de Investigação e Inovação em Saúde da Universidade do Porto

INEB, Instituto de Engenharia Biomédica da Universidade do Porto,

Microenvironments for NEWTherapies Group, Porto, Portugal

The research described in this thesis was financially supported by:

- FEDER funds through the Programa Operacional Factores de Competitividade– COMPETE;

- Portuguese funds through FCT − Fundacão para a Ciência e a Tecnologia in the framework of the project EXPL/BIM-MED/0022/2013.

"O INFANTE

Deus quer, o homem sonha, a obra nasce.
Deus quis que a terra fosse toda uma,
Que o mar unisse, já não separasse.
Sagrou-te, e foste desvendando a espuma.
E a orla branca foi de ilha em continente,
Clareou, correndo, até ao fim do mundo,
E viu-se a terra inteira, de repente,
Surgir, redonda, do azul profundo.
Quem te sagrou criou-te português.
Do mar e nós em ti nos deu sinal.
Cumpriu-se o Mar, e o Império se desfez.
Senhor, falta cumprir-se Portugal!"

s.d.

Mensagem. Fernando Pessoa. Lisboa, 1934 (Lisboa: Ática, 10ª ed. 1972). - 57.

AGRADECIMENTOS / ACKNOWLEDGMENTS

O fim revela a fonte dos nossos começos.

A pessoa incontornável nos agradecimentos especiais deste meu percurso é a Catarina Almeida, a minha orientadora. Nunca terei palavras suficientes para te agradecer por tudo. Obrigada pelo incentivo e acima de tudo pela objetividade, rigor e foco que me incutiste durante estes últimos anos. Certamente das coisas mais valiosas que guardo desta minha etapa para o futuro. Obrigada por me fazeres crescer como pessoa e investigador.

I would also like to thank Melba Navarro, my co-supervisor, who received me at IBEC and gave me the opportunity to work closely to Tiziano and their 3D Rapid Prototyping machine. Thank you for always being there when I needed.

I would like to express my gratitude for all the co-authors of the publications for their important contribution, for their suggestions and commitment which greatly improved this thesis work. Maria Lázaro, Carla Oliveira, David Gomes, Denise Mateus, Patrícia Silva, Tiago Esteves, Pedro Quelhas, Carla Oliveira, Cristina Barrias, Mário Barbosa, Melba Navarro and Catarina Almeida thank you for helping me reaching there!

Faço também um agradecimento em particular à Professora Doutora Fátima Gärtner pela incansável disponibilidade que sempre manifestou na qualidade de directora do programa doutoral em Patologia e Genética Molecular.

Gostaria de fazer um agradecimento especial à Maria José Oliveira por ter sido o meu primeiro contacto no mundo da investigação, ter falado com o professor Mário, e alimentado o meu sonho! Obrigada por todos os momentos de amizade, pela simpatia e bondade que tão bem a caracteriza. E com isto irei continuar a agradecer ao meu “núcleo duro” do antigo Lab INEB no IPATIMUP. Um grande obrigado do fundo da alma à Marta Pinto, Helena Brigas, Maria Lázaro, Flávia Castro, Ana Freitas, Joana Caldeira (Xu), Ana Pinto e Eliana Vale. Estiveram sempre lá quando precisei e foram para mim um apoio inabalável e fonte de esperança/resiliência nestes últimos momentos difíceis. Vocês foram e são, sem dúvida alguma, parte essencial da concretização desta tese.

Obrigada também Patrícia Oliveira, Patrícia Silva, Dinis Faustino e Maria Molinos pelos bons momentos partilhados (lanches, almoços, cafés e que bons momentos foram!) mas

também desilusões e desabafos. Obrigado pela vossa companhia sem a qual não seria a mesma coisa porque a investigação faz-se de pessoas para pessoas.

Gostaria também de agradecer ao Professor Mário Barbosa por me ter recebido no INEB e ter tutelado a minha orientação à Catarina Almeida. Obrigado por ter criado o microambiente necessário para me fazer crescer como investigador.

Gostaria de agradecer à minha equipa NEWTherapies porque apesar de distantes na "casa mãe" mantiveram-se sempre perto. Obrigada Susana Santos, Raquel Gonçalves, Marta Oliveira, Daniel Vasconcelos, Daniela Vasconcelos, Catarina Pereira, Cristina Ribeiro, Judite Barbosa, Arantxa Blazquez, Graciosa Teixeira, José Teixeira, Carla Cunha, Andreia Silva, Inês Almeida, Ana Lourenço, Amadeu e Ana Paula Lima e por fim mas não por última obrigada Joana Antunes pela tua resiliência.

Deixo também um sinal de apreço a todos os colegas e amigos do IPATIMUP pelos momentos partilhados e pelo incentivo durante estes últimos anos, especialmente durante esta minha etapa "final". Obrigada Nuno Mendes, Ricardo Coelho, Luísa Amaral, Lara Silva, Sandra Carvalho, Ana Dias, Daniela Freitas, Henrique Duarte, Márcia Micaela, Paula Boaventura, Filipa Valente, Raquel Lima, Filipa Reis, Vanessa Rodrigues e Diana Sousa.

Não me esqueço também da boa disposição e simpatia da Zezinha, da Dona Eduarda, da Dona Teresa, do Sr. Oliveira, do Sr. Mendes, do Sr. Mário e dos elementos do departamento de informática do IPATIMUP nomeadamente do Marco César, do Rui Sousa e do Wagner Amaral. Um grande obrigado!

Gostaria também de agradecer a toda a minha família e amigos que sempre me apoiaram e estiveram presentes ao longo destes últimos anos.

Mãe, Pai e little sister. Obrigada por toda a compreensão e apoio durante todos os tempos difíceis, porque mesmo longe estiveram sempre perto, sempre com uma palavra de alento e esperança. Obrigado pela perseverança e valores que me transmitiram, pelo vosso amor incondicional. Tenho imensa sorte em vos ter comigo. Sempre!

Diana Sousa. De longe a minha fonte de inspiração e vontade. Parte de mim sempre presente. Sempre com amor, cuidado e apoio incondicional.

Obrigada pelo teu olhar e sorriso.

Esta tese é incontestavelmente vossa !

SUMÁRIO

Mobilização de MSC (Células Mesenquimais Estaminais / do Estroma) durante respostas imunes a biomateriais 3D: em direção à regeneração *in situ*

A engenharia de tecidos *in situ* visa intervir terapeuticamente no exíguo processo de regeneração endógena através do uso de matrizes biodegradáveis fabricadas para instruir, melhorar e acelerar a capacidade de regeneração do hospedeiro. Atualmente, biomateriais fabricados com o intuito de modular a inflamação ou de promover a mobilização de células progenitoras para o implante biomédico têm sido utilizadas com sucesso para potenciar a regeneração endógena. Neste contexto, o avanço da regeneração de tecidos *in situ* exige um conhecimento mais aprofundado sobre como as diferentes células do sistema imune interagem com os biomateriais implantados. Tal informação irá permitir compreender e modelar esta interação para promover a mobilização e recrutamento de células estaminais/progenitoras endógenas em detrimento de tipos de células pró-fibróticas para o local do implante por forma a potenciar a regeneração da lesão ao invés da sua cicatrização/fibrose.

Neste contexto, o objetivo global desta tese consiste em fornecer uma análise abrangente sobre qual o impacto das respostas imunes primárias humanas no recrutamento de células mesenquimais estaminais primárias da medula óssea (BM-MSC) e de fibroblastos que são desencadeadas pelo implante de diferentes biomateriais 3D.

A nossa hipótese explora a mobilização endógena de células de carácter regenerativo para os biomateriais implantados. Desta forma foi primeiramente desenvolvida uma nova plataforma de imagiologia que possibilitasse a investigação do comportamento dinâmico das células estaminais mesenquimais em diferentes microambientes tridimensionais. Para tal, BM-MSC humanas foram transfectadas para expressar uma proteína fluorescente fotoconversora, designada proteína Dendra2, a qual foi utilizada para distinguir e seguir o mesmo grupo de células de forma estável ao longo de mais de sete dias, mesmo com a remoção da amostra do microscópio para a incubadora. Esta técnica imagiológica, baseada na proteína Dendra2, permitiu a análise da morfologia celular acoplada com quantificação da migração celular em tempo real numa variedade de matrizes biomédicas, com propriedades distintas, de origem natural ou sintética. De especial interesse, através desta técnica de imagiologia foram revelados perfis de migração celulares específicos para cada uma mas matrizes tridimensionais testadas ao longo de sete dias.

Tendo em conta o foco principal, procedeu-se à caracterização das respostas imunes desencadeadas pela interação das células imunes com distintos biomateriais e foi estabelecido qual o seu impacto no recrutamento de MSC e/ou de fibroblastos para o implante. Especificamente, foi determinado que os biomateriais modelo de Ácido Poli-Láctico (PLA) e de quitosano levam a um aumento da atividade metabólica dos macrófagos mas não das células mononucleares do sangue periférico (PBMC), das células exterminadoras naturais (NK) ou dos monócitos. As PBMC e as células NK aumentam o seu número quando interagem com matrizes de PLA, e expressam um perfil de secreção que não promove o recrutamento de MSC ou de fibroblastos. Por outro lado, os monócitos secretam mais IL-8 quando em matrizes de PLA que é acompanhada por uma tendência para promover um maior recrutamento de fibroblastos mas não de MSC. A interação com quitosano aumentou a secreção de IL-8, MIP-1, MCP-1 e de RANTES por parte dos macrófagos diferenciados enquanto a interação com PLA estimulou a produção de IL-6, IL-8 e MCP-1, todas elas quimiocinas que podem conduzir ao recrutamento de MSC e/ou de fibroblastos. De especial importância, este perfil de secreção de macrófagos em contacto com os biomateriais foi correlacionado com a indução preferencial da invasão por parte de determinadas células do estroma em função do material. Desta forma, os macrófagos foram as células imunes que em contacto com os biomateriais tornam-se ativados para secretar moléculas bioativas capazes de estimular o recrutamento de MSC e de fibroblastos. Subsequentemente, investigámos se os macrófagos poderiam também regular a velocidade de colonização das matrizes implantadas pelas MSC recrutadas. Para tal, utilizou-se a plataforma de imagiologia, baseada na proteína Dendra2, previamente desenvolvida. Surpreendentemente, verificou-se que apesar da motilidade das células estaminais no interior das matrizes 3D de PLA e de quitosano ser semelhante na ausência de células imunes, a sua motilidade foi significativamente aumentada na presença de macrófagos diferenciados em quitosano.

Foi desenvolvido um ensaio de competição fisiologicamente relevante que combina a câmara de Boyden com a tripla co-cultura celular. Surpreendentemente, este ensaio revelou que quando as MSC e os fibroblastos co-habitam no mesmo ambiente (câmara superior) existem diferenças no recrutamento preferencial de cada tipo de célula do estroma em função do tipo de biomaterial com que os macrófagos interagem. Neste contexto, tem sido sugerido que as MSC diminuem a fibrose e melhoram a integração dos implantes biomédicos. Desta forma, foi investigado se a suposta chegada das MSC e interação com os macrófagos na interface do implante poderia influenciar a dinâmica de recrutamento de fibroblastos. Verificou-se que esta interação reprime o recrutamento de

fibroblastos para o biomaterial. Este resultado sugere um mecanismo de regulação das MSC sobre a mobilização de fibroblastos para implante que não depende do tipo de biomaterial.

Na sua globalidade, os resultados desta tese proporcionam uma expansão do conhecimento sobre a resposta imune despoletada por distintos biomateriais e estabelece qual a sua consequência funcional na indução de recrutamento de células do estroma com potencial regenerador ou fibrótico para o local do implante. Mais especificamente, os nossos resultados destacam um novo conceito integrador na engenharia de tecidos *in situ* fornecendo um dos primeiros passos na definição de regras de *design* para o desenvolvimento de biomateriais imunomoduladores com um carácter regenerativo mais eficaz.

SUMMARY

MSC (Mesenchymal Stem / Stromal Cell) mobilization following immune responses to 3D biomaterials: a road towards *in situ* regeneration

In situ tissue engineering strategies aim to therapeutically target our rather limited endogenous regenerative process through the use of off-the-shelf biodegradable scaffolds specifically designed to instruct, enhance and accelerate the hosts self-healing ability. Until now independent approaches that modulate inflammation or promote mobilization of progenitor cells towards the implanted scaffold have been successfully used to achieve endogenous regeneration. Predictably, advances in this field require deep insights on how different immune cell populations interact with biomaterials and how this can be modulated to promote mobilization of endogenous stem/progenitor cells in detriment of pro-fibrotic cell types towards the implant site.

In this framework, the overall thesis objective is to provide a comprehensive analysis on the impact of primary human immune responses, triggered by distinct 3D scaffold models, on the recruitment of primary human bone marrow MSC and fibroblasts.

Since our hypothesis focuses on exploiting mobilization of regenerative cells towards implanted materials, an imaging platform was developed to interrogate MSC dynamical behaviour within distinct 3D microenvironments. For that, human MSC were transfected to express a fluorescent photoconvertible protein, Dendra2, which was used to stably highlight and follow the same group of cells for more than seven days, even if removed from the microscope to the incubator. Dendra2 imaging allowed to couple an analysis of the cells morphology with quantification of cell migration in real-time, in a range of natural and bioengineered matrices with distinct properties. Interestingly, specific cell migration profiles throughout seven days were revealed for each of the tested matrices with this imaging technique.

The immune cell responses triggered by distinct scaffolds were characterized and their impact on MSC and/or fibroblast recruitment towards the implant established. It was found that Poly-Lactic Acid (PLA) and chitosan scaffold models lead to increased metabolic activity of macrophages but not of peripheral blood mononuclear cells (PBMC), natural killer (NK) cells or monocytes. PBMC and NK cells increased their cell number in PLA scaffolds and expressed a secretion profile that did not promote MSC or fibroblast recruitment. On the other hand, monocytes secreted more IL-8 when in PLA, which was followed by a trend to increase fibroblast recruitment but not MSC. Importantly, chitosan lead to increased IL-8, MIP-1, MCP-1 and RANTES secretion by monocyte derived-

macrophages while PLA stimulated IL-6, IL-8 and MCP-1 production, all of which are chemokines that can lead to MSC and/or fibroblast recruitment. This secretion profile of macrophages in contact with biomaterials correlated with the highest stromal cell invasion, which was biomaterial-dependent. Thus, macrophages were the cells that in contact with engineered biomaterials become activated to secrete bioactive molecules capable of stimulating MSC and fibroblast recruitment. Subsequently, we have investigated whether macrophages could also modulate the MSC colonization rate of implanted scaffolds using the Dendra2 imaging platform previously developed. Strikingly, it was found that although stem cell motility within PLA and chitosan 3D matrices was similar in the absence of immune cells, MSC motility significantly increased in the presence of macrophages differentiated in chitosan.

Interestingly, using a physiologically relevant triple co-culture competitive Boyden chamber assay it was revealed that when MSC and fibroblasts co-habited within the same environment (upper chamber) there were biomaterial-dependent differences on preferential stromal cell type recruitment induced by macrophages. In line with this, MSC have been recently suggested to decrease fibrosis and improve scaffold integration. Therefore, it was investigated whether a putative MSC arrival and interaction with macrophages at the implant interface could influence the dynamics of fibroblast recruitment. It was found that MSC interaction with the scaffolds interface repressed macrophage-mediated fibroblast recruitment. This suggests a biomaterial-independent MSC regulatory mechanism over macrophage-mediated fibroblast mobilization.

Taken together, the results of this thesis provide new knowledge on the scaffold-evoked immune responses and established their functional consequence on recruitment of stromal cells with regenerative or reparative potential. More specifically, our findings highlight a novel integrative concept for *in situ* tissue engineering providing one of the first steps towards defining design rules for a more effective development of immunomodulatory scaffold.

ABREVIATIONS

2D: two-dimensional
3D: three-dimensional

A

ADP: adenosine diphosphate
AKT: protein kinase B
ALCAM: activated leukocyte cell adhesion molecule
ALP: alkaline phosphatase activity
ANOVA: analysis of variance
APC: allophycocyanin

B

Bcl-2: B-cell lymphoma 2
Bcl-xL: B-cell lymphoma-extra large
bFGF: basic fibroblast growth factor
BM-MSC: bone marrow mesenchymal stem/stromal cells
BSA: bovine serum albumin

C

CAM: cell adhesion molecule
CCL: chemokine (C-C motif) ligand
CCR: C-C chemokine receptor
CD: cluster of differentiation
CFU: colony forming capacity
CG: Collagen
Ch: chitosan
CIs: Confidence intervals
CO_2: carbon dioxide
CT: computed tomography
CXCL: chemokine (C-X-C motif) ligand
CXCR: C-X-C chemokine receptor
CX3CL: chemokine (C-X_3-C motif) ligand

D

DAMPs: damage-associated molecular patterns
DAPI: 4',6-diamidino-2-phenylindole
DMEM: Dulbecco's modified eagle medium
DNA: deoxyribonucleic acid

E

EC: extinction coefficient
ECM: extracellular matrix
EDTA: ethylenediamine tetraacetic acid
ELISA: enzyme-linked immunosorbent assay

F

FBGCs: foreign body giant cells
FBR: foreign body reaction
FBS: fetal bovine serum
FDA: Food and Drug Administration
FRAP: fluorescence recovery after photobleaching

G

GDL: δ-gluconolactone
GFP: green fluorescent protein

$Green_{ac}$: green fluorescence intensity after conversion
$Green_{bc}$: green fluorescence intensity before conversion

H

HA: hyaluronic acid
HDF: human dermal fibroblast
HGF: hepatocyte growth factor
HIF-1α: hypoxia-inducible factor-1 alpha
HLA-DR: human leukocyte antigen - antigen D Related
HSC: hematopoietic stem cell
HSP: heat shock protein

I

ICAM-1: intercellular adhesion molecule - 1
IDO: indoleamine
IFN-γ: interferon gamma
IGF: insulin growth factor
IgG: immunoglobulin G
IL: interleukin
IL-6R: interleukin-6 receptor
IP-10: IFN-gamma-inducible protein 10
ISCT: International Society for Cellular Therapy

L

LPS: lipopolysaccharides

M

Mac-1: macrophage adhesion molecule-1
MCP-1: monocyte chemotactic protein 1
MIP-1α: macrophage inflammatory protein-1 alpha
MIP-1β: macrophage inflammatory protein-1 beta
MMP: matrix metalloproteinase
MRI: magnetic resonance imaging
MSC: mesenchymal stem/stromal cells
MT1-MMP: membrane-type 1-matrix metalloproteinase

N

NAP-2: neutrophil-activating protein-2
NETs: neutrophils extracellular traps
NF-κB: factor nuclear kappa B
NK: natural killer
NKT: natural killer t
NO: oxide nitric

O

OCT: optical coherence tomography

P

PAM: photoacoustic microscopy
PAMPs: pathogen-associated molecular patterns
PBMC: peripheral blood mononuclear cells
PBS: phosphate buffered saline
pDendra2: Dendra2 plasmid
PDGF: platelet-derived growth factor

PDGFR: platelet-derived growth factor receptor
pDNA: plasmid DNA
PE: phycoerythrin
PEG: poly(ethylene glycol)
PEO: poly(ethylene oxide)
PET: positron emission tomography
PGA: polyglycolic acid
PGE_2: prostaglandin E2
PLA: poly-lactic acid
PLGA: poly(lactic-co-glycolic acid)
PLLA: poly(L-lactic acid)
PLDL: poly(l-lactide-co-dl-lactide)
PMNs: polymorphonuclear neutrophils
POC: poly(1,8-octanediol-co-citrate)
proMMP-2: pro-matrix metalloproteinase 2
PSGL1: P-selectin glycoprotein ligand 1

R

RANTES: regulated upon activation normal t cell expressed and secreted
Red_{ac}: red fluorescence intensity after conversion
Red_{bc}: red fluorescence intensity before conversion
RFU: relative fluorescence units
RGD: arginine-glycine-aspartic acid
Rho-GTPase: Ras homolog hydrolase enzyme of guanosine triphosphate
ROI: region of interest
ROS: reactive oxygen species
RT: room temperature

S

SDF-1: stromal cell-derived factor 1
SEM: standard error of the mean
SPECT: single-photon emission computed tomography
STAT-1: signal transducer and activator of transcription 1

T

TCPS: tissue culture polystyrene
TGF-β: transforming growth factor beta
Th2: helper T cell response type 2
TIMP: tissue inhibitors of metalloproteinases
TLRs: toll like receptors
TNF-α: tumor necrosis factor alpha
T_{regs}: regulatory T cells
TSG6: tumor necrosis factor-inducible gene 6 protein
TXA2: tromboxane A2

U

UV: ultravioleta
US: Ultrasounds

V

V-CAM: vascular cell adhesion molecule
VEGF: vascular endothelial growth factor
VLA-4: very late antigen-4

Q

QY: quantum yield

LIST OF FIGURES

CHAPTER 1

CHAPTER 2

CHAPTER 3

CHAPTER 4

CHAPTER 5

LIST OF TABLES

CHAPTER 1

CHAPTER 2

TABLE OF CONTENTS

CHAPTER 1

"Da minha aldeia vejo quanto da terra se pode ver do Universo…

Da minha aldeia vejo quanto da terra se pode ver do Universo...
Por isso a minha aldeia é tão grande como outra terra qualquer,
Porque eu sou do tamanho do que vejo
E não do tamanho da minha altura...

Nas cidades a vida é mais pequena
Que aqui na minha casa no cimo deste outeiro.
Na cidade as grandes casas fecham a vista à chave,
Escondem o horizonte, empurram o nosso olhar para longe de todo o céu,
Tornam-nos pequenos porque nos tiram o que os nossos olhos nos podem dar,
E tornam-nos pobres porque a nossa única riqueza é ver."

s.d.
"O Guardador de Rebanhos". In Poemas de Alberto Caeiro. Fernando Pessoa. Lisboa: Ática, 1946 (10ª ed. 1993). - 32.

INTRODUCTION &

SCOPE OF THE THESIS

The contents of this chapter are based on:

MSC DYNAMICS UPON SCAFFOLD IMPLANTATION: CHALLENGES AND OPPORTUNITIES FOR IMPROVED *IN SITU* REGENERATION

Hugo R. Caires [1,2,3]

Catarina R. Almeida [2,3,4]

[1] ICBAS - Instituto de Ciências Biomédicas Abel Salazar, Universidade do Porto, Rua Jorge Viterbo Ferreira, 228, 4050-313 Porto, Portugal

[2] i3S - Instituto de Investigação e Inovação em Saúde da Universidade do Porto, Rua Alfredo Allen, 208, 4200-135 Porto, Portugal Portugal

[3] INEB - Instituto de Engenharia Biomédica, Porto, Portugal

[4] Department of Medical Sciences and Institute for Biomedicine - iBiMED, University of Aveiro, 3810-193 Aveiro, Portugal (current address)

Manuscript in preparation, **(2016)**

1.1 The physiology of tissue repair and/or regeneration

The human body has the ability to regenerate certain organs over time as part of natural tissue turnover[1]. For instance, organs as bone, intestinal epithelia and skin can self-renewal at distinct rates with new cells replacing the exhausted/damaged ones to maintain the original tissue structure and function during life-time. Hence regeneration is defined as the biological process that leads to the restitution of native tissue architecture and function. Unfortunately, this regenerative potential is largely hindered in a severe injury scenario[2]. When an emergency response is required the body rushes to repair the damaged tissue. Upon injury, healing occurs mostly by laying down a fibrotic connective tissue "patch" to seal the lesion/wound rather than fully restoring the native tissue structure and function. Thus, while tissue regeneration leads to the restitution of native tissue architecture and function, tissue repair is defined as the replacement of native parenchyma tissue for a relative acellular and fibrotic deposit of extracellular matrix (ECM) with consequent loss of function[3]. Importantly, the recognition of tissue injury and recruitment of inflammatory cells to the lesion site is a key pre-requisite to clear out debris and initiate the healing mechanisms either by regeneration or fibrotic repair[4,5]. The local release of "danger signals" by damaged cells triggers an inflammatory response. This sets in motion a sequence of events that signal the innate immune system to rush into the injury site, eliminate the injurious agents, contain damage and orchestrate the repair or regeneration of the lost tissue[6,7]. Importantly, the amount of regeneration *versus* repair is highly dependent on the integrity of the connective-tissue framework (tissue that supports the parenchyma), on the recruitment of progenitor cells, and on the duration and extent of the inflammatory process (Figure 1).

1.1.1 Haemostasis: vasculature disruption

Following tissue injury, there is disruption of the blood hemodynamics at the damaged area. Blood contact with interstitial collagen matrix at the injury site triggers blood platelets to degranulate several inflammatory mediators including adenosine diphosphate (ADP), serotonin and tromboxane A2 (TXA2)[8]. This instals a strong positive feedback for further platelet aggregation and degranulation at the injured area[9]. These series of events leads to a fibrin clot formation that stops blood extravasation to the extravascular space. The formed fibrin clot provides a provisional matrix, rich in growth factors and chemokines that establish the foundations to support and initiate immune cell influx to the injured site which later gives rise to granulation tissue[10]. Notably, the activated platelets also release a

range of chemokines that can promote mobilization, adhesion and proliferation of different progenitor cells with regenerative potential in this early phase[11-13].

1.1.2 Acute inflammation

The aforementioned sequence of events initiates the inflammatory phase. Acute inflammation is a pivotal response to tissue damage that signals the injury to the immune system, neutralizes the injurious agents, removes necrotic cells and initiates healing mechanisms[14]. The innate immune system senses the presence of an injury stimuli through pattern recognition receptors that detect either exogenous pathogen-associated molecular patterns (PAMPs) or endogenous damage-associated molecular patterns (DAMPs)[15]. These “danger signals” may comprise damaged/degraded extracellular matrix (ECM) proteins[16-18], cell stress-induced proteins[19] and chemicals or cytokines released by necrotic/damaged cells[20,21]. Simultaneously, the newly formed fibrin clot at the injury site releases inflammatory mediators that increase blood flow, haemostasis and vessel permeabilization to synergistically promote immune cell influx and initiate the healing process[22].

The local release of inflammatory mediators such as tumour necrosis factor alpha (TNF-α) and interleukin-1 beta (IL-1β) at the injury site mediates expression of adhesion molecules on the plasma membrane of leukocytes[23]. Their expression is essential to bind to their complementary integrin and selectin receptors on the inflamed endothelial wall[24,25]. Altered blood flow dynamics force incoming leukocytes to position near the margins of blood vessels, promoting their slowly roll over the endothelium and subsequent firm adhesion to activated endothelial cells[26]. Leukocyte rolling is mediated mostly by low affinity interactions between L-, P-, and E-selectin (CD62-L,-P,-E) with P-selectin glycoprotein ligand 1 (PSGL1)[27,28]. Then, leukocytes firmly adhere to the inflamed endothelium under sheer stress through vascular cell adhesion molecule (V-CAM) and intercellular adhesion molecule 1 (ICAM-1) integrins[29]. Noteworthy, PSGL1-L-selectin can also mediate additional leukocyte-leukocyte interactions by which the adhered leukocytes may facilitate secondary leukocyte tethering and thus increase immune cell influx to injury site[30,31].

Before crossing the endothelial wall, leukocytes spread and crawl inside blood vessels in a macrophage adhesion molecule 1- (MAC-1) and ICAM-1-dependent manner seeking a site to transmigrate to the extravascular space either by paracellular[32] or transcellular routes[26,33]. Once the endothelial-cell barrier is crossed, leukocytes then migrate through the endothelial basement membrane and pericyte sheath to reach the injury site in a

chemotactic gradient-dependent manner[34]. The type of expressed receptor at the endothelium and chemotactic signal gradient regulates the recruitment of distinct immune cells to the injury site in a timely fashion[35]. Hence, the profile of infiltrated immune cells and their interaction with local tissue cells influences many aspects of the healing process, facilitating or not tissue regeneration.

This acute inflammatory process is relatively short in time, ranging from hours to a few days, and it is tightly regulated by the immune system to avoid excessive tissue damage and spill over to normal tissue[14]. However, depending on the severity of tissue injury and on the ability of progenitor cells to be mobilized towards the damaged tissue, proliferate and replace the damaged cells through differentiation, acute inflammation can progress to one of three outcomes: tissue regeneration, repair by fibrosis and/or chronic inflammation (Figure 1).

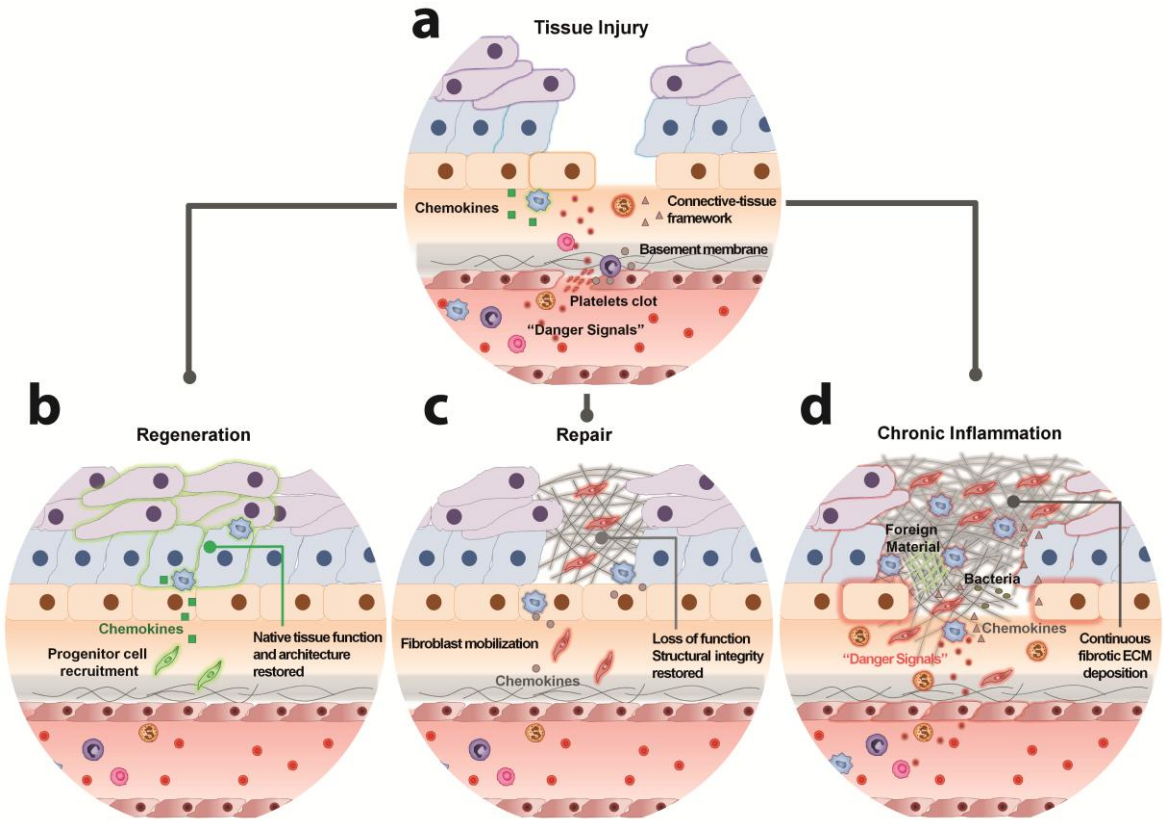

Figure 1 - Framework of healing mechanisms upon tissue injury largely depends on the integrity of the connective-tissue, on the duration and extent of the inflammatory process, and on the type of mobilized stromal cells. (a) Tissue injury triggers local release of danger signals that mediates recruitment and activation of immune cells to the damaged site. The mobilized immune cells phagocyte cell debris and secrete inflammatory cytokines and chemokines that drive the inflammatory process

required to initiate the healing mechanisms. (b) In minor lesions the immune response is fine-tuned and has the ability to mobilize progenitor cells to replace the lost cells. Inflammation is timely resolved and the native tissue function and architecture is restored. (c) Larger necrotic debris areas require a more intense inflammatory response and the body rushes to patch the defect with connective tissue. Fibroblast mobilization and proliferation drives the fibrotic repair of the injury. Although the structural integrity of the affected area is restored the native parenchymal tissue function is irreversibly lost. (d) Interference with the normal process of healing, caused for example by the persistence of a foreign material within the wound, perpetuates inflammation which might drive further tissue damage and exacerbate concurrent fibrotic repair.

1.1.3 Tissue regeneration

Regeneration involves complete restitution of the native tissue architecture and function. However, in humans it is usually restricted to natural tissue turnover of some tissues and to minor tissue injuries[36]. Certain tissues of the body are more capable of self-renewing (and hence regenerating) than others and can be broadly divided into three main types: continuously dividing (e.g. skin and gut), quiescent (e.g. liver and bone) and non-dividing tissues (e.g. heart and brain). The regenerative potential of these tissues lies not in the parenchymal cells (which are terminally differentiated and with limited proliferative potential) but in the progenitor cells located in the stem cell niches[37]. Therefore in an injury scenario, regeneration can only occur if the connective-tissue framework is relatively intact and/or the tissue maintains the ability to mobilize progenitor cells to replace the lost tissue-specific cells[14]. Extensive destruction of connective tissue in severe wounds limits the structural support to the regenerative process. In such scenario, the tissue-specific stem cell niches were probably obliterated, and a more prominent immune/inflammatory response for a longer time period is required to fully remove/remodel the damaged tissue. In the lack of the proper structural support, provided by the connective tissue, healing often occurs by remodelling the exudates/blood clot at the injury site into granulation tissue and ultimately in a fibrotic scar with limited blood supply. In opposition, in a well-approximated surgical incision the healing is usually fast as the defect is relatively small[38]. Moreover, the fine-tuned inflammatory response triggered by the minor tissue damage might initiate mobilization of stem cells and subsequent injury resolution and regeneration with minimal scarring (Figure 1b).

1.1.4 Tissue repair by fibrosis

Few types of tissue injury can result in complete restoration of native tissue and the majority of our body's healing takes place via fibrotic scarring with very little regeneration. This type of repair occurs when there is substantial damage to the stromal tissue framework (as occurs in most injuries) and/or the inflammatory process lacks the ability to mobilize progenitor cell to replace the lost specialized cells[14,39]. In these instances, the margins of the damaged area are not easily approximated, such as in infractions, ulcers and large tissue resections (e.g. upon tumour excision). Since larger necrotic debris areas require a more intense inflammatory response to resolve, an abundant layer of fibrotic tissue is deposited to fill in the defect[40]. Despite the loss of some specialised cells and architectural distortion by fibrous scar, structural integrity is re-established at the expenses of tissue function (Figure 1c). This repair by connective tissue requires a massive influx of immune cells that remove all the damaged tissue and mediate the mobilization and activation of fibroblasts. In turn, recruited fibroblasts remodel the granulation tissue into a fibrotic scar to fill in the defect[41]. Although this type of repair rapidly seals the wound, it leads to a major loss of tissue function which can be potentially life threatening depending on the site and extent of injury[42].

1.1.5 Chronic inflammation: impaired healing response

Acute to chronic transition occurs when the acute inflammatory response cannot be resolved. This can occur owing either to the persistence of the injurious agent, foreign material or to some interference with the normal process of healing, such as infection[14]. Although inflammation has a pivotal role in orchestrating the healing process after injury, the perpetuation of the inflammatory component can also severely compromise the healing outcome[43].

In chronic inflammation the prolonged presence of inflammatory macrophages at the injury site directly contributes to maintenance of a pro-inflammatory environment. These macrophages can secrete an array of bioactive molecules that continuously promote tissue damage spill-over, as well as proliferation and activation of recruited fibroblasts. The originated tissue destruction/reconstruction cycles often result in excessive fibrosis[44] in a wound that often fails to heal spontaneously (Figure 1d).

1.2 Regenerative medicine and tissue engineering approaches

The ability of human tissues to regenerate following severe injuries is rather limited during adulthood. Within this framework, regenerative medicine and tissue engineering seek to develop therapeutic strategies that restore the structure and function of the native tissue upon injury, by providing the required microenvironment to direct tissue regeneration[45]. To this end, a number of approaches have been proposed in the last decades and can be broadly divided into (i) stem cell transplantation[46], (ii) implantation of ex-vivo tissue constructs (which comprises biodegradable materials that provide a temporary template for tissue formation seeded with stem cells and growth factors)[47] or (iii) the use of scaffolds alone or in combination with chemotactic agents to assist and enhance the hosts endogenous regenerative potential[48]. We will briefly overview the last two tissue engineering strategies, proposed to address deficits in repair of serious injuries by relying on the use of instructive biomaterials. The idea is to implant artificial matrix (scaffold) to fill/replace the lesion volume and temporarily provide the mechanical and biochemical support for cell ingrown and tissue regeneration. For successful regeneration the implanted scaffold should (i) be biocompatible, (ii) be timely reabsorbed /degraded by the organism over the regenerative process, (iii) be porous, with an interconnected network to enable rapid tissue ingrowth and diffusion of nutrients, oxygen and metabolites, (iii) have surface properties (chemistry, roughness and stiffness) that support cell adhesion, proliferation and differentiation and (iv) should also provide adequate mechanical support accordingly to organ demands[49,50].

1.2.1 Scaffolds, Cells and Growth Factors triad: filling in the gap

The traditional tissue engineering paradigm to regenerate damaged tissues relies on harnessing autologous bone marrow mesenchymal stem/stromal cells (BM-MSC) from patients, expanding the cells *in vitro* and subsequently seeding these cells into a biodegradable scaffold. Then, the cell-scaffold constructs can be further conditioned or not in bioreactors to promote additional cell growth, differentiation and extracellular matrix formation, before implantation[47,51]. Although this approach can lead to an autologous tissue substitute, the *in vitro* process is a very costly, time consuming procedure, and it has safety issues related with excessive *ex-vivo* stem cell manipulation[52].

1.2.2 In situ tissue engineering: the smarter way?

Therefore, a novel approach emerged from this, in which the *in vitro* phase is obliterated, the so-called *in situ* tissue engineering, or scaffold-guided endogenous regeneration[53]. The endeavour of *in situ* tissue engineering is to develop scaffolds that can therapeutically interfere with our otherwise limited regenerative potential by creating a regenerative microenvironment capable of accelerating and enhancing our self-healing ability[54,55]. And this might be achieved by modulating inflammation or by promoting the mobilization of the endogenous mesenchymal stem/stromal cells (MSC) towards the implanted scaffold[48,56,57]. The development of such immunomodulatory materials have been recently reviewed elsewhere[58].

1.3 Inflammation, foreign body response and regeneration

One of the main challenges for tissue engineering is to stimulate native tissue formation while avoiding fibrosis. Nevertheless, implantation of the so called “regenerative biomaterials” triggers two opposing types of host response: activation of regenerative mechanisms at the injured area but also an immune reaction against the implanted foreign material[59,60]. Although these biological responses are very distinct they share inflammation as a common denominator. While the beneficial aspects of this immune reaction, such as debris clearance and progenitor cell recruitment must occur to initiate healing, their damaging effects as chronic inflammation, fibroblast mobilization, activation and subsequent fibrotic encapsulation of the biomaterial should be minimized for scaffold-guided regeneration to succeed.

1.3.1 Foreign body response to implanted biomaterial

Biomaterial implantation triggers a foreign body reaction (FBR) that consists of five crucial steps: (i) adsorption of blood proteins at materials surface, (ii) recruitment of immune cells, (iii) acute and (iv) chronic inflammation and, finally, (v) fibrotic encapsulation[59,61]. This alternative healing response is sustained by chronic inflammation and characterized by formation of foreign body giant cells (FBGCs), which ultimately leads to encapsulation of the foreign object[62] (Figure 2). Typically, 2-4 weeks upon implantation, the foreign material is encapsulated within an almost avascular and acellular fibrous connective tissue which impairs the scaffolds regenerative function. Fibrotic thickness largely depends on the extent of the inflammatory response which is intrinsically related to biomaterial properties[63,64].

1.3.2 The immune players

The inflammatory response is mainly driven by colonization of the scaffold by blood-derived immune cells. Immune cell activation upon interaction with a biomaterial can occur by two means: (i) binding of adhesion receptors (e.g. integrins) to the pre-adsorbed fibrinogen, Immunoglobulin G (IgG), fibronectin and vitronectin proteins at the surface of materials or (ii) through activation of Toll Like Receptors (TLRs) by local PAMPs and DAMPs related to scaffold implantation[64]. The nature of the infiltrating immune cells and their activation state were demonstrated to be pivotal in the delicate balance between fibrotic or functional ECM formation[65,66]. Table 1 illustrates the immune cell populations present in human peripheral blood that can be recruited to the implant site. Activation of immune cells leads to production of inflammatory cytokines and chemokine-mediated recruitment of more immune cells but also of circulating BM-MSC and fibroblasts to the site of implantation. Importantly, the type of recruited cells can shift the healing outcome. Nevertheless, the specific contribution to stem cell or fibroblast recruitment by each immune cell population upon biomaterial interaction remains largely unknown.

Table 1 – Frequencies of immune cell types present in human peripheral blood [67,68]. +percentage relative to number of peripheral blood leukocytes. *percentage relative to number of peripheral blood mononuclear cells.

	Cell type	Morphology	Size (μm)	Frequencies in human blood (x10^6 cells/mL)	Life-span	Primary function
	Erythrocytes		6-8	93-96% (3800 – 6200)	100-120 days	O_2 and CO_2 transportation
Leukocytes (0.1-0.2% of blood cells)	**Granulocytes**			35-80%+ (2.13 – 6.35)		
	Neutrophils		10-14	30-80%+ (2.09 – 5.97)	6-48 hours	To phagocyte bacteria and fungi
	Basophils		10-14	0-7%+ (0.01 – 0.08)	8-12 days	To kill parasites;
	Eosinophils		10-12	0-2%+ (0.03 – 0.30)	hours-days	To release histamine
	Mononuclear cells (PBMC)			20-65%+		
	Monocytes		12-14	10 – 30%* (0.20-0.90)	hours-days	Angiogenesis; phagocytosis
	Macrophages					Phagocytosis; to mediate inflammation
	Dendritic cells			1-2%* (0.02-0.06)		To recognize and present antigens; T cell activation
	Lymphocytes		5-17	70-90%* (1.1 – 3.5)	weeks-years	
	NK cells			10-15%* (0.08 – 0.43)		Lysis of tumour or virally-infected cells; production of IFN-α and TNF-γ
	T cells			45 – 70%* (0.54 – 1.79)		To mediate adaptive immunity
	B cells			15%* (0.07 – 0.53)		Antibody production
	Platelets		2-4	4-7% (140 – 450)	5-10 days	Blood clotting; release of factors

1.3.2.1 Neutrophils

Following biomaterial implantation, cells of the innate immune system are the first to respond yielding a classical FBR. The early immune cell influx is characterized by polymorphonuclear neutrophils (PMNs). Neutrophils are CD15+/CD68+ phagocytic leukocytes containing granules and are activated by pro-inflammatory cytokines such as IL-1β, TNF-α and Interferon gamma (IFN-γ). Despite their relatively short life span of 24-48 hrs these cells display a rather destructive role[64]. Neutrophils destroy the foreign particles by phagocytosis and their activation triggers their degranulation of proteolytic enzymes and reactive oxygen species (ROS). Additionally, formation of neutrophils extracellular traps (NETs) on implant surfaces renders an inhospitable environment for nearby foreign entities preventing the spread of a potential biomaterial-derived infection[69].

1.3.2.2 NK cells

Even though Natural killer (NK) cells are one of the first immune cell populations to arrive at an injury site, their role in biomaterial-mediated immune reaction is considerably less studied[70]. NK cells are CD56+/CD3- granular cytotoxic lymphocyte effector cells involved in wound healing processes and in uterine tissue remodelling during pregnancy[71,72]. These cells play a major role in both innate and adaptive immune responses and could mediate cytotoxicity against implanted allografts and tissue-constructs due to their ability to distinguish between self and non-self. This ability could be crucial to kill potential pathogens associated with implanted biomaterials through degranulation of lytic granules on target cells. NK cells can also secrete several cytokines including TNF-α, interleukin-10 (IL-10), IFN-γ, transforming growth factor beta (TGF-β) and neutrophil-activating protein-2 (NAP-2), known to impact other immune cells and/or mediate MSC recruitment[73-75].

1.3.2.3 Monocytes

Sequentially to neutrophil and NK cell engraftment, circulating monocytes are recruited from the blood to the implant site in response to monocyte chemotactic protein 1 (MCP-1)[76] produced by recruited neutrophils[77] and tissue-derived macrophages[78]. Monocytes are CD14+/CD3- phagocytic cells that replace the short-lived neutrophils and reach maximum numbers 24-36 hrs after injury[79]. Upon arrival, monocytes became activated by local DAMPs and binding to the fibrinogen layer on the biomaterials surface. These cells also phagocyte cell debris resulting from the initial immune cell response and secrete chemokines such as IL-8 and MCP-1 to foster invasion of additional inflammatory cells[59].

1.3.2.4 Macrophages

Eventually, monocytes gradually differentiate into long-lived macrophages that became the predominant cell type at the tissue-implant interface. Macrophages are phagocytes with a remarkable plasticity that enables them to assume diverse and context-dependent polarization states[80]. These are broadly categorized by their functional properties and patterns of cytokine secretion into M1 and M2 types. Although this classification provides an important framework to study their roles during many processes including tissue repair/regeneration it is simplistic. *In vivo*, macrophages adopt continuum phenotypes with overlapping functions in which classically activated (M1), wound-healing ($M2_{wound\text{-}healing}$), and regulatory macrophages ($M2_{regulatory}$) occupy different points of the spectrum[81].

Upon injury, macrophage exposure to pro-inflammatory cytokines as IFN-γ and TNF-α and/or necrotic cellular or bacterial debris drives cells into a pro-inflammatory (M1) phenotype. Macrophages activated by biomaterials are typically M1 and secrete high levels of IL-1β, IL-6, IL-8, MCP-1 and macrophage inflammatory protein-1β (MIP-1β) which can recruit more inflammatory cells and exacerbate inflammation. Although this M1 state is essential to mount the inflammatory response to injury and initiate healing their prolonged activation is detrimental and leads to further tissue damage and chronic inflammation[82,83].

A prominent acute inflammatory response is required to cleanse the wound and to mobilize progenitor cells and other stromal cell types as fibroblasts to assist in tissue regeneration and/or repair, respectively (Figure 2). This phase is followed by a M1 to M2 phenotype transition of macrophages. Wound healing macrophages ($M2_{wound\text{-}healing}$) are induced by IL-4 and IL-13 secreted into the inflammatory milieu by mast cells, granulocytes and T helper cells that were recruited during the previous acute inflammatory phase. $M2_{wound\text{-}healing}$ macrophages assists in tissue repair through secretion of TGF-β, basic fibroblast growth factor (bFGF), platelet-derived growth factor (PDGF), vascular endothelial growth factor (VEGF) to promote angiogenesis, pro-fibrotic activity by fibroblasts and the secretion of a myriad of proteolytic enzymes to remodel the damaged ECM[84]. As the inflammatory process progresses, the cytokine environment gradually changes and accumulates increased levels of anti-inflammatory signals such as IL-10, prostaglandin E2 (PGE_2), and TGF-β produced by regulatory T cells (T_{regs}), B cells and recruited MSC. This combined with TLR4 activation on macrophages, by apoptotic bodies, drives regulatory macrophage ($M2_{regulatory}$) polarization[85]. Subsequently, $M2_{regulatory}$ macrophages can themselves secrete high amounts of these anti-inflammatory cytokines.

Their main task is to dampen the immune response, resolve inflammation and promote regeneration while limiting development of fibrosis[86].

Despite the sequential role of macrophages M1, $M2_{wound\text{-}healing}$ and $M2_{regulatory}$ during the physiologic healing process, persistence of a foreign material (e.g. a regenerative scaffold) at the injury site often disrupts this sequence of events and prolongs the presence of pro-inflammatory (M1) and $M2_{wound\text{-}healing}$ macrophages[64,87]. In this scenario, biomaterial-adherent M1 macrophages attempt to phagocyte the material or degrade it through secretion of reactive oxygen species (ROS). Since solid biomaterials are typically larger than a cell this results in “frustrated phagocytosis”. This promotes macrophage fusion into FBGCs which display enhanced ability to degrade the material surface and to orchestrate the fibrotic encapsulation of the implant in close interaction with fibroblasts[59].

1.3.2.5 T and B lymphocytes

The immune system employs tissue-resident antigen presenting cells (APC: dendritic cells, macrophages, B cells) to identify and present antigens/epitopes to B and T cells for development of an adaptive immune response. These epitopes are usually peptide sequences, which can be incorporated into biomaterials or can arise *in situ* as APCs process larger antigens, proteins, cells, or debris associated with the biomaterial.

Noteworthy, accumulation of T lymphocytes (CD3+) is associated with the expression of MCP-1 a few days after injury and coincides with macrophage predominance in a FBR. These cells are part of cell-mediated adaptive immune responses and can display effector (CD8+ cytotoxic T cells) or regulatory (CD4+ helper T cell or CD4+/CD25+ Treg cell) roles. Activated T cells will undergo proliferation during injury and upon interaction with antigen presenting cells (APCs) will secrete the pro-inflammatory cytokines IL-1β, IL-6, IL-8, TNF-α, MCP-1 and MIP-1β[88]. However their specific role in regeneration remains controversial. During healing, it has been reported that increased T lymphocytes correlate with delayed bone regeneration[89]. However, Saddler et al.[90] recently showed that regeneration upon implantation of decellularized tissue-derived scaffolds requires an mTOR/Rictor-dependent T helper 2 pathway to guide an IL-4-dependent M2 macrophage polarization. Moreover, this IL-4 up-regulation is driven by an early adaptive response (at week 1) which is then maintained by an innate response (at week 3) later in the wound-healing and regenerative processes. Together, this unveils the potential role of CD4+ Th2 T cells to induce a pro-regenerative transcriptome on scaffold-associated macrophages[90-92]. Nevertheless, it remains the question whether this putative CD4+ T cell role is maintained upon implantation of artificial/engineered scaffolds.

B cells are lymphocytes that are responsible for the humoral immune response. Interestingly, in biomaterials that trigger Th2 type responses, B cells are rarely observed in the implant site which suggests limited antibody production[93]. Despite their potential involvement in mediating an adaptive response towards implanted materials their specific role and interplay with other cells in FBR is considerable less studied.

1.4 Cell recruitment in regeneration

Mobilization and recruitment of specific stromal cell types towards implanted biomaterials is a crucial step for the regenerative outcome. This is justified by the need to recruit a sufficient number of pro-regenerative stem cells in the best time frame in order to have accelerated recovery. In this regard, several chemoattractant molecules released by immune cells upon biomaterial interaction may have an important role in mediating a preferential recruitment of stem cells, which ultimately may impact on the healing outcome (Figure 2).

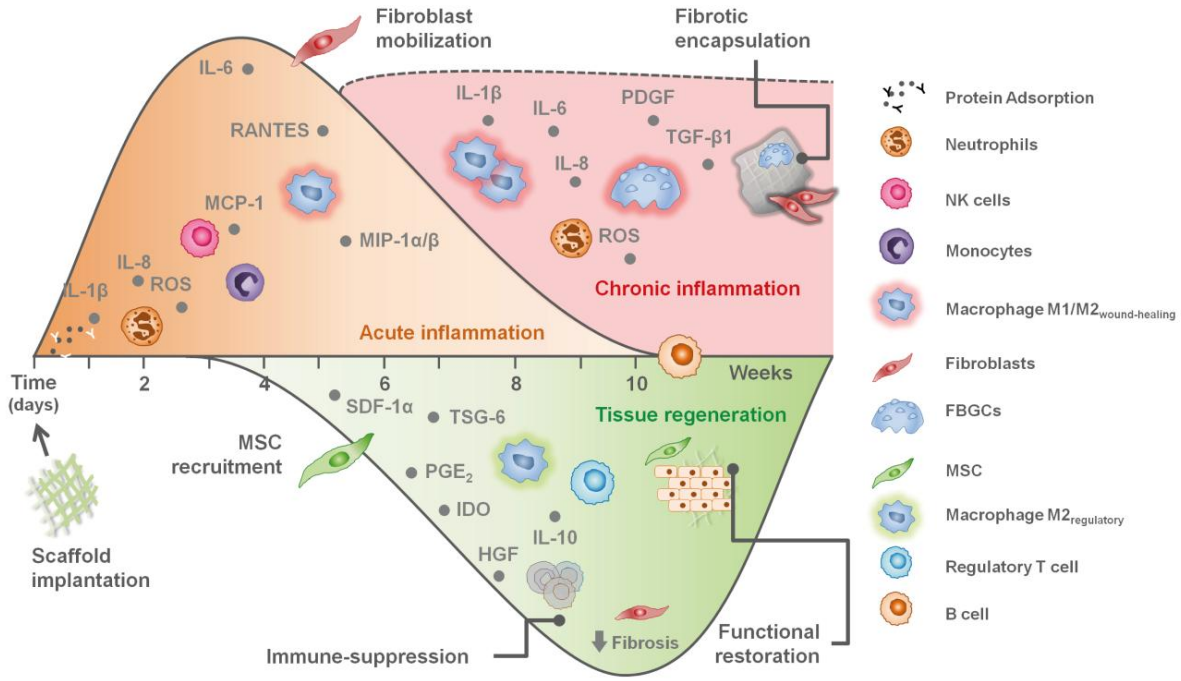

Figure 2 – Overview of the chemokines, growth factors and cell players involved in acute inflammation, chronic inflammation, and/or tissue regeneration triggered upon scaffold implantation. Upon implantation, the scaffold surface is immediately coated by blood proteins. The surgical implantation of the biomaterial injuries the tissue and initiates an inflammatory process mediated by the local production of IL-1β and IL-8 inflammatory signals. Local inflammation triggers the influx of neutrophils and NK cells to the implant site to remove cell debris and other injurious agents. Increased IL-6 and MCP-

1 expression promotes recruitment of monocytes which gradually differentiate into macrophages replacing the short-lived neutrophils. Pro-inflammatory macrophages (M1) secrete chemokines as RANTES and MIP-1α/β that recruit additional immune and/or stromal cells to initiate healing mechanisms. Excessive fibroblasts mobilization and activation and/or the persistence of foreign material stimuli prolong the presence of pro-inflammatory and wound-healing macrophages and perpetuate the inflammatory cytokine environment. The inability of macrophages to phagocyte the scaffold drives formation of FBGCs which ultimately orchestrate fibrotic encapsulation of the scaffold and impair scaffold colonization. On the other hand, MSC recruitment can assist tissue regeneration through secretion of SDF-1 to attract additional progenitor cells and PGE_2, IDO, TSG-6 and IL-10 to polarize macrophages and other immune cells such as T cells towards a regulatory phenotype. This ameliorates inflammation and creates a feed-back loop to resolve inflammation allowing scaffold-guided regeneration to succeed. This pathway is facilitated by the synchronized biodegradation of the implanted scaffold over the regenerative process. Abbreviations: FBGCs, foreign body giant cells.

1.4.1 Chemokines and growth factors

1.4.1.1 SDF-1

Stromal cell-derived factor 1 (SDF-1), also known as CXCL12, is a chemokine produced by resident endothelial cells and stromal fibroblasts and it is specially up-regulated following tissue injury and/or hypoxia[(94)]. SDF-1, recognized by the CXCR4 receptor, is involved in mobilization and recruitment of MSC and endothelial progenitor cells from the bone marrow to the injury site but also of other immune cells including B lymphocytes[(95)]. Hence, a number of *in situ* tissue engineering SDF-1 delivery strategies have been shown to promote MSC migration towards implanted scaffolds and improve tissue regeneration[(96,97)]. Depending on the local concentration of SDF-1, this chemokine can act as chemoattractant as well as repellent for leukocytes[(98,99)].

1.4.1.2 IL-6

Interleukin 6 (IL-6) is promptly and transiently produced in response to tissue injuries and is an important mediator of acute inflammatory phase[(100)]. IL-6 binds to the IL6R receptor and can be produced by several cell types including endothelial cells, fibroblasts, monocytes and macrophages[(101)]. Depending on the environment, IL-6 production may act as pro-inflammatory or pro-regenerative cytokine. For instance, IL-6 secreted by fibroblasts in an autocrine fashion has a central role in pathologic fibrosis which drives

fibroblast proliferation and collagen synthesis while perpetuating inflammation[102,103]. On the other hand, proteolytic processing of the IL-6R from invading neutrophils subsequently drives IL-6 trans-signaling in resident tissue cells, leading to a switch from neutrophil to monocyte recruitment by suppressing neutrophil-attracting (CXCL1/Gro-α, CXCL8/IL-8, CX3CL1/fractalkine) and enhancing monocyte-attracting chemokines (CCL2/MCP-1, CCL8/MCP-2, CXCL5/ENA-78, CXCL6/GCP-2), a instrumental event for the progression of the inflammatory process[104,105].

1.4.1.3 IL-8

Interleukin 8 (IL-8), or CXCL8, is a chemokine primarily involved in neutrophil accumulation during the inflammatory response that also primes phagocytosis and respiratory burst at the injury site[106]. IL-8 can be recognized by the receptors CXCR1 and CXCR2 and is transiently expressed upon tissue damage or ischemia by several cells including endothelial cells, fibroblasts, NK cells, monocytes and macrophages[107,108]. Interestingly, BM-MSC show a dose-dependent chemotactic response to IL-8[109,110].

1.4.1.4 MCP-1

Monocyte chemotactic protein 1 (MCP1), also known as CCL2, signals by binding to the CCR2 receptor. This chemokine that can be secreted upon tissue damage or stress by many cell types including endothelial cells, fibroblasts, smooth muscle cells and monocytes/macrophages[111,112]. Although MCP-1 is primarily involved in monocyte/macrophage recruitment to sites of inflammation, it also promotes chemotaxis of BM-MSC, dendritic cells, NK cells and memory T cells[112-115].

1.4.1.5 MIP-1α/β

Macrophage inflammatory protein 1α (MIP-1α), also known as CCL3, and MIP-1β (CCL4) play critical roles in recruitment of leukocytes to the site of inflammation and signal through CCR1, CCR4, and CCR5. Their expression is induced by inflammatory stimuli, mainly in macrophages, lymphocytes and dendritic cells but also in other cells, including fibroblasts and smooth muscle cells[116]. While CCL3 and CCL4 are both chemoattractant for monocytes, macrophages, and dendritic cells, they differ in their responses with T cells. While MIP-1α preferentially attracts CD8+ T cells, CD4+ T cells are more responsive to MIP-1β. In addition to its chemotactic and co-activator functions, MIP-1α also induces inflammatory cytokine secretion, mast cell degranulation, and NK cell activation. MIP-1α has been shown to encourage BM-MSC migration. Therefore it has been proposed as one of the mechanisms for stem cell recruitment to the injury site[117-119].

1.4.1.6 RANTES

Regulated upon Activation Normal T cell Expressed and Secreted (RANTES), also known as CCL5, is produced by synovial fibroblasts, NK cells, monocytes, macrophages, T lymphocytes, mast cells, and platelets. RANTES signals through the receptors CCR1, CCR3, CCR4 and CCR5 and plays an important role in the immune response by initiating the recruitment of leukocytes and other cells to the injury site. RANTES is chemoattractant for monocytes, NK cells, dendritic cells and T cells but also for non-inflammatory cells such as BM-MSC[120]. Interestingly, BM-MSC chemotaxis towards RANTES was found to be greatly increased in inflammatory environments[121]. The activity of RANTES is not restricted to chemotaxis, since it is also involved in proliferation and activation of certain immune cells[122].

1.4.1.7 PDGF-BB

Platelet-derived growth factor BB (PDGF-BB) is a growth factor, recognized by PDGF-R, and can be produced upon tissue injury by a plethora of cells including activated platelets, macrophages, mast cells and endothelial cells. The secreted PDGF-BB promotes neutrophil and macrophage infiltration, triggers fibroblasts migration, proliferation and fibrotic activity and has a key role in angiogenesis. PDGF also mediates recruitment of BM-MSC, which express high levels of PDGFRs. Nevertheless, while other chemokines (as SDF-1 and MCP-1) greatly increase their ability to promote MSC recruitment under inflammatory stimuli the same does not seem to occur with growth factors, including PDGF-BB[121].

1.5 The stromal compartment: MSC and fibroblasts

The type of healing adopted upon injury is intrinsically related with the stromal compartment. Stroma refers to the tissue that provides the structural support for the parenchyma/functional tissue of the organs. Since the parenchyma is avascular, it largely depends on the integrity of the underlying stromal tissue to access to oxygen, nutrients, waste disposal and eventually to the immune system for surveillance. Thus, upon tissue injury two key stromal cell types, MSC and fibroblasts (Table 2), can be mobilized to participate in wound healing and most likely determine the healing outcome.

Table 2 – Overview MSC and fibroblasts features. Phenotypic markers are denoted as (–) absent or (+) present. Chemokine receptor expression is graded from + to ++++.

		MSC	Fibroblasts	Refs.
Morphology				
Distribution		Bone-marrow Throughout vascularised tissues, possibly as pericytes	Ubiquitous	(123-125)
Frequency		Rare (0.001-0.08% in bone-marrow; Lower frequencies in other tissues)	Common in stromal compartments	(123,126)
Primary function		Support haematopoiesis Tissue turn-over and regeneration	ECM production Wound healing/fibrosis	(127-129)
Phenotype	**CD14**	-	-	(130)
	CD19	-	-	(131)
	CD34	-	-	(130)
	CD45	-	-	(130)
	CD73	+	+	(125,132)
	CD90	+	+	(125)
	CD105	+	+	(125,132)
	CD106	+	-	(125)
	CD146	+	-	(125)
	HLA-DR	-	-	(133)
Chemokine receptors	**CCR1**	-	+++	(117,121,134)
	CCR2	++++	+++	(121,134,135)
	CCR3	+++	+	(121,135)
	CCR4	++	++	(109,121,136,137)
	CCR5	+++	+++	(109,121,135)
	CXCR1	++++	+	(109,138)
	CXCR2	++++	+	(109)
	CXCR4	++++	+	(117,121,139)
	IL-6R	-	+	(140-142)
	PDGF-R	+++	+++	(121,143)
Immumodulatory ability		Immunoenhancing (MSC1) or Immunosupressive (MSC2)	Pro-inflammatory	(144,145)

1.5.1 MSC

In 1961 Freidenstein *et al.*[146] experimentally demonstrated that a bone marrow transplant into a heterotypic site could give rise to a functional bone organoid. MSC characterized by their fibroblastic morphology were then identified as the bone marrow stem cell component responsible for the *in vivo* regeneration and support of ectopic bone, stroma and hematopoietic tissues upon transplantation[147-149]. These stromal cells isolated by plastic adherence, were characterized by their colony forming capacity (CFU) at low densities and by their ability to differentiate and form bone, cartilage and adipose tissues upon single stem cell transplantation[127]. In the following decades, MSC were also identified, isolated and expanded by *in vitro* culture from a myriad of other tissues including adipose tissue, umbilical cord blood, skin, tendon, muscle and dental pulp. The widespread research on MSC became plagued by the lack of uniform criteria to define these cells which hampered the possibility to compare the results obtained by the different research groups[150]. This major obstacle, lead the International Society for Cellular Therapy (ISCT) in 2006 to formulate the minimal standard criteria to define MSC[151] as: (i) plastic-adherence cells under standard culture conditions, (ii) with positive expression of CD73, CD90 and CD105 and lack of hematopoietic cell surface marker expression, namely CD14, CD19, CD34, CD45 and human leukocyte antigen (HLA-DR) and (iii) ability for *in vitro* differentiation into osteoblasts adipocytes and chondrocytes when chemically stimulated. Although the characterization of this broad population of MSC is still under debate[127,152], these cells seem to exhibit stem cell function *in vivo*, and were hence named Mesenchymal Stromal/Stem cells (MSC)[153]. Although not included in the ISCT minimal criteria for defining these cells, MSC have been increasingly recognized to participate in tissue regeneration not only as building blocks through differentiation but more importantly by their role in immune modulation, recruitment of tissue-specific progenitor cells and release of trophic factors in response to injury[128,154,155].

The gradual understanding of stem cell biology has lead to a notorious MSC paradigm evolution over the last decades, with direct implications on their therapeutic application. Indeed, within the first decades upon their discovery MSC were explored as feeder cells that provided the niche for culture of hematopoietic stem cell (HSC). The experimental demonstration, in 1999 by Pittenger and colleagues[123], that MSC could be cultured *ex-vivo* and chemically induced to differentiate into other tissue-specific lineages as osteoblasts, adipocytes and chondrocytes has led to a novel paradigm: MSC as a regenerative medicine workhorse which could be used to replace the damaged cells/organs. However, as the knowledge on stem cell biology increases it is now apparent

that only a small fraction of MSC actually differentiates into tissue-specific cells upon recruitment to assist regeneration. In fact, MSC seem to act also as a transient first aid responder in injured tissues. Their ability to (a) modulate excessive inflammation and immune reactions, (b) secrete bioactive factors that lead to diminished fibrosis and apoptosis of damaged cells, and (c) that promote proliferation and differentiation of tissue-specific progenitor cells seems instrumental to minimize tissue damage and orchestrate tissue regeneration[156]. Within the current paradigm, in-depth understanding on how endogenous MSC function upon tissue injury is crucial to develop novel and more efficient *in situ* tissue engineering strategies to improve tissue regeneration.

1.5.1.1 MSC: a first aid responder

MSC can differentiate into multiples tissue-specific cell types. Since their differentiated progeny is not limited to one specific anatomical position it has been suggested that these cells can participate in the regeneration of multiple tissues throughout the body[124,126,157]. Conceptually, this implies that MSC are localized (i) within an anatomical site or "niche" with access to systemic danger signals and (ii) have the ability to reach the damaged tissues throughout the body.

In an effort to regenerate damaged tissue, it is thus essential to efficiently recruit sufficient number of endogenous MSC to the implanted scaffold[116]. This recruitment is a multistep process and involves complex inflammatory signals from the injury site causing the release of MSC from their storage niche into circulation (mobilization), which may then migrate towards the injury site (homing), colonize the implanted scaffold, secrete bioactive molecules to support the regenerative process and eventually some will directly replace the damaged tissue through differentiation (Figure 3a).

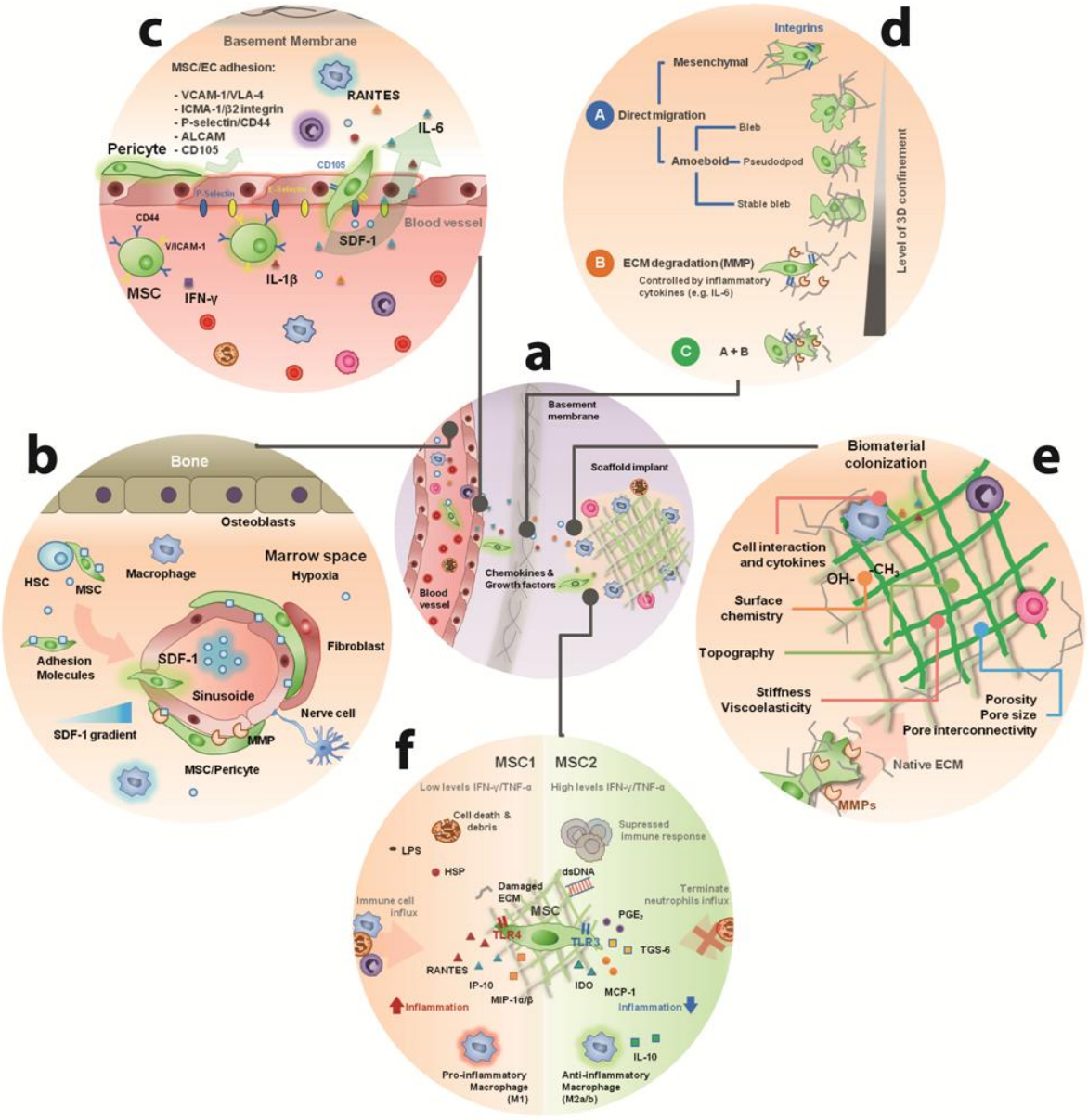

Figure 3 - Model of the dynamical behavior of MSC upon biomaterial implantation. (a) Overall view of MSC mobilization, homing, interstitial migration, scaffold colonization and immunomodulation upon scaffold implantation. Colonization of an implanted scaffold by immune cells drives the inflammatory process through secretion of chemokines and inflammatory mediators. (b) The release of inflammatory signals from the injury site is sensed in the bone marrow and mediates mobilization of MSC from their niche into the blood stream. The presence of activated immune cells within the bone marrow niche together with SDF-1 and other inflammatory mediators released from the injury site decreases the adhesion of MSC to the niche and facilitate their migration towards the blood stream into the injury site. (c) The continuous release of inflammatory mediators and chemokines from the injury site activate the endothelium to express P- and E-selectins and incoming MSC to express CD44, CD105 and V-CAM, which mediates the

slow rolling of MSC and subsequently the firm adhesion and transmigration through the inflamed endothelial cells into the interstitial space. (d) Upon transmigration MSC need to overcome the physical constrains imposed by the basement membrane and interstitial ECM before reaching the implanted scaffold. Here, MSC motility modes include mesenchymal motility, or various forms of amoeboid motility characterized by blebs, pseudopods, or stable blebs. Additionally, cells can degrade/cleave ECM proteins through secretion of MMPs. The adopted motility mode is influenced by environmental factors, including the strength of adhesion to the substrate, or the extent of physical confinement and contractility. (e) Biomaterial colonization rate by recruited MSC and their fate is influenced by the physical-chemical features of the scaffold, by the inflammatory microenvironment and cell-cell interactions. (f) Upon arrival to the implanted scaffold MSC interaction with the surrounding environment can trigger their polarization into a pro-inflammatory (MSC1) or anti-Inflammatory (MSC2) phenotype. In the onset of inflammation (low levels of TNF-α and IFN-γ), recruited MSC may adopt a pro-inflammatory phenotype (MSC1) and enhance immune cell responses by secreting chemokines that recruit lymphocytes to the implanted biomaterial (e.g. MIP-1α and MIP-1β, RANTES and IP-10). In the presence of an inflammatory environment (high levels of TNF-α and IFN-γ), MSC become activated to adopt an immune-suppressive phenotype (MSC2) by secreting high levels of soluble factors such as IDO, PGE_2, TSG-6 and MCP-1, which suppress inflammatory immune cell responses and drive their polarization into a regulatory phenotype. The switch toward MSC1 or MSC2 type may also depend on MSC stimulation through TLRs expressed on their surface.

1.5.1.2 MSC niches

MSC reside primarily in bone marrow niche, comprising approximately 0.001-0.08% of bone marrow cells, but were identified in almost every vascularised tissues throughout the body[123,157]. The close association of many stem cells types with vasculature and the fact that MSC and CD146+ pericytes, that reside in close proximity with the vascular wall, share the same phenotypic profile and multipotency lead to the hypothesis of vascular pericytes as a possible *in vivo* source of MSC[158,159].

The stem cell “niche” hypothesis was first proposed by R. Schofield for hematopoetic stem cells (HSC) [160]. Niche was then defined as a specialized environment within tissues that can preserve the adult stem cells proliferative potential and block maturation. Removal of stem cells from the niche results in loss of stem cell identity, self-renewal capacity and the onset of differentiation[161]. Every stem cell niche represents a dynamic entity with different cells interacting to modulate MSC function[162] (Figure 3b). Within this microenvironment

there are two types of niche cells: resident and transitory cells. The permanent cells include endothelial cells, nerve cells and connective-tissue fibroblasts while immune cells and MSC itself account for the transitory component, especially during host response to tissue damage[163,164]. Importantly the close proximity of MSC niches with blood vessels ensures their responsiveness to systemic signals and provides a conduit for recruitment of stem cells into and from the niche[165-167].

The stem cell pool within the niches are maintained by two cell division mechanisms: (i) asymmetric self-renewal into which a stem cell divides into one stem and one differentiated cell to maintain tissue homeostasis and/or (ii) symmetric self-renewal in which a stem cell gives rise to two daughter stem cells leading to the re-establishment of the stem cells pool, a condition required upon tissue injury[168].

Although distinct tissue-specific stem cell niches can be identified they share common features. These niches are physical entities with specific ECM proteins and environmental properties as hypoxia. Stem cell niches are typically governed by heterotypic cell-cell interactions, where secreted and membrane-bound factors as chemokines gradients regulate stem cell fate: quiescence or mobilization into blood stream/injury site. Interestingly, immune cells seem to provide the needed dynamic regulation of the niche during inflammation and tissue damage, which in turn can transiently modify the specific local environmental properties and chemokine gradients of the niche setting off the release of MSC[163].

1.5.1.3 MSC mobilization from niches

The release of MSC from their niche into circulation is defined as mobilization[169]. The bone marrow acts as a major reservoir for multiple stem cell populations including MSC, which are mobilized at different extents to the peripheral circulation following tissue injury[170-172]. However, the nature of signals released from the injured tissue and the molecular mechanism that sets off MSC mobilization from the niche are poorly understood. Under physiologic conditions, bone marrow MSC are maintained within their niche through tightly controlled interactions of chemokines, cytokines and growth factors as well the presence of specific adhesion molecules. SDF-1/CXCR4 axis seems to be pivotal for MSC maintenance within the niche. Moreover, their maintenance in discrete hypoxic regions of bone marrow promotes cell adhesion to the niche possibly through local increase in SDF-1 due to stabilization of hypoxia related hypoxia-inducible factor 1-alpha (HIF-1α) transcription factor[173].

However, injury leads to upregulation of inflammatory cytokines and chemokines that are released into circulation from remote damaged tissues, thus creating a transient imbalance on niche gradients. This stimulates the downregulation of adhesion molecules in MSC and ultimately sets off their mobilization from the niche (Figure 3b). For instance, blood vessel disruption upon injury leads to tissue hypoxia with stabilization of HIF-1α. Consequently there is SDF-1 expression and its release from the damaged tissue to the circulation triggers a spike on SDF-1 systemic levels[174]. This is sensed in bone marrow MSC niches, inducing CXCR4 receptor desensitization on resting MSC and increases in matrix metalloproteinase 9 (MMP-9) protease activity on the stromal component of the niche, hence triggering the release of stem cells from the bone marrow reservoir[175].

Additionally it is also possible that MSC participating in tissue regeneration following injury can originate from local tissues or nearby vasculature (pericytes) as these cells only need to travel short distances to arrive to the site of injury avoiding the need for circulation[176] (Figure 3c).

1.5.1.4 MSC homing

Upon release from their niches into circulation, MSC then need to home and engraft at the injury site[177]. Homing mechanisms of circulating MSC to the site of injury involve a cascade of events, including rolling of MSC along the blood vessels, adhesion onto inflamed endothelial cell surface, transendothelial migration and finally, migration and invasion through ECM towards the target tissue[178]. Although the exact mechanism used by MSC remains largely unknown it seems to rely on a complex interplay between inflammatory cytokines, chemokines, adhesion molecules and ECM-degrading proteases[179,180]. This process is thought to be similar to the one used by leukocytes homing to sites of inflammation since many of the molecules involved are also expressed by MSC. Importantly, maximal engraftment of stem cells was correlated with peak production of inflammatory cytokines, such as IL-6, which supports the notion that the intensity of inflammation is an important modulator for enhanced homing and migration of stem cells to damaged tissues[181].

Several studies implicated P- and E-selectin in endothelial cells to be involved on MSC rolling over the inflamed endothelial wall. The specific P-selectin ligand used by human MSC seems to be a modified CD44 isoform since these cells do not express neither PSGL-1 (CD162) nor CD24 on their surface[182,183]. For subsequent firm adhesion, MSC seem to use several protein-integrin interactions as VCAM-1/ very late antigen-4 (VLA-4), ICAM-1-β2 integrin[179,184]. This could be facilitated by local production of pro-inflammatory

cytokines such as IFN-γ, TNF-α and IL-1β in response to injury, all of which upregulate expression of ICAM-1 and VCAM-1 on the surface of MSC[185,186] (Figure 3c). Moreover, a myriad of other cell adhesion molecules (CAM) such as a1, a2, a3, a4, a5, av, b1, b3, b4, ICAM-3, activated leukocyte cell adhesion molecule (ALCAM), and endoglin/CD105 have also been implicated in mediating MSC-endothelial cell adhesion[187,188]. Interestingly, the integrin-dependent adhesion of several progenitor cells can be regulated by several chemokines including SDF-1[189]. Nevertheless, further studies are required to understand whether bone marrow-derived circulating MSC and tissue-derived MSC operate through identical trafficking mechanisms.

1.5.1.5 MSC interstitial migration

Regardless of MSC origin from circulation or local tissues, their ability to migrate and invade is critical for their functional integration within the inflamed tissue. In two-dimensional (2D) surfaces the matrix stiffness directly modulates the velocity of cells[190]. However, for navigation in three-dimensional (3D) substrates cells interpret not only adhesive and mechanical features of increased complexity from their environment but also the steric hindrances created by the ECM itself. And to navigate effectively MSC can either migrate directly through the matrix pores, use cell-mediated degradation of the matrix or a combination of both[191,192]. Direct migration of MSC in 3D depends on deformability of cells and cell sub-structures with cell nucleus being the rate-limiting organelle in 3D migration[193]. For direct migration, single MSC can adopt two broadly defined motility modes: mesenchymal or amoeboid[194]. MSC in the mesenchymal mode exhibit elongated, spindle-like shape morphology and their movement relies on strong cell-substrate adhesions to exert traction via focal adhesions, with actin rich leading edge structures including lamellipodia or filopodia protrusions. On the other hand, cells undergoing amoeboid migration adopt round or irregular shapes and undergo cycles of expansion and contraction to squeeze through gaps in the ECM, a process that does not rely so heavily on cell-substrate adhesions[191] (Figure 3d). The cells velocity in amoeboid mode is higher than that of cells in mesenchymal one and it appears to involve a range of different sub-modes, depending if cells use a bleb-, pseudopod- or stable bleb-based motility[195]. Mesenchymal and amoeboid migration modes are not mutually exclusive, and the ECM features seem to influence which mode predominates. This plasticity in the motility mode is an important aspect of immune cells and MSC migration, as the cells mobilized by acute inflammation have to navigate through a range of extracellular matrix geometries to escape their niche and engraft at the injury site. The degree of cell

confinement that cells encounter in the different tissues seems to be one of the most important factors for cells to use a given motility mode[195](Figure 3d).

The transendothelial and thereafter interstitial migration of MSC requires degradation of the basement membrane that underlies all epithelia and endothelia surrounding muscle and fat tissues. This process largely depends on the production of matrix-degrading enzymes[196]. This thin, yet dense and highly cross-linked ECM is composed mainly by laminin and collagen type IV but also contains nidogen/enactin and proteoglycans[197]. Notably, all cell types that migrate through endothelial walls, including leukocytes, tumor cells, HSC and MSC, express matrix metalloproteinases (MMPs) -2 and MMP-9, which degrade the two major basement membrane components - collagen type IV and laminin[198,199].

The majority of MMP activity exhibited by MSC is associated with the membrane/pericellular vicinity rather than on the secreted proteolytic factors[200]. Importantly, MSC proteolytic activity experiences a complex regulation by the inflammatory cytokines present at the injury site that can further encourage their ability to invade into the damaged tissue. For instance, TGF-β1, IL-1β and TNF-α promote BM-MSC recruitment through up-regulation of MMP-2, -9 MT1-MMP and TIMP metallopeptidase inhibitor (TIMP) -1 and -2. Similarly, IL-6 seems to do the same by increased expression of MMP-13 alone[180,200,201] while PDGF-BB modulates MSC migration by inducing a decrease on TIMP secretion, counterbalanced with an increased expression of MMP-2[200]. Besides their MMP and TIMP secretion these cells were also found to activate proMMP-2 inactive form already present within the inflammatory milieu in a process that appears to involve TIMP-2 and MT1-MMP[180]. Although SDF-1 can play an important role on MSC mobilization several studies suggest that this chemokine does not influence MMP/TIMP production by MSC and therefore their ability to degrade the basement membrane[201].

1.5.1.6 Scaffold colonization by recruited MSC

Upon arrival, MSC and other cells attracted by local inflammation should colonize the implanted engineered ECM that gaps the wound limits. It is important to notice that without cellular colonization of the implanted scaffold, little if any new tissue could be formed. Cell migration within such scaffolds is a critical process governing tissue integration. Thus, improved understanding on how matrix physico-chemical cues affect MSC behaviour led to the design of dynamic and multifunctional scaffolds with fine-tuned features to facilitate cell ingrown and to instruct MSC fate decisions upon scaffold

colonization. The colonization rate of the engineered matrix by endogenous MSC is highly dependent on the 3D architectural features of the porous scaffold, stiffness and cell-material interactions[50] (Figure 3e).

Implantation of highly porous scaffolds is desirable since it provides high surface area for cell-matrix interactions, which combined with increased pore interconnectivity facilitates cell adhesion, deposition of ECM elements and uniform cell migration within the implanted matrix[49]. Importantly, the matrix pore size not only plays a major role in immune responses triggered but also on cell migration. Although the "optimal pore size range" may vary depending on the cell type and application, several reports state that pores within the range of 100-150 μm are adequate to support most mature cell ingrown[202-204]. Surface chemistry and roughness are other features that can impact migration of cells. Differences in expression of focal adhesion components and Rho GTPases were found to be modulated by different surface chemistry which in turn enhanced endothelial cell migration in the order CH_3>NH_2>OH>COOH[205]. Similarly, MSC expression of cell-substrate and cell-cell adhesion proteins has been shown to be regulated by substrate roughness with consequences on cell spreading and migration [206,207]. The understanding that most cells interact with the Arginine-Glycine-Aspartic acid (RGD) binding domains present in many of ECM proteins prompted the manufacture of biomaterials tailored with these small RGD peptide sequences to improve cell adhesion, proliferation and migration[208,209].

Additionally, matrix stiffness and viscoelasticity can also have an important role on scaffold colonization since MSC can actively deform and re-arrange more compliant matrices to move directly through the ECM while in more resistive matrices degradation of the ECM components may be necessary for cell movement[50]. These physical properties of the matrix not only influence cell migration but also MSC proliferation and differentiation. Human MSC have been shown to increase their proliferation rate with increasing substrate stiffness[210-212]. Moreover, MSC tend to differentiate into the cell type relevant to the substrate stiffness on the long run[213]. For instance, soft matrices that resemble soft brain tissue induce MSC differentiation into neuronal lineages, a 10 fold stiffer matrices promote myoblast differentiation while harder substrates that match cortical bone stiffness triggers osteogenic differentiation[214-218]. Interestingly, in the absence of regenerative intervention, formed scar tissue stiffness following injury is usually 2 to 3 times higher than the native tissue where it is paved-down[219,220]. Notably, fibrotic ECM properties have been shown to hinder MSC differentiation into the native tissue-specific cell type and thus contributing for poor healing outcomes [221,222].

Therefore, it is the biophysical properties of the material scaffold and how the cells interact that will influence the MSC phenotypic decisions and thus the healing outcome.

1.5.1.6.1 Imaging MSC ability to integrate 3D bioengineered matrices

Multiple features such as matrix porosity, pore size, surface chemistry and stiffness impact cells dynamical behaviour within engineered 3D matrices. Therefore, scaffold properties should be carefully optimized to facilitate MSC ingrowth upon recruitment. In this regard 3D cell-based tissue models have been increasingly useful[223,224]. While the use and complexity of 3D models have advanced, there has been an increasing demand for methods to monitor and compare the MSC dynamical behaviour within distinct engineered matrices/models. Surprisingly, histology of fixed samples remains the "gold standard" technique for imaging tissue constructs to access cells ability to integrate the implanted matrix[225]. Unfortunately, this requires destruction of the samples which limits longitudinal 3D assessment. Thus, non-destructive imaging technologies for live 3D analysis have been identified as a strategic priority in tissue engineering research, required to accelerate progress this field[226]. To this end a number of live cell imaging techniques were developed for tissue engineering and regenerative medicine purposes, namely, Ultrasound (US), Resonance imaging (MRI), X-ray Imaging, Nuclear Imaging, Photoacoustic microscopy (PAM) and Optical imaging. Imaging techniques often display an intrinsic trade-off between spatial resolution and imaging depth/sensibility (Table 3). These features make US, MRI, X-ray and nuclear imaging techniques more suitable for *in vivo* applications and optical microscopy more promising for detailed *in vitro* monitoring of 3D cell-scaffold interactions. To access advanced tissue-engineered constructs, versatile 3D live cell imaging methods to monitor morphological and, more importantly, functional and molecular information are needed. Importantly each imaging method has a specific range of applications and provides distinct types of information. For *in vitro* 3D models, confocal imaging techniques are the most promising due to their high spatial resolution which enables visualization of sub-cellular features. The fact that a plethora of fluorescent probes are commercially available makes the ability to target specific sub-cellular structures/processes a powerful ally to interrogate cell morphology and function within engineered microenvironments. Moreover, since materials can exhibit inherent auto-fluorescence this can be further exploited to image 3D structure of the matrix[227]. Several studies illustrate confocal ability to track cell movement within engineered matrices and potential to interrogate how specific ECM features can be optimized to facilitate cell motility[228-231]. However, such imaging platforms do not allow to follow MSC dynamical behaviour in these matrices for more than a couple of days due to photo-bleaching

constrains. Therefore, imaging methods with improved longitudinal perspective of MSC movement are required and will greatly benefit advances in biomaterial design.

Although scaffold properties can have an important role in regeneration, other key environmental features must be considered for improving the healing outcome. These include the type of cells recruited to colonize the implanted scaffold and the inflammatory state encountered at the biomaterial-tissue interface. Importantly, each of these factors can be modulated by MSC mostly through secretion of an array of key chemokines and cytokines with tremendous impact on the regenerative microenvironment.

Table 3 – Properties of imaging modalities for tissue engineering applications[225,226].
Abbreviations: PLDL: poly(l-lactide-co-dl-lactide); PEG: poly(ethylene glycol); PLLA: poly(L-lactic acid); ECM: extracellular matrix; PEO: poly(ethylene oxide); PGA: polyglycolic acid; PLGA: poly(lactic-co-glycolic acid); POC: poly(1,8-octanediol-co-citrate); CG: collagen; HA: hyaluronic acid; CT: computed tomography; PET: positron emission tomography; SPECT: single-photon emission computed tomography.

	Imaging technique		Endpoint	3D Scaffold	Imaging resolution/ depth	Real-time?	Markers (molecular imaging)	Cost	Refs.
Clinical / Pre-clinical	X-ray imaging (μ-CT)		Changes in mineralization; Scaffold structure	PLDL; Bioceramic scaffolds; PEG hydrogels	5 μm / Full body	No	Poor	Medium	(232-234)
	Nuclear imaging (μ-PET; μ-SPECT)		Cell adhesion, metabolism; MSC tracking	Bioceramic, chitosan and PLLA scaffolds; Decellularized ECM	1-2 mm / Full body	No	Excellent	High	(235-239)
	μ-MRI		Changes in ECM, MSC tracking	PEO hydrogel; PGA/PLLA scaffolds; Cartilage tissue-constructs; pullulan/dextran scaffolds	100-200 μm / Full body	Yes	Good	High	(240-244)
	μ-Ultrasound		Changes in ECM content and stiffness	PLGA scaffolds; Cartilage constructs; PEG hydrogels; POC scaffolds.	20-100 μm / 10 mm	Yes	Good	Low	(245-248)
Organs	Optical microscopy	Bioluminescence	Cell proliferation/survival, hypoxia, MSC differentiation, tracking	Matrigel; Decellularized matrix; bioceramic, chitosan and PLLA scaffolds;	2-3 mm / 10 mm	Yes	Excellent	Low	(239,249-253)
Tissues		Photoacoustic microscopy	Vascularisation; Cell distribution, invasion, tracking and proliferation; Scaffold structure	Matrigel, Gelatin and PEGylated fibrin gels; PLGA scaffolds	50-150 μm / 20 mm	Yes	Good	Medium	(254-258)
Cells		Optical Coherence Tomography	Cell metabolism, migration, proliferation and distribution; Scaffold structure	PLLA, PLGA, calcium phosphate scaffolds; Matrigel and agarose hydrogels	15 μm / 2-3 mm	Yes	Good	Low	(259-262)
Molecules		Confocal microscopy (Fluorescence)	Cell tracking and motility dynamics; Cell viability, invasion; Cytoskeleton dynamics; Molecule diffusion	Matrigel; CG, PLGA, PEG, silk-fibroin, chitosan, scaffolds; Alginate- and HA-RGD hydrogels, Tissue engineered models	0.2-1 μm / 100-500 μm	Yes	Excellent	Low	(208,228-231,263-265)

1.5.1.7 MSC immunomodulatory and paracrine properties

Upon arrival at the injury site, MSC encounter a rather hypoxic, pro-inflammatory microenvironment with extensive immune cell infiltration. Stimulation of MSC with pro-inflammatory cytokines up-regulates the expression of a subset of toll-like receptors (TLRs) to grant MSC increased sensitivity to the damage/danger signals following injury[266]. Moreover, during inflammation many DAMPs are released from necrotic cells which will trigger TLRs not just on immune cells but also on MSC at the injury site[267].

MSC ability to sense and integrate many of these inflammatory signals allows them to adopt a pro-inflammatory (MSC1) or anti-inflammatory (MSC2) phenotype accordingly shaping their responses[268] (Figure 3f). Human BM-MSC have been reported to express all TLR1-10 with TLR3 and TLR4 having the highest expression[269]. And recently, MSC1/MSC2 polarization based on TLR4/TLR3 priming has been proposed[145]. This putative dual MSC phenotype relies on the presence of inflammatory cytokines together with specific danger signals that activate these cells TLRs at the injury site[270].

During onset of acute inflammation, tissue-specific stem cells and early recruited MSC can actually help to mount and enhance the inflammatory response to boost host defence. In fact, low levels of IFN-γ, TNF-α together with activation of TLR4 signalling by exogenous bacterial LPS or endogenous HSP released from necrotic cells and fibronectin fragments from damaged ECM promotes a pro-inflammatory MSC1 phenotype. This triggers secretion of low levels of indoleamine (IDO), oxide nitric (NO) and PGE2 and high levels of pro-inflammatory cytokines as IFN-gamma-inducible protein 10 (IP-10), MIP-1α, MIP-1β and RANTES by MSC that can exacerbate inflammation through the recruitment of additional leukocytes to clear the injured area[268]. Interestingly, several of these cytokines have also been reported as powerful inducers of MSC recruitment[121].

When high levels of these pro-inflammatory cytokines are achieved and there is activation of TLR3 signalling, then MSC adopt an anti-inflammatory MSC2 profile. This renders MSC to secrete high levels of anti-inflammatory cytokines as IDO, IL-10, MCP-1 chemokine, TGF-β, tumor necrosis factor-inducible gene 6 protein (TSG6) and PGE_2 that suppress immune cell responses counteracting the excessive inflammation. These paracrine factors can ameliorate the immune response by preventing the proliferation and function of a myriad of inflammatory cells including T cells, B cells, dendritic cells, NK cells, monocytes and macrophages[271,272]. MSC2 can also induce IL-10 expression by monocytes and macrophages which in turn prevents neutrophils migration into the damaged tissue, avoiding further oxidative damage[273,274]. Notably, prolonged stimulation with TLR ligands induces down-regulation of TLR2 and TLR4 on MSC, which constitutes another self-

regulatory mechanism to prevent chronic inflammation and thus impaired healing[268,275]. Importantly, the balance between these opposing pathways can therefore encourage host defence mechanisms at the beginning of acute inflammation while at the same time it creates a loop that prevents excessive inflammation later on to initiate tissue regeneration/repair mechanisms.

Apart from shaping the immune responses and inflammation MSC-secreted bioactive molecules also play an important role in limiting damage and re-establishing the native tissue architecture following injury. For instance, many of the MSC-secreted molecules can rescue apoptotic cells due to traumatic hypoxia, acidic environments and mechanical injury. IGF-1 and IL-6 secretion by MSC increases protein kinase B (AKT), Wnt and factor nuclear kappa B (NF-κB) signalling in damaged cells which in turn can regulate the expression of B-cell lymphoma 2 (Bcl-2), B-cell lymphoma-extra large (Bcl-xL) and heat-shock proteins that revert and limit cell apoptosis upon injury[276,277]. Moreover, VEGF, hepatocyte growth factor (HGF) and TGF-β1 cytokines secreted by MSC can also revert hypoxia-related apoptosis of endothelial cells while at the same time these molecules are instrumental to promote angiogenesis and support tissue regeneration later on[278,279].

A persistent and exacerbated inflammatory state is a pre-requisite for healing through fibrotic repair/scaring. Notably, it was found that MSC in implanted tissue constructs decrease the fibrous capsule thickness that circumvents the biomaterial[280,281]. Therefore, MSC secreted molecules can inhibit excessive fibrosis both indirectly - by suppressing immune responses and damping the inflammatory state - and directly through modulation of myofibroblasts ECM protein deposition rate. Indeed, MSC can secrete molecules as IL-10, TNF-α, HGF and PGE2 that have been shown to inhibit collagen synthesis and proliferation of fibroblast like cells[282-285].

1.5.2 Fibroblasts and fibrosis

Fibroblasts are a heterogeneous population of stromal cells characterized by their spindle shape morphology and plastic adherence. Although no universal fibroblast marker exists to identify this population they are reported to lack hematopoietic and endothelial lineage markers[125] (Table 2). Fibroblasts have an important role in the structural maintenance of ECM through production and secretion of all ECM components including structural proteins (fibrous collagens and elastin), adhesive proteins (laminin and fibronectin) and ground substance (glycosaminoglycans)[129]. This property combined with their ability to remodel the ECM, respond and secrete a broad range of pro-inflammatory cytokines,

chemokines and growth factors during injury makes them a key player on tissue repair, pathological fibrosis and foreign body reactions[286].

1.5.2.1 Fibroblast recruitment and activation during inflammation

The array of inflammatory cytokines and chemokines produced upon injury by immune cells promotes recruitment of many cell types to the injury site to initiate healing, including fibroblasts. Fibroblasts main role upon recruitment is to replace and remodel the blood clot provisional matrix with collagen and other ECM components[287]. Despite the fact that resident stromal fibroblasts seem to be the most significant cell source for the fibrotic response, they can originate from a variety of precursor cells and are not terminally differentiated cells. Following injury, TGF-β1, TNF-α, IL-1β, IL-6, IL-8 and PDGF are among the cytokines that are normally encountered within the inflammatory milieu that can drive the development of a fibrotic response[287] (Figure 4). Fibroblast activation by these inflammatory signals promotes their migration, proliferation and differentiation into myofibroblasts[288]. Fibroblast differentiation renders increased responsiveness to inflammatory stimuli, exaggerated ECM component synthesis and a constitutive pro-inflammatory cytokine secretion. Among these cytokines are MCP-1, MIP-1α, MIP-1β, RANTES and IP-10 which can have an important role in the recruitment of more inflammatory cells[289]. Together, these features endow them the ability to assist on biomaterials fibrotic encapsulation and simultaneously promote the recruitment and activation of more immune cells towards the implant site, exacerbating inflammation[59].

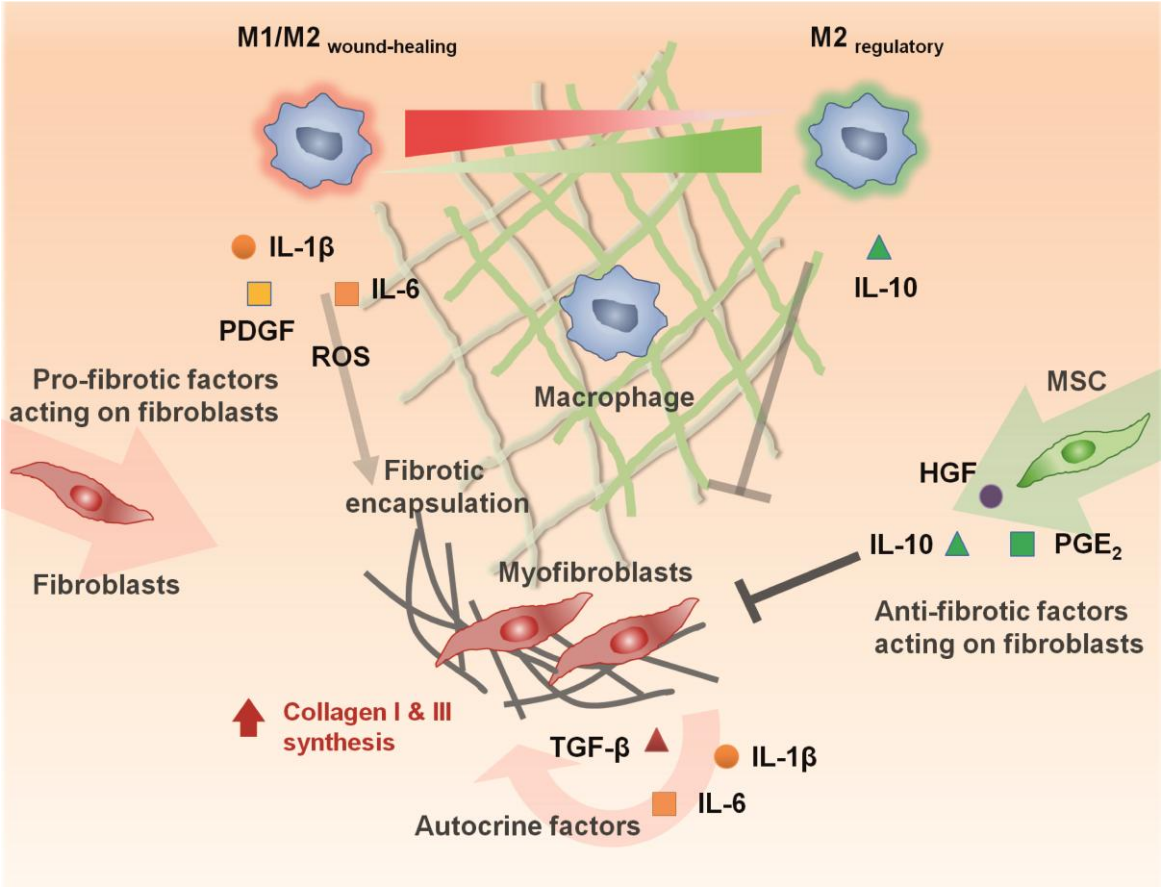

Figure 4 - Overview of the factors involved in profibrotic myofibroblast phenotype that mediate the fibrotic encapsulation of implanted scaffold (green mesh). Macrophage polarization into pro-inflammatory (M1) or wound-healing ($M2_{wound}$) phenotypes impacts secretion of IL-1β, IL6 and PDGF and production of ROS, which drives fibroblast activation and differentiation into myofibroblasts. This, in turn perpetuates the inflammatory environment and mediates fibrotic encapsulation of the implant. On the other hand, mobilized MSC secrete HGF, PGE_2 and IL-10 that drive macrophage polarization into the M2 regulatory phenotype to synergistically resolve inflammation and inhibit excessive deposition of ECM components by fibroblasts.

1.5.2.2 Chronic inflammation and fibrotic encapsulation

Continuous activation of recruited immune cells due to prolonged presence of a foreign body (regenerative scaffold) leads to a chronic inflammation state which deregulates the normal course of healing. This pro-inflammatory environment maintains a positive feedback loop that perpetuates inflammation and consequently drives fibrotic encapsulation of the implanted scaffold. In turn, activated fibroblasts secrete molecules as IL-1β, IL-6, TGF-β that sustain inflammation and can act in an autocrine fashion to further enhance their own fibrotic activity[287,290].

Although fibrotic tissue production immediately after injury can limit the damage it is an inappropriate environment for regeneration over the long term. Excessive deposition of ECM components at the biomaterial-tissue interface results in a thick and dense fibrotic capsule circumventing the biomaterial. This rather hypo -cellular and -vascular fibrotic region composed by highly crosslinked collagen type I and III fibbers isolates the regenerative scaffold from host's cells, severely compromising their colonization by endogenous MSC and consequently scaffold-guided tissue regeneration.

SCOPE OF THE THESIS

Rationale & thesis aims

In situ tissue engineering approaches rely on the use of scaffolds designed to stimulate endogenous healing mechanisms, which intimately involves the immune system. While the beneficial aspects of the immune response, namely debris clearance and progenitor cell recruitment, initiate healing, their potentially damaging effects, due to excessive inflammation followed by fibrotic encapsulation of a biomaterial should be minimized for a successful regeneration. Consequently, two independent research lines are currently being pursued with significant effects on scaffold integration and remodelling. These are based on the implantation of scaffolds designed to (i) enhance the recruitment of endogenous MSC or to (ii) ameliorate the foreign body reaction and fibrotic encapsulation.

As an alternative, I propose that scaffolds should be designed to modulate inflammation as a mean of controlling the type of regenerative/fibrotic cells mobilized towards the implanted material. However, the potential of the immune cell populations to promote stem cell and/or fibroblast recruitment, upon interaction with distinct 3D biomaterials, remains largely uncharacterized.

Hypothesis and goal

Here I explore the idea that biomaterials can modulate the immune response to control the recruitment and motility of specific stromal cell types, pivotal to determine the likelihood of tissue regeneration/fibrosis.

To test the aforementioned hypothesis, experiments were conducted in a 3D model with multiple scaffolds and cell types. Within this framework, the main objective of this work is to provide a comprehensive analysis on the impact of primary human immune responses, triggered by distinct 3D scaffold models, on primary human bone-marrow MSC and fibroblasts recruitment. The specific aims of this thesis are as follows:

Specific aims

1. **Develop a bioimaging platform to characterize MSC dynamical behaviour within 3D engineered matrices.**

Upon scaffold implantation, mobilized MSC need to move through distinct 3D environments to colonize the engineered scaffold. Nevertheless, there is a scarcity of imaging tools to access and longitudinally monitor MSC dynamical behaviour within such

3D microenvironments. This has been identified as a strategic priority to accelerate progress in the tissue engineering and regenerative medicine field[291].

Therefore, in **Chapter 2** I describe the development and characterization of a novel imaging tool that takes advantage of the photoswitchable Dendra2 protein to directly compare MSC migration within distinct 3D engineered matrices over long periods of time.

2. **Profile which immune cell populations promote MSC recruitment upon interaction with distinct 3D biomaterial models.**

Once developed the needed technology to monitor MSC motility within 3D engineered matrices, I sought to establish a link between the immune responses triggered by different 3D biomaterial models and their predisposition to mobilize endogenous MSC towards the implanted material.

Accordingly, in **Chapter 3**, the responses elicited by interactions of PBMCs, NK cells, monocytes and macrophages with 3D scaffolds were first characterized. Then, the ability of those responses to promote bone-marrow MSC invasion towards the implanted scaffolds was directly compared. Additionally, this characterization made use of the Dendra2 imaging platform, developed in Chapter 2, in order to analyse whether the immune responses could also modulate the scaffolds colonization rate by the recruited MSC.

3. **Map which immune cell populations induce fibroblast mobilization upon interaction with distinct 3D scaffold models.**

Recently, the extent of fibrocytic cell recruitment towards the implant site was correlated with a poor healing outcome[292]. Indeed fibroblasts are one of the major contributors for the biomaterials fibrotic encapsulation observed following foreign body response to implanted materials.

Thus, in **Chapter 4,** I sought to clarify which type of immune responses and which biomaterials promoted the highest fibroblast mobilization.

4. **Develop a 3-cell platform to screen how the immune responses triggered by model 3D biomaterials regulate the recruitment of stromal cells.**

In a physiologic environment, several cell types will reciprocally influence each other behaviour. For example, recruited MSC and fibroblasts compete for the chemokines and/or growth factors produced by the immune cells reacting to the implanted

biomaterials. Thus in **Chapter 4**, a 3-cell platform was developed to investigate whether those biomaterial-evoked immune responses promoted the competitive recruitment of one specific stromal cell type in detriment of another. Also, MSC at the implant site have been suggested to decrease biomaterials fibrotic encapsulation and improve the regenerative outcome[280]. Thus, I sought to investigate the consequence of endogenous MSC arrival and interaction with immune cells at the implant site on the recruitment of fibroblasts.

Finally, this thesis closes with a general discussion on the data gathered (**Chapter 5**), integrating the knowledge from preceding chapters, and highlights the challenges that should be addressed for the development of next generation immunomodulatory scaffolds.

It is expected that this work provides one of the first steps towards defining rules for the creation of biomaterials that trigger the desired immunological pathways for enhanced stem cell recruitment in detriment of pro-fibrotic cell types.

1.6 References

[1] Baddour, J. A., Sousounis, K. & Tsonis, P. A. Organ repair and regeneration: an overview. *Birth defects research. Part C, Embryo today : reviews*, 96, 1, 2012, 1-29.

[2] Atala, A., Irvine, D. J., Moses, M. & Shaunak, S. Wound Healing Versus Regeneration: Role of the Tissue Environment in Regenerative Medicine. *MRS bulletin / Materials Research Society*, 35, 8, 2010.

[3] Gurtner, G. C., Werner, S., Barrandon, Y. & Longaker, M. T. Wound repair and regeneration. *Nature*, 453, 7193, 2008, 314-321.

[4] Fairweather, M. *et al.* Celecoxib inhibits early cutaneous wound healing. *The Journal of surgical research*, 194, 2, 2015, 717-724.

[5] Endo, K. *et al.* Cyclooxygenase-2 inhibitor delays fracture healing in rats. *Acta orthopaedica*, 76, 4, 2005, 470-474.

[6] Chazaud, B. Macrophages: supportive cells for tissue repair and regeneration. *Immunobiology*, 219, 3, 2014, 172-178.

[7] Bianchi, M. E. DAMPs, PAMPs and alarmins: all we need to know about danger. *Journal of leukocyte biology*, 81, 1, 2007, 1-5.

[8] Eldor, A., Vlodavsky, I., Martinowicz, U., Fuks, Z. & Coller, B. S. Platelet interaction with subendothelial extracellular matrix: platelet-fibrinogen interactions are essential for platelet aggregation but not for the matrix-induced release reaction. *Blood*, 65, 6, 1985, 1477-1483.

[9] Li, Z., Delaney, M. K., O'Brien, K. A. & Du, X. Signaling during platelet adhesion and activation. *Arteriosclerosis, thrombosis, and vascular biology*, 30, 12, 2010, 2341-2349.

[10] Lam, F. W., Vijayan, K. V. & Rumbaut, R. E. Platelets and Their Interactions with Other Immune Cells. *Comprehensive Physiology*, 5, 3, 2015, 1265-1280.

[11] Langer, H. F. *et al.* Platelet derived bFGF mediates vascular integrative mechanisms of mesenchymal stem cells in vitro. *Journal of molecular and cellular cardiology*, 47, 2, 2009, 315-325.

[12] de Boer, H. C. *et al.* Fibrin and activated platelets cooperatively guide stem cells to a vascular injury and promote differentiation towards an endothelial cell phenotype. *Arteriosclerosis, thrombosis, and vascular biology*, 26, 7, 2006, 1653-1659.

[13] Lev, E. I. *et al.* Potential role of activated platelets in homing of human endothelial progenitor cells to subendothelial matrix. *Thrombosis and haemostasis*, 96, 4, 2006, 498-504.

[14] Kumar, V., Abbas, A. K. & Aster, J. C. *Robbins Basic Pathology*. (Elsevier Health Sciences, 2012).

[15] Kono, H. & Rock, K. L. How dying cells alert the immune system to danger. *Nature reviews. Immunology*, 8, 4, 2008, 279-289.

[16] Horton, M. R. *et al.* Hyaluronan fragments synergize with interferon-gamma to induce the C-X-C chemokines mig and interferon-inducible protein-10 in mouse macrophages. *The Journal of biological chemistry*, 273, 52, 1998, 35088-35094.

[17] Noble, P. W., Lake, F. R., Henson, P. M. & Riches, D. W. Hyaluronate activation of CD44 induces insulin-like growth factor-1 expression by a tumor necrosis factor-alpha-dependent mechanism in murine macrophages. *The Journal of clinical investigation*, 91, 6, 1993, 2368-2377.

[18] Smiley, S. T., King, J. A. & Hancock, W. W. Fibrinogen stimulates macrophage chemokine secretion through toll-like receptor 4. *Journal of immunology*, 167, 5, 2001, 2887-2894.

[19] Chen, W., Syldath, U., Bellmann, K., Burkart, V. & Kolb, H. Human 60-kDa heat-shock protein: a danger signal to the innate immune system. *Journal of immunology*, 162, 6, 1999, 3212-3219.

[20] Tran, T. T., Groben, P. & Pisetsky, D. S. The release of DNA into the plasma of mice following hepatic cell death by apoptosis and necrosis. *Biomarkers : biochemical indicators of exposure, response, and susceptibility to chemicals*, 13, 2, 2008, 184-200.

[21] Rovere-Querini, P. *et al.* HMGB1 is an endogenous immune adjuvant released by necrotic cells. *EMBO reports*, 5, 8, 2004, 825-830.

[22] Esmon, C. T. The interactions between inflammation and coagulation. *British journal of haematology*, 131, 4, 2005, 417-430.

[23] Rios-Navarro, C. *et al.* Differential effects of anti-TNF-alpha and anti-IL-12/23 agents on human leukocyte-endothelial cell interactions. *European journal of pharmacology*, 765, 2015, 355-365.

[24] Muller, W. A. Leukocyte-endothelial-cell interactions in leukocyte transmigration and the inflammatory response. *Trends in immunology*, 24, 6, 2003, 327-334.

[25] Meisel, S. R. *et al.* Increased expression of neutrophil and monocyte adhesion molecules LFA-1 and Mac-1 and their ligand ICAM-1 and VLA-4 throughout the acute phase of myocardial infarction: possible implications for leukocyte aggregation and microvascular plugging. *Journal of the American College of Cardiology*, 31, 1, 1998, 120-125.

[26] Ley, K., Laudanna, C., Cybulsky, M. I. & Nourshargh, S. Getting to the site of inflammation: the leukocyte adhesion cascade updated. *Nature reviews. Immunology*, 7, 9, 2007, 678-689.

[27] McEver, R. P. & Cummings, R. D. Role of PSGL-1 binding to selectins in leukocyte recruitment. *The Journal of clinical investigation*, 100, 11 Suppl, 1997, S97-103.

[28] Ley, K. *et al.* Lectin-like cell adhesion molecule 1 mediates leukocyte rolling in mesenteric venules in vivo. *Blood*, 77, 12, 1991, 2553-2555.

[29] Herter, J. & Zarbock, A. Integrin Regulation during Leukocyte Recruitment. *Journal of immunology*, 190, 9, 2013, 4451-4457.

[30] Eriksson, E. E., Xie, X., Werr, J., Thoren, P. & Lindbom, L. Importance of primary capture and L-selectin-dependent secondary capture in leukocyte accumulation in inflammation and atherosclerosis in vivo. *The Journal of experimental medicine*, 194, 2, 2001, 205-218.

[31] Sperandio, M. *et al.* P-selectin glycoprotein ligand-1 mediates L-selectin-dependent leukocyte rolling in venules. *The Journal of experimental medicine*, 197, 10, 2003, 1355-1363.

[32] Yang, L. *et al.* ICAM-1 regulates neutrophil adhesion and transcellular migration of TNF-alpha-activated vascular endothelium under flow. *Blood*, 106, 2, 2005, 584-592.

[33] Watson, R. L. *et al.* Endothelial CD99 signals through soluble adenylyl cyclase and PKA to regulate leukocyte transendothelial migration. *The Journal of experimental medicine*, 212, 7, 2015, 1021-1041.

[34] Vestweber, D. How leukocytes cross the vascular endothelium. *Nature reviews. Immunology*, 15, 11, 2015, 692-704.

[35] Schnoor, M., Alcaide, P., Voisin, M. B. & van Buul, J. D. Crossing the Vascular Wall: Common and Unique Mechanisms Exploited by Different Leukocyte Subsets during Extravasation. *Mediators of inflammation*, 2015, 2015, 946509.

[36] Dorin, R. P., Pohl, H. G., De Filippo, R. E., Yoo, J. J. & Atala, A. Tubularized urethral replacement with unseeded matrices: what is the maximum distance for normal tissue regeneration? *World journal of urology*, 26, 4, 2008, 323-326.

[37] Lutolf, M. P., Gilbert, P. M. & Blau, H. M. Designing materials to direct stem-cell fate. *Nature*, 462, 7272, 2009, 433-441.

[38] Krafts, K. P. Tissue repair: The hidden drama. *Organogenesis*, 6, 4, 2010, 225-233.

[39] Oberpenning, F., Meng, J., Yoo, J. J. & Atala, A. De novo reconstitution of a functional mammalian urinary bladder by tissue engineering. *Nature biotechnology*, 17, 2, 1999, 149-155.

[40] Pellicoro, A., Ramachandran, P., Iredale, J. P. & Fallowfield, J. A. Liver fibrosis and repair: immune regulation of wound healing in a solid organ. *Nature reviews. Immunology*, 14, 3, 2014, 181-194.

[41] Klingberg, F., Hinz, B. & White, E. S. The myofibroblast matrix: implications for tissue repair and fibrosis. *The Journal of pathology*, 229, 2, 2013, 298-309.

[42] Moerkamp, A. T. & Goumans, M. J. Cardiac regeneration: stem cells and beyond. *Current medicinal chemistry*, 19, 35, 2012, 5993-6002.

[43] Forbes, S. J. & Rosenthal, N. Preparing the ground for tissue regeneration: from mechanism to therapy. *Nature medicine*, 20, 8, 2014, 857-869.

[44] Ueha, S., Shand, F. H. & Matsushima, K. Cellular and molecular mechanisms of chronic inflammation-associated organ fibrosis. *Frontiers in immunology*, 3, 2012, 71.

[45] Katari, R., Peloso, A. & Orlando, G. Tissue engineering and regenerative medicine: semantic considerations for an evolving paradigm. *Frontiers in bioengineering and biotechnology*, 2, 2014, 57.

[46] Bernardo, M. E., Pagliara, D. & Locatelli, F. Mesenchymal stromal cell therapy: a revolution in Regenerative Medicine? *Bone marrow transplantation*, 47, 2, 2012, 164-171.

[47] Atala, A. Engineering tissues, organs and cells. *Journal of tissue engineering and regenerative medicine*, 1, 2, 2007, 83-96.

[48] Ko, I. K., Lee, S. J., Atala, A. & Yoo, J. J. In situ tissue regeneration through host stem cell recruitment. *Experimental & molecular medicine*, 45, 2013, e57.

[49] Lawrence, B. J. & Madihally, S. V. Cell colonization in degradable 3D porous matrices. *Cell adhesion & migration*, 2, 1, 2008, 9-16.

[50] Akhmanova, M., Osidak, E., Domogatsky, S., Rodin, S. & Domogatskaya, A. Physical, Spatial, and Molecular Aspects of Extracellular Matrix of In Vivo Niches and Artificial Scaffolds Relevant to Stem Cells Research. *Stem cells international*, 2015, 2015, 167025.

[51] Raya-Rivera, A. M. *et al.* Tissue-engineered autologous vaginal organs in patients: a pilot cohort study. *Lancet*, 384, 9940, 2014, 329-336.

[52] Fisher, M. B. & Mauck, R. L. Tissue engineering and regenerative medicine: recent innovations and the transition to translation. *Tissue engineering. Part B, Reviews*, 19, 1, 2013, 1-13.

[53] Evans, C. H. *et al.* Facilitated endogenous repair: making tissue engineering simple, practical, and economical. *Tissue engineering*, 13, 8, 2007, 1987-1993.

[54] Andreas, K., Sittinger, M. & Ringe, J. Toward in situ tissue engineering: chemokine-guided stem cell recruitment. *Trends in biotechnology*, 32, 9, 2014, 483-492.

[55] Chen, F. M., Wu, L. A., Zhang, M., Zhang, R. & Sun, H. H. Homing of endogenous stem/progenitor cells for in situ tissue regeneration: Promises, strategies, and translational perspectives. *Biomaterials*, 32, 12, 2011, 3189-3209.

[56] Yu, Y., Wu, R.-X., Yin, Y. & Chen, F.-M. Directing immunomodulation using biomaterials for endogenous regeneration. *Journal of Materials Chemistry B*, 4, 4, 2016, 569-584.

[57] Herrmann, M., Verrier, S. & Alini, M. Strategies to Stimulate Mobilization and Homing of Endogenous Stem and Progenitor Cells for Bone Tissue Repair. *Frontiers in bioengineering and biotechnology*, 3, 2015, 79.

[58] Vishwakarma, A. *et al.* Engineering Immunomodulatory Biomaterials To Tune the Inflammatory Response. *Trends in biotechnology*, 34, 6, 2016, 470-482.

[59] Anderson, J. M., Rodriguez, A. & Chang, D. T. Foreign body reaction to biomaterials. *Seminars in immunology*, 20, 2, 2008, 86-100.

[60] Jones, K. S. Effects of biomaterial-induced inflammation on fibrosis and rejection. *Seminars in immunology*, 20, 2, 2008, 130-136.

[61] Kastellorizios, M., Tipnis, N. & Burgess, D. J. Foreign Body Reaction to Subcutaneous Implants. *Advances in experimental medicine and biology*, 865, 2015, 93-108.

[62] Tang, L. & Eaton, J. W. Natural responses to unnatural materials: A molecular mechanism for foreign body reactions. *Molecular medicine*, 5, 6, 1999, 351-358.

[63] Veiseh, O. *et al.* Size- and shape-dependent foreign body immune response to materials implanted in rodents and non-human primates. *Nature materials*, 14, 6, 2015, 643-651.

[64] Franz, S., Rammelt, S., Scharnweber, D. & Simon, J. C. Immune responses to implants - a review of the implications for the design of immunomodulatory biomaterials. *Biomaterials*, 32, 28, 2011, 6692-6709.

[65] Koh, T. J. & DiPietro, L. A. Inflammation and wound healing: the role of the macrophage. *Expert reviews in molecular medicine*, 13, 2011, e23.

[66] Bryers, J. D., Giachelli, C. M. & Ratner, B. D. Engineering biomaterials to integrate and heal: the biocompatibility paradigm shifts. *Biotechnology and bioengineering*, 109, 8, 2012, 1898-1911.

[67] Silverthorn, D. U. *Fisiologia Humana: Uma Abordagem Integrada*. (Artmed Editora, 2009).

[68] Mak, T. W., Saunders, M. E. & Jett, B. D. *Primer to the Immune Response*. (Elsevier Science, 2013).

[69] Jhunjhunwala, S. *et al.* Neutrophil Responses to Sterile Implant Materials. *PloS one*, 10, 9, 2015, e0137550.

[70] Agaiby, A. D. & Dyson, M. Immuno-inflammatory cell dynamics during cutaneous wound healing. *J Anat*, 195 (Pt 4), 1999, 531-542.

[71] Liippo, J., Toriseva, M. & Kähäri, V.-M. in *Natural Killer cells - Basic Science and Clinical Application* (eds M. Lotze & A. Thomson) Ch. 39, 519-525 (Academic Press, 2009).

[72] Moffett, A. & Colucci, F. Uterine NK cells: active regulators at the maternal-fetal interface. *The Journal of clinical investigation*, 124, 5, 2014, 1872-1879.

[73] Almeida, C. R. *et al.* Human NK cells differ more in their KIR2DL1-dependent thresholds for HLA-Cw6-mediated inhibition than in their maximal killing capacity. *PloS one*, 6, 2011, e24927.

[74] Fauriat, C., Long, E. O., Ljunggren, H.-G. & Bryceson, Y. T. Regulation of human NK-cell cytokine and chemokine production by target cell recognition. *Blood*, 115, 11, 2010, 2167-2176.

[75] Almeida, C. R., Caires, H. R., Vasconcelos, D. P. & Barbosa, M. A. NAP-2 Secreted by Human NK Cells Can Stimulate Mesenchymal Stem/Stromal Cell Recruitment. *Stem cell reports*, 6, 4, 2016, 466-473.

[76] Tsou, C. L. *et al.* Critical roles for CCR2 and MCP-3 in monocyte mobilization from bone marrow and recruitment to inflammatory sites. *The Journal of clinical investigation*, 117, 4, 2007, 902-909.

[77] Chan, J. K. *et al.* Low-dose TNF augments fracture healing in normal and osteoporotic bone by up-regulating the innate immune response. *EMBO molecular medicine*, 7, 5, 2015, 547-561.

[78] Brieland, J. K. *et al.* Expression of monocyte chemoattractant protein-1 (MCP-1) by rat alveolar macrophages during chronic lung injury. *American journal of respiratory cell and molecular biology*, 9, 3, 1993, 300-305.

[79] Tsirogianni, A. K., Moutsopoulos, N. M. & Moutsopoulos, H. M. Wound healing: immunological aspects. *Injury*, 37 Suppl 1, 2006, S5-12.

[80] Mantovani, A., Biswas, S. K., Galdiero, M. R., Sica, A. & Locati, M. Macrophage plasticity and polarization in tissue repair and remodelling. *The Journal of pathology*, 229, 2, 2013, 176-185.

[81] Sica, A. & Mantovani, A. Macrophage plasticity and polarization: in vivo veritas. *The Journal of clinical investigation*, 122, 3, 2012, 787-795.

[82] Badylak, S. F. *Host Response to Biomaterials: The Impact of Host Response on Biomaterial Selection*. (Elsevier Science, 2015).

[83] Sridharan, R., Cameron, A. R., Kelly, D. J., Kearney, C. J. & O'Brien, F. J. Biomaterial based modulation of macrophage polarization: a review and suggested design principles. *Materials Today*, 18, 6, 2015, 313-325.

[84] Murray, P. J. & Wynn, T. A. Protective and pathogenic functions of macrophage subsets. *Nature reviews. Immunology*, 11, 11, 2011, 723-737.

[85] Soehnlein, O. & Lindbom, L. Phagocyte partnership during the onset and resolution of inflammation. *Nature reviews. Immunology*, 10, 6, 2010, 427-439.

[86] Kou, P. M. & Babensee, J. E. Macrophage and dendritic cell phenotypic diversity in the context of biomaterials. *Journal of biomedical materials research. Part A*, 96, 1, 2011, 239-260.

[87] Badylak, S. F., Valentin, J. E., Ravindra, A. K., McCabe, G. P. & Stewart-Akers, A. M. Macrophage phenotype as a determinant of biologic scaffold remodeling. *Tissue engineering. Part A*, 14, 11, 2008, 1835-1842.

[88] Anderson, J. M. & McNally, A. K. Biocompatibility of implants: lymphocyte/macrophage interactions. *Seminars in immunopathology*, 33, 3, 2011, 221-233.

[89] Gouttefangeas, C. *et al.* Functional T lymphocytes infiltrate implanted polyvinyl alcohol foams during surgical wound closure therapy. *Clinical and experimental immunology*, 124, 3, 2001, 398-405.

[90] Sadtler, K. *et al.* Developing a pro-regenerative biomaterial scaffold microenvironment requires T helper 2 cells. *Science*, 352, 6283, 2016, 366-370.

[91] Allman, A. J. *et al.* Xenogeneic extracellular matrix grafts elicit a TH2-restricted immune response. *Transplantation*, 71, 11, 2001, 1631-1640.

[92] Laranjeira, P. *et al.* Effect of human bone marrow mesenchymal stromal cells on cytokine production by peripheral blood naive, memory, and effector T cells. *Stem cell research & therapy*, 6, 2015, 3.

[93] Ducheyne, P., Healy, K., Hutmacher, D. E., Grainger, D. W. & Kirkpatrick, C. J. *Comprehensive Biomaterials*. (Elsevier Science, 2015).

[94] Hitchon, C. *et al.* Hypoxia-induced production of stromal cell-derived factor 1 (CXCL12) and vascular endothelial growth factor by synovial fibroblasts. *Arthritis and rheumatism*, 46, 10, 2002, 2587-2597.

[95] Brandes, M., Legler, D. F., Spoerri, B., Schaerli, P. & Moser, B. Activation-dependent modulation of B lymphocyte migration to chemokines. *International immunology*, 12, 9, 2000, 1285-1292.

[96] Thevenot, P. T. *et al.* The effect of incorporation of SDF-1alpha into PLGA scaffolds on stem cell recruitment and the inflammatory response. *Biomaterials*, 31, 14, 2010, 3997-4008.

[97] Schantz, J. T., Chim, H. & Whiteman, M. Cell guidance in tissue engineering: SDF-1 mediates site-directed homing of mesenchymal stem cells within three-

dimensional polycaprolactone scaffolds. *Tissue engineering*, 13, 11, 2007, 2615-2624.

[98] Poznansky, M. C. *et al.* Active movement of T cells away from a chemokine. *Nature medicine*, 6, 5, 2000, 543-548.

[99] Buckley, C. D. *et al.* Fibroblasts regulate the switch from acute resolving to chronic persistent inflammation. *Trends in immunology*, 22, 4, 2001, 199-204.

[100] Tanaka, T., Narazaki, M. & Kishimoto, T. IL-6 in inflammation, immunity, and disease. *Cold Spring Harbor perspectives in biology*, 6, 10, 2014, a016295.

[101] Hagiwara, E., Abbasi, F., Mor, G., Ishigatsubo, Y. & Klinman, D. M. Phenotype and frequency of cells secreting IL-2, IL-4, IL-6, IL-10, IFN and TNF-alpha in human peripheral blood. *Cytokine*, 7, 8, 1995, 815-822.

[102] Feghali, C. A., Bost, K. L., Boulware, D. W. & Levy, L. S. Mechanisms of pathogenesis in scleroderma. I. Overproduction of interleukin 6 by fibroblasts cultured from affected skin sites of patients with scleroderma. *The Journal of rheumatology*, 19, 8, 1992, 1207-1211.

[103] Tiggelman, A. M. *et al.* Interleukin-6 production by human liver (myo)fibroblasts in culture. Evidence for a regulatory role of LPS, IL-1 beta and TNF alpha. *Journal of hepatology*, 23, 3, 1995, 295-306.

[104] Scheller, J., Chalaris, A., Schmidt-Arras, D. & Rose-John, S. The pro- and anti-inflammatory properties of the cytokine interleukin-6. *Biochimica et biophysica acta*, 1813, 5, 2011, 878-888.

[105] Le, T. T. *et al.* Blockade of IL-6 Trans signaling attenuates pulmonary fibrosis. *Journal of immunology*, 193, 7, 2014, 3755-3768.

[106] Harada, A. *et al.* Essential involvement of interleukin-8 (IL-8) in acute inflammation. *Journal of leukocyte biology*, 56, 5, 1994, 559-564.

[107] Wolff, B., Burns, A. R., Middleton, J. & Rot, A. Endothelial cell "memory" of inflammatory stimulation: human venular endothelial cells store interleukin 8 in Weibel-Palade bodies. *The Journal of experimental medicine*, 188, 9, 1998, 1757-1762.

[108] Liechty, K. W., Crombleholme, T. M., Cass, D. L., Martin, B. & Adzick, N. S. Diminished interleukin-8 (IL-8) production in the fetal wound healing response. *The Journal of surgical research*, 77, 1, 1998, 80-84.

[109] Ringe, J. *et al.* Towards in situ tissue repair: human mesenchymal stem cells express chemokine receptors CXCR1, CXCR2 and CCR2, and migrate upon stimulation with CXCL8 but not CCL2. *Journal of cellular biochemistry*, 101, 1, 2007, 135-146.

[110] Wang, L. *et al.* MCP-1, MIP-1, IL-8 and ischemic cerebral tissue enhance human bone marrow stromal cell migration in interface culture. *Hematology*, 7, 2, 2002, 113-117.

[111] Cushing, S. D. *et al.* Minimally modified low density lipoprotein induces monocyte chemotactic protein 1 in human endothelial cells and smooth muscle cells. *Proceedings of the National Academy of Sciences of the United States of America*, 87, 13, 1990, 5134-5138.

[112] Deshmane, S. L., Kremlev, S., Amini, S. & Sawaya, B. E. Monocyte chemoattractant protein-1 (MCP-1): an overview. *Journal of interferon & cytokine research : the official journal of the International Society for Interferon and Cytokine Research*, 29, 6, 2009, 313-326.

[113] Yoshimura, T. *et al.* Human monocyte chemoattractant protein-1 (MCP-1). Full-length cDNA cloning, expression in mitogen-stimulated blood mononuclear leukocytes, and sequence similarity to mouse competence gene JE. *FEBS letters*, 244, 2, 1989, 487-493.

[114] Belema-Bedada, F., Uchida, S., Martire, A., Kostin, S. & Braun, T. Efficient homing of multipotent adult mesenchymal stem cells depends on FROUNT-mediated clustering of CCR2. *Cell stem cell*, 2, 6, 2008, 566-575.

[115] Dwyer, R. M. *et al.* Monocyte chemotactic protein-1 secreted by primary breast tumors stimulates migration of mesenchymal stem cells. *Clinical cancer research : an official journal of the American Association for Cancer Research*, 13, 17, 2007, 5020-5027.

[116] Vanden Berg-Foels, W. S. In situ tissue regeneration: chemoattractants for endogenous stem cell recruitment. *Tissue engineering. Part B, Reviews*, 20, 1, 2014, 28-39.

[117] Sordi, V. *et al.* Bone marrow mesenchymal stem cells express a restricted set of functionally active chemokine receptors capable of promoting migration to pancreatic islets. *Blood*, 106, 2, 2005, 419-427.

[118] Koch, A. E. *et al.* Macrophage inflammatory protein-1 alpha. A novel chemotactic cytokine for macrophages in rheumatoid arthritis. *The Journal of clinical investigation*, 93, 3, 1994, 921-928.

[119] Boomsma, R. A. & Geenen, D. L. Mesenchymal stem cells secrete multiple cytokines that promote angiogenesis and have contrasting effects on chemotaxis and apoptosis. *PloS one*, 7, 4, 2012, e35685.

[120] Maghazachi, A. A., al-Aoukaty, A. & Schall, T. J. C-C chemokines induce the chemotaxis of NK and IL-2-activated NK cells. Role for G proteins. *Journal of immunology*, 153, 11, 1994, 4969-4977.

[121] Ponte, A. L. *et al.* The in vitro migration capacity of human bone marrow mesenchymal stem cells: comparison of chemokine and growth factor chemotactic activities. *Stem cells*, 25, 7, 2007, 1737-1745.

[122] Maghazachi, A. A. & Al-Aoukaty, A. Chemokines activate natural killer cells through heterotrimeric G-proteins: implications for the treatment of AIDS and cancer. *FASEB journal : official publication of the Federation of American Societies for Experimental Biology*, 12, 11, 1998, 913-924.

[123] Pittenger, M. F. *et al.* Multilineage potential of adult human mesenchymal stem cells. *Science*, 284, 5411, 1999, 143-147.

[124] Caplan, A. I. All MSCs are pericytes? *Cell stem cell*, 3, 3, 2008, 229-230.

[125] Halfon, S., Abramov, N., Grinblat, B. & Ginis, I. Markers distinguishing mesenchymal stem cells from fibroblasts are downregulated with passaging. *Stem cells and development*, 20, 1, 2011, 53-66.

[126] da Silva Meirelles, L., Chagastelles, P. C. & Nardi, N. B. Mesenchymal stem cells reside in virtually all post-natal organs and tissues. *Journal of cell science*, 119, Pt 11, 2006, 2204-2213.

[127] Bianco, P. "Mesenchymal" stem cells. *Annual review of cell and developmental biology*, 30, 2014, 677-704.

[128] Caplan, A. I. MSCs: The Sentinel and Safe-Guards of Injury. *Journal of cellular physiology*, 2015.

[129] Darby, I. A., Laverdet, B., Bonte, F. & Desmouliere, A. Fibroblasts and myofibroblasts in wound healing. *Clinical, cosmetic and investigational dermatology*, 7, 2014, 301-311.

[130] Lorenz, K. *et al.* Multilineage differentiation potential of human dermal skin-derived fibroblasts. *Experimental dermatology*, 17, 11, 2008, 925-932.

[131] Kozdon, K., Fitchett, C., Rose, G. E., Ezra, D. G. & Bailly, M. Mesenchymal Stem Cell-Like Properties of Orbital Fibroblasts in Graves' Orbitopathy. *Investigative ophthalmology & visual science*, 56, 10, 2015, 5743-5750.

[132] Alt, E. *et al.* Fibroblasts share mesenchymal phenotypes with stem cells, but lack their differentiation and colony-forming potential. *Biology of the cell / under the auspices of the European Cell Biology Organization*, 103, 4, 2011, 197-208.

[133] Cappellesso-Fleury, S. *et al.* Human fibroblasts share immunosuppressive properties with bone marrow mesenchymal stem cells. *Journal of clinical immunology*, 30, 4, 2010, 607-619.

[134] Scholten, D. *et al.* Migration of fibrocytes in fibrogenic liver injury. *The American journal of pathology*, 179, 1, 2011, 189-198.

[135] Moore, B. B. *et al.* CCR2-mediated recruitment of fibrocytes to the alveolar space after fibrotic injury. *The American journal of pathology*, 166, 3, 2005, 675-684.

[136] Kato, T. *et al.* Thymus and activation-regulated chemokine (TARC)/CC chemokine ligand (CCL) 17 accelerates wound healing by enhancing fibroblast migration. *Experimental dermatology*, 20, 8, 2011, 669-674.

[137] McLane, J. S. & Ligon, L. A. Palladin mediates stiffness-induced fibroblast activation in the tumor microenvironment. *Biophysical journal*, 109, 2, 2015, 249-264.

[138] Marotte, H., Ruth, J. H., Campbell, P. L., Koch, A. E. & Ahmed, S. Green tea extract inhibits chemokine production, but up-regulates chemokine receptor expression, in rheumatoid arthritis synovial fibroblasts and rat adjuvant-induced arthritis. *Rheumatology*, 49, 3, 2010, 467-479.

[139] Smadja, D. M. *et al.* Cooperation between human fibrocytes and endothelial colony-forming cells increases angiogenesis via the CXCR4 pathway. *Thrombosis and haemostasis*, 112, 5, 2014, 1002-1013.

[140] Kondo, M. *et al.* Contribution of the Interleukin-6/STAT-3 Signaling Pathway to Chondrogenic Differentiation of Human Mesenchymal Stem Cells. *Arthritis & rheumatology*, 67, 5, 2015, 1250-1260.

[141] Erices, A., Conget, P., Rojas, C. & Minguell, J. J. Gp130 activation by soluble interleukin-6 receptor/interleukin-6 enhances osteoblastic differentiation of human bone marrow-derived mesenchymal stem cells. *Experimental cell research*, 280, 1, 2002, 24-32.

[142] Sporri, B., Muller, K. M., Wiesmann, U. & Bickel, M. Soluble IL-6 receptor induces calcium flux and selectively modulates chemokine expression in human dermal fibroblasts. *International immunology*, 11, 7, 1999, 1053-1058.

[143] Novosyadlyy, R., Dudas, J., Pannem, R., Ramadori, G. & Scharf, J. G. Crosstalk between PDGF and IGF-I receptors in rat liver myofibroblasts: implication for liver fibrogenesis. *Laboratory investigation; a journal of technical methods and pathology*, 86, 7, 2006, 710-723.

[144] Donlin, L. T., Jayatilleke, A., Giannopoulou, E. G., Kalliolias, G. D. & Ivashkiv, L. B. Modulation of TNF-induced macrophage polarization by synovial fibroblasts. *Journal of immunology*, 193, 5, 2014, 2373-2383.

[145] Waterman, R. S., Tomchuck, S. L., Henkle, S. L. & Betancourt, A. M. A new mesenchymal stem cell (MSC) paradigm: polarization into a pro-inflammatory MSC1 or an Immunosuppressive MSC2 phenotype. *PloS one*, 5, 4, 2010, e10088.

[146] Friedenstein, A. J. Osteogenetic activity of transplanted transitional epithelium. *Acta anatomica*, 45, 1961, 31-59.

[147] Friedenstein, A. J. Stromal mechanisms of bone marrow: cloning in vitro and retransplantation in vivo. *Haematology and blood transfusion*, 25, 1980, 19-29.

[148] Friedenstein, A. J., Petrakova, K. V., Kurolesova, A. I. & Frolova, G. P. Heterotopic of bone marrow. Analysis of precursor cells for osteogenic and hematopoietic tissues. *Transplantation*, 6, 2, 1968, 230-247.

[149] Friedenstein, A. J., Piatetzky, S., II & Petrakova, K. V. Osteogenesis in transplants of bone marrow cells. *Journal of embryology and experimental morphology*, 16, 3, 1966, 381-390.

[150] Horwitz, E. M. *et al.* Clarification of the nomenclature for MSC: The International Society for Cellular Therapy position statement. *Cytotherapy*, 7, 5, 2005, 393-395.

[151] Dominici, M. *et al.* Minimal criteria for defining multipotent mesenchymal stromal cells. The International Society for Cellular Therapy position statement. *Cytotherapy*, 8, 4, 2006, 315-317.

[152] Bianco, P. *et al.* The meaning, the sense and the significance: translating the science of mesenchymal stem cells into medicine. *Nature medicine*, 19, 1, 2013, 35-42.

[153] Bianco, P., Robey, P. G. & Simmons, P. J. Mesenchymal stem cells: revisiting history, concepts, and assays. *Cell stem cell*, 2, 4, 2008, 313-319.

[154] Caplan, A. I. & Sorrell, J. M. The MSC curtain that stops the immune system. *Immunology letters*, 168, 2, 2015, 136-139.

[155] Caplan, A. I. & Correa, D. The MSC: an injury drugstore. *Cell stem cell*, 9, 1, 2011, 11-15.

[156] Prockop, D. J., Kota, D. J., Bazhanov, N. & Reger, R. L. Evolving paradigms for repair of tissues by adult stem/progenitor cells (MSCs). *Journal of cellular and molecular medicine*, 14, 9, 2010, 2190-2199.

[157] Murphy, M. B., Moncivais, K. & Caplan, A. I. Mesenchymal stem cells: environmentally responsive therapeutics for regenerative medicine. *Experimental & molecular medicine*, 45, 2013, e54.

[158] Blocki, A. *et al.* Not all MSCs can act as pericytes: functional in vitro assays to distinguish pericytes from other mesenchymal stem cells in angiogenesis. *Stem cells and development*, 22, 17, 2013, 2347-2355.

[159] Crisan, M. *et al.* A perivascular origin for mesenchymal stem cells in multiple human organs. *Cell stem cell*, 3, 3, 2008, 301-313.

[160] Schofield, R. The relationship between the spleen colony-forming cell and the haemopoietic stem cell. *Blood cells*, 4, 1-2, 1978, 7-25.

[161] Watt, F. M. & Hogan, B. L. Out of Eden: stem cells and their niches. *Science*, 287, 5457, 2000, 1427-1430.

[162] Wagers, A. J. The stem cell niche in regenerative medicine. *Cell stem cell*, 10, 4, 2012, 362-369.

[163] Lane, S. W., Williams, D. A. & Watt, F. M. Modulating the stem cell niche for tissue regeneration. *Nature biotechnology*, 32, 8, 2014, 795-803.

[164] Garrett, R. W. & Emerson, S. G. Bone and blood vessels: the hard and the soft of hematopoietic stem cell niches. *Cell stem cell*, 4, 6, 2009, 503-506.

[165] Christopher, M. J., Rao, M., Liu, F., Woloszynek, J. R. & Link, D. C. Expression of the G-CSF receptor in monocytic cells is sufficient to mediate hematopoietic progenitor mobilization by G-CSF in mice. *The Journal of experimental medicine*, 208, 2, 2011, 251-260.

[166] Chow, A. *et al.* Bone marrow CD169+ macrophages promote the retention of hematopoietic stem and progenitor cells in the mesenchymal stem cell niche. *The Journal of experimental medicine*, 208, 2, 2011, 261-271.

[167] Ehninger, A. & Trumpp, A. The bone marrow stem cell niche grows up: mesenchymal stem cells and macrophages move in. *The Journal of experimental medicine*, 208, 3, 2011, 421-428.

[168] Voog, J. & Jones, D. L. Stem cells and the niche: a dynamic duo. *Cell stem cell*, 6, 2, 2010, 103-115.

[169] Lapidot, T. & Petit, I. Current understanding of stem cell mobilization: the roles of chemokines, proteolytic enzymes, adhesion molecules, cytokines, and stromal cells. *Experimental hematology*, 30, 9, 2002, 973-981.

[170] Hannoush, E. J. *et al.* Impact of enhanced mobilization of bone marrow derived cells to site of injury. *The Journal of trauma*, 71, 2, 2011, 283-289; discussion 289-291.

[171] Rennert, R. C., Sorkin, M., Garg, R. K. & Gurtner, G. C. Stem cell recruitment after injury: lessons for regenerative medicine. *Regenerative medicine*, 7, 6, 2012, 833-850.

[172] Kumar, S. & Ponnazhagan, S. Mobilization of bone marrow mesenchymal stem cells in vivo augments bone healing in a mouse model of segmental bone defect. *Bone*, 50, 4, 2012, 1012-1018.

[173] Ceradini, D. J. *et al.* Progenitor cell trafficking is regulated by hypoxic gradients through HIF-1 induction of SDF-1. *Nature medicine*, 10, 8, 2004, 858-864.

[174] Youn, S. W. *et al.* COMP-Ang1 stimulates HIF-1alpha-mediated SDF-1 overexpression and recovers ischemic injury through BM-derived progenitor cell recruitment. *Blood*, 117, 16, 2011, 4376-4386.

[175] Heissig, B. *et al.* Recruitment of stem and progenitor cells from the bone marrow niche requires MMP-9 mediated release of kit-ligand. *Cell*, 109, 5, 2002, 625-637.

[176] Eggenhofer, E., Luk, F., Dahlke, M. H. & Hoogduijn, M. J. The life and fate of mesenchymal stem cells. *Frontiers in immunology*, 5, 2014, 148.

[177] Zhuang, Y., Chen, X., Xu, M., Zhang, L. Y. & Xiang, F. Chemokine stromal cell-derived factor 1/CXCL12 increases homing of mesenchymal stem cells to injured myocardium and neovascularization following myocardial infarction. *Chinese medical journal*, 122, 2, 2009, 183-187.

[178] Karp, J. M. & Leng Teo, G. S. Mesenchymal Stem Cell Homing: The Devil Is in the Details. *Cell stem cell*, 4, 3, 2009, 206-216.

[179] Steingen, C. *et al.* Characterization of key mechanisms in transmigration and invasion of mesenchymal stem cells. *Journal of molecular and cellular cardiology*, 44, 6, 2008, 1072-1084.

[180] Ries, C. *et al.* MMP-2, MT1-MMP, and TIMP-2 are essential for the invasive capacity of human mesenchymal stem cells: differential regulation by inflammatory cytokines. *Blood*, 109, 9, 2007, 4055-4063.

[181] Malek, S. *et al.* Successful implantation of intravenously administered stem cells correlates with severity of inflammation in murine myocarditis. *Pflugers Archiv : European journal of physiology*, 452, 3, 2006, 268-275.

[182] Thankamony, S. P. & Sackstein, R. Enforced hematopoietic cell E- and L-selectin ligand (HCELL) expression primes transendothelial migration of human mesenchymal stem cells. *Proceedings of the National Academy of Sciences of the United States of America*, 108, 6, 2011, 2258-2263.

[183] Herrera, M. B. *et al.* Exogenous mesenchymal stem cells localize to the kidney by means of CD44 following acute tubular injury. *Kidney international*, 72, 4, 2007, 430-441.

[184] Segers, V. F. *et al.* Mesenchymal stem cell adhesion to cardiac microvascular endothelium: activators and mechanisms. *American journal of physiology. Heart and circulatory physiology*, 290, 4, 2006, H1370-1377.

[185] Ren, G. *et al.* Mesenchymal stem cell-mediated immunosuppression occurs via concerted action of chemokines and nitric oxide. *Cell stem cell*, 2, 2, 2008, 141-150.

[186] Ren, G. *et al.* Inflammatory cytokine-induced intercellular adhesion molecule-1 and vascular cell adhesion molecule-1 in mesenchymal stem cells are critical for immunosuppression. *Journal of immunology*, 184, 5, 2010, 2321-2328.

[187] Minguell, J. J., Erices, A. & Conget, P. Mesenchymal stem cells. *Experimental biology and medicine*, 226, 6, 2001, 507-520.

[188] Krampera, M., Pizzolo, G., Aprili, G. & Franchini, M. Mesenchymal stem cells for bone, cartilage, tendon and skeletal muscle repair. *Bone*, 39, 4, 2006, 678-683.

[189] De Falco, E. *et al.* SDF-1 involvement in endothelial phenotype and ischemia-induced recruitment of bone marrow progenitor cells. *Blood*, 104, 12, 2004, 3472-3482.

[190] Vincent, L. G., Choi, Y. S., Alonso-Latorre, B., del Alamo, J. C. & Engler, A. J. Mesenchymal stem cell durotaxis depends on substrate stiffness gradient strength. *Biotechnology journal*, 8, 4, 2013, 472-484.

[191] Welch, M. D. Cell migration, freshly squeezed. *Cell*, 160, 4, 2015, 581-582.

[192] Driscoll, M. K. & Danuser, G. Quantifying Modes of 3D Cell Migration. *Trends in cell biology*, 25, 12, 2015, 749-759.

[193] Wolf, K. *et al.* Physical limits of cell migration: control by ECM space and nuclear deformation and tuning by proteolysis and traction force. *The Journal of cell biology*, 201, 7, 2013, 1069-1084.

[194] Friedl, P. & Wolf, K. Plasticity of cell migration: a multiscale tuning model. *The Journal of cell biology*, 188, 1, 2010, 11-19.

[195] Liu, Y. J. *et al.* Confinement and low adhesion induce fast amoeboid migration of slow mesenchymal cells. *Cell*, 160, 4, 2015, 659-672.

[196] Kelley, L. C., Lohmer, L. L., Hagedorn, E. J. & Sherwood, D. R. Traversing the basement membrane in vivo: a diversity of strategies. *The Journal of cell biology*, 204, 3, 2014, 291-302.

[197] Pöschl, E. *et al.* Collagen IV is essential for basement membrane stability but dispensable for initiation of its assembly during early development. *Development*, 131, 7, 2004, 1619-1628.

[198] Ratzinger, G. *et al.* Matrix metalloproteinases 9 and 2 are necessary for the migration of Langerhans cells and dermal dendritic cells from human and murine skin. *Journal of immunology*, 168, 9, 2002, 4361-4371.

[199] Smart, N. & Riley, P. R. The Stem Cell Movement. *Circulation research*, 102, 10, 2008, 1155-1168.

[200] Lozito, T. P., Jackson, W. M., Nesti, L. J. & Tuan, R. S. Human mesenchymal stem cells generate a distinct pericellular zone of MMP activities via binding of MMPs and secretion of high levels of TIMPs. *Matrix biology : journal of the International Society for Matrix Biology*, 34, 2014, 132-143.

[201] Tondreau, T. *et al.* In vitro study of matrix metalloproteinase/tissue inhibitor of metalloproteinase production by mesenchymal stromal cells in response to inflammatory cytokines: the role of their migration in injured tissues. *Cytotherapy*, 11, 5, 2009, 559-569.

[202] Huang, Y., Onyeri, S., Siewe, M., Moshfeghian, A. & Madihally, S. V. In vitro characterization of chitosan-gelatin scaffolds for tissue engineering. *Biomaterials*, 26, 36, 2005, 7616-7627.

[203] Yannas, I. V., Lee, E., Orgill, D. P., Skrabut, E. M. & Murphy, G. F. Synthesis and characterization of a model extracellular matrix that induces partial regeneration of adult mammalian skin. *Proceedings of the National Academy of Sciences of the United States of America*, 86, 3, 1989, 933-937.

[204] Loh, Q. L. & Choong, C. Three-dimensional scaffolds for tissue engineering applications: role of porosity and pore size. *Tissue engineering. Part B, Reviews*, 19, 6, 2013, 485-502.

[205] Shen, Y. *et al.* Effect of surface chemistry on the integrin induced pathway in regulating vascular endothelial cells migration. *Colloids and surfaces. B, Biointerfaces*, 126, 2015, 188-197.

[206] Menon, N. V. *et al.* Microfluidic Assay To Study the Combinatorial Impact of Substrate Properties on Mesenchymal Stem Cell Migration. *ACS applied materials & interfaces*, 7, 31, 2015, 17095-17103.

[207] Han, J., Menon, N. V., Kang, Y. & Tee, S.-Y. An in vitro study on the collective tumor cell migration on nanoroughened poly(dimethylsiloxane) surfaces. *Journal of Materials Chemistry B*, 3, 8, 2015, 1565-1572.

[208] Caires, H. R. *et al.* Finding and tracing human MSC in 3D microenvironments with the photoconvertible protein Dendra2. *Scientific reports*, 5, 2015, 10079.

[209] Wang, X., Ye, K., Li, Z., Yan, C. & Ding, J. Adhesion, proliferation, and differentiation of mesenchymal stem cells on RGD nanopatterns of varied nanospacings. *Organogenesis*, 9, 4, 2013, 280-286.

[210] Li, Z. *et al.* Differential regulation of stiffness, topography, and dimension of substrates in rat mesenchymal stem cells. *Biomaterials*, 34, 31, 2013, 7616-7625.

[211] Kim, T. H. *et al.* Creating stiffness gradient polyvinyl alcohol hydrogel using a simple gradual freezing-thawing method to investigate stem cell differentiation behaviors. *Biomaterials*, 40, 2015, 51-60.

[212] Rowlands, A. S., George, P. A. & Cooper-White, J. J. Directing osteogenic and myogenic differentiation of MSCs: interplay of stiffness and adhesive ligand presentation. *American journal of physiology. Cell physiology*, 295, 4, 2008, C1037-1044.

[213] MacQueen, L., Sun, Y. & Simmons, C. A. Mesenchymal stem cell mechanobiology and emerging experimental platforms. *Journal of the Royal Society, Interface / the Royal Society*, 10, 84, 2013, 20130179.

[214] Her, G. J. *et al.* Control of three-dimensional substrate stiffness to manipulate mesenchymal stem cell fate toward neuronal or glial lineages. *Acta biomaterialia*, 9, 2, 2013, 5170-5180.

[215] Wang, L. S., Boulaire, J., Chan, P. P., Chung, J. E. & Kurisawa, M. The role of stiffness of gelatin-hydroxyphenylpropionic acid hydrogels formed by enzyme-mediated crosslinking on the differentiation of human mesenchymal stem cell. *Biomaterials*, 31, 33, 2010, 8608-8616.

[216] Wen, J. H. *et al.* Interplay of matrix stiffness and protein tethering in stem cell differentiation. *Nature materials*, 13, 10, 2014, 979-987.

[217] Wang, L. S., Du, C., Chung, J. E. & Kurisawa, M. Enzymatically cross-linked gelatin-phenol hydrogels with a broader stiffness range for osteogenic differentiation of human mesenchymal stem cells. *Acta biomaterialia*, 8, 5, 2012, 1826-1837.

[218] Wang, P. Y., Tsai, W. B. & Voelcker, N. H. Screening of rat mesenchymal stem cell behaviour on polydimethylsiloxane stiffness gradients. *Acta biomaterialia*, 8, 2, 2012, 519-530.

[219] Berry, M. F. *et al.* Mesenchymal stem cell injection after myocardial infarction improves myocardial compliance. *American journal of physiology. Heart and circulatory physiology*, 290, 6, 2006, H2196-2203.

[220] Mueller, S. & Sandrin, L. Liver stiffness: a novel parameter for the diagnosis of liver disease. *Hepatic medicine : evidence and research*, 2, 2010, 49-67.

[221] Li, Z., Guo, X., Palmer, A. F., Das, H. & Guan, J. High-efficiency matrix modulus-induced cardiac differentiation of human mesenchymal stem cells inside a thermosensitive hydrogel. *Acta biomaterialia*, 8, 10, 2012, 3586-3595.

[222] Breitbach, M. *et al.* Potential risks of bone marrow cell transplantation into infarcted hearts. *Blood*, 110, 4, 2007, 1362-1369.

[223] van Duinen, V., Trietsch, S. J., Joore, J., Vulto, P. & Hankemeier, T. Microfluidic 3D cell culture: from tools to tissue models. *Current opinion in biotechnology*, 35, 2015, 118-126.

[224] Knight, E. & Przyborski, S. Advances in 3D cell culture technologies enabling tissue-like structures to be created in vitro. *J Anat*, 227, 6, 2015, 746-756.

[225] Smith, L. E., Smallwood, R. & Macneil, S. A comparison of imaging methodologies for 3D tissue engineering. *Microscopy research and technique*, 73, 12, 2010, 1123-1133.

[226] Nam, S. Y., Ricles, L. M., Suggs, L. J. & Emelianov, S. Y. Imaging strategies for tissue engineering applications. *Tissue engineering. Part B, Reviews*, 21, 1, 2015, 88-102.

[227] Chiu, Y. C., Brey, E. M. & Perez-Luna, V. H. A study of the intrinsic autofluorescence of poly (ethylene glycol)-co-(L-lactic acid) diacrylate. *Journal of fluorescence*, 22, 3, 2012, 907-913.

[228] Mandal, B. B. & Kundu, S. C. Cell proliferation and migration in silk fibroin 3D scaffolds. *Biomaterials*, 30, 15, 2009, 2956-2965.

[229] Lei, Y., Gojgini, S., Lam, J. & Segura, T. The spreading, migration and proliferation of mouse mesenchymal stem cells cultured inside hyaluronic acid hydrogels. *Biomaterials*, 32, 1, 2011, 39-47.

[230] Peyton, S. R. *et al.* Marrow-derived stem cell motility in 3D synthetic scaffold is governed by geometry along with adhesivity and stiffness. *Biotechnology and bioengineering*, 108, 5, 2011, 1181-1193.

[231] Schultz, K. M., Kyburz, K. A. & Anseth, K. S. Measuring dynamic cell-material interactions and remodeling during 3D human mesenchymal stem cell migration in hydrogels. *Proceedings of the National Academy of Sciences of the United States of America*, 112, 29, 2015, E3757-3764.

[232] Cartmell, S., Huynh, K., Lin, A., Nagaraja, S. & Guldberg, R. Quantitative microcomputed tomography analysis of mineralization within three-dimensional scaffolds in vitro. *Journal of biomedical materials research. Part A*, 69, 1, 2004, 97-104.

[233] Komlev, V. S. *et al.* Biodegradation of porous calcium phosphate scaffolds in an ectopic bone formation model studied by X-ray computed microtomograph. *European cells & materials*, 19, 2010, 136-146.

[234] Chatterjee, K. *et al.* The effect of 3D hydrogel scaffold modulus on osteoblast differentiation and mineralization revealed by combinatorial screening. *Biomaterials*, 31, 19, 2010, 5051-5062.

[235] Zhou, J. *et al.* The repair of large segmental bone defects in the rabbit with vascularized tissue engineered bone. *Biomaterials*, 31, 6, 2010, 1171-1179.

[236] Bai, F. *et al.* The correlation between the internal structure and vascularization of controllable porous bioceramic materials in vivo: a quantitative study. *Tissue engineering. Part A*, 16, 12, 2010, 3791-3803.

[237] Mertsching, H., Walles, T., Hofmann, M., Schanz, J. & Knapp, W. H. Engineering of a vascularized scaffold for artificial tissue and organ generation. *Biomaterials*, 26, 33, 2005, 6610-6617.

[238] Walles, T. *et al.* Experimental generation of a tissue-engineered functional and vascularized trachea. *The Journal of thoracic and cardiovascular surgery*, 128, 6, 2004, 900-906.

[239] Hwang do, W. *et al.* Real-time in vivo monitoring of viable stem cells implanted on biocompatible scaffolds. *European journal of nuclear medicine and molecular imaging*, 35, 10, 2008, 1887-1898.

[240] Ramaswamy, S. *et al.* Magnetic resonance imaging of chondrocytes labeled with superparamagnetic iron oxide nanoparticles in tissue-engineered cartilage. *Tissue engineering. Part A*, 15, 12, 2009, 3899-3910.

[241] Poirier-Quinot, M. *et al.* High-resolution 1.5-Tesla magnetic resonance imaging for tissue-engineered constructs: a noninvasive tool to assess three-dimensional scaffold architecture and cell seeding. *Tissue engineering. Part C, Methods*, 16, 2, 2010, 185-200.

[242] Nugent, A. E. *et al.* Characterization of ex vivo-generated bovine and human cartilage by immunohistochemical, biochemical, and magnetic resonance imaging analyses. *Tissue engineering. Part A*, 16, 7, 2010, 2183-2196.

[243] Martinez, C., Henao, A., Rodriguez, J. E., Padgett, K. R. & Ramaswamy, S. Monitoring steady flow effects on cell distribution in engineered valve tissues by magnetic resonance imaging. *Molecular imaging*, 12, 7, 2013, 1-13.

[244] Lalande, C. *et al.* Magnetic resonance imaging tracking of human adipose derived stromal cells within three-dimensional scaffolds for bone tissue engineering. *European cells & materials*, 21, 2011, 341-354.

[245] Fite, B. Z. *et al.* Noninvasive multimodal evaluation of bioengineered cartilage constructs combining time-resolved fluorescence and ultrasound imaging. *Tissue engineering. Part C, Methods*, 17, 4, 2011, 495-504.

[246] Sun, Y. *et al.* Nondestructive evaluation of tissue engineered articular cartilage using time-resolved fluorescence spectroscopy and ultrasound backscatter microscopy. *Tissue engineering. Part C, Methods*, 18, 3, 2012, 215-226.

[247] Rice, M. A., Waters, K. R. & Anseth, K. S. Ultrasound monitoring of cartilaginous matrix evolution in degradable PEG hydrogels. *Acta biomaterialia*, 5, 1, 2009, 152-161.

[248] Kim, K., Jeong, C. G. & Hollister, S. J. Non-invasive monitoring of tissue scaffold degradation using ultrasound elasticity imaging. *Acta biomaterialia*, 4, 4, 2008, 783-790.

[249] Vilalta, M. *et al.* Dual luciferase labelling for non-invasive bioluminescence imaging of mesenchymal stromal cell chondrogenic differentiation in demineralized bone matrix scaffolds. *Biomaterials*, 30, 28, 2009, 4986-4995.

[250] Geuze, R. E. *et al.* Luciferase labeling for multipotent stromal cell tracking in spinal fusion versus ectopic bone tissue engineering in mice and rats. *Tissue engineering. Part A*, 16, 11, 2010, 3343-3351.

[251] Liu, J. *et al.* In vitro and in vivo bioluminescent imaging of hypoxia in tissue-engineered grafts. *Tissue engineering. Part C, Methods*, 16, 3, 2010, 479-485.

[252] Cresce, A., Dandu, R., Burger, A., Cappello, J. & Ghandehari, H. Characterization and real-time imaging of gene expression of adenovirus embedded silk-elastinlike protein polymer hydrogels. *Molecular pharmaceutics*, 5, 5, 2008, 891-897.

[253] Bago, J. R. *et al.* In vivo bioluminescence imaging of cell differentiation in biomaterials: a platform for scaffold development. *Tissue engineering. Part A*, 19, 5-6, 2013, 593-603.

[254] Zhang, Y. *et al.* Chronic label-free volumetric photoacoustic microscopy of melanoma cells in three-dimensional porous scaffolds. *Biomaterials*, 31, 33, 2010, 8651-8658.

[255] Pan, D. *et al.* Molecular photoacoustic imaging of angiogenesis with integrin-targeted gold nanobeacons. *FASEB journal : official publication of the Federation of American Societies for Experimental Biology*, 25, 3, 2011, 875-882.

[256] Nam, S. Y., Ricles, L. M., Suggs, L. J. & Emelianov, S. Y. In vivo ultrasound and photoacoustic monitoring of mesenchymal stem cells labeled with gold nanotracers. *PloS one*, 7, 5, 2012, e37267.

[257] Cai, X., Paratala, B. S., Hu, S., Sitharaman, B. & Wang, L. V. Multiscale photoacoustic microscopy of single-walled carbon nanotube-incorporated tissue engineering scaffolds. *Tissue engineering. Part C, Methods*, 18, 4, 2012, 310-317.

[258] Zhang, Y. *et al.* Noninvasive photoacoustic microscopy of living cells in two and three dimensions through enhancement by a metabolite dye. *Angewandte Chemie*, 50, 32, 2011, 7359-7363.

[259] Yang, Y. *et al.* Investigation of optical coherence tomography as an imaging modality in tissue engineering. *Physics in medicine and biology*, 51, 7, 2006, 1649-1659.

[260] Xu, X., Wang, R. K. & El Haj, A. Investigation of changes in optical attenuation of bone and neuronal cells in organ culture or three-dimensional constructs in vitro with optical coherence tomography: relevance to cytochrome oxidase monitoring. *European biophysics journal : EBJ*, 32, 4, 2003, 355-362.

[261] Tan, W., Oldenburg, A. L., Norman, J. J., Desai, T. A. & Boppart, S. A. Optical coherence tomography of cell dynamics in three-dimensional tissue models. *Optics express*, 14, 16, 2006, 7159-7171.

[262] Chen, C. W., Betz, M. W., Fisher, J. P., Paek, A. & Chen, Y. Macroporous hydrogel scaffolds and their characterization by optical coherence tomography. *Tissue engineering. Part C, Methods*, 17, 1, 2011, 101-112.

[263] Teo, G. S., Yang, Z., Carman, C. V., Karp, J. M. & Lin, C. P. Intravital imaging of mesenchymal stem cell trafficking and association with platelets and neutrophils. *Stem cells*, 33, 1, 2015, 265-277.

[264] Saha, S., Kirkham, J., Wood, D., Curran, S. & Yang, X. B. Informing future cartilage repair strategies: a comparative study of three different human cell types for cartilage tissue engineering. *Cell Tissue Res*, 352, 3, 2013, 495-507.

[265] Hearnden, V. *et al.* Diffusion studies of nanometer polymersomes across tissue engineered human oral mucosa. *Pharmaceutical research*, 26, 7, 2009, 1718-1728.

[266] Raicevic, G. *et al.* Inflammation modifies the pattern and the function of Toll-like receptors expressed by human mesenchymal stromal cells. *Human immunology*, 71, 3, 2010, 235-244.

[267] Matzinger, P. The danger model: a renewed sense of self. *Science*, 296, 5566, 2002, 301-305.

[268] Bernardo, M. E. & Fibbe, W. E. Mesenchymal stromal cells: sensors and switchers of inflammation. *Cell stem cell*, 13, 4, 2013, 392-402.

[269] Tomchuck, S. L. *et al.* Toll-like receptors on human mesenchymal stem cells drive their migration and immunomodulating responses. *Stem cells*, 26, 1, 2008, 99-107.

[270] van den Akker, F., de Jager, S. C. & Sluijter, J. P. Mesenchymal stem cell therapy for cardiac inflammation: immunomodulatory properties and the influence of toll-like receptors. *Mediators of inflammation*, 2013, 2013, 181020.

[271] Spaggiari, G. M., Abdelrazik, H., Becchetti, F. & Moretta, L. MSCs inhibit monocyte-derived DC maturation and function by selectively interfering with the generation of immature DCs: central role of MSC-derived prostaglandin E2. *Blood*, 113, 26, 2009, 6576-6583.

[272] Selmani, Z. *et al.* Human leukocyte antigen-G5 secretion by human mesenchymal stem cells is required to suppress T lymphocyte and natural killer function and to induce CD4+CD25highFOXP3+ regulatory T cells. *Stem cells*, 26, 1, 2008, 212-222.

[273] Nemeth, K. *et al.* Bone marrow stromal cells attenuate sepsis via prostaglandin E(2)-dependent reprogramming of host macrophages to increase their interleukin-10 production. *Nature medicine*, 15, 1, 2009, 42-49.

[274] Hall, S. R. *et al.* Mesenchymal stromal cells improve survival during sepsis in the absence of heme oxygenase-1: the importance of neutrophils. *Stem cells*, 31, 2, 2013, 397-407.

[275] Mo, I. F. *et al.* Prolonged exposure to bacterial toxins downregulated expression of toll-like receptors in mesenchymal stromal cell-derived osteoprogenitors. *BMC cell biology*, 9, 2008, 52.

[276] Mirotsou, M., Jayawardena, T. M., Schmeckpeper, J., Gnecchi, M. & Dzau, V. J. Paracrine mechanisms of stem cell reparative and regenerative actions in the heart. *Journal of molecular and cellular cardiology*, 50, 2, 2011, 280-289.

[277] Gnecchi, M. *et al.* Evidence supporting paracrine hypothesis for Akt-modified mesenchymal stem cell-mediated cardiac protection and functional improvement. *FASEB journal : official publication of the Federation of American Societies for Experimental Biology*, 20, 6, 2006, 661-669.

[278] Hung, S. C., Pochampally, R. R., Chen, S. C., Hsu, S. C. & Prockop, D. J. Angiogenic effects of human multipotent stromal cell conditioned medium activate the PI3K-Akt pathway in hypoxic endothelial cells to inhibit apoptosis, increase survival, and stimulate angiogenesis. *Stem cells*, 25, 9, 2007, 2363-2370.

[279] Rehman, J. *et al.* Secretion of angiogenic and antiapoptotic factors by human adipose stromal cells. *Circulation*, 109, 10, 2004, 1292-1298.

[280] Swartzlander, M. D. *et al.* Immunomodulation by mesenchymal stem cells combats the foreign body response to cell-laden synthetic hydrogels. *Biomaterials*, 41, 2015, 79-88.

[281] Hanson, S., D'Souza, R. N. & Hematti, P. Biomaterial-mesenchymal stem cell constructs for immunomodulation in composite tissue engineering. *Tissue engineering. Part A*, 20, 15-16, 2014, 2162-2168.

[282] Wang, J. *et al.* Inhibition of hepatic stellate cells proliferation by mesenchymal stem cells and the possible mechanisms. *Hepatology research : the official journal of the Japan Society of Hepatology*, 39, 12, 2009, 1219-1228.

[283] Berardis, S., Dwisthi Sattwika, P., Najimi, M. & Sokal, E. M. Use of mesenchymal stem cells to treat liver fibrosis: current situation and future prospects. *World journal of gastroenterology*, 21, 3, 2015, 742-758.

[284] Ortiz, L. A. *et al.* Mesenchymal stem cell engraftment in lung is enhanced in response to bleomycin exposure and ameliorates its fibrotic effects. *Proceedings of the National Academy of Sciences of the United States of America*, 100, 14, 2003, 8407-8411.

[285] Meier, R. P. *et al.* Microencapsulated human mesenchymal stem cells decrease liver fibrosis in mice. *Journal of hepatology*, 62, 3, 2015, 634-641.

[286] Duffield, J. S., Lupher, M., Thannickal, V. J. & Wynn, T. A. Host responses in tissue repair and fibrosis. *Annual review of pathology*, 8, 2013, 241-276.

[287] Van Linthout, S., Miteva, K. & Tschope, C. Crosstalk between fibroblasts and inflammatory cells. *Cardiovascular research*, 102, 2, 2014, 258-269.

[288] Shinde, A. V. & Frangogiannis, N. G. Fibroblasts in myocardial infarction: a role in inflammation and repair. *Journal of molecular and cellular cardiology*, 70, 2014, 74-82.

[289] Lukacs, N. W. *et al.* Stimulus and cell-specific expression of C-X-C and C-C chemokines by pulmonary stromal cell populations. *The American journal of physiology*, 268, 5 Pt 1, 1995, L856-861.

[290] Braga, T. T., Agudelo, J. S. & Camara, N. O. Macrophages During the Fibrotic Process: M2 as Friend and Foe. *Frontiers in immunology*, 6, 2015, 602.

[291] Appel, A. A., Anastasio, M. A., Larson, J. C. & Brey, E. M. Imaging challenges in biomaterials and tissue engineering. *Biomaterials*, 34, 28, 2013, 6615-6630.

[292] Thevenot, P. T., Baker, D. W., Weng, H., Sun, M. W. & Tang, L. The pivotal role of fibrocytes and mast cells in mediating fibrotic reactions to biomaterials. *Biomaterials*, 32, 33, 2011, 8394-8403.

CHAPTER 2

“DA NOSSA SEMELHANÇA COM OS DEUSES

Da nossa semelhança com os deuses
Por nosso bem tiremos
Julgarmo-nos deidades exiladas
E possuindo a Vida
Por uma autoridade primitiva
E coeva de Jove.

Altivamente donos de nós-mesmos,
Usemos a existência
Como a vila que os deuses nos concedem
Para esquecer o Estio.

Não de outra forma mais apoquentada
Nos vale o esforço usarmos
A existência indecisa e afluente
Fatal do rio escuro.

Como acima dos deuses o Destino
É calmo e inexorável,
Acima de nós-mesmos construamos
Um fado voluntário
Que quando nos oprima nós sejamos
Esse que nos oprime,
E quando entremos pela noite dentro
Por nosso pé entremos.”

30-7-1914
Odes de Ricardo Reis . Fernando Pessoa. Lisboa: Ática, 1946 (imp.1994). - 40.

The contents of this chapter are based on:

FINDING AND TRACING HUMAN MSC IN 3D MICROENVIRONMENTS WITH THE PHOTOCONVERTIBLE PROTEIN DENDRA2

Hugo R. Caires [1,2,3]
Maria Gómez-Lázaro [2,3,4]
Carla Oliveira [2,3,5]
David Gomes [2,3]
Denise D. Mateus [2,6]
Carla Oliveira [2,6,7]
Cristina C. Barrias [2,3]
Mário A. Barbosa [1,2,3]
Catarina R. Almeida [2,3]

[1] ICBAS - Instituto de Ciências Biomédicas Abel Salazar, Universidade do Porto, Rua Jorge Viterbo Ferreira, 228, 4050-313 Porto, Portugal

[2] i3S - Instituto de Investigação e Inovação em Saúde da Universidade do Porto, Rua Alfredo Allen, 208, 4200-135 Porto, Portugal Portugal

[3] INEB - Instituto de Engenharia Biomédica, Porto, Portugal

[4] b.IMAGE - Bioimaging Center for Biomaterials and Regenerative Therapies

[5] ISPUP - Instituto de Saúde Pública da Universidade do Porto, Rua das Taipas, 135, 4050-600 Porto, Portugal.

[6]IPATIMUP - Instituto de Patologia e Imunologia Molecular da Universidade do Porto, Rua Dr. Roberto Frias s/n,4200-465 Porto, Portugal

[7]Medical Faculty of the University of Porto, Alameda Hernani Monteiro, 4200-319 Porto, Portugal

SCIENTIFIC REPORTS 5, 10079 (2015)

2.1 Abstract

Mesenchymal Stem/Stromal Cells (MSC) are a promising cell type for cell-based therapies - from tissue regeneration to treatment of autoimmune diseases - due to their capacity to migrate to damaged tissues, to differentiate in different lineages and to their immunomodulatory and paracrine properties. Here, a simple and reliable imaging technique was developed to study MSC dynamical behaviour in natural and bioengineered 3D matrices. Human MSC were transfected to express a fluorescent photoswitchable protein, Dendra2, which was used to stably highlight and follow the same group of cells for more than seven days, even if removed from the microscope to the incubator. This strategy provided reliable tracking in 3D microenvironments with different properties, including the hydrogels Matrigel and alginate as well as chitosan porous scaffolds. Comparison of cells motility within matrices with tuned physicochemical properties revealed that MSC embedded in Matrigel migrated 64% more with 5.2 mg protein/mL than with 9.6 mg/mL and that MSC embedded in RGD-alginate migrated 51% faster with 1% polymer concentration than in 2% RGD-alginate. This platform thus provides a straightforward approach to characterize MSC dynamics in 3D and has applications in the field of stem cell biology and for the development of biomaterials for tissue regeneration.

Keywords: Matrigel; RGD-Alginate; Chitosan; Dendra2; 3D imaging; Human MSC

2.2 Introduction

MSC are an attractive cell source for regenerative cell-based therapies due to its well established multipotency, immunomodulatory and paracrine properties, combined with their ability to migrate into damaged tissues. Most strategies being currently explored involve either stem cell transplantation to patients[1], implantation of the triad scaffolds/stem cells/growth factors[2,3], or the use of materials that stimulate endogenous stem cell recruitment[4]. Regardless of the approach, to improve the effectiveness of such applications it is critical to understand the determinants of stem cell migration in 3D microenvironments.

Despite the worldwide effort to modulate and direct stem cell fate for tissue regeneration, the influence of 3D extracellular matrix (ECM) features on MSC motility still remains largely unknown. A tool to longitudinally follow MSC in 3D is essential to better understand cell migration and organization in 3D microenvironments. To this end, a number of cell labelling techniques have been developed. Some studies have suggested that cell transfection with fluorescent proteins[5-7] will be required for long term cell tracking and others are pursuing magnetic nanoparticles[8], bioluminescent probes[9-11], quantum dots[12,13] and radioactive isotope alternatives[14] for stem cell labelling.

Most of these bioimaging techniques are well established but are more oriented to localize the final homing site of transplanted cells or to roughly quantify cell survival after implantation, being rather limited for studying the effect of cell-ECM interactions on MSC dynamical behaviour. There are some reports on the use of fluorescent proteins or dyes to track stem cells, but most use labelling in order to find the cells at one fixed time point and not to follow them by time-lapse analysis[6,15]. As MSC are slowly moving cells when in 3D, tracing the same cells through time requires imaging performed for several days and it is usually not feasible to keep the cells under the microscope for long periods. Apart from unpractical to perform continuous 3D live cell imaging for more than a day, the increased probability of photo-damaging cells or photobleach the fluorophore over time is often the limiting factor. When imaging cells at discrete daily intervals, it is extremely difficult to find exactly the same cells that were being imaged[16]. Thus, studies aiming to compare the dynamic MSC behaviour within distinct 3D microenvironments would benefit from new bioimaging tools that allow finding and tracing the same cells over long periods of time.

A class of fluorescent proteins that can change irreversibly the emission fluorescence spectrum upon laser excitation offers a promising and flexible opportunity for solving this problem[17,18]. With these fluorescent photoconvertible proteins, it is possible to create a

reference by selecting and photo-marking cells of interest in precisely defined positions, which will then be easier to track with no mistaken identity issues. It has been shown that photoswitchable or photoconvertible proteins can indeed be applied to accurately track a discrete sub-population of tumor cells even with imaging sessions spaced over days[19,20]. Dendra2 is such a photoswitchable protein, with a fluorescence spectrum similar to Green Fluorescent Protein (GFP), but that upon exposure to blue light (e.g., 405 nm) suffers an irreversible shift to red (>150 nm). Dendra2 is highly photostable after switching to its red form, and some of the advantages compared with other photoswitchable proteins are: its predominant monomeric form (generating less aggregates than tetrameric proteins); the fact that it forms a completely functional chromophore at 37ºC, and its great brightness in relation to other photoconvertible proteins[21,22].

Here, Dendra2+ human bone marrow MSC were generated and characterized, and the influence of optimized photoconversion on MSC properties was analyzed. Finally, the feasibility and flexibility of Dendra2 imaging to quantify MSC dynamics in distinct 3D environments was verified. A tool to investigate and compare the dynamical behaviour of MSC in bioengineered materials was thus developed.

2.3 Results

2.3.1 Transfection of human MSC to express the photoswitchable protein Dendra2

To follow living MSC in 3D for long periods of time it is vital to develop a strategy that allows imaging of the same cells at different time-points. Here, human bone marrow MSC were transfected to express a photoswitchable fluorescent protein, Dendra2, which enables green-to-red photo-conversion of labelled MSC, and subsequently highlighting and tracking the same group of cells over long time periods. Transfection of MSC by electroporation yielded more than 80% of cells expressing Dendra2 protein, with most cells expressing high levels of this fluorescent protein (Figure 1a, b). Transfection with the pDendra2 plasmid did not affect cell number or metabolic activity of MSC, which remained constant for up to eight days, when comparing with cells electroporated in the absence of a plasmid. However, electroporation in itself affected the kinetics of both the cell number and metabolism (Figure 1c, d). Importantly, almost 70% of the transfected cell population still expressed Dendra2 ten days after transfection (Figure 1e, f). Additionally, MSC morphology was not affected by transfection; transfected MSC started to exhibit an elongated spindle shape after ten days due to extended cell culture time (Figure 1f).

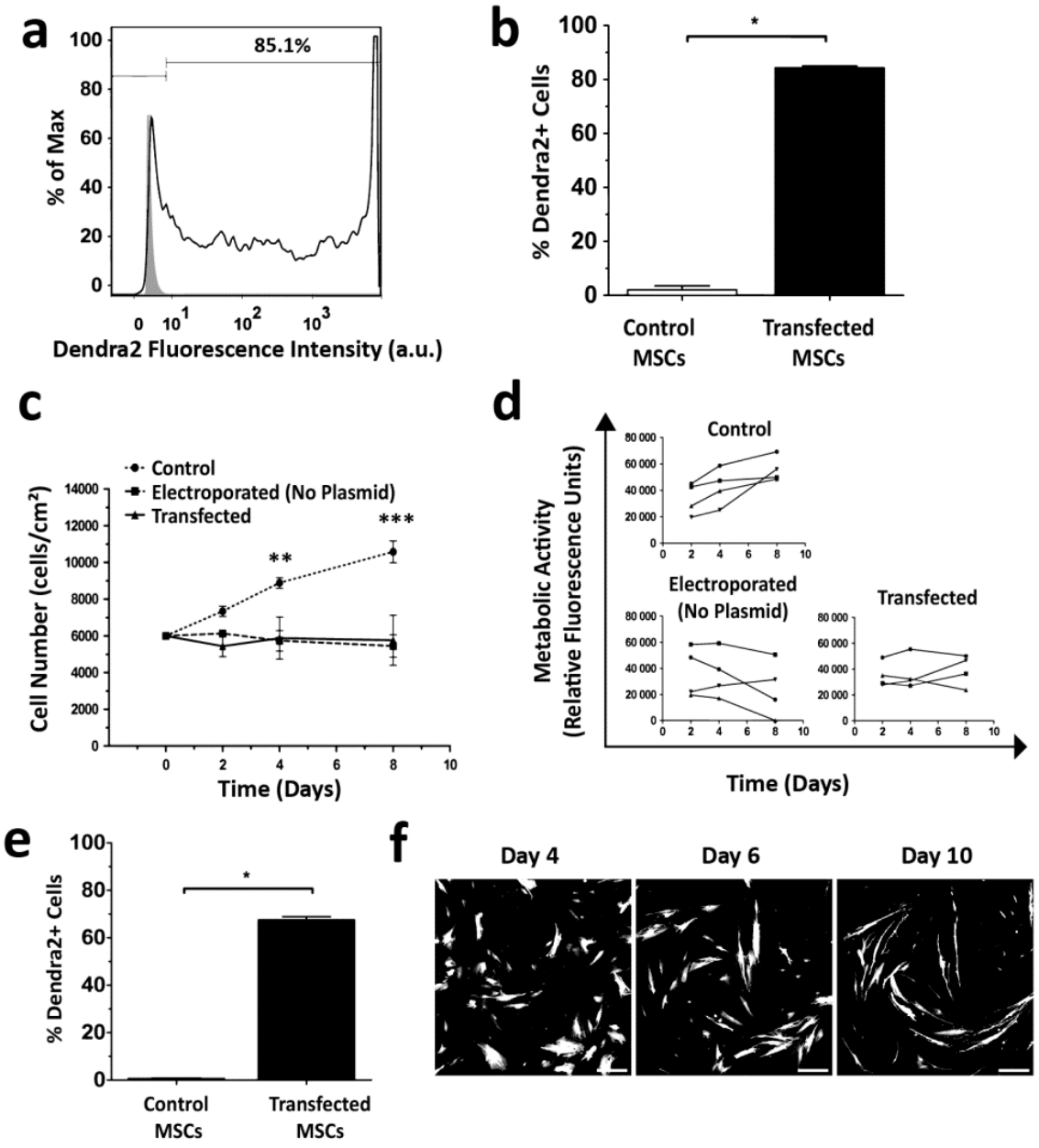

Figure 1. Transfection of human MSC to express Dendra2. (a) Flow cytometry histogram showing the fluorescence intensity of control (grey, filled) and transfected (open) MSC two days after electroporation. Data is representative of 3 experiments. (b) The percentage of Dendra2+ MSC upon electroporation was measured by flow cytometry. Graphs show mean ± SEM of three experiments.*, $p > 0.05$ by Mann-Whitney test. (c) Growth curve of MSC over a period of 8 days after an initial seeding of 6,000 cells/cm^2. Number of cells was determined by trypan blue exclusion. Graph shows mean ± SEM of three experiments. **, $p > 0.01$ and ***, $p > 0.001$ by two-way ANOVA with Bonferroni post-test for comparison with control group. (d) Relative fluorescence unit (RFU) as a measure of metabolic activity determined by resazurin assays. Graph shows mean ± SEM of four experiments. Differences are not statistically significant, two-way ANOVA with

Bonferroni post-test for comparison with control group. (e) The percentage of Dendra2+ cells was determined 10 days after transfection by flow cytometry. Graphs show mean ± SEM of three experiments.*, $p > 0.05$ by Mann-Whitney test. (f) Fluorescence microscopy images of transfected cells 4, 6 and 10 days after electroporation. Scale bar, 250 μm.

2.3.2 Characterization of Dendra2+ MSC

In order to analyze whether Dendra2 expression affected MSC properties, we firstly analyzed the expression profile of MSC-related cell surface antigens. MSC were electroporated to obtain a mixed population with Dendra2 positive and negative cells, to correlate with expression of the surface markers. Importantly, neither electroporation nor Dendra2 expression influenced surface marker expression, with more than 90-95% of cells being positive for CD73, CD90 and CD105 and negative for CD14, CD19, CD34, CD45, HLA-DR (Figure 2a).

To test whether Dendra2 transfection affects MSC differentiation capacity, control and transfected cells were induced into osteogenic and adipogenic differentiation. Both transfected and control cells were able to differentiate when cultured under osteogenic or adipogenic stimuli but not under basal condition, as detected by Alkaline Phosphatase activity (ALP), von Kossa and oil red O stainings (Supplementary Figure S1a, b). Furthermore, both Dendra2+ and Dendra2- MSC could be visualized by fluorescence microscopy to express ALP and stain with oil red O under the appropriate stimuli (Supplementary Figure S1c). Moreover, the percentage of ALP+ MSC increased after culture with osteogenic stimuli for 7 days both on Dendra2+ and Dendra2- cells (Figure 2b, c). Thus, Dendra2 expression did not interfere with either MSC surface marker expression nor MSC differentiation capacity.

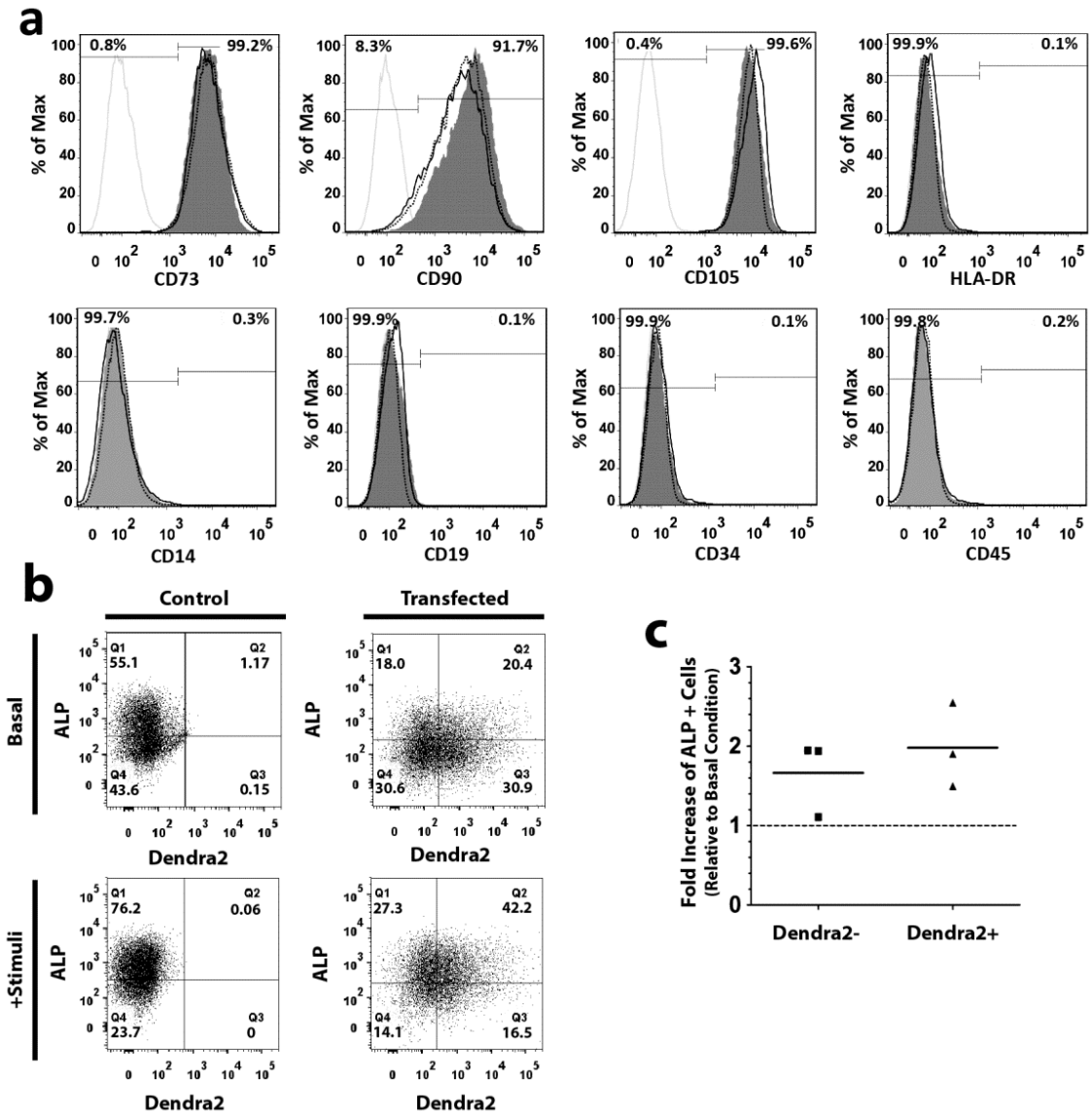

Figure 2. Dendra2 expression does not interfere with MSC properties. (a) Flow cytometry histograms showing expression of CD14, CD19, CD34, CD45, HLA-DR, CD73, CD90 and CD105 by control (grey filled) and transfected (Dendra2+, solid line; Dendra2-, dashed line). Isotype control is displayed as the grey line. Numbers indicate the percentage of cells in each gate for the Dendra2+ cells. Figure is representative of three experiments. (b) Representative flow cytometry dot plots showing ALP surface staining on control or transfected MSC cultured under basal or osteogenic medium for 7 days (n=3). (c) Fold increase of the percentage of ALP+ cells in Dendra2+ and Dendra2- MSC cultured in osteogenic conditions for 7 days, in relation to cells cultured in basal medium (n=3). Each dot represents data from one experiment and bars represent the mean. Differences are not statistically significant, Friedman test with Dunns post-test comparison.

2.3.3 Efficient Photoswitching of Dendra2 protein expressed by MSC

Maximized photoconversion efficiency should result in enhanced signal-to-noise ratio of photo-marked MSC and therefore in improved imaging quality and extended tracking time. Excitation at 488 nm with high power could lead to photoconversion but using a 405 nm laser was much more efficient. Hence, parameters were optimized for efficient photoconversion with a 405 nm laser in a region of interest (ROI), without complete fluorescence bleaching and without photoconverting nearby cells (Figure 3a, b). To determine the optimal conditions for Dendra2 green-to-red photoconversion, we incrementally increased laser power and tested different numbers of iterations (Figure 3c). Laser power below 15% was insufficient for noticeable photoconversion. Efficient photoconversion was achieved using 60-70% of laser power with 60 iterations, which allowed obtaining an intense red signal to track MSC for an extended time (Figure 3d). UV irradiation with these optimized settings did not affect cells metabolic activity, indicating that it was not cytotoxic (Figure 3e). Photoconversion could also be achieved at the subcellular level (Supplementary Figure S2).

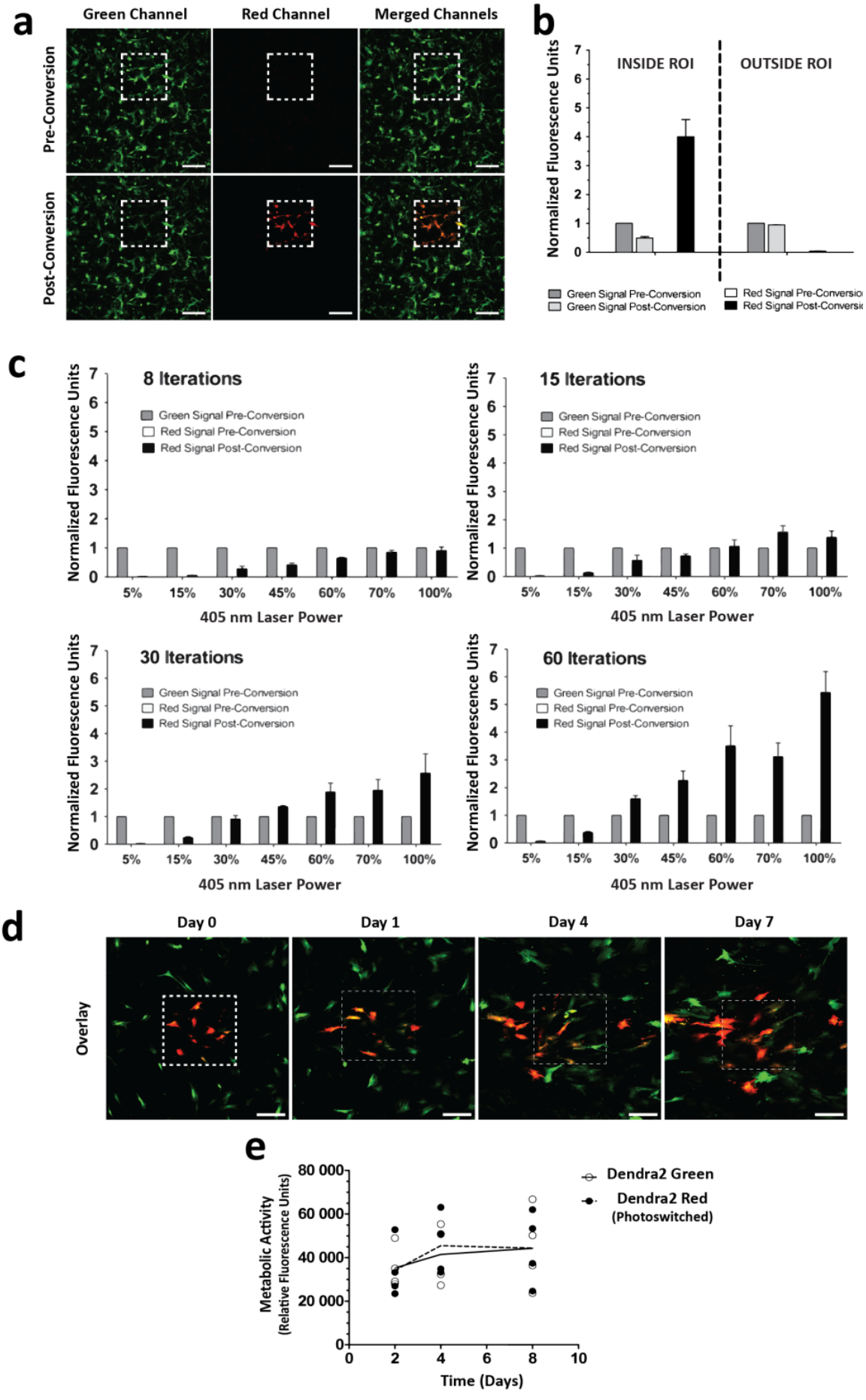
a
Green Channel
Red Channel
Merged Channels
Pre-Conversion
Post-Conversion
b
INSIDE ROI
OUTSIDE ROI
Normalized Fluorescence Units
Green Signal Pre-Conversion
Green Signal Post-Conversion
Red Signal Pre-Conversion
Red Signal Post-Conversion
c
8 Iterations
15 Iterations
30 Iterations
60 Iterations
Normalized Fluorescence Units
Green Signal Pre-Conversion
Red Signal Pre-Conversion
Red Signal Post-Conversion
5%
15%
30%
45%
60%
70%
100%
405 nm Laser Power
d
Day 0
Day 1
Day 4
Day 7
Overlay
e
Metabolic Activity
(Relative Fluorescence Units)
80 000
60 000
40 000
20 000
0
0
2
4
6
8
10
Time (Days)
Dendra2 Green
Dendra2 Red
(Photoswitched)

Figure 3. Photoswitching Dendra2 protein expressed by MSC. (a) Confocal microscopy images in green, red and merged channels of Dendra2+ MSC taken before (top) and after (bottom) irradiation with a 405 nm laser. Photoconversion was achieved by laser irradiation of a square region of interest (ROI) targeting a selected cell population (dashed line). Scale bar, 250 µm. (b) Green-to-red conversion did not induce photoconversion of cells located outside the defined ROI. Fluorescence intensity in each channel was measured and normalized relatively to the fluorescence intensity in the green channel before conversion. (c) The laser power and number of iterations affected photoconversion efficiency of Dendra2 on MSC. (b) and (c) Mean ± SEM of normalized fluorescence units (n=3 experiments, 3 cells analyzed in each). (d) Confocal microscopy images (merged green and red channels) of Dendra2 expressing MSC taken after irradiation. Green-to-red conversion for a selected group of cells was achieved at time-point zero and used to track this group of cells for 7 days after conversion. Scale bar, 250 µm. (e) Relative fluorescence units (RFU) as a measure of metabolic activity of Dendra2 Green and Dendra2 Red MSC, determined 2, 4 and 8 days after an initial seeding of 6,000 cells/cm^2. Photoconversion was performed at day 2. Each dot represents data of one individual experiment, lines represent the mean. Differences are not statistically significant, two-way ANOVA with Bonferroni post-test.

2.3.4 Migration of Dendra2+ MSC in 2D

To examine the ability of Dendra2+ MSC to migrate, time-lapse microscopy of an *in vitro* wound healing assay was performed (Figure 4). MSC migrated using lamellipodia mode with visible cell extensions and rear body retraction. Cells motility was oriented towards the centre of the wound with a similar directness index for all groups (Figure 4b). However, the velocity of MSC showed some differences: control cells migrated at 0.33 ± 0.15 µm/min, electroporated cells without pDNA at 0.35 ± 0.16 µm/min, transfected green cells at 0.23 ± 0.09 µm/min and photoswitched red cells at 0.20 ± 0.07 µm/min (Figure 4c). Therefore, even though transfected cells moved slightly slower than control cells, photoswitching did not interfere with the cells velocity.

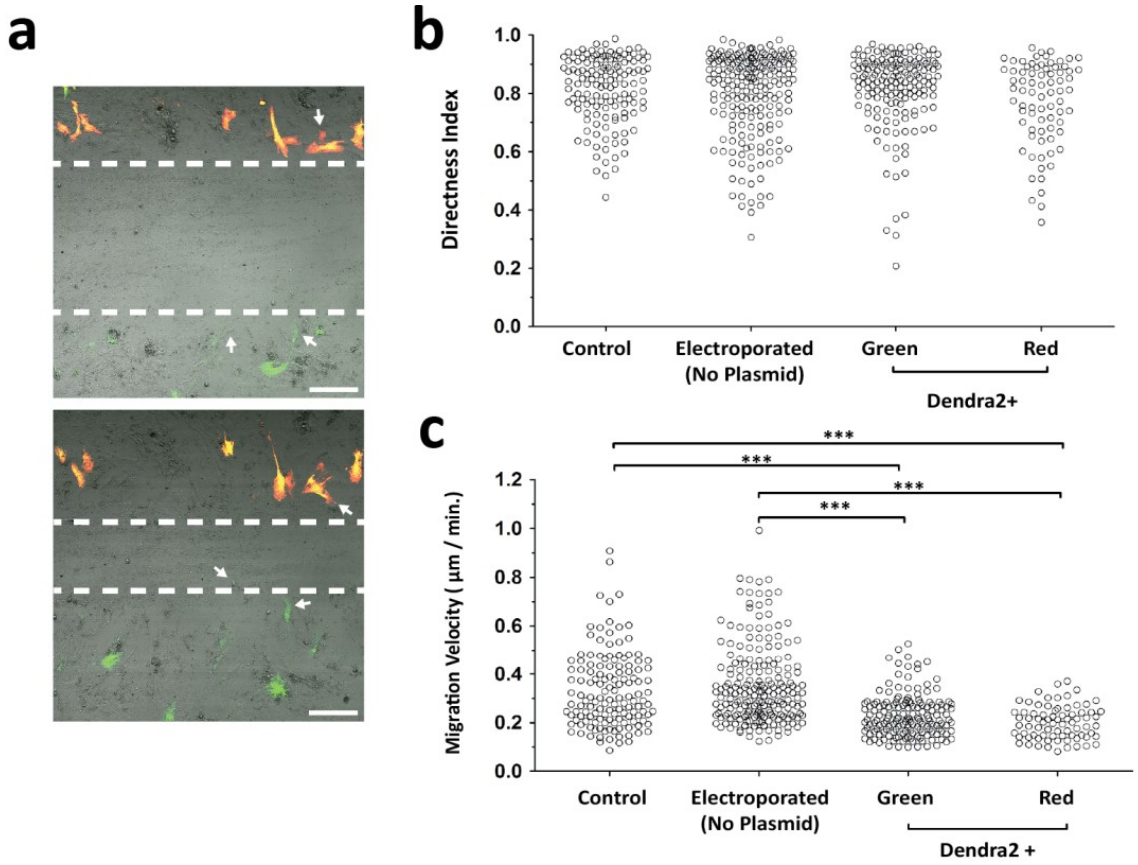

Figure 4. Migration of Dendra2+ MSC in 2D. (a) Representative images of *in vitro* wound healing time-lapse microscopy at time-points 0 (top) and 16.5 hrs (bottom) post wound. Dashed lines represent the migrating front and arrows show Dendra2-, Dendra2+ Green and Dendra2+ Red cells. Scale bar, 250 µm. (b) Directness index and (c) migration velocity were determined for Control, Electroporated (without plasmid), Dendra2 Green and Red single cells (n=4). Only cells initially at the migrating front were analyzed. ***, p > 0.001, linear mixed model.

2.3.5 Tracking Migration of MSC in different 3D matrices

To assess the feasibility of this tool to analyze MSC dynamics in 3D, experiments were performed in microenvironments with distinct properties, including the hydrogels Matrigel and alginate as well as chitosan porous scaffolds. Transfected MSC were embedded in the hydrogels or seeded on top of chitosan scaffolds and tracked for up to seven days. It was possible to photoconvert cells, enabling finding and imaging the same cells at discrete daily intervals, after placing them in the 37ºC/CO_2 incubator instead of leaving them for 7 days under the microscope. Thus it was possible to trace photoconverted cells over extended periods of cell culture, and to compare MSC motility in different matrices (Figure 5). Labelling cells with a fluorescent protein such as GFP would not allow tracing

the same cells over these long periods of time, as evident when cells were imaged only at the green channel (Supplementary Figure S3). Approximately 400-500 μm in depth were effectively imaged for Matrigel and RGD-alginate hydrogels and approximately 100 μm for chitosan scaffolds due to lower light penetration properties of the later. To avoid any inaccuracy related with photoconversion in stiffer/opaque materials, which may derive from laser scattering, data was normalized to the photoconverted area at time-point zero. Unwanted photoconversion due to routine imaging with low power 488 / 561 nm lasers was not observed over the time points imaged.

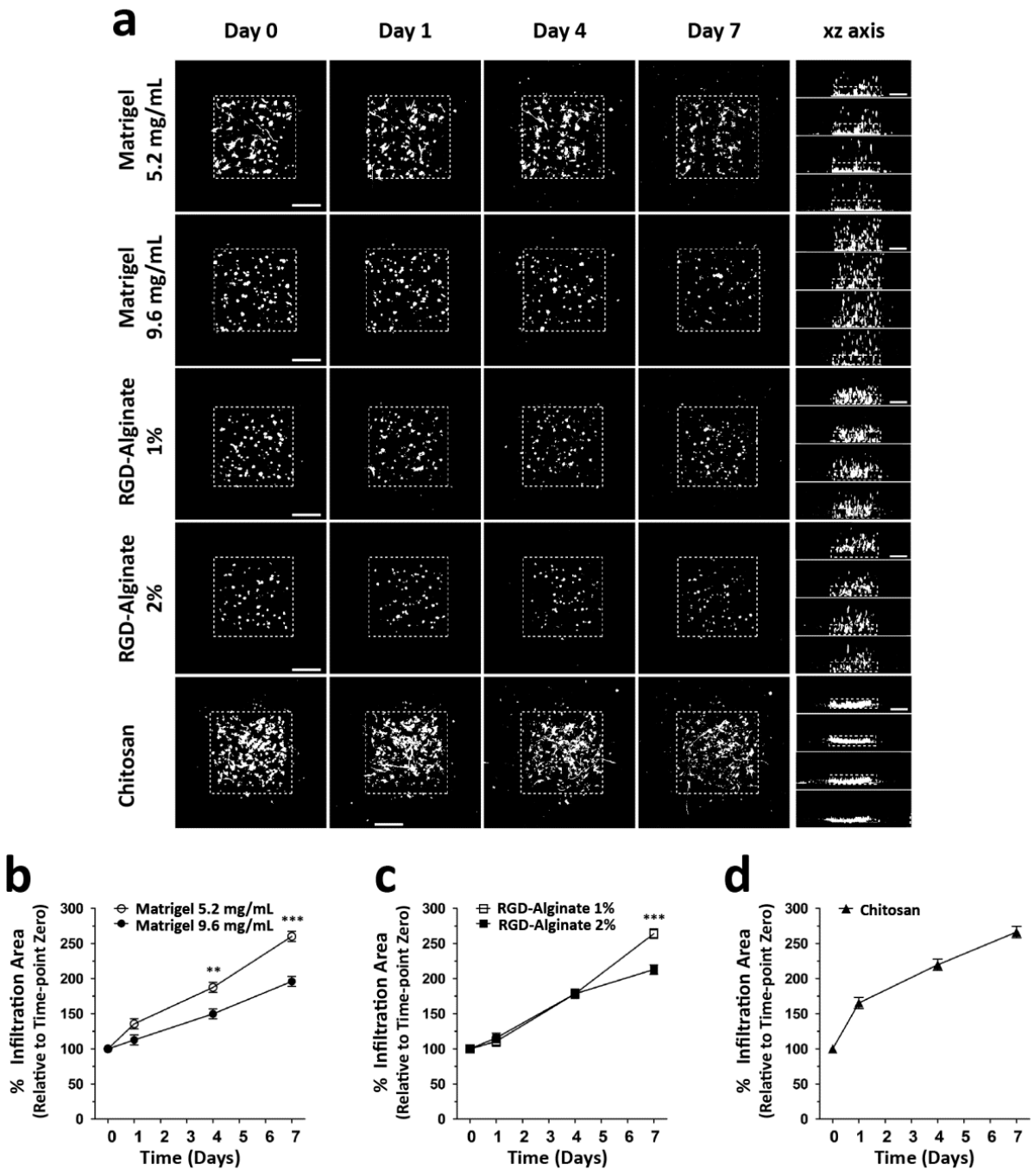

Figure 5. MSC motility in 3D microenvironments. (a) Representative maximum projection images of cells in Matrigel, RGD-alginate and Chitosan matrices obtained over a period of 7 days (first four columns in xy; right column in xz). Cell migration can be determined by the increasing infiltration area over time in maximum projection images. White dotted square line represents the photoconverted area at time-point zero. Scale bar, 250 μm. The infiltration area at time-points 1, 4 and 7 days was normalized to time-point zero, for cells in (b) Matrigel (5.2 or 9.6 mg/mL), (c) RGD-alginate (1% or 2%) hydrogels or in (d) Chitosan scaffolds. **, $p > 0.01$ and ***, $p > 0.001$ by linear mixed model.

This approach could be used to discriminate differences in MSC dynamics in 3D matrices with tuned physicochemical properties. Dendra2+ MSC were embedded in Matrigel with a protein content of 5.2 mg/mL and 9.6 mg/mL or in RGD-alginate at 1% and 2% (wt) polymer concentration. Then, a square region was photoswitched and the population was traced over a period of seven days. In Matrigel, MSC were able to migrate 64% more at 5.2 mg/mL than at 9.6 mg/mL (Figure 5). Moreover, Matrigel 5.2 mg/mL favoured a more elongated morphology than cells embedded in Matrigel 9.6 mg/mL (Figure 6a,d). In RGD-alginate, MSC embedded in a 1% polymer concentration migrated 51% more than in 2% concentration after seven days of incubation (Figure 5c), with more elongated and clustered cells in 1% RGD-alginate (Figure 6b,e). Interestingly, cells seeded in the much different chitosan scaffolds showed an infiltration area similar to Matrigel 5.2 mg/mL and RGD-alginate 1% hydrogels at day 7, even though the increase in infiltration area was higher for early time points. MSC in chitosan scaffolds were the most elongated for all time-points (Figure 6c,f). MSC embedded in Matrigel 9.6 mg/mL, 1% and 2% RGD-alginate but not in Matrigel 5.2 mg/mL or chitosan matrices displayed a statistically significant trend to decrease cell sphericity over time. In summary, Dendra2 photoswitching in MSC allowed analysis of the cells morphology and quantification of MSC motility in different 3D microenvironments.

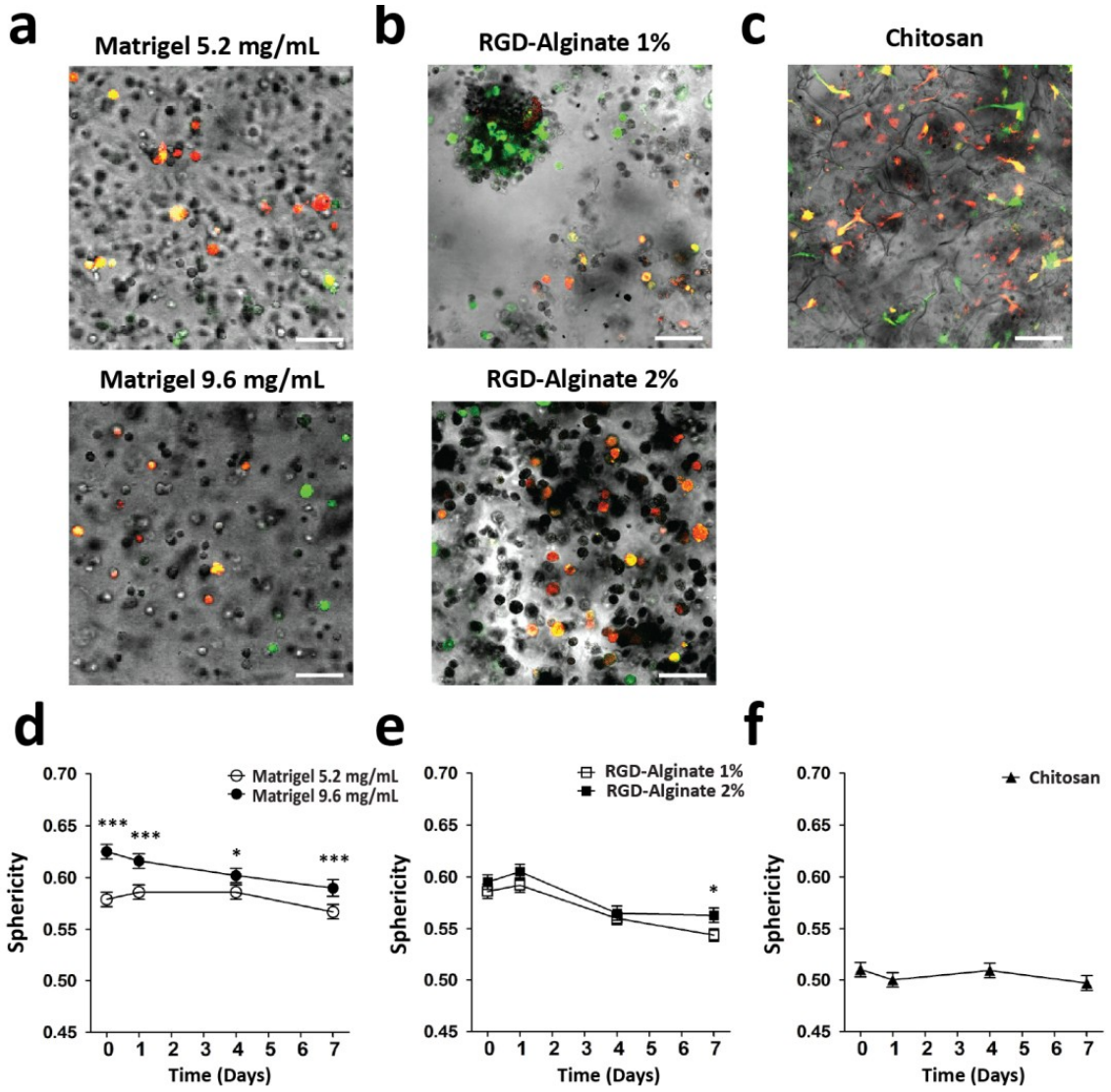

Figure 6. Dendra2+ MSC morphology in 3D microenvironments. Representative merged bright-field and fluorescence images of cells when embedded in (a) Matrigel (5.2 or 9.6 mg/mL), (b) RGD-alginate (1% or 2%) hydrogels or seeded in (c) Chitosan scaffolds at day eight. Scale bar, 100 μm. Cells sphericity for (d) Matrigel, (e) RGD-alginate and (f) Chitosan was determined throughout 7 days. Data are mean ± SEM of more than 150 cells per time point (3 experiments). *, $p > 0.05$ and ***, $p > 0.001$ by linear mixed model.

2.4 Discussion

Here we describe an imaging tool to follow the dynamical behavior of human MSC in complex 3D microenvironments. The idea behind this method is to photo-mark Dendra2+ MSC in precisely defined positions, being then able to follow the same group of cells for long periods of time.

High transfection efficiency with minimal loss of Dendra2 expression after ten days was achieved by electroporation. Analysis of cell number suggests that there is equilibrium between proliferation and cell death in electroporated cells, an effect that was not affected by Dendra2 protein expression. Electroporation in itself (without any plasmid) affected the proliferation of these slowly dividing cells, whose number remained constant over time. However, the metabolic activity of the cells does not show statistically significant differences, indicating that the cells are alive and probably recovering from the electroporation. These data highlights the need that future studies involving Dendra2 transfection, which may be used to study the role of other proteins, also perform these controls. A diminished cell proliferation rate due to electroporation is a limitation of this technology, but at the same time it avoids the problem of signal loss due to fluorescence signal dilution to daughter cells which could limit cell tracking to a couple of days or less depending on the cells proliferation rate[23,24].

Nevertheless, others report that electroporation does not influence cell proliferation, and therefore this effect could be related to MSC donor used. Photo-marked red cells could be clearly distinguished from the green non-converted cells and exhibited a 3-fold increase in red fluorescence. This increase in red fluorescence intensity was coupled with a decrease in green fluorescence intensity, consistent with conversion of both the green and neutral forms of Dendra2 into the red form[21,22,25]. Photoswitching did not lead to diminished metabolic activity, suggesting that it was not cytotoxic. Also, cells could be tracked for at least seven days, indicating that the degradation rate of Dendra2 red form is low. Importantly, photoconversion only targeted cells inside a pre-defined ROI, with minimal photoconversion occurring outside the ROI. Photoswitching did not adversely affect MSC properties, nor the cells migration directionality and velocity. As transfection affected MSC motility, this tool does not allow quantification of the cells speed but it allows the comparison of the dynamic behaviour when cells are subjected to different treatments or microenvironments.

To analyze whether Dendra2 imaging allows detection of changes in MSC dynamics in 3D, we compared MSC migration in Matrigel, RGD-alginate hydrogels and in porous

chitosan scaffolds. Matrigel is a reconstituted basement membrane widely used to study cellular invasion and interactions with the basement membrane. Cells embedded in diluted Matrigel 5.2 mg/mL migrated more than in Matrigel 9.6 mg/mL matrices. Also, cells in diluted Matrigel adopted a more elongated shape, which is usually associated with increased cell migration. The slower migration in denser Matrigel matrix could be explained by the tighter mesh size, the increased gel stiffness, the lower diffusion of soluble factors from culture medium and/or sub-optimal adhesion ligand density[26]. Alginate is a natural hydrogel forming polysaccharide that can be tailored with specific biofunctional moieties to modulate cell behaviour and thus is currently being widely explored for tissue engineering[27,28]. A higher motility in 1% as compared with RGD-alginate 2% was seen after seven days of culture. Here, cell motility probably depends more on gel stiffness than on pore size, as cells are embedded and need to rearrange the mesh to create the physical space to move inside this matrix. Furthermore, mechano-sensing molecules can modulate cytoskeleton organization, which affects migration mode and speed[29-32].

To further demonstrate the usefulness of this method in biomaterials where cells are seeded on top instead of embedded inside, MSC dynamical behaviour was analyzed in porous chitosan scaffolds. Chitosan is a natural biodegradable polysaccharide obtained by N-deacetylation of chitin, currently being explored for many applications, from bone repair to gene therapy, amongst others. In chitosan scaffolds cells exhibited an elongated morphology through seven days of imaging possibly due to the high porosity and large pore size (larger pores and smaller interconnecting pores measure on average 147 μm and 58 μm in diameter[33,34]). On the other hand, the lack of physical constrain can impact negatively on cells migration velocity, as less adhesion sites could be available to support an efficient cell movement. Cells could be seen to migrate, with an infiltrated area similar to the values obtained for Matrigel 5.2 mg/mL and RGD-alginate 1% after seven days of incubation.

Applying this tool to access the behaviour of the cells in different materials revealed some of the issues that may arise when dealing with matrices with varied optical properties. Indeed, the more opaque chitosan allowed imaging a smaller depth and led to some light scattering when photoswitching was performed. In was possible to overcome this by normalizing data to the photoconverted area at time-point zero. Table 1 compares some characteristics of the analysed scaffolds, as well as differences in the imaging strategies and the cellular behaviour in the 3D matrices.

In summary, a tool that takes advantage of the photoswitchable Dendra2 was developed to characterize and compare MSC migration in distinct 3D microenvironments. Applying photoconvertible proteins has clear advantages to trace cells in 3D when comparing with fluorescent dyes or proteins such as GFP (Table 2). Importantly, this method allowed quantification of differences in cell migration in bioengineered matrices with fine-tuned physicochemical modifications. Furthermore, it also allowed coupling cell morphology analysis with quantification of cell migration in real-time, to study cell-ECM interactions. This method provides reliable tracking over at least seven days with an easy and straightforward analysis of cell migration using open source software. Thus, this novel platform to characterize MSC dynamics in matrices will likely have an important role in the development of biomaterials with improved characteristics for stem cell recruitment and migration or even for the study of stem cell biology in 3D microenvironments.

Table 1 - Comparison of scaffold characteristics, imaging strategies and MSC behaviour in 3D Matrigel.

		Matrigel		RGD-Alginate		Chitosan
		5.2 mg protein/mL	9.6 mg protein/mL	1% polymer	2% polymer	
Scaffold characteristics	Mesh/Pore Size	≈2 µm[26]	<0.5 µm[26]	≈12.1 nm[32]	≈5.3 nm[32]	≈147 µm (large pore) and 58 µm (small pore)[27]
	Stiffness (storage modulus)	≈10 Pa[26]	≈50 Pa[26]	≈99 Pa[32]	≈461 Pa[32]	≈83 KPa[50]
Cell seeding		Embedded	Embedded	Embedded	Embedded	On top
Imaging features	Depth (µm)	400-500	400-500	400-500	400-500	100
	Laser scattering	Low	Low	Low	Low	High
Cellular behaviour	Cell sphericity (over 7 days)	Maintain	Decrease	Decrease	Decrease	Maintain
	% Infiltration area (after 7 days)	259	193	262	207	265

Table 2 - Key characteristics of using photoconvertible or fluorescent proteins to label and quantify cell motility in 3D matrices over long periods of time *Brightness is calculated as a product of molar extinction coefficient (EC) and fluorescence quantum yield (QY) in $mM \bullet cm^{-1}$.

	Photoconvertible Proteins (e.g. Dendra2)	Fluorescent Proteins (e.g. GFP)
Brightness	19.3*	16.17*
Photostability	+++	+++
Need for continuous live imaging	No. Allows imaging for more than 15 days.	Preferable. Sample should not be moved from the initial position throughout imaging.
Imaging of the same cell(s) over days	Yes. Technically easy to create a reference by photomarking single cells or a defined subpopulation that fluoresce at a specific wavelength.	Need for cell registry strategies that are technically demanding. Small movement of the scaffold will result in misalignment of the tracked cells[16].
Effect of cell density on 3D tracking	Efficient in a range of cell densities.	Limited to imaging at low cell densities as otherwise it is difficult to follow cell trajectories.

2.5 Materials & Methods

2.5.1 Cells

Human bone marrow MSC (purchased from Lonza) were cultured in MSC growth medium (DMEM with low glucose and Glutamax plus 10% selected inactivated FBS and 1% penicillin/streptomycin (all from Invitrogen)). Cells were incubated at 37ºC/5% (V/V) CO_2 and medium was changed twice per week until cells reached approximately 80% confluence. For expansion, cells were detached by treatment with 0.05% trypsin/EDTA (Invitrogen) and replaced in 150 cm^2 tissue culture flasks (BD Falcon). Cells were used at passages 6-10.

2.5.2 MSC transfection

MSC were ressuspended in OptiMEM (Invitrogen) at 1.25 $x10^6$ cells/mL. Then, 200 µl of cell suspension were transferred to a 4 mm electroporation cuvette (BioRad), mixed with 60 µg Dendra2 plasmid DNA (pDendra2, Clontech) per $1x10^6$ cells and electroporated using a X-Cell Gene Pulser (BioRad). For optimal cell electroporation, an exponential

pulse protocol was used with 250V, 950 uF and 200 Ω[35]. After electroporation, cells were cultured in MSC growth medium at 37ºC/5%CO_2. After 16-18 hrs, medium was changed to remove debris and dead cells. Cells were incubated for 48 hrs to allow Dendra2 expression. Electroporation was performed with 200 µl of cell suspension for all experiments except for surface marker expression and 2D motility analysis, where 500 µl were used to obtained an evenly proportion of Dendra2+ and Dendra2- cells.

To determine transfection efficiency, the percentage of Dendra2+ cells was determined 48 hrs after electroporation by flow cytometry (FACSCalibur, Becton Dickinson) and analysis with FlowJo software.

2.5.3 Cell number, metabolic activity, and morphology

Cells were seeded in triplicate at 6,000 cells/cm^2 in 24 well plates and metabolic activity was assessed as described[36]. To analyze the effects of photoconversion on cells metabolic activity, photoswitching was performed 2 days after transfection. To estimate cell number, three wells for each condition were analyzed by trypan blue exclusion. Morphology was visualized by confocal microscopy (Leica TCS SP5 II, Leica Microsystems, Wetzlar, Germany, model DMI6000B-CS).

2.5.4 Surface marker expression

Cells were harvested 72 hrs after electroporating 500 µl cell suspension per cuvette. Surface staining was performed in 96-well plates by incubating for 30 min on ice with all antibodies diluted at 1.25:50, except for anti-CD73, at 2.5:50, in staining buffer (PBS, 0.5% BSA, 0.01% sodium azide), as determined after an initial titration. The antibodies used were: PerCP eFluor® 710 conjugated anti-human CD73 (clone AD2), APC conjugated anti-human CD90 (clone 5E10), eFluor® 450 conjugated anti-human CD45 (clone HI30), PE conjugated anti-human CD105 (clone SN6), eFluor® 450 conjugated anti-human HLA-DR (clone L243, eBioscience) and eFluor® 450 conjugated anti-human CD34 (clone 4H11), all from eBioscience, and PE conjugated anti-human CD14 (clone MEM-15), APC conjugated anti-human CD19 (clone LT19), from Immunotools. Appropriate isotype controls were used. Samples were washed four times in staining buffer before acquisition in a flow cytometer (FACSCanto II, Becton Dickinson). Data were analyzed with FlowJo software. Only samples resulting in more than 10,000 events were analyzed.

2.5.5 Measuring ALP expression by flow cytometry

MSC were plated at 30,000 cells/well in 24 well plates with basal or osteogenic medium. Cell surface staining for flow cytometry was performed using anti-human ALP antibody Alexa Fluor 700 (Clone B4-78, R&D Systems) as[37].

2.5.6 Photoswitching Dendra2

Photoswitching was optimized in a Leica TCS SP5 II laser scanning confocal microscope (Leica Microsystems) by using the Leica LAS AF software FRAP Wizard application (version 2.6.0.7266, Leica Microsystems) and applying a ROI (region of interest) scan, with a 10x HCX PL APO CS dry objective (0.4 N.A.) with the pinhole set to Airy1 (53.07 µm), image size 1024x1024 pixels with 16 bits and bidirectional scanning at 400 Hz. Cells were firstly imaged by sequentially acquiring green and red images with a 488 nm and 561 nm laser lines in low power. Dendra2 was converted to its red form by exposure to 405 nm laser using distinct iteration number (defined as one complete pass with the 405 nm laser, 1.303 s/frame, laser power at 2.466 mW) for a ROI with 470,000 μm^2. Finally, cells were imaged again in the green and red channels to quantify photoconversion efficiency. For 3D cell tracking 3 to 6 spots were photoswitched for each material in each individual experiment.

2.5.7 Wound healing assay combined with time-lapse microscopy

MSC were plated at 25,000 cells/well in 24-well plates in MSC growth medium. When cells reached 100% confluence a scratch was made using a 200 µL pipette tip. Cell monolayer was washed twice with PBS, MSC growth medium was added and cells were imaged in a confocal microscope (Leica TCS SP5 II, Leica Microsystems, Wetzlar, Germany), at 37°C/5% CO_2 (incubator from OKO lab). Bright-field and fluorescence images were collected using the Live Data Mode application, with 10x dry objective. Images were captured every 15 min for 16-24 hrs. Each experiment was run in triplicate and repeated 4 times. For each replicate 3 distinct positions were imaged. Photoswitching of transfected MSC located at the edges of the wound was performed immediately after the scratch. Single cell trajectories in time-lapse movies were analyzed using Gradientech Tracking Tool™ v1.07 software (Gradientech). Only cells initially at the migrating front were considered for analysis. The directness index is a measure of the cell directionality and is calculated by comparing euclidean and accumulated distances. This value can range from 0 to 1, with a value closer to 1 indicating oriented cell migration.

2.5.8 Preparation of 3D matrices

Matrigel: Matrigel Matrix Phenol Red-free (BD Biosciences) was mixed with cells following manufacturer's instructions and allowed to gel at 37ºC.

RGD-alginate disks: PRONOVA ultrapure sodium alginate (FMC Biopolymers, 70% guluronic acid) was covalently modified with cell-adhesion peptide sequence GGGGRGDSP (abbreviated as RGD, custom-made at GenScript (U.S.A.)) using aqueous carbodiimide chemistry, as previously described[36,38,39]. Solutions composed of a 1:1 mixture of high (HMW, 1.5 $\times 10^5$ Da) and low molecular weight (LMW, 2.5 $\times 10^4$ Da) alginate (both RGD-modified) were prepared in 0.9 wt-% sodium chloride (NaCl, Sigma) and combined with crosslinking agents ($CaCO_3$ and δ-gluconolactone (GDL)) to trigger hydrogel formation by internal gelation[40,41].

Chitosan scaffolds: Chitosan (France-Chitine) was purified as described[42]. Chitosan sponges were prepared by freeze-drying using a 2% solution of chitosan (degree of acetylation: 12.00 ± 2.35%, molecular weight: 324 ± 27 x 10^3) and disinfected as previously described[42,43]. Scaffolds were cut in parallelepiped shape with a dimension of 4x4 mm and a height of 2 mm (1 ± 0.2 mg average weight).

2.5.9 MSC seeding in 3D matrices

Matrigel: 1.8 x 10^5 transfected cells were mixed with Matrigel solution pre-cooled at 4ºC at 5.2 or 9.6 mg/mL of protein content. Solution was cast into a 0.8 cm^2 Lab-Tek II chamber and incubated at 37ºC/5%CO_2 for 30 min, until gelling was complete.

RGD-alginate: transfected MSC were homogeneously mixed with gel precursor solutions, prepared as described above, for a final concentration of 8x10^6 cells/mL and 1 or 2% (wt) alginate (both with RGD at 100 µM). Crosslinking of hydrogel disks was promoted in teflon plates by placing 15 µL of the solution into the plate surface. Small and uniform hydrogel disks (1.5 mm height, 3 mm diameter) were obtained by mechanical pressing during the gelling process using 3 mm spacers. Samples were incubated at 37ºC/5%CO_2 for 1hrs, until crosslinking was completed.

Chitosan: 2.5x10^5 cells in 10 µL of MSC growth medium were added to each side (top and bottom) of a scaffold in non-treated 24 well tissue culture plates. Cells were allowed to adhere to the scaffold for 4 hrs and 400 µL of MSC growth medium was added.

Prior to imaging, chitosan and RGD-alginate matrices were transferred to a 10 cm^2 dish with a bottom coverslip and to a 0.8 cm^2 Lab-Tek II chamber, respectively. After 24 hrs of

incubation cells were photoswitched and imaged. The cell-loaded matrices were cultured during seven days and medium was changed every 48 hrs.

2.5.10 Tracking Photoswitched MSC

The reference red cell population (3-6 spots per scaffolds in each individual experiment) was centred and imaged 0, 1, 4 and 7 days after conversion. Each spot was imaged by sequentially acquiring green and red images with 3% power of the 488 nm laser and with a 30% power of the 561 nm laser using a 10x dry objective, pinhole set to Airy1, image size 512x512 pixels with 8 bits, bidirectional scanning at 400 Hz, using xyz mode with a Z-stack of 50 frames, each with 9.99 µm thickness, building a Z-stack with 499.5 µm. After imaging, cells were returned to the incubator and cultured at 37ºC/5%CO_2, until the next imaging time-point.

2.5.11 Data processing

2.5.12 Photoconversion efficiency

Fluorescence intensity of both green and red forms of the Dendra2 protein were measured in 16 bits images using ImageJ software. The increase in fluorescence of Green and Red Signal Post-Conversion (relative fluorescence intensity, RFU) was normalized to take into account the initial number of Dendra2 green fluorescence molecules by calculating:

$$RFU_{\text{red}} = \frac{red_{ac} - red_{bc}}{green_{bc}}; \quad (1)$$

$$RFU_{green} = \frac{green_{ac}}{green_{bc}}; \quad (2)$$

where red_{ac} = red fluorescence intensity after conversion; red_{bc} = red fluorescence intensity before conversion; $green_{ac}$ = green fluorescence intensity after conversion; $green_{bc}$ = green fluorescence intensity before conversion.

2.5.13 Cell tracking and shape analysis

To quantify the cells infiltration area, 2D maximum projection images of Z-stacks for both green and red channels were generated using Leica LAS AF software for each photoswitched spot. The same manual threshold (threshold value ≥ 30; scale 0 - 255) was

applied to all images using ImageJ software. The area occupied by red cells was quantified by drawing a manual ROI around this area (Supplementary Figure S3). The infiltration area was then normalized to the area measured at time-point 0.

For shape analysis, ICY software was used[44]. Images were threshold by the Otsu method with the Best Threshold plugin (developed by Thomas Provoost)[45]. Then, Spot Detector plugin (developed by Fabrice de Chaumont)[46] was used for detection of the 3D objects followed by 3D Analysis (developed by Thomas Boudier)[47] to calculate object sphericity.

2.5.14 Statistical analysis

Statistical analysis was performed using Prism5 software, v5.01 for data on MSC characterization (Figure 1-3). One tailed Mann-Whitney test was used to compare two samples, whereas comparison between more than two samples was performed using the Friedman-matched paired test followed by Dunns comparison test. For grouped samples, two-way ANOVA test was used followed by Bonferroni post-test.

R software (v2.14.1) was used for statistical analysis of cells motility and shape (Figure 4–6). To test cell velocity, directness index, relative infiltration area and cell sphericity for significant differences between groups we used a linear mixed model[48], as detailed in Supplementary Methods. For 2D migration experiments, groups were treated as fixed effects and individual cells nested within each experiment were treated as random factors. For infiltration area and cell sphericity, spots and cells, respectively, were considered nested, with days nested within each experiment, which was treated as a random effect to take into account possible variability. The detailed results of this statistical analysis are in Supplementary Tables 1-5.

Data are mean ± Standard Error of the Mean (SEM) unless stated otherwise. Confidence intervals (CIs) for the desired comparisons were computed as[49].

Parameters were estimated by computing the maximum likelihood estimators using R software (www.R-project.org, R Development Core Team) and the lme and multcomp package. Values of $p < 0.05$ (*), $p < 0.01$ (**) and $p < 0.001$ (***) were considered statistically significant.

2.6 Acknowledgements

This work was financed by FEDER funds -Programa Operacional Factores de Competitividade – COMPETE and by Portuguese funds through FCT – Fundação para a Ciência e a Tecnologia in the framework of project EXPL/BIM-MED/0022/2013.

2.7 Competing financial interests

The authors declare no competing financial interests.

2.8 References

[1] Bartunek, J. *et al.* Cardiopoietic stem cell therapy in heart failure: the C-CURE (Cardiopoietic stem Cell therapy in heart failURE) multicenter randomized trial with lineage-specified biologics. *Journal of the American College of Cardiology*, 61, 23, 2013, 2329-2338.

[2] Elliott, M. J. *et al.* Stem-cell-based, tissue engineered tracheal replacement in a child: a 2-year follow-up study. *Lancet*, 380, 9846, 2012, 994-1000.

[3] Shekaran, A. *et al.* Bone regeneration using an alpha 2 beta 1 integrin-specific hydrogel as a BMP-2 delivery vehicle. *Biomaterials*, 35, 21, 2014, 5453-5461.

[4] Goncalves, R. M., Antunes, J. C. & Barbosa, M. A. Mesenchymal stem cell recruitment by stromal derived factor-1-delivery systems based on chitosan/poly(gamma-glutamic acid) polyelectrolyte complexes. *European cells & materials*, 23, 2012, 249-260; discussion 260-241.

[5] Guo, Y. *et al.* Assessment of the green florescence protein labeling method for tracking implanted mesenchymal stem cells. *Cytotechnology*, 64, 4, 2012, 391-401.

[6] Polzer, H. *et al.* Long-term detection of fluorescently labeled human mesenchymal stem cell in vitro and in vivo by semi-automated microscopy. *Tissue engineering. Part C, Methods*, 18, 2, 2012, 156-165.

[7] Taghizadeh, R. R. & Sherley, J. L. CFP and YFP, but not GFP, provide stable fluorescent marking of rat hepatic adult stem cells. *Journal of biomedicine & biotechnology*, 2008, 2008, 453590.

[8] Lalande, C. *et al.* Magnetic resonance imaging tracking of human adipose derived stromal cells within three-dimensional scaffolds for bone tissue engineering. *European cells & materials*, 21, 2011, 341-354.

[9] Bago, J. R. *et al.* In vivo bioluminescence imaging of cell differentiation in biomaterials: a platform for scaffold development. *Tissue engineering. Part A*, 19, 5-6, 2013, 593-603.

[10] Granero-Molto, F. *et al.* Regenerative effects of transplanted mesenchymal stem cells in fracture healing. *Stem cells*, 27, 8, 2009, 1887-1898.

[11] Teo, G. S., Yang, Z., Carman, C. V., Karp, J. M. & Lin, C. P. Intravital Imaging of Mesenchymal Stem Cell Trafficking and Association with Platelets and Neutrophils. *Stem cells*, 2014.

[12] Muller-Borer, B. J., Collins, M. C., Gunst, P. R., Cascio, W. E. & Kypson, A. P. Quantum dot labeling of mesenchymal stem cells. *Journal of nanobiotechnology*, 5, 2007, 9.

[13] Collins, M. C., Gunst, P. R., Cascio, W. E., Kypson, A. P. & Muller-Borer, B. J. Labeling and imaging mesenchymal stem cells with quantum dots. *Methods in molecular biology*, 906, 2012, 199-210.

[14] Gildehaus, F. J. *et al.* Impact of indium-111 oxine labelling on viability of human mesenchymal stem cells in vitro, and 3D cell-tracking using SPECT/CT in vivo. *Molecular imaging and biology : MIB : the official publication of the Academy of Molecular Imaging*, 13, 6, 2011, 1204-1214.

[15] Ji, F., Duan, H. G., Zheng, C. Q. & Li, J. Comparison of chloromethyl-dialkylcarbocyanine and green fluorescent protein for labeling human umbilical mesenchymal stem cells. *Biotechnology letters*, 2014.

[16] Bins, A. D. *et al.* Intravital imaging of fluorescent markers and FRET probes by DNA tattooing. *BMC biotechnology*, 7, 2007, 2.

[17] Chernet, B. T., Adams, D. S. & Levin, M. Photoconversion for tracking the dynamics of cell movement in Xenopus laevis embryos. *Cold Spring Harbor protocols*, 2012, 6, 2012, 683-690.

[18] Nowotschin, S. & Hadjantonakis, A. K. Use of KikGR a photoconvertible green-to-red fluorescent protein for cell labeling and lineage analysis in ES cells and mouse embryos. *BMC developmental biology*, 9, 2009, 49.

[19] Baker, S. M., Buckheit, R. W., 3rd & Falk, M. M. Green-to-red photoconvertible fluorescent proteins: tracking cell and protein dynamics on standard wide-field mercury arc-based microscopes. *BMC cell biology*, 11, 2010, 15.

[20] Kedrin, D. *et al.* Intravital imaging of metastatic behavior through a mammary imaging window. *Nature methods*, 5, 12, 2008, 1019-1021.

[21] Chudakov, D. M., Lukyanov, S. & Lukyanov, K. A. Using photoactivatable fluorescent protein Dendra2 to track protein movement. *BioTechniques*, 42, 5, 2007, 553, 555, 557 passim.

[22] Chudakov, D. M., Lukyanov, S. & Lukyanov, K. A. Tracking intracellular protein movements using photoswitchable fluorescent proteins PS-CFP2 and Dendra2. *Nature protocols*, 2, 8, 2007, 2024-2032.

[23] Griswold, S. L., Sajja, K. C., Jang, C. W. & Behringer, R. R. Generation and characterization of iUBC-KikGR photoconvertible transgenic mice for live time-lapse imaging during development. *Genesis*, 49, 7, 2011, 591-598.

[24] Carlson, A. L. *et al.* Correction: Tracking Single Cells in Live Animals Using a Photoconvertible Near-Infrared Cell Membrane Label. *PloS one*, 8, 11, 2013.

[25] Wu, S., Koizumi, K., Macrae-Crerar, A. & Gallagher, K. L. Assessing the utility of photoswitchable fluorescent proteins for tracking intercellular protein movement in the Arabidopsis root. *PloS one*, 6, 11, 2011, e27536.

[26] Zaman, M. H. *et al.* Migration of tumor cells in 3D matrices is governed by matrix stiffness along with cell-matrix adhesion and proteolysis. *Proceedings of the National Academy of Sciences of the United States of America*, 103, 29, 2006, 10889-10894.

[27] Fonseca, K. B. *et al.* Injectable MMP-sensitive alginate hydrogels as hMSC delivery systems. *Biomacromolecules*, 15, 1, 2014, 380-390.

[28] Bidarra, S. J. *et al.* Injectable in situ crosslinkable RGD-modified alginate matrix for endothelial cells delivery. *Biomaterials*, 32, 31, 2011, 7897-7904.

[29] Discher, D. E., Janmey, P. & Wang, Y. L. Tissue cells feel and respond to the stiffness of their substrate. *Science*, 310, 5751, 2005, 1139-1143.

[30] Ghibaudo, M., Di Meglio, J. M., Hersen, P. & Ladoux, B. Mechanics of cell spreading within 3D-micropatterned environments. *Lab on a chip*, 11, 5, 2011, 805-812.

[31] Ridley, A. J. *et al.* Cell migration: integrating signals from front to back. *Science*, 302, 5651, 2003, 1704-1709.

[32] Maia, F. R., Fonseca, K. B., Rodrigues, G., Granja, P. L. & Barrias, C. C. Matrix-driven formation of mesenchymal stem cell-extracellular matrix microtissues on soft alginate hydrogels. *Acta biomaterialia*, 10, 7, 2014, 3197-3208.

[33] Santos, S. G. *et al.* Adsorbed fibrinogen leads to improved bone regeneration and correlates with differences in the systemic immune response. *Acta biomaterialia*, 9, 7, 2013, 7209-7217.

[34] Barbosa, J. N., Amaral, I. F., Aguas, A. P. & Barbosa, M. A. Evaluation of the effect of the degree of acetylation on the inflammatory response to 3D porous chitosan scaffolds. *Journal of biomedical materials research. Part A*, 93, 1, 2010, 20-28.

[35] Helledie, T., Nurcombe, V. & Cool, S. M. A simple and reliable electroporation method for human bone marrow mesenchymal stem cells. *Stem cells and development*, 17, 4, 2008, 837-848.

[36] Bidarra, S. J., Barrias, C. C., Barbosa, M. A., Soares, R. & Granja, P. L. Immobilization of human mesenchymal stem cells within RGD-grafted alginate microspheres and assessment of their angiogenic potential. *Biomacromolecules*, 11, 8, 2010, 1956-1964.

[37] Almeida, C. R., Vasconcelos, D. P., Goncalves, R. M. & Barbosa, M. A. Enhanced mesenchymal stromal cell recruitment via natural killer cells by incorporation of inflammatory signals in biomaterials. *Journal of the Royal Society, Interface / the Royal Society*, 9, 67, 2012, 261-271.

[38] Evangelista, M. B. *et al.* Upregulation of bone cell differentiation through immobilization within a synthetic extracellular matrix. *Biomaterials*, 28, 25, 2007, 3644-3655.

[39] Rowley, J. A., Madlambayan, G. & Mooney, D. J. Alginate hydrogels as synthetic extracellular matrix materials. *Biomaterials*, 20, 1, 1999, 45-53.

[40] Fonseca, K. B., Bidarra, S. J., Oliveira, M. J., Granja, P. L. & Barrias, C. C. Molecularly designed alginate hydrogels susceptible to local proteolysis as three-dimensional cellular microenvironments. *Acta Biomater*, 7, 4, 2011, 1674-1682.

[41] Kuo, C. K. & Ma, P. X. Ionically crosslinked alginate hydrogels as scaffolds for tissue engineering: part 1. Structure, gelation rate and mechanical properties. *Biomaterials*, 22, 6, 2001, 511-521.

[42] Antunes, J. C. *et al.* Layer-by-layer self-assembly of chitosan and poly(gamma-glutamic acid) into polyelectrolyte complexes. *Biomacromolecules*, 12, 12, 2011, 4183-4195.

[43] Amaral, I. F., Sampaio, P. & Barbosa, M. A. Three-dimensional culture of human osteoblastic cells in chitosan sponges: the effect of the degree of acetylation. *Journal of biomedical materials research*, 76, 2, 2006, 335-346.

[44] de Chaumont, F. *et al.* Icy: an open bioimage informatics platform for extended reproducible research. *Nature methods*, 9, 7, 2012, 690-696.

[45] Otsu, N. A Threshold Selection Method from Gray-Level Histograms. *Systems, Man and Cybernetics, IEEE Transactions on*, 9, 1, 1979, 62-66.

[46] Olivo-Marin, J.-C. Extraction of spots in biological images using multiscale products. *Pattern Recognition*, 35, 9, 2002, 1989-1996.

[47] Ollion, J., Cochennec, J., Loll, F., Escude, C. & Boudier, T. TANGO: a generic tool for high-throughput 3D image analysis for studying nuclear organization. *Bioinformatics*, 29, 14, 2013, 1840-1841.

[48] Pinheiro, J. C. B. D. M. *Mixed-effects models in S and S-PLUS*. (Springer, 2000).

[49] Richardson, A. Multiple Comparisons Using R by Frank Bretz, Torsten Hothorn, Peter Westfall. *International Statistical Review*, 79, 2, 2011, 297-297.

[50] Oliveira, S. M., Amaral, I. F., Barbosa, M. A. & Teixeira, C. C. Engineering endochondral bone: in vitro studies. *Tissue engineering. Part A*, 15, 3, 2009, 625-634.

2.9 Supplementary Data

2.9.1.1 Oil Red O / ALP / Von Kossa Stainings

For adipogenesis or osteogenesis, hMSCs were plated in 24 well plates until reaching confluence and were stimulated with DMEM with low glucose and glutamax plus 10% FBS (PAA) and penicillin/streptomycin and with or without the adipogenic or osteogenic supplements as previously described[1]. Cells were washed with distilled water twice and analyzed both under an inverted microscope (Olympus CKX Inverted Microscope) and in a confocal microscope (Leica TCS SP5 II) for co-localization of Oil Red O stained lipid droplets or ALP with cells Dendra2 fluorescence.

2.9.1.2 Statistical analysis: Linear Mixed Model Analysis

For 2D migration experiments, groups were treated as fixed effects and individual cells nested within each experiment were treated as random factors. For infiltration area and cell sphericity, spots and cells, respectively, were considered nested, with days nested within each experiment, which was treated as a random effect to take into account possible variability. The fixed effect materials and days interaction was tested for significance. The random factor experiment described the between-experiment variability of infiltration area and sphericity from one experiment to another, the days described the between-days-within-experiment variability from one day to another one, and the random factor cells described the between-cells-within-days-within-experiment variability of infiltration area and sphericity. This random effect was assumed to follow a normal distribution centred on 0 with standard deviations for experiment, days and cells.

To assess the importance of random factors in our model, we tested their significance by removing terms one at a days and comparing the difference between the log likelihoods of the reduced and complete models using a qui-square test. In each model random terms were retained if they significantly improved likelihood.

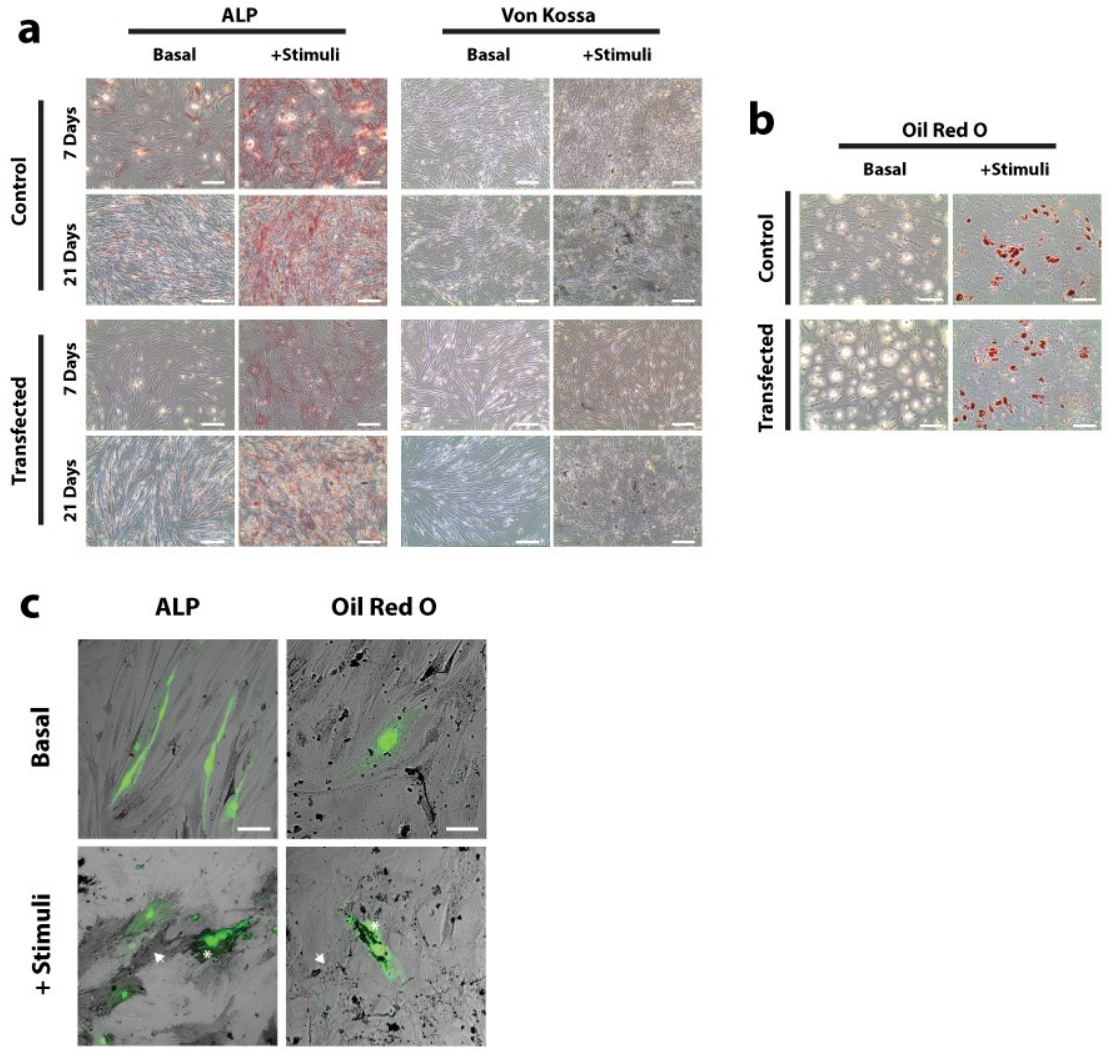

Supplementary Figure S1. Transfected MSC are capable of multilineage differentiation when appropriately stimulated but not in basal condition. (a) Control and transfected MSC differentiate into osteoblasts as determined by staining for ALP activity (left: ALP staining) and late calcium-containing mineral deposits in extracellular matrix (right: von Kossa staining). (b) Lipid vacuoles accumulation stained with Oil Red O solution at 21 days indicates differentiating adipocytes on both control and transfected MSC. Scale bar, 250 μm. (c) Both Dendra2+ (asterisk) and Dendra2- MSC (arrowhead) were able to differentiate into osteogenic or adipogenic lineages when appropriately stimulated as denoted by expression of ALP showed as black staining (left) or oil droplets illustrated as black droplets (right), respectively. Scale bar, 75 μm. Pictures are representative of 3 individual experiments in duplicate.

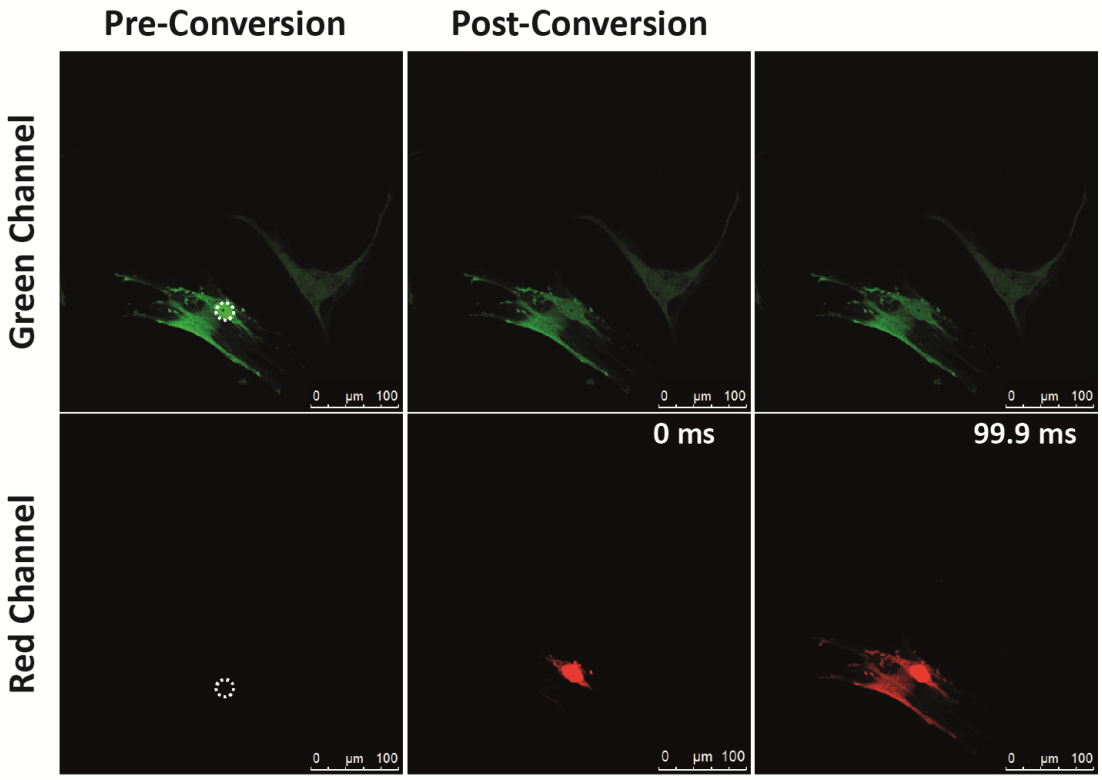

Supplementary Figure S2. Photoconversion at sub-cellular resolution. Confocal microscopy images in Green (top) and Red (bottom) channels of Dendra2+ MSC. Photoconversion was achieved with 405nm laser in the circular region of Interest indicated (dashed line). Photoswitched red Dendra2 redistributed throughout the cell cytoplasm within 99.9 ms after conversion.

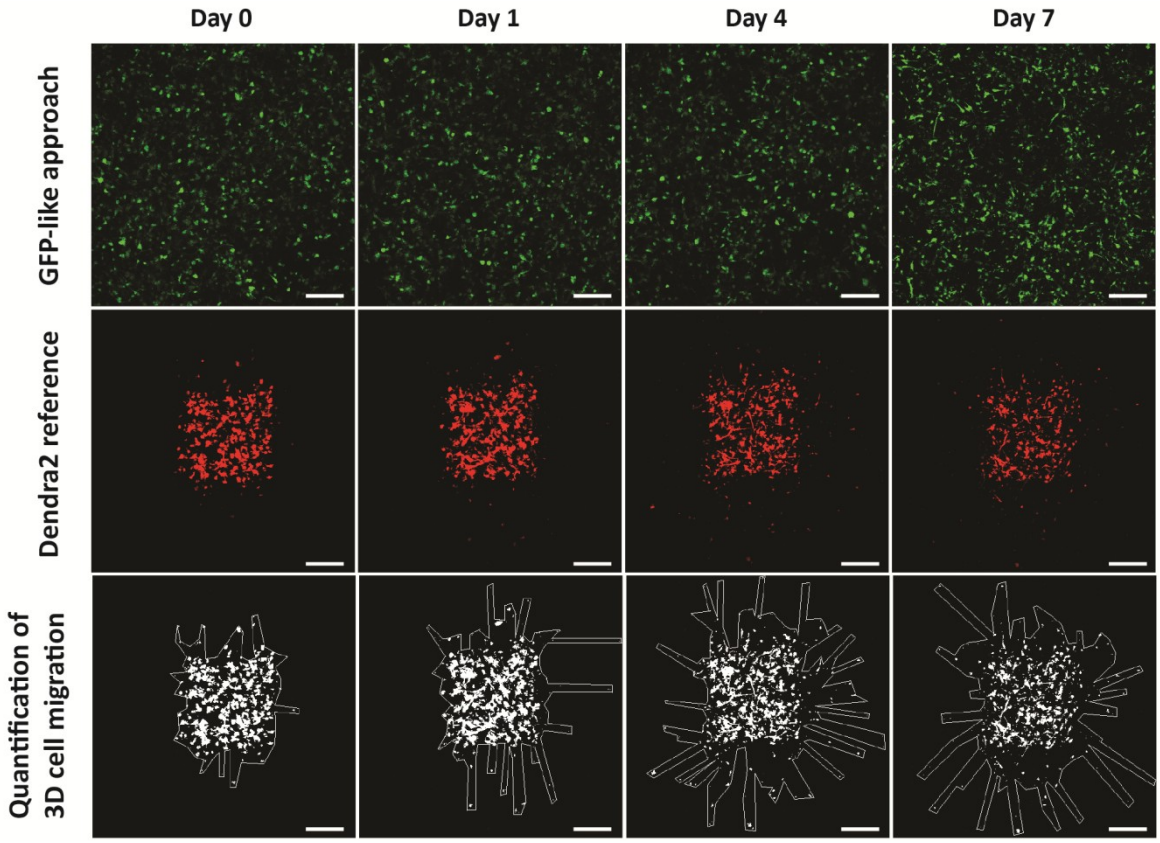

Supplementary Figure S3. Using Dendra2 photoconversion to track MSC. (top) It is difficult to quantify cell motility in 3D when MSC are all labelled with the same fluorescent protein (GFP-like approach, cells were imaged in the green channel only). In this scenario, it is extremely hard to find the same cells when imaging sessions have to be performed at discrete daily intervals and samples cannot be kept under a microscope. (middle) Dendra2 photoconversion of a group of cells creates a fixed reference with defined geometric shapes that allows repositioning the same cells over the different imaging sessions. (bottom) Infiltration area quantified in xy maximum projection images by manual drawing a ROI. Scale bar, 250 μm.

Supplementary Table 1 - Contrast comparison using mixed effect model fit to test differences in mean directness index between groups. Group1: Control ; Group2: Electroporated without plasmid ; Group3: Dendra2+ Green ; Group4: Dendra2+ Red.

Materials	Estimate	Std. Error	95%CI	z value	Pr(>|z|)
Group2 vs. Group1	-0.017	0.015	(-0.055; 0.020)	-1.179	0.637
Group3 vs. Group1	-0.001	0.015	(-0.041; 0.039)	-0.056	1.000
Group4 vs. Group1	-0.047	0.019	(-0.096; 0.002)	-2.452	0.066
Group3 vs. Group2	0.017	0.014	(-0.020; 0.053)	1.176	0.639
Group4 vs. Group2	-0.029	0.018	(-0.075; 0.017)	-1.630	0.358
Group4 vs. Group3	-0.046	0.019	(-0.094; 0.002)	-2.476	0.062
Variance Component				**StdDev**	
Between-experiment				0.000002	
Between-cells-within-experiments				0.000009	
Residuals				0.1335	

Supplementary Table 2 - Contrast comparison using mixed effect model fit to test differences in mean velocity between groups. Group1: Control ; Group2: Electroporated without plasmid ; Group3: Dendra2+ Green ; Group4: Dendra2+ Red.

	Estimate	Std. Error	95%CI	z value	Pr(>|z|)	
Group2 vs. Group1	0.030216	0.013872	(-0.005; 0.066)	2.178	0.128	
Group3 vs. Group1	-0.10191	0.014061	(-0.138; -0.066)	-7.248	p<0.001	***
Group4 vs. Group1	-0.11584	0.01737	(-0.160; -0.071)	-6.669	p<0.001	***
Group3 vs. Group2	-0.13212	0.013375	(-0.166; -0.098)	-9.879	p<0.001	***
Group4 vs. Group2	-0.14605	0.016651	(-0.189; -0.103)	-8.772	p<0.001	***
Group4 vs. Group3	-0.01393	0.016884	(-0.057; 0.029)	-0.825	0.841	
Variance Component				StdDev		
between-experiment				0.0585		
between-cell-within-experiment				0.0043		
Residual				0.1209		

Supplementary Table 3 - Contrast comparison using mixed effect model fit to test differences in the mean % infiltration area between material in each time point and within material in each time point. Group1: Matrigel 5.2 mg/mL ; Group2: Matrigel 9.6 mg/mL ; Group3: 1% RGD-alginate ; Group4: 2% RGD-alginate ; Group5: Chitosan.

Material	Estimate	Std. Error	IC95%	z value	Pr(>|z|)	
TimePoint1: Group2 vs. Group1	-22.866	9.959	(-50.019; 4.287)	-2.296	0.146	
TimePoint1: Group3 vs. Group1	-24.884	9.651	(-51.195; 1.428)	-2.578	0.074	
TimePoint1: Group4 vs. Group1	-19.920	9.658	(-46.252; 6.413)	-2.062	0.236	
TimePoint1: Group5 vs. Group1	29.815	10.629	(0.835; 58.795)	2.805	0.040	*
TimePoint1: Group3 vs. Group2	-2.017	9.651	(-28.329; 24.294)	-0.209	1.000	
TimePoint1: Group4 vs. Group2	2.946	9.658	(-23.386; 29.279)	0.305	0.998	
TimePoint1: Group5 vs. Group2	52.681	10.629	(23.701; 81.661)	4.956	0.000	***
TimePoint1: Group4 vs. Group3	4.964	9.330	(-20.474; 30.402)	0.532	0.984	
TimePoint1: Group5 vs. Group3	54.699	10.341	(26.506; 82.892)	5.290	0.000	***
TimePoint1: Group5 vs. Group4	49.735	10.341	(21.540; 77.930)	4.809	0.000	***
TimePoint4: Group2 vs. Group1	-37.789	9.959	(-64.938; -10.64)	-3.794	0.001	**
TimePoint4: Group3 vs. Group1	-9.145	9.651	(-35.454; 17.163)	-0.948	0.878	
TimePoint4: Group4 vs. Group1	-9.075	9.658	(-35.404; 17.254)	-0.940	0.881	
TimePoint4: Group5 vs. Group1	32.153	10.629	(3.178; 61.129)	3.025	0.021	*
TimePoint4: Group3 vs. Group2	28.644	9.651	(2.336; 54.952)	2.968	0.025	*
TimePoint4: Group4 vs. Group2	28.715	9.658	(2.386; 55.044)	2.973	0.024	*
TimePoint4: Group5 vs. Group2	69.943	10.629	(40.967; 98.918)	6.580	0.000	***
TimePoint4: Group4 vs. Group3	0.071	9.330	(-25.364; 25.506)	0.008	1.000	
TimePoint4: Group5 vs. Group3	41.299	10.341	(13.110; 69.488)	3.994	0.001	***
TimePoint4: Group5 vs. Group4	41.228	10.341	(13.037; 69.419)	3.987	0.001	***
TimePoint7: Group2 vs. Group1	-64.232	9.959	(-91.389; -37.074)	-6.450	0.000	***
TimePoint7: Group3 vs. Group1	3.796	9.651	(-22.520; 30.113)	0.393	0.995	
TimePoint7: Group4 vs. Group1	-47.273	9.658	(-73.610; -20.935)	-4.895	0.000	***
TimePoint7: Group5 vs. Group1	6.079	10.629	(-22.906; 35.063)	0.572	0.979	
TimePoint7: Group3 vs. Group2	68.028	9.651	(41.711; 94.344)	7.049	0.000	***
TimePoint7: Group4 vs. Group2	16.959	9.658	(-9.378; 43.297)	1.756	0.399	
TimePoint7: Group5 vs. Group2	70.310	10.629	(41.326; 99.295)	6.615	0.000	***
TimePoint7: Group4 vs. Group3	-51.069	9.330	(-76.512; -25.626)	-5.474	0.000	***
TimePoint7: Group5 vs. Group3	2.282	10.341	(-25.916; 30.480)	0.221	0.999	
TimePoint7: Group5 vs. Group4	53.351	10.341	(25.151; 81.551)	5.159	0.000	***
Material	**Estimate**	**Std. Error**	**IC95%**	**z value**	**Pr(>|z|)**	
Group1: Time1 vs. Time0	35.634	9.959	(10.054; 61.213)	3.578	0.002	**
Group1: Time4 vs. Time0	87.683	9.959	(62.103; 113.262)	8.804	0.000	***
Group1: Time7 vs. Time0	160.315	9.959	(134.736; 185.895)	16.097	0.000	***
Group1: Time4 vs. Time1	52.049	9.959	(26.470; 77.628)	5.226	0.000	***
Group1: Time7 vs. Time1	124.682	9.959	(99.102; 150.261)	12.519	0.000	***
Group1: Time7 vs. Time4	72.633	9.959	(47.053; 98.212)	7.293	0.000	***
Group2: Time1 vs. Time0	12.767	9.959	(-12.741; 38.276)	1.282	0.601	

Group2: Time4 vs. Time0	64.817	14.084	(28.742; 100.891)	4.602	0.000	***
Group2: Time7 vs. Time0	137.449	14.084	(101.375; 173.523)	9.759	0.000	***
Group2: Time4 vs. Time1	37.126	9.959	(11.617; 62.634)	3.728	0.001	**
Group2: Time7 vs. Time1	83.316	9.959	(57.808; 108.824)	8.366	0.000	***
Group2: Time7 vs. Time4	46.190	9.959	(20.682; 71.699)	4.638	0.000	***
Group3: Time1 vs. Time0	10.627	9.316	(-13.649; 34.903)	1.141	0.768	
Group3: Time4 vs. Time0	67.472	13.637	(31.935; 103.008)	4.948	0.000	***
Group3: Time7 vs. Time0	189.605	15.014	(150.481; 228.729)	12.629	0.000	***
Group3: Time4 vs. Time1	67.787	9.316	(43.511; 92.063)	7.277	0.000	***
Group3: Time7 vs. Time1	153.362	9.316	(129.085; 177.638)	16.462	0.000	***
Group3: Time7 vs. Time4	85.574	9.316	(61.298; 109.850)	9.186	0.000	***
Group4: Time1 vs. Time0	15.422	9.316	(-8.475; 39.320)	1.656	0.359	
Group4: Time4 vs. Time0	67.472	13.637	(32.489; 102.455)	4.948	0.000	***
Group4: Time7 vs. Time0	140.104	13.637	(105.121; 175.087)	10.274	0.000	***
Group4: Time4 vs. Time1	62.894	9.316	(38.996; 86.792)	6.751	0.000	***
Group4: Time7 vs. Time1	97.329	9.316	(73.431; 121.227)	10.448	0.000	***
Group4: Time7 vs. Time4	34.435	9.316	(10.537; 58.333)	3.696	0.001	**
Group5: Time1 vs. Time0	64.923	11.235	(36.216; 93.631)	5.778	0.000	***
Group5: Time4 vs. Time0	116.972	15.014	(78.610; 155.335)	7.791	0.000	***
Group5: Time7 vs. Time0	189.605	15.014	(151.243; 227.967)	12.629	0.000	***
Group5: Time4 vs. Time1	54.387	11.235	(25.680; 83.095)	4.841	0.000	***
Group5: Time7 vs. Time1	100.945	11.235	(72.238; 129.653)	8.985	0.000	***
Group5: Time7 vs. Time4	46.558	11.235	(17.850; 75.265)	4.144	0.000	***

Variance Component	**StdDev**
between-experiment	0.0027
between-spot-within-experiment	4.4
between-days-within-spot-within-experiment	0.0002
Residual	26.349

Supplementary Table 4 - Contrast comparison using mixed effect model fit to test differences in cell sphericity between material in each time point and within material over time. Group1: Matrigel 5.2 mg/mL ; Group2: Matrigel 9.6 mg/mL ; Group3: 1% RGD-alginate ; Group4: 2% RGD-alginate ; Group5: Chitosan.

Material	Estimate	Std. Error	IC95%	z value	Pr(>|z|)	
TimePoint0: Group2 vs. Group1	0.046	0.007	(0.027; 0.065)	6.500	0.000	***
TimePoint0: Group3 vs. Group1	0.007	0.007	(-0.011; 0.025)	1.085	0.814	
TimePoint0: Group4 vs. Group1	0.016	0.007	(-0.003; 0.035)	2.263	0.157	
TimePoint0: Group5 vs. Group1	-0.069	0.007	(-0.09; -0.049)	-9.319	0.000	***
TimePoint0: Group3 vs. Group2	-0.039	0.006	(-0.056; -0.021)	-5.936	0.000	***
TimePoint0: Group4 vs. Group2	-0.030	0.007	(-0.049; -0.011)	-4.275	0.000	***
TimePoint0: Group5 vs. Group2	-0.115	0.007	(-0.135; -0.095)	-15.658	0.000	***
TimePoint0: Group4 vs. Group3	0.009	0.006	(-0.009; 0.026)	1.367	0.648	
TimePoint0: Group5 vs. Group3	-0.077	0.007	(-0.095; -0.058)	-11.131	0.000	***
TimePoint0: Group5 vs. Group4	-0.085	0.007	(-0.105; -0.066)	-11.698	0.000	***
TimePoint1: Group2 vs. Group1	0.029	0.007	(0.029; 0.011)	4.269	0.000	***
TimePoint1: Group3 vs. Group1	0.005	0.007	(0.005; -0.013)	0.772	0.939	
TimePoint1: Group5 vs. Group1	-0.087	0.007	(-0.087; -0.106)	-12.157	0.000	***
TimePoint1: Group4 vs. Group1	0.019	0.007	(0.019; 0.000)	2.682	0.056	
TimePoint1: Group3 vs. Group2	-0.024	0.007	(-0.024; -0.042)	-3.62	0.003	**
TimePoint1: Group4 vs. Group2	-0.011	0.007	(-0.011; -0.029)	-1.546	0.532	
TimePoint1: Group5 vs. Group2	-0.116	0.007	(-0.116; -0.135)	-16.375	0.000	***
TimePoint1: Group4 vs. Group3	0.013	0.007	(0.013; -0.005)	2.016	0.258	
TimePoint1: Group5 vs. Group3	-0.092	0.007	(-0.092; -0.111)	-13.43	0.000	***
TimePoint1: Group5 vs. Group4	-0.106	0.007	(-0.106; -0.125)	-14.971	0.000	***
TimePoint4: Group2 vs. Group1	0.016	0.006	(0.016; 0.000)	2.777	0.043	*
TimePoint4: Group3 vs. Group1	-0.027	0.005	(-0.027; -0.042)	-4.983	0.000	***
TimePoint4: Group4 vs. Group1	-0.021	0.006	(-0.021; -0.037)	-3.721	0.002	**
TimePoint4: Group5 vs. Group1	-0.078	0.007	(-0.078; -0.096)	-11.946	0.000	***
TimePoint4: Group3 vs. Group2	-0.043	0.005	(-0.043; -0.057)	-8.017	0.000	***
TimePoint4: Group4 vs. Group2	-0.037	0.006	(-0.037; -0.053)	-6.58	0.000	***
TimePoint4: Group5 vs. Group2	-0.094	0.006	(-0.094; -0.111)	-14.575	0.000	***
TimePoint4: Group4 vs. Group3	0.006	0.005	(0.006; -0.009)	1.053	0.829	
TimePoint4: Group5 vs. Group3	-0.051	0.006	(-0.051; -0.068)	-8.258	0.000	***
TimePoint4: Group5 vs. Group4	-0.057	0.006	(-0.057; -0.074)	-8.771	0.000	***
TimePoint7: Group2 vs. Group1	0.046	0.007	(0.046; 0.026)	6.5	0.000	***
TimePoint7: Group3 vs. Group1	0.007	0.007	(0.007; -0.011)	1.085	0.892	
TimePoint7: Group4 vs. Group1	0.016	0.007	(0.016; -0.003)	2.263	0.175	
TimePoint7: Group5 vs. Group1	-0.069	0.007	(-0.069; -0.090)	-9.319	0.000	***
TimePoint7: Group3 vs. Group2	-0.046	0.007	(-0.046; -0.066)	-6.51	0.000	***
TimePoint7: Group4 vs. Group2	-0.027	0.008	(-0.027; -0.048)	-3.525	0.004	**
TimePoint7: Group5 vs. Group2	-0.093	0.007	(-0.093; -0.113)	-12.811	0.000	***
TimePoint7: Group4 vs. Group3	0.020	0.006	(0.020; 0.002)	3.131	0.016	*

TimePoint7: Group5 vs. Group3	-0.047	0.006	(-0.047; -0.064)	-7.671	0.000	***
TimePoint7: Group5 vs. Group4	-0.066	0.007	(-0.066; -0.084)	-10.099	0.000	***

Material	Estimate	Std. Error	IC95%	z value	Pr(>|z|)	
Group1: Time1 vs. Time0	0.007	0.009	(0.007; -0.017)	0.784	0.862	
Group1: Time4 vs. Time0	0.007	0.009	(0.007; -0.016)	0.817	0.846	
Group1: Time7 vs. Time0	-0.012	0.009	(-0.012; -0.036)	-1.282	0.574	
Group1: Time4 vs. Time1	0.000	0.009	(0.000; -0.023)	-0.001	1.000	
Group1: Time7 vs. Time1	-0.019	0.009	(-0.019; -0.043)	-2.090	0.156	
Group1: Time7 vs. Time4	-0.019	0.009	(-0.019; -0.042)	-2.182	0.128	
Group2: Time1 vs. Time0	-0.009	0.009	(-0.009; -0.033)	-1.000	0.797	
Group2: Time4 vs. Time0	-0.009	0.011	(-0.009; -0.038)	-0.825	0.889	
Group2: Time7 vs. Time0	-0.028	0.011	(-0.028; -0.058)	-2.476	0.065	
Group2: Time4 vs. Time1	-0.013	0.009	(-0.013; -0.036)	-1.520	0.451	
Group2: Time7 vs. Time1	-0.025	0.010	(-0.025; -0.050)	-2.610	0.045	*
Group2: Time7 vs. Time4	-0.012	0.009	(-0.012; -0.036)	-1.299	0.601	
Group3: Time1 vs. Time0	0.005	0.009	(0.005; -0.017)	0.608	0.976	
Group3: Time4 vs. Time0	0.010	0.011	(0.010; -0.019)	0.878	0.896	
Group3: Time7 vs. Time0	-0.029	0.012	(-0.029; -0.060)	-2.481	0.069	
Group3: Time4 vs. Time1	-0.032	0.008	(-0.032; -0.054)	-3.837	0.001	***
Group3: Time7 vs. Time1	-0.048	0.009	(-0.048; -0.070)	-5.608	0.000	***
Group3: Time7 vs. Time4	-0.016	0.008	(-0.016; -0.037)	-1.961	0.230	
Group4: Time1 vs. Time0	0.010	0.009	(0.010; -0.014)	1.073	0.751	
Group4: Time4 vs. Time0	0.010	0.011	(0.010; -0.019)	0.878	0.863	
Group4: Time7 vs. Time0	-0.009	0.012	(-0.009; -0.039)	-0.817	0.892	
Group4: Time4 vs. Time1	-0.040	0.009	(-0.040; -0.062)	-4.573	0.000	***
Group4: Time7 vs. Time1	-0.042	0.009	(-0.042; -0.065)	-4.544	0.000	***
Group4: Time7 vs. Time4	-0.002	0.009	(-0.002; -0.024)	-0.200	1.000	
Group5: Time1 vs. Time0	-0.010	0.010	(-0.010; -0.035)	-1.067	0.752	
Group5: Time4 vs. Time0	-0.010	0.012	(-0.010; -0.040)	-0.884	0.858	
Group5: Time7 vs. Time0	-0.029	0.012	(-0.029; -0.060)	-2.481	0.063	
Group5: Time4 vs. Time1	0.009	0.009	(0.009; -0.015)	0.968	0.812	
Group5: Time7 vs. Time1	-0.002	0.009	(-0.002; -0.026)	-0.266	0.999	
Group5: Time7 vs. Time4	-0.011	0.009	(-0.011; -0.035)	-1.274	0.614	

Variance Component	StdDev
between-experiment	0.005
between-days-within-experiment	0.007
between-cells-within-days-within-experiment	0.000002
Residual	0.0796

Supplementary Table 5 - Contrast comparison using mixed effect model fit to test differences in mean cell sphericity within material over time (consider time continuous).

Trend per Material	Estimate	Std. Error	IC95%	z value	Pr(>|z|)	
Trend in Matrigel 5.2 mg/mL	-0.002	0.001	(-0.005; 0.001)	-1.486	0.459	
Trend in Matrigel 9.6 mg/mL	-0.005	0.001	(-0.008; -0.002)	-3.929	0.000	***
Trend in 1% RGD-alginate	-0.007	0.001	(-0.010; -0.004)	-6.613	0.000	***
Trend in 2% RGD-alginate	-0.006	0.001	(-0.009; -0.003)	-5.288	0.000	***
Trend in Chitosan	-0.001	0.001	(-0.004; 0.002)	-0.935	0.840	

2.9.1.3 References

[1] Almeida CR, Vasconcelos DP, Goncalves RM, Barbosa MA. Enhanced mesenchymal stromal cell recruitment via natural killer cells by incorporation of inflammatory signals in biomaterials. *J R Soc Interface,* **9**, 2012, 261-271.

CHAPTER 3

“O QUE HÁ EM MIM É SOBRETUDO CANSAÇO

(…)
Há sem dúvida quem ame o infinito,
Há sem dúvida quem deseje o impossível,
Há sem dúvida quem não queira nada
Três tipos de idealistas, e eu nenhum deles:
Porque eu amo infinitamente o finito,
Porque eu desejo impossivelmente o possível,
Porque eu quero tudo, ou um pouco mais, se puder ser,
Ou até se não puder ser...
(…)”

9-10-1934
Poesias de Álvaro de Campos. Fernando Pessoa. Lisboa: Ática, 1944 (imp. 1993) - 64.

The contents of this chapter are based on:

MACROPHAGE INTERACTIONS WITH PLA AND CHITOSAN SCAFFOLDS LEAD TO IMPROVED RECRUITMENT OF HUMAN MSC: A COMPREHENSIVE STUDY WITH DIFFERENT IMMUNE CELLS

Hugo R. Caires [1,2,3]

Tiago Esteves [2,3,4]

Pedro Quelhas [2,3]

Mário A. Barbosa [1,2,3]

Melba Navarro [5]

Catarina R. Almeida [2,3,6]

[1] ICBAS - Instituto de Ciências Biomédicas Abel Salazar, Universidade do Porto, Rua Jorge Viterbo Ferreira, 228, 4050-313 Porto, Portugal

[2] i3S - Instituto de Investigação e Inovação em Saúde da Universidade do Porto, Rua Alfredo Allen, 208, 4200-135 Porto, Portugal Portugal

[3] INEB - Instituto de Engenharia Biomédica, Porto, Portugal

[4] Faculdade de Engenharia, Universidade do Porto, Rua Dr. Roberto Frias, s/n 4200-465 Porto, Portugal

[5] International Center for Numerical Methods in Engineering (CIMNE), Edificio Nexus (103) Carrer del Gran Capità, 2-4, 08034, Barcelona, Spain

[6] Department of Medical Sciences and Institute for Biomedicine - iBiMED, University of Aveiro, 3810-193 Aveiro, Portugal (current address)

JOURNAL OF THE ROYAL SOCIETY INTERFACE 13, 122, (2016)

3.1 Abstract

Despite the importance of immune cell - biomaterial interactions for the regenerative outcome, few studies have investigated how distinct 3D biomaterials modulate the immune cell-mediated MSC recruitment and function. Thus, this work compares the response of varied primary human immune cell populations triggered by different model scaffolds and describes its functional consequence on recruitment and motility of bone marrow MSC. It was found that Poly-Lactic Acid (PLA) and chitosan scaffolds lead to an increase in the metabolic activity of macrophages but not of peripheral blood mononuclear cells (PBMC), NK cells or monocytes. PBMC and NK cells increase their cell number in PLA scaffolds and express a secretion profile that does not promote MSC recruitment. Importantly, chitosan increases IL-8, MIP-1, MCP-1 and RANTES secretion by macrophages while PLA stimulates IL-6, IL-8 and MCP-1 production, all chemokines that can lead to MSC recruitment. This secretion profile of macrophages in contact with biomaterials correlates with the highest MSC invasion. Furthermore, macrophages enhance stem cell motility within chitosan scaffolds by 44% but not in PLA scaffolds. Thus, macrophages are the cells that in contact with engineered biomaterials become activated to secrete bioactive molecules that stimulate MSC recruitment.

KEYWORDS: Biomaterials; Inflammation; regeneration; Mesenchymal stem cell; Recruitment; human

3.2 Introduction

Implantation of tissue engineered scaffolds triggers simultaneously two types of host response: an immune reaction against the foreign material and activation of tissue repair mechanisms at the injured area. Although the nature of these biological processes is very distinct they share inflammation as a common denominator. If perpetuated, inflammation can be detrimental, leading to tissue damage and fibrotic encapsulation of the biomaterial, but at the same time inflammation is essential to promote progenitor cell recruitment and initiate healing mechanisms[1]. The requirement of fine-tuning inflammation for a beneficial regenerative outcome prompted the design of "immuno-informed" biomaterials to control the host response[2]. The great majority of regenerative medicine strategies aim for spatial and temporal control of stem cell differentiation. But for effective tissue repair, it is also necessary to tightly control the coordinated movement of different cell types to the injury site. Thus, strategies that modulate the immune response to attract endogenous stem cells are appealing, as we start to understand that recruitment, and not only proliferation and differentiation of progenitor cells is important for effective regeneration.

Mesenchymal stem/stromal cells (MSC) have a pivotal role in supporting the regenerative process due to their ability to migrate to inflamed tissues, to differentiate in different lineages and to their paracrine and immunomodulation properties[3]. Importantly, it was shown in a murine model that upon biomaterial subcutaneous implantation there is first recruitment of inflammatory cells, which is then correlated with recruitment of MSC[4-7]. MSC recruitment can then lead to subsequent modulation of inflammation and is essential to promote the constructive remodelling of the tissue[8,9]. Nevertheless, the specific contribution of different immune cell populations interacting with implanted biomaterials for MSC recruitment remains unexplored.

In the first 48 hrs upon implantation, Natural Killer (NK) cells and polymorphonuclear neutrophils become the predominant cells at the tissue-implant interface[10,11]. NK cells are lymphocytes crucial for remodelling of the endometrium during pregnancy, and which can promote MSC recruitment, possibly through secretion of different chemokines[12]. Monocyte recruitment from the blood to the implant site thrives under its inflammatory environment, where they gradually differentiate into macrophages that replace the short-lived neutrophils and NK cells. Macrophages are master regulators of the foreign body response and tissue regeneration through secretion of bioactive molecules which can impact inflammation, angiogenesis, extracellular matrix remodelling and stem cell recruitment and differentiation[2]. And indeed, Macrophages are potent inducers of MSC recruitment, mainly through the production of the chemokine RANTES[12,13]. The

remarkable plasticity of macrophages allows them to adopt a dynamic profile between M1 pro-inflammatory and M2 pro-regenerative functional programmes which can shift the regenerative outcome. Essentially, these over-simplistic functional phenotypes are not exclusive and the overall response is the net result of a combination of distinct macrophage phenotypes dictated by the specific microenvironment, cell-cell interaction and biomaterial properties[14,15].

Even though biomaterials impact on immune cells, few studies compared the response of different populations to 3D matrices. But more importantly, its consequence on the dynamical behaviour of stem cells is not understood. Here, we analysed the ability of human immune cells interacting with different scaffolds to promote human stem cells recruitment. Thus, two different types of materials were used as models for biomaterials with distinct physic-chemical properties: Poly-Lactic Acid (PLA), an FDA approved synthetic polymer used for bone repair or as internal fracture fixation device [16]; and chitosan which is a natural polysaccharide, currently explored for many applications, including wound dressings and bone regeneration[17,18]. Firstly, the effect of PLA and chitosan scaffolds on the behaviour of primary human PBMC, NK cells, monocytes and macrophages isolated from peripheral blood of healthy donors was characterized. Then, it was determined how the responses of these immune cell populations affected human bone marrow MSC recruitment and motility within 3D matrices **(Figure 1)**.

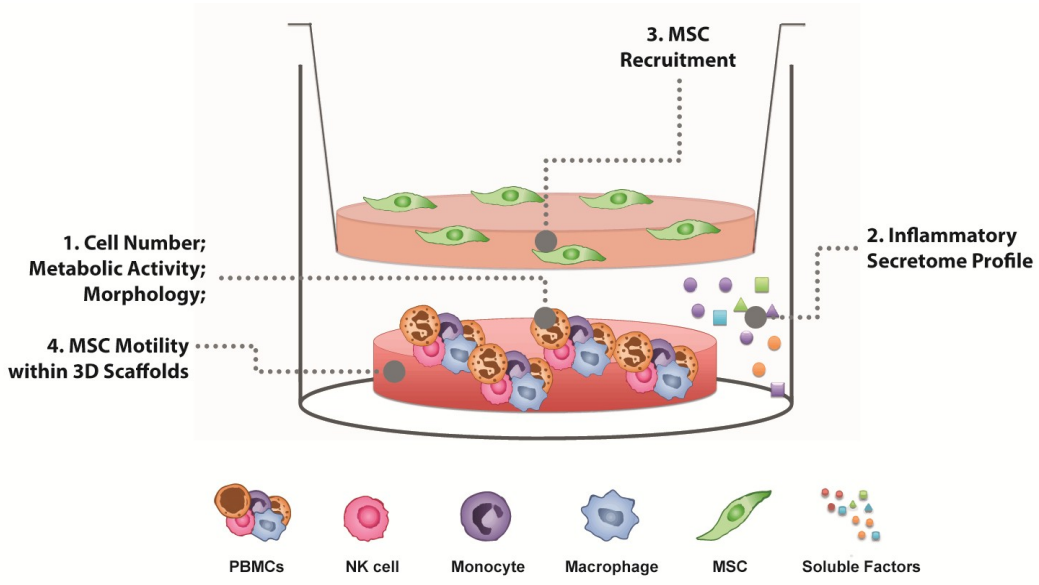

Figure 1 - Schematic representation of the study performed. Experiments were performed with 3D PLA or chitosan scaffolds on a well of a 24 well plate, and, for invasion assays, a Matrigel-coated transwell chamber on top of it, with a spacer to compensate for scaffolds height. Different immune cell populations, namely, PBMC, NK cells, monocytes

and macrophages were seeded on the scaffolds to analyse cell number, metabolic activity, cell morphology, secretory profile and MSC recruitment. Furthermore, motility of MSC seeded on scaffolds was also analysed.

3.3 Results

3.3.1 Scaffold characterization

To compare the behaviour of immune cell populations incubated with materials with a different chemistry, we prepared PLA and chitosan scaffolds with approximately the same pore size **(Supplementary Figure S1)**, which can be instrumental in defining the inflammatory response towards biomaterials. Both types of scaffolds showed a homogeneous porosity with the large pores having an average diameter of 141±44 μm for PLA and 125±25 μm for chitosan, in agreement with previous reports[19,20]. PLA had a rougher surface compared to chitosan and displayed micropores with a mean diameter of 25±10 μm against 42±24 μm for chitosan. Both types of scaffold had endotoxin levels lower than 0.2 EU/ml, which are below the recommended FDA limit for implanted biomaterials.

3.3.2 Metabolism, cell number and morphology

Upon biomaterial implantation, distinct immune cell populations are recruited and activated in a highly regulated manner over the acute and chronic phases of inflammation. Here, the behaviour of PBMC, NK cells and monocytes was evaluated after 2 days in contact with the materials while macrophages were analyzed after differentiation through 9 days of contact with the scaffolds. Although not statistically significant, there was a tendency for the metabolic activity of macrophages, but not monocytes, to increase in contact with PLA and chitosan scaffolds as opposed to 2D TCPS. In contrast, PBMC and NK cells metabolism was significantly reduced upon interaction with PLA or chitosan scaffolds **(Figure 2a)**.

Immune cells metabolism was not correlated with cell number as DNA quantification suggests that NK cells showed a significantly higher number of cells when incubated with PLA. This indicates that there was cell proliferation even in the absence of any exogenous stimulus apart from the scaffold, but that the metabolic activity per cell is diminished **(Figure 2b)**. The number of macrophages was maintained in both types of 3D scaffolds but the cells disappeared on TCPS. Therefore, caution must be taken when comparing

data from macrophages differentiated on TCPS with cells in biomaterials. No major differences were observed with monocytes.

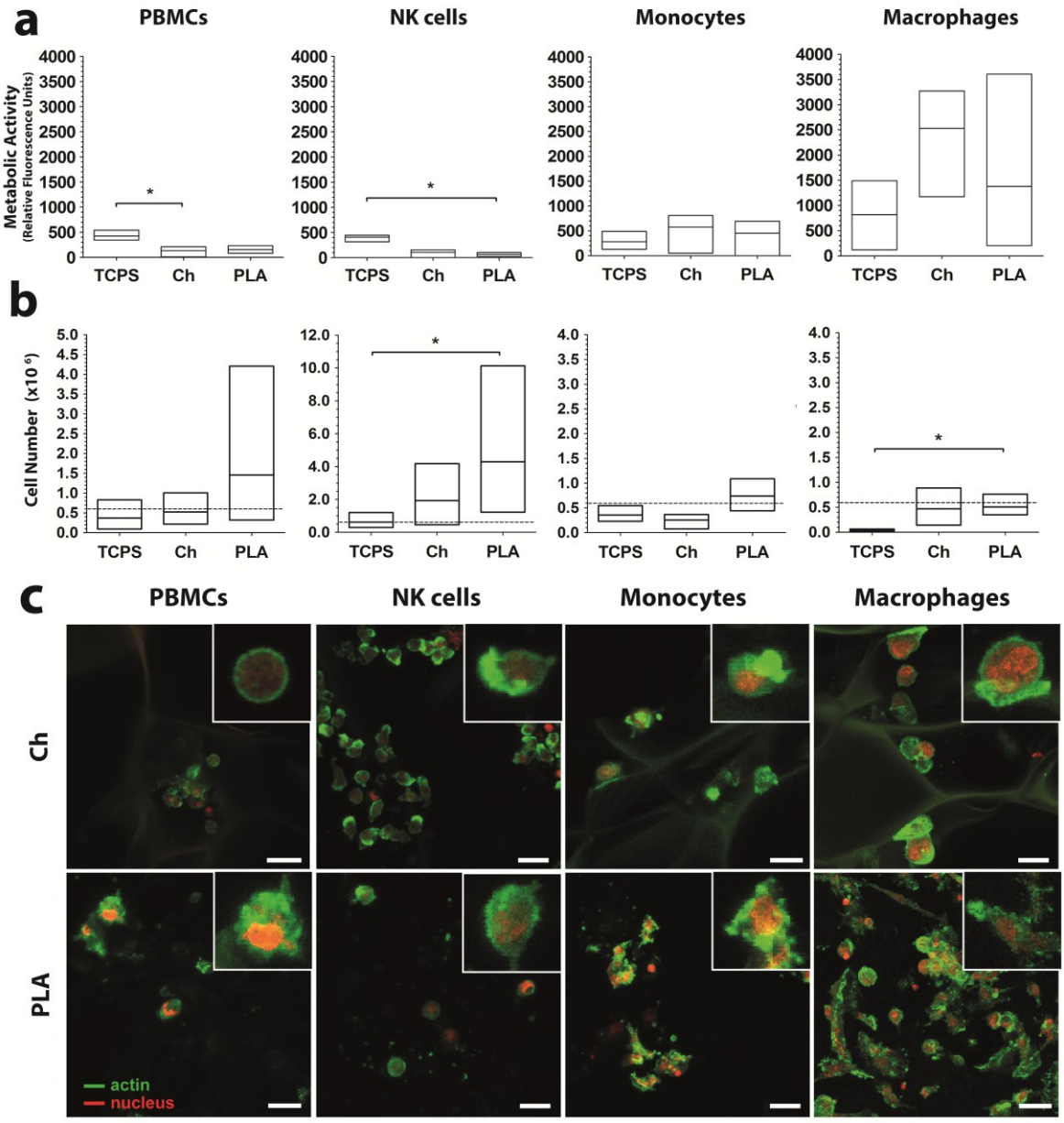

Figure 2 - Modulation of immune cell behaviour by distinct materials. (a) Metabolic activity, (b) cell number and (c) morphology were determined for immune cells incubated for 48 hrs or 9 days (Macrophages) on 2D TCPS or in 3D scaffolds of chitosan or PLA. n=3 (a) Metabolic activity was estimated with a resazurin assay. The background fluorescence intensity obtained in the presence of each material was subtracted to experimental values. (b) Cell number was estimated by quantifying the amount of DNA with Quant-IT Picogreen. The dashed line indicates the number of cells initially seeded. (c) To visualize cells, scaffolds were fixed and stained for actin (green) and the nuclei (red) before being visualized by laser scanning confocal microscopy. Chitosan scaffolds

can be observed in green due to their autofluorescence. Scale Bar, 12.5 μm. Data is represented as floating bars with line at the mean ± maximum to minimum value.

Visualization of the cells upon actin staining revealed that in all cases cells were distributed throughout the scaffolds (Supplementary Figure S2). A more detailed observation suggests that NK cells adopted a more elongated morphology, with polarized actin, when in chitosan scaffolds than in PLA (Figure 2c). Furthermore, an irregular morphology with extensive actin protrusions was frequently observed for macrophages in PLA but not in chitosan. Some cell fragmentation was noticed, consistent with minor cell death within the scaffolds, as anticipated from the results obtained when estimating the number of cells by DNA quantification (Figure 2b). Very few giant cells were observed for either PLA or chitosan scaffolds.

3.3.3 Cytokine secretion

Since macrophages showed the highest metabolic activity in the presence of 3D biomaterials their supernatants were analyzed for the presence of 40 inflammatory mediators with antibody arrays. Importantly, materials had a profound effect on the secretion profile of these macrophages **(Figure 3a)**. ELISA was performed to quantify the inflammatory mediators that achieved quotients of signal intensity higher than 0.3: IL-6, IL-8, MIP-1α, MIP-1β, MCP-1 and RANTES **(Figure 3b)**.

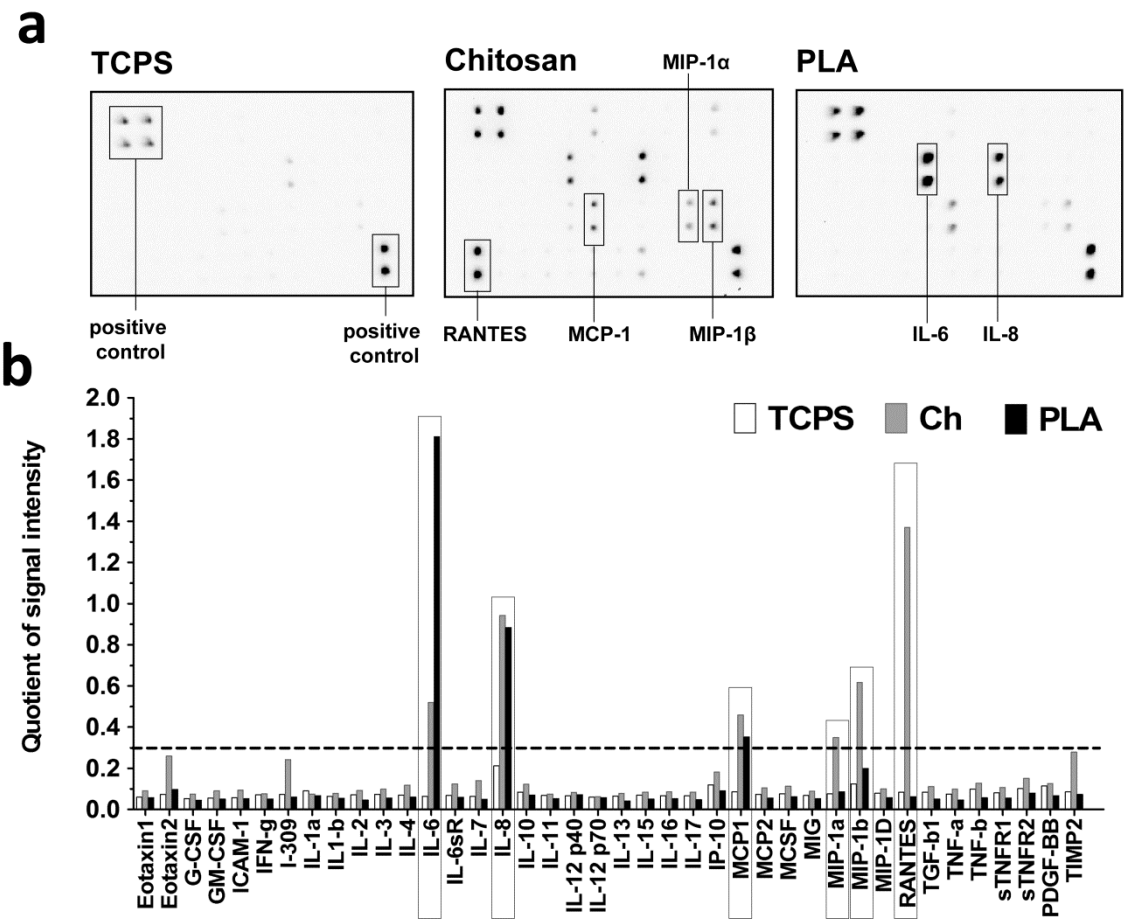

Figure 3 - Protein array of macrophage-secreted cytokines upon culture on distinct materials. Macrophages were allowed to differentiate in the materials for 7 days, washed and cultured in serum free medium for another 48 hrs. Media was collected and analysed by protein arrays. (a) Developed membranes of a protein array used to analyse supernatants from macrophages cultured in different materials. (b) The average intensity of signal detected for each molecule in the protein arrays was divided by the average intensity of signal detected for the positive controls. Cytokines reaching a quotient of signal intensity (Q.S.I.) higher than 0.3 (dashed line) were selected for ELISA quantification (box).

Distinct immune populations were cultured in the different materials **(Figure 4)** and it was found that PBMC secreted low amounts of IL-6, MIP-1α and MCP-1 and expressed high levels of IL-8 with no statistical differences when incubating with the different materials. NK cells secreted more RANTES when cultured on 2D TCPS than in 3D chitosan or PLA scaffolds. Monocytes showed a trend to express more IL-6 and MIP-1α when in chitosan and PLA scaffolds than when with TCPS while their culture in PLA induced a significantly higher expression of IL-8 than on 2D TCPS or in 3D chitosan scaffolds. No differences

were found for MCP-1 between materials and MIP-1β was not detected in monocyte supernatants. Most interestingly, when these cells were allowed to differentiate into mature macrophages there was secretion of IL-6, IL-8 and MCP-1 for PLA while the interaction with chitosan scaffolds lead to secretion of IL-8, MIP-1α, MIP-1β, MCP-1 and RANTES. There was no correlation between the purity of the immune cell populations and the concentration of secreted cytokines **(Supplementary Figure S3).**

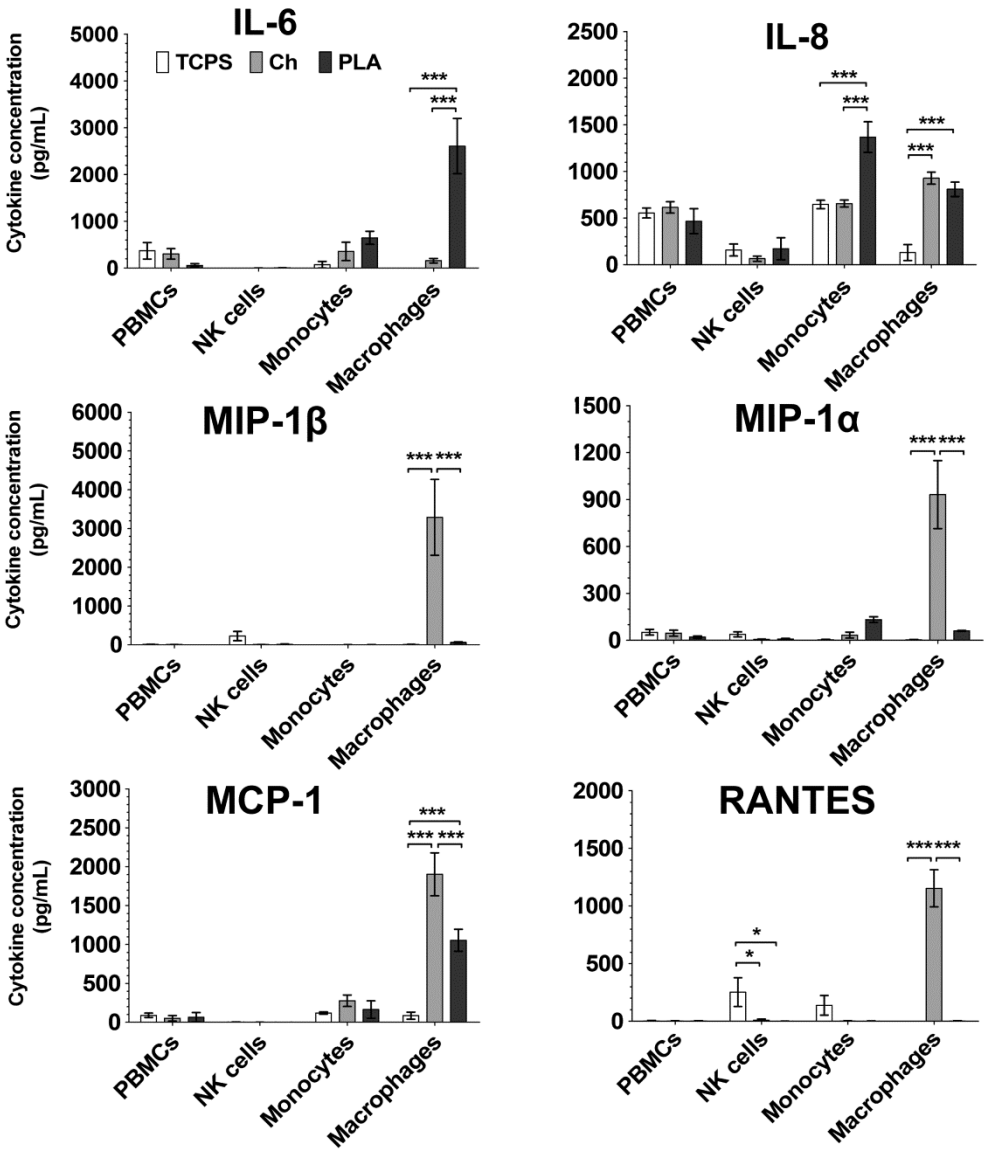

Figure 4 - Cytokine secretion profile of PBMC, NK cells, monocytes and macrophages cultured on distinct materials. PBMC, NK cells and monocytes were cultured for 48 hrs on 2D TCPS or in 3D chitosan and PLA scaffolds. Macrophages were allowed to differentiate in the materials for 7 days, washed and cultured in serum free medium for another 48 hrs. Media was collected and analysed by ELISA. The amounts of IL-6, IL-8, MIP-1α, MIP-1β, MCP-1 and RANTES present in the supernatants from immune cells from 5 donors were quantified by ELISA. $p < 0.05$ (*) and $p < 0.001$ (***).

Thus, the secretion profile of PBMC was not affected by the material while NK cells showed decreased production of RANTES in the 3D biomaterials. And of significant importance, differentiation of monocyte-derived macrophages on PLA and chitosan scaffolds led to secretion of inflammatory mediators known to stimulate MSC recruitment.

3.3.4 MSC recruitment and motility in 3D microenvironments

Different materials impacted on different immune cells, with PLA and even more strongly chitosan stimulating macrophage activity and chemokine secretion. Therefore, we sought to understand the functional consequences of this material-cell interaction on human stem cell recruitment. To investigate this, a modified Boyden chamber invasion assay was performed. PLA or chitosan scaffolds were placed on a well of a 24 well plate, and a Matrigel-coated transwell chamber was inserted on top of it. Then, human MSC were allowed to migrate for 24 hrs towards the bottom well with the scaffolds seeded with different immune populations (PBMC, NK cells, monocytes or macrophages). To ensure that immune cells had time to produce paracrine factors, immune cells were cultured in DMEM without serum for 24 hrs and only then was the invasion assay performed. To analyse the role of macrophages, monocytes were allowed to differentiate in the different materials for 7 days.

Chitosan scaffolds by itself showed a trend to recruit more MSC compared with TCPS and PLA negative controls **(Figure 5)**. PBMC were not capable of relevant MSC recruitment independently of the substrate, with the number of recruited MSC being very similar to the negative controls. On the other hand, NK cells on 2D TCPS were able to recruit 4.5 times more MSC than in the control. This value decreased to 1.9 and 2.1 times in chitosan and PLA 3D scaffolds, respectively. Monocytes on 2D TCPS showed a 5.8 fold increase in MSC recruitment compared with the negative control. However, monocyte interaction with chitosan and PLA scaffolds hindered this increase to 1.2 and 1.5 fold, respectively. Importantly, when these cells were differentiated into macrophages the number of recruited MSC was decreased on 2D TCPS but was markedly higher when in contact with chitosan and PLA scaffolds. Indeed, macrophages were able to recruit 3 and 2.1 times more MSC for chitosan and PLA against 1.9 fold observed for TCPS. Thus, NK cells and monocytes on 2D TCPS led to a high number of recruited MSC but when differentiated in the presence of either chitosan or PLA scaffolds macrophages were the most effective in recruiting MSC **(Figure 5)**, in agreement with the secretion profile found for these cells.

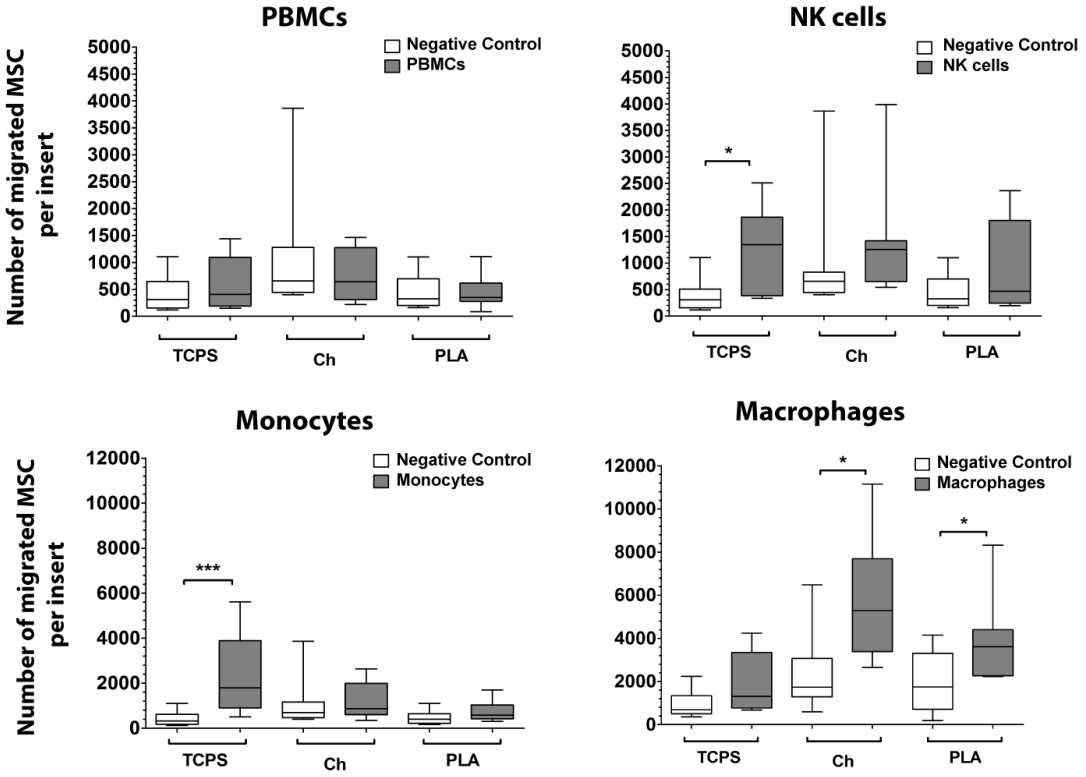

Figure 5 - MSC recruitment promoted by immune cells in different materials. Invasion assays were performed in the presence of the indicated immune cells that were pre-incubated for 24 hrs on 2D TCPS or in chitosan (Ch) or PLA 3D scaffolds. MSC were placed on the top chamber and allowed to migrate for 24 hrs. Graphs are box and whiskers plots with median ± maximum to minimum value. n=6-8, $p < 0.05$ (*) and $p < 0.001$ (***).

To understand whether the presence of macrophages would encourage not only MSC recruitment but also MSC motility within the 3D scaffolds, the dynamical behaviour of the cells was imaged throughout 7 days as previously described[21]. Tracking Dendra2 labelled and photo-marked MSC revealed that 3D MSC motility in the absence of immune cells was similar for PLA and chitosan scaffolds. But interestingly, there was a 44% increase in the cells motility within chitosan scaffolds at day 7 when MSC were co-cultured with macrophages **(Figure 6a and b)**. The same co-culture led to a 17% decrease in cells motility in PLA scaffolds **(Figure 6c)**. Thus, interactions between macrophages and chitosan scaffolds led to the highest increase in both MSC recruitment and motility.

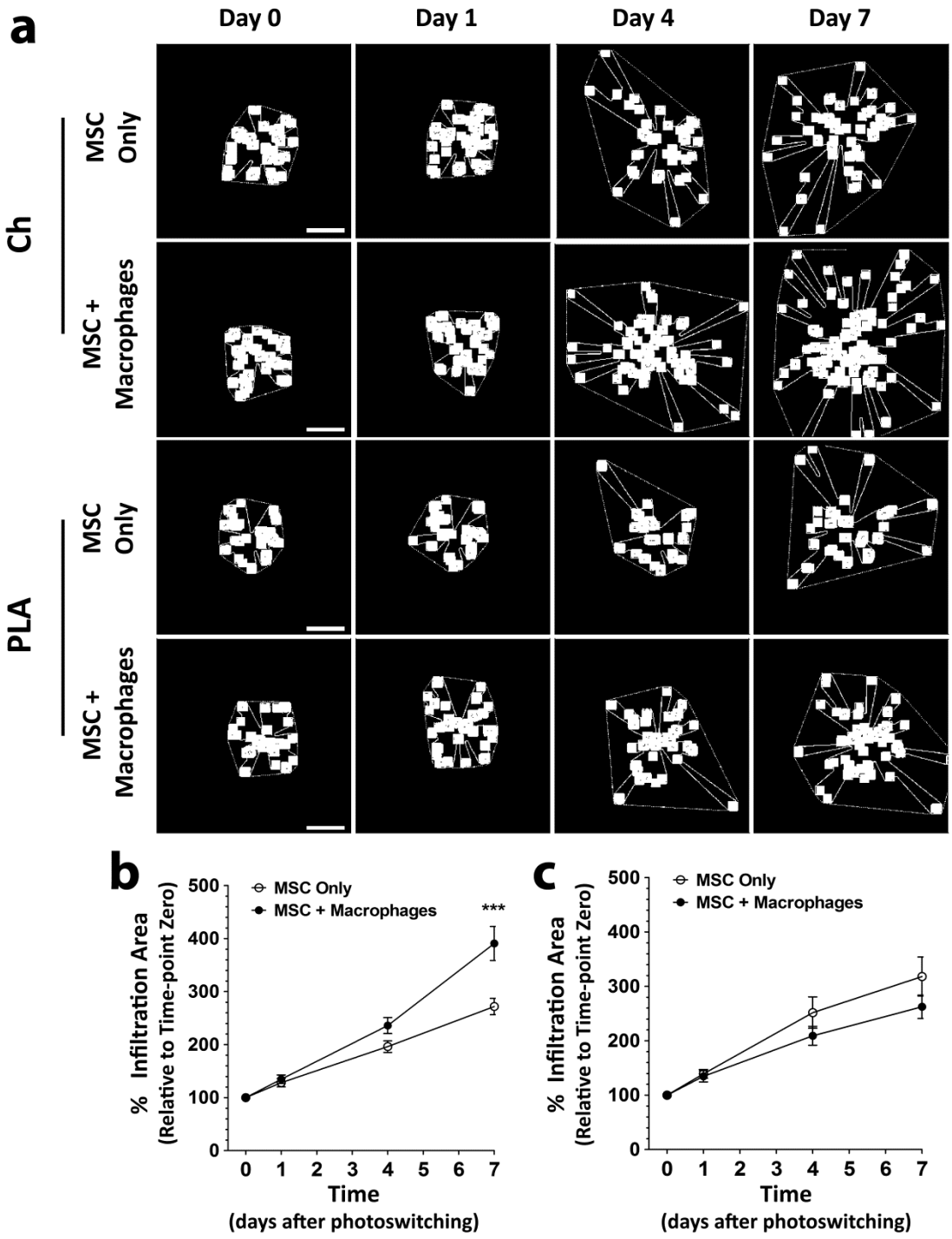

Figure 6 - MSC motility is stimulated by macrophages in chitosan but not in PLA scaffolds. (a) Processed images of MSC in chitosan and PLA 3D matrices alone or co-cultured with macrophages (1:3 ratio) over a period of 7 days obtained by a customized Matlab® plugin. The infiltration area increase over time in a 3D image stack was estimated using *Dendra2imaging* Matlab® plugin. White squares represent the photomarked cells position. The outer circle represents convex hull contour while internal radial dotted line represents the area occupied by photo-marked cells automatically quantified over distinct time-points. Scale bar, 250 μm. The infiltration area at time-points

1, 4 and 7 days was calculated and normalized to time-point zero, for cells in (b) chitosan and (c) PLA scaffolds. $p < 0.001$ (***), n=5 donors.

3.4 Discussion

Here, we investigated which immune cells are activated by PLA and chitosan scaffolds in such a way that promotes stem cell recruitment and motility. While the type of scaffold influenced the extent and type of immune cell responses, it was the cell type that led to major differences in promoting MSC recruitment.

In this study, to avoid interference of unknown molecules in the secretion profile and cell recruitment assays, experiments were performed after washing and in the absence of serum. However, immune responses can depend on the proteins adsorbed to the materials surface and this should be addressed in future studies. Also, provisional matrix formation includes dynamic adsorption and desorption of several serum proteins, the Vroman effect, and this can lead to another level of complexity: activation of complement and coagulation systems, which are difficult to mimic.

Here, the number of NK cells increased when cultured on 3D materials for 48 hrs without any other stimuli, especially on PLA, suggesting that these biomaterials can trigger NK cell proliferation. Indeed, cell culture in a 3D spatial arrangement has been reported to affect a range of cellular functions, including cell proliferative index and gene expression, compared with 2D substrates [22,23]. Moreover, similar observations were found between 3D matrices with distinct properties[24]. Nevertheless, the cells metabolism was reduced when in contact with the scaffolds, indicating that individual cells are less active. Since resazurin conversion rate depends on the cells metabolic pathway, which is modulated by oxygen availability[25], the decreased metabolic activity in the scaffolds could be related to hypoxic gradients created by the matrix architecture and culture density in these 3D biomaterials[26,27]. Similarly to other studies, NK cells on 2D TCPS secreted high levels of RANTES and IL-8 and low amounts of MIP-1α and MIP-1β[28]. It has also been recently shown that NK cells secrete NAP-2 when on TCPS but its production in the presence of biomaterials remains unknown[29]. However, secretion of MIP-1α, MIP-1β and RANTES which can stimulate MSC recruitment was abrogated when NK cells were cultured with chitosan or PLA scaffolds. In agreement with this, NK cells were able to recruit MSC when on TCPS but not in the 3D biomaterials. Thus, the role of these cells as promoters of stem cell recruitment may be hindered during the acute response to biomaterials.

As for monocytes, their number and metabolic activity was maintained upon incubation with the different materials. However, monocytes secreted higher levels of IL-8 in PLA while RANTES was expressed on TCPS but absent in the biomaterials. Similar to NK cells, monocytes had an improved capacity to promote MSC recruitment on TCPS but lost this ability in the presence of the 3D biomaterials. RANTES can impact on MSC chemotaxis and also on other key functions linked with their regenerative potential. Indeed, it was recently shown that the immunosuppressive ability of MSC relies on STAT-1 signalling [30], which in these cells can be specifically activated by RANTES [31,32]. Therefore, interactions of monocytes and NK cells with biomaterials hamper expression of key chemokines and, as a consequence, MSC recruitment. It will be of interest to find strategies to modify biomaterials to stimulate NK cells and monocyte-mediated MSC recruitment.

The purity of the enriched population is an important issue to consider when interpreting the results of secreted inflammatory mediators. The percentage of NK cells and monocytes used specifically for the ELISA measurements was higher than 81%, being on average 89% and 90%, respectively. The contaminant population was CD3- and thus probably includes B cells, dendritic cells and monocytes or NK cells, respectively. It is unlikely that these contaminant cells are the contributors to the cytokine levels since there was no correlation between the percentage of cells of each population and the levels of secreted mediators **(Supplementary Figure S3)**.

Contrary to the other immune cell populations analysed, macrophages differentiated in the presence of PLA or chitosan scaffolds showed high levels of metabolic activity. This difference was not perceived for their precursor cell, suggesting that monocyte to macrophage differentiation is needed to yield this response. There was probably an increased conversion of resazurin to resorufin due to abundant mitochondrial ROS production by macrophages interacting with the scaffolds. Indeed, we noticed that macrophage culture in 3D biomaterials lowered the pH of culture medium to levels below 3.8, particularly with chitosan, suggesting a more intense reaction in the presence of this material. Although monocytes could be cultured for 48 hrs on 2D TCPS surfaces, their prolonged incubation on this surface led to poor cell survival. This suggests that monocytes failed to remain attached on TCPS for a 7 day period, which led to a decrease in the number of monocyte-derived macrophages probably due to anoikis[33,34]. Interestingly, the same outcome was not verified for macrophages incubated in the 3D biomaterials, indicating that the 3D scaffold microenvironment stimulated macrophage metabolism and survival. This will have an impact on the levels of cytokines being

produced by monocyte-derived macrophages on 2D TCPS, which thus cannot be compared with the levels found for cells incubated with the 3D biomaterials.

It has previously been shown that 3D PLA and chitosan scaffolds lead to production of a mixture of cytokines characteristic of both M1 and M2 macrophages[14]. However, the over simplistic M1 or M2 classification remains controversial and analysis of the functional outcome of macrophage behaviour induced by biomaterials on MSC behaviour recruitment might be more useful[35]. Distinct biomaterials had a profound effect on macrophages secretion profile, with PLA stimulating secretion of IL-6 and IL-8 while chitosan led to increased IL-8, MCP-1, MIP-1α and MIP-1β and RANTES production. IL-6, IL-8, MIP-1α, MIP-1β, MCP-1 and RANTES have all been implicated as potent chemotactic agents for MSC recruitment[32,36-39]. Also, upon biomaterial interaction macrophages can produce an array of pro-inflammatory cytokines and chemokines that have been reported to exacerbate the expression of CCR2, CCR3 and CCR4 receptors on MSC[31,32]. Thus, this synergism could be the basis for the ability of monocyte-derived macrophages to recruit MSC when interacting with the 3D materials. Interestingly, analysis of the cells motility within 3D matrices has revealed that MSC motility within PLA and chitosan is very similar but that macrophages stimulated MSC movement when in chitosan but not in PLA. MSC movement in 3D microenvironments might be favoured by increased local concentrations of collagenases and gelatinases, which is promoted by pro-inflammatory environments. In fact, a strong increase in expression of MMP-1, -3, -9 and MMP-13 has been reported for MSC upon treatment with inflammatory cytokines[32,40]. Moreover, it has been previously demonstrated that chitosan leads to enhanced activity of MMP-9 produced by macrophages[41]. Therefore, differences in the inflammatory milieu could explain why macrophages encouraged MSC motility within chitosan scaffolds but not for PLA.

PBMC consist of a heterogeneous population that includes mostly monocytes and T lymphocytes but also B, NK and NKT lymphocytes, thus allowing immune cell crosstalk to occur. PBMC showed no significant differences in their cell number when in the presence of scaffolds. Moreover, metabolism did not correlate with the cell number as there was a significant decrease of cells metabolic activity when cultured in 3D materials, similarly to what was observed with NK cells. Additionally, PBMC secreted low amounts of IL-6, MCP-1 and MIP-1α with a reasonable expression of IL-8 that was material-independent. Concomitantly, PBMC did not stimulate MSC recruitment, independently of the material, suggesting that either the total number of monocytes/macrophages or NK cells found in PBMC was not sufficiently high to stimulate MSC recruitment or that interactions between the different immune cell populations might inhibit production of important chemokines.

3.5 Conclusion

In summary, this work provides a comprehensive analysis of primary human responses triggered by different 3D biomaterials and the functional consequence of those responses on recruitment and motility of primary human MSC **(Figure 7)**. PBMC and NK cells showed an increased cell number in PLA and expressed an unfavourable secretion profile when interacting with chitosan or PLA scaffolds, and did not stimulate MSC recruitment. Importantly, monocyte-derived macrophages but not monocytes yielded the highest MSC recruitment when interacting with these biomaterials. This may imply that stem cell recruitment is only signalled at later stages of host response and that it is promoted by mature macrophages. Moreover, the impact of macrophages on MSC motility was biomaterial-dependent. This stem cell dynamical behaviour can be essential for the regenerative switch from detrimental inflammatory response to constructive remodelling.

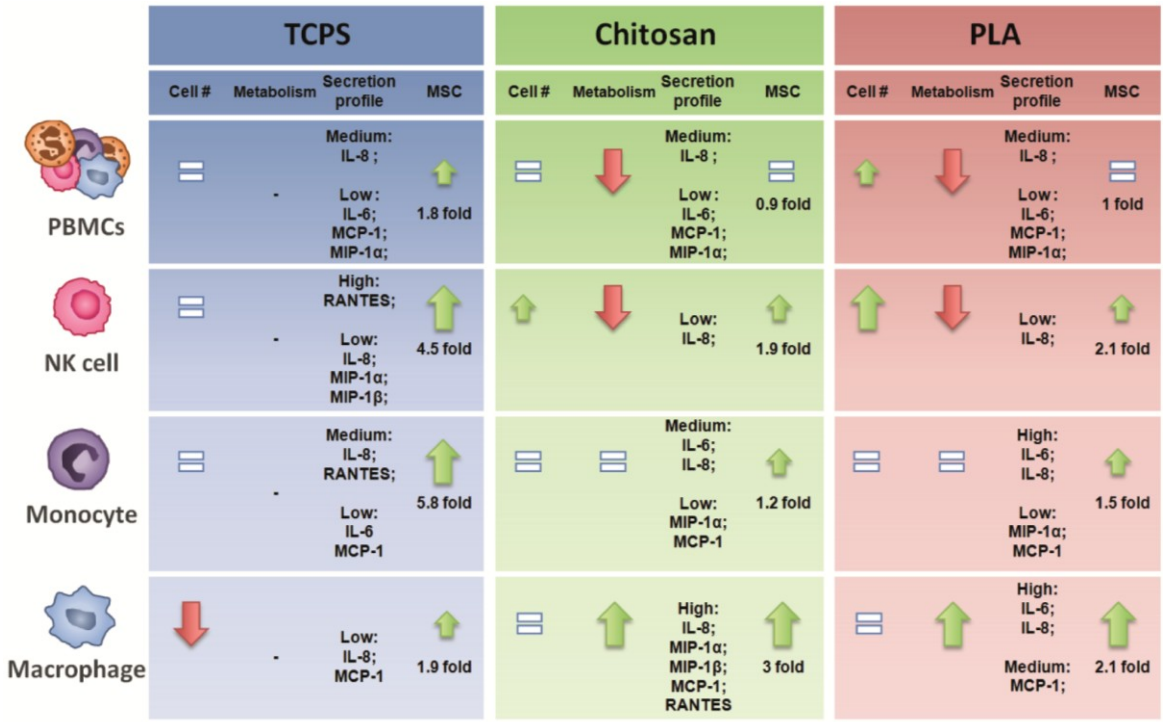

Figure 7 - Summary of PBMC, NK cell, monocyte and macrophage behaviour when in contact with 2D TCPS or 3D chitosan and PLA scaffolds and their impact on MSC recruitment. Cell number (#) is compared with the initial number of seeded cells. Metabolic activity of cells in 2D TCPS was considered baseline (-) for comparisons with chitosan and PLA scaffolds. Recruitment of MSC in relation to each negative control is indicated.

3.6 Material & Methods

3.6.1 Scaffold Fabrication

PLA scaffolds: Poly-96L/4DL-lactic acid (from PURAC, Netherlands) was used. PLA scaffolds were fabricated by solvent casting and particle leaching as previously described[42]. A 5% (w/v%) PLA solution in chloroform was mixed with sieved sodium chloride (NaCl) measuring between 75 and 150 µm. The slurry was cast into 24 well Teflon moulds until complete chloroform evaporation. NaCl particles were dissolved by immersing the cylinders in distilled water.

Chitosan scaffolds: Chitosan (France-Chitine) was purified as described[43]. Chitosan sponges were prepared by freeze-drying using a 2% solution of chitosan (degree of acetylation: 12.00 ± 2.35%, molecular weight: 324 ± 27 x 10^3) as in [19,43]. Briefly, chitosan was hydrated overnight at 4 ºC and dissolved by adding acetic acid (Panreac) to a final concentration of 0.2 M under strong vortex agitation. The chitosan solution was incubated for 24 hrs at 4 ºC, was centrifuged at 4165 g for 5 min and then 800 µl was added to each well of a 48-well plate. Plates were placed at -20 ºC and freeze-dried at -80 ºC for 48 hrs to produce scaffolds.

Both PLA and chitosan scaffolds were cut into a cylinder shape of 11 mm diameter and 2 mm height (20.2 ± 0.5 mg and 5.8 ± 0.5 mg average weight for PLA and chitosan, respectively) and disinfected as in [19].

3.6.2 Scanning electron microscopy characterization of 3D scaffolds

Cross-sections of 2 mm thickness were cut in liquid nitrogen and mounted with carbon tape for scanning electron microscopy (SEM) analysis. Samples were sputter-coated with gold and observed with a JEOL JSM-6301F SEM, at 1 kV and amplifications of 1000X or 250X. Pore diameter was measured with ImageJ software.

3.6.3 Measurement of endotoxin levels

PLA and chitosan extracts were prepared by cutting the scaffolds into small pieces that were suspended in 40 ml endotoxin-free water per gram of dry polymer, and incubated for 24 h at 50 ºC under continuous shaking (250 rpm), as described elsewhere[44]. Endotoxin detection was performed by Analytical Services Unit of iBET, Oeiras, Portugal using a Charles River endotoxin detection kit.

3.6.4 Cells

Human bone marrow MSC (Lonza) were cultured in MSC growth medium (DMEM with low glucose supplemented with Glutamax plus 10% MSC selected inactivated FBS and 1% penicillin/streptomycin (all from Invitrogen)). Cells were incubated at 37ºC/5% (V/V) CO_2 and medium was changed twice per week until cells reached approximately 80% confluence. For expansion, cells were detached by treatment with 0.05% trypsin/EDTA (Invitrogen) and replaced in 150 cm^2 tissue culture flasks (BD Falcon). MSC were used at passages 5-8. PBMC, NK cells and monocytes were obtained from buffy coats of healthy human donors, kindly provided by Centro Hospitalar de São João after patients informed consent and ethics committee approval. Briefly, a PBMC suspension was prepared by density gradient centrifugation and NK cells were purified by negative selection using the EasySep human NK cell enrichment kit (StemCell Technologies), as detailed elsewhere[12]. Human monocytes were isolated by negative selection using a RosetteSep human monocyte enrichment cocktail (StemCell Technologies), as previously described[14]. PBMC, NK cells and monocytes used in the following experiments were isolated from the same donor. The percentages of CD56+CD3- cells for the isolated NK cells and CD14+CD3- for monocytes were on average 89±6% and 87±8%, respectively, as confirmed by flow cytometry. Macrophages were differentiated from monocyte-enriched populations by culturing directly on 2D TCPS (Tissue Culture Polystyrene) surfaces or in PLA and chitosan 3D scaffolds for 7 days in RPMI medium supplemented with 1% penicillin/streptomycin and 10% inactivated FBS. Cells were cultured in the absence of any additional growth factors/cytokines such as M-CSF or GM-CSF.

3.6.5 Cell seeding

To understand how distinct materials affected immune cells, PBMC, NK cells or monocytes isolated from the same donor were ressuspended in DMEM without serum and seeded on 2D TCPS or in PLA or chitosan 3D scaffolds. For that, 25 µl of cell suspension was added to each side of the scaffold with a total of 6×10^5 immune cells per scaffold. Then, the seeded scaffolds were incubated for 4 hrs at 37ºC/5% (V/V) CO_2 to promote cell adhesion before adding 750 µl of DMEM without serum. Cell culture proceeded for 48 hrs. For macrophages, 6×10^5 monocytes were seeded as described and allowed to differentiate in the materials for 7 days in 750 µl of RPMI medium supplemented with 1% penicillin/streptomycin and 10% inactivated FBS. Then, this culture medium was carefully removed and washed with PBS before adding 750 µl DMEM medium without serum and culturing for another 48 hrs.

3.6.6 Metabolic activity

The metabolic activity of PBMC, NK cells and monocytes that had interacted for 48 hrs with the materials, or macrophages that had been in culture for 9 days with the scaffolds was assessed with a resazurin assay as described elsewhere[45]. Values obtained with scaffolds incubated in the absence of cells were subtracted in the final analysis.

3.6.7 DNA quantification

PLA and chitosan scaffolds were washed in PBS, thinly cut and incubated in 1% triton X-100 (Sigma) at 4°C under agitation for 1 hr. To reduce the effects of triton X-100 (Sigma) in DNA quantification, the solutions were diluted in PBS for a final concentration of 0.1% triton X-100. Then, scaffolds were vortexed and Quant-iT™ PicoGreen dsDNA Reagent (Invitrogen) was used according to the manufacturer's protocol to quantify DNA content. To estimate the number of cells on the scaffolds, a standard curve was prepared using samples with a known number of PBMC, NK cells and monocytes.

3.6.8 Nuclei and actin staining

For analysis of cellular morphology, cells were stained for actin and nuclei. After 48 hrs (for PBMC, NK cells and monocytes) or 9 days (for macrophages) of culture in the scaffolds, cells were washed with PBS and fixed with 4% paraformaldehyde for 30 min at 4ºC and washed with PBS. Cells were incubated with phalloidin–AlexaFluor633 (50 µl, Invitrogen) in PBS (1:40) for 1 hr on ice and washed with PBS. Nuclei were then counterstained with propidium iodide (20 µg/ml) for 10 min followed by washing with PBS. Scaffolds were imaged on a laser scanning confocal microscope (Leica TCS SP5 II, model DMI6000B-CS, Bioimaging Center for Biomaterials and Regenerative Therapies, b.IMAGE, Porto).

3.6.9 Protein arrays

Monocyte-derived macrophages were cultured for 7 days on 2D TCPS or in 3D chitosan or PLA scaffolds in RPMI medium supplemented with 1% penicillin/streptomycin and 10% inactivated FBS. Then, culture medium was carefully removed and wells washed with PBS, before adding fresh 750 µl of DMEM without serum. Supernatants were then collected after 48 hrs of cell culture in the designated materials, centrifuged and kept at -80ºC until analysis. A membrane-based Inflammation Array III (Raybiotech) was used to analyse secretion of 40 cytokines according to manufacturer's instructions. Supernatants from chitosan scaffolds incubated without cells were used as a control.

3.6.10 ELISA assays

ELISA assays were performed to quantify secreted cytokines. Supernatants were collected after 48 hrs of immune cell – material interaction, centrifuged and kept at -80ºC until analysis. IL-6, IL-8, MIP-1α, MIP-1β, MCP-1 and RANTES levels were quantified according to manufacturer's instructions (Mini ELISA Development Kits, PeproTech). Concentrations were determined for five donors per condition and values were corrected with the amount determined for materials incubated in the absence of cells.

3.6.11 Invasion assay

Studies on invasion of MSC were performed using a modified transwell chamber system. Membrane filters with a pore size of 8 μm that had been coated with Matrigel (BD Biosciences) were used for the top compartment. Matrigel mimics the extracellular matrix that cells need to invade through in order to arrive to the implant site. The lower compartments of the invasion chamber contained 750 μl of DMEM medium, as a negative control, or immune cells (PBMC, NK cells, monocytes and macrophages) seeded on 2D TCPS or PLA and chitosan 3D scaffolds as already described. Custom spacer rings with 2 mm height were used to maintain the distance between the seeded scaffolds and the transwell insert. Matrigel-coated inserts were pre-incubated for 1 hr with serum-free DMEM before adding MSC at $4x10^4$ cells in 500 μl serum-free DMEM medium. The invasion chambers were incubated for 24 hrs at 37ºC/5% CO_2. After incubation, inserts were washed with PBS and cells were fixed in 4% paraformaldehyde for 20 min at room temperature (RT). Inserts were washed with PBS and kept at 4ºC until analysis. Cells on the top surfaces of filters were wiped off with cotton swabs and the membrane was carefully cut and mounted on a slide with Vectashield and DAPI. Cells that had migrated into the lower compartment and attached to the lower surface of the filter were counted in an inverted fluorescence microscope (ZeissAxiovert). Cell nuclei were counted in ten 200X fields of view for each membrane. The number of migrated cells was estimated by taking into account the area of a field of view and the total area of the membrane.

3.6.12 Photoswitching and imaging Dendra2+ MSC to measure cells motility

MSC motility was estimated by following the behaviour of photo-switched Dendra2+ MSC for up to 7 days, as previously described[21]. Dendra2+ MSC can be converted from green to red fluorescence in defined regions, being then easier to track the cells over long incubation periods that require placing the cells in the incubator between time points. Briefly, cells were transfected by electroporation with Dendra2 plasmid DNA (pDendra2, Clontech) using a X-Cell Gene Pulser (BioRad), with 80% efficiency, as described in [21].

MSC were then seeded on PLA or chitosan scaffolds with a square shape of 4x4 mm and 2 mm height. When mentioned, scaffolds had been previously seeded with 6×10^5 human monocytes which were allowed to differentiate into macrophages for 7 days. Then, 2 $x10^5$ MSC in 25 µL of DMEM medium were added to each side (top and bottom) of a scaffold in non-treated 24 well tissue culture plates. Cells were allowed to adhere to the scaffold for 4 hrs at 37ºC/5% CO_2 and then 400 µL of medium was added. MSC to macrophage ratio was 1:3. Green-to-red Photoconversion was performed with a laser scanning confocal microscope (Leica TCS SP5 II, model DMI6000B-CS, Bioimaging Center for Biomaterials and Regenerative Therapies, b.IMAGE, Porto). The reference red cell population was then used to centre the scaffold, which was imaged 1, 4 and 7 days after conversion (3-5 spots per scaffolds in each individual experiment). After imaging, cells were returned to the incubator and cultured at 37ºC/5%CO_2, until the next imaging time-point.

3.6.13 Dendra2 imaging data analysis - MatLab Plugin

MatLab Plugin: An automatic tool named *Dendra2imaging* was implemented in *MATLAB*^{TM}. This tool enabled analysis of the infiltrated area covered by photo-marked cells in microscopy images acquired in different days. The algorithm defines a threshold value used to bin the input image in order to extract the objects (cells) from their background[46]. For standardization purposes, the same threshold value was applied to images of the same series in distinct experimental conditions, allowing unbiased comparison of cell motility. Based on the segmented image the algorithm automatically estimates the region occupied by cells as well as the convex hull contour of that same region. The region occupied by photo-marked cells was then normalized to the area measured at time-point 0.

3.6.14 Statistical analysis

Statistical analysis was performed using Prism5 software, v5.01. Friedman matched paired test followed by Dunns comparison test was used to compare more than two samples. For grouped samples, two-way ANOVA test was used followed by Bonferroni post-test. Data are mean ± Standard Error of the Mean (SEM) unless stated otherwise. Values of $p < 0.05$ (*), $p < 0.01$ (**) and $p < 0.001$ (***) were considered statistically significant.

3.7 Acknowledgements

The authors would like to thank Centro Hospitalar de São João for kindly donating the buffy coats. This work had the financial support of FCT / MEC through National Funds

and, when applicable, co-financed by the FEDER through the PT2020 Partnership Agreement under the 4293 Unit I&D.

3.8 References

[1] Anderson, J. M. & McNally, A. K. Biocompatibility of implants: lymphocyte/macrophage interactions. *Seminars in immunopathology*, 33, 3, 2011, 221-233.

[2] Sridharan, R., Cameron, A. R., Kelly, D. J., Kearney, C. J. & O'Brien, F. J. Biomaterial based modulation of macrophage polarization: a review and suggested design principles. *Materials Today*, 18, 6, 2015, 313-325.

[3] Caplan, A. I. & Correa, D. The MSC: an injury drugstore. *Cell stem cell*, 9, 1, 2011, 11-15.

[4] Nair, A. *et al.* Biomaterial implants mediate autologous stem cell recruitment in mice. *Acta Biomater*, 7, 11, 2011, 3887-3895.

[5] Herdrich, B. J. *et al.* Regenerative healing following foetal myocardial infarction. *European journal of cardio-thoracic surgery : official journal of the European Association for Cardio-thoracic Surgery*, 38, 6, 2010, 691-698.

[6] Liu, Y. *et al.* Mesenchymal stem cell-based tissue regeneration is governed by recipient T lymphocytes via IFN-gamma and TNF-alpha. *Nature medicine*, 17, 12, 2011, 1594-1601.

[7] Chang, J. *et al.* NF-kappaB inhibits osteogenic differentiation of mesenchymal stem cells by promoting beta-catenin degradation. *Proceedings of the National Academy of Sciences of the United States of America*, 110, 23, 2013, 9469-9474.

[8] Thevenot, P. T. *et al.* The effect of incorporation of SDF-1alpha into PLGA scaffolds on stem cell recruitment and the inflammatory response. *Biomaterials*, 31, 14, 2010, 3997-4008.

[9] Ko, I. K. *et al.* Combined systemic and local delivery of stem cell inducing/recruiting factors for in situ tissue regeneration. *FASEB journal : official publication of the Federation of American Societies for Experimental Biology*, 26, 1, 2012, 158-168.

[10] Agaiby, A. D. & Dyson, M. Immuno-inflammatory cell dynamics during cutaneous wound healing. *J Anat*, 195 (Pt 4), 1999, 531-542.

[11] Anderson, J. M., Rodriguez, A. & Chang, D. T. Foreign body reaction to biomaterials. *Seminars in immunology*, 20, 2, 2008, 86-100.

[12] Almeida, C. R., Vasconcelos, D. P., Goncalves, R. M. & Barbosa, M. A. Enhanced mesenchymal stromal cell recruitment via natural killer cells by incorporation of inflammatory signals in biomaterials. *Journal of the Royal Society, Interface / the Royal Society*, 9, 67, 2012, 261-271.

[13] Anton, K., Banerjee, D. & Glod, J. Macrophage-associated mesenchymal stem cells assume an activated, migratory, pro-inflammatory phenotype with increased IL-6 and CXCL10 secretion. *PloS one*, 7, 4, 2012, e35036.

[14] Almeida, C. R. *et al.* Impact of 3-D printed PLA- and chitosan-based scaffolds on human monocyte/macrophage responses: unraveling the effect of 3-D structures on inflammation. *Acta biomaterialia*, 10, 2, 2014, 613-622.

[15] Sica, A. & Mantovani, A. Macrophage plasticity and polarization: in vivo veritas. *The Journal of clinical investigation*, 122, 3, 2012, 787-795.

[16] Suuronen, R., Pohjonen, T., Hietanen, J. & Lindqvist, C. A 5-year in vitro and in vivo study of the biodegradation of polylactide plates. *Journal of oral and maxillofacial surgery : official journal of the American Association of Oral and Maxillofacial Surgeons*, 56, 5, 1998, 604-614; discussion 614-605.

[17] Dai, T., Tanaka, M., Huang, Y. Y. & Hamblin, M. R. Chitosan preparations for wounds and burns: antimicrobial and wound-healing effects. *Expert review of anti-infective therapy*, 9, 7, 2011, 857-879.

[18] Oliveira, S. M. *et al.* Engineering endochondral bone: in vivo studies. *Tissue engineering. Part A*, 15, 3, 2009, 635-643.

[19] Santos, S. G. *et al.* Adsorbed fibrinogen leads to improved bone regeneration and correlates with differences in the systemic immune response. *Acta biomaterialia*, 9, 7, 2013, 7209-7217.

[20] Navarro, M., Ginebra, M. P., Planell, J. A., Zeppetelli, S. & Ambrosio, L. Development and cell response of a new biodegradable composite scaffold for guided bone regeneration. *Journal of materials science. Materials in medicine*, 15, 4, 2004, 419-422.

[21] Caires, H. R. *et al.* Finding and tracing human MSC in 3D microenvironments with the photoconvertible protein Dendra2. *Scientific reports*, 5, 2015, 10079.

[22] Baharvand, H., Hashemi, S. M., Kazemi Ashtiani, S. & Farrokhi, A. Differentiation of human embryonic stem cells into hepatocytes in 2D and 3D culture systems in vitro. *The International journal of developmental biology*, 50, 7, 2006, 645-652.

[23] Daneshmandi, S., Dibazar, S. P. & Fateh, S. Effects of 3-dimensional culture conditions (collagen-chitosan nano-scaffolds) on maturation of dendritic cells and their capacity to interact with T-lymphocytes. *Journal of immunotoxicology*, 13, 2, 2016, 235-242.

[24] Seo, Y. K. *et al.* Correlation between scaffold in vivo biocompatibility and in vitro cell compatibility using mesenchymal and mononuclear cell cultures. *Cell biology and toxicology*, 25, 5, 2009, 513-522.

[25] Karakashev, D., Galabova, D. & Simeonov, I. A simple and rapid test for differentiation of aerobic from anaerobic bacteria. *World Journal of Microbiology and Biotechnology*, 19, 3, 2003, 233-238.

[26] Jenkins, J., Dmitriev, R. I., Morten, K., McDermott, K. W. & Papkovsky, D. B. Oxygen-sensing scaffolds for 3-dimensional cell and tissue culture. *Acta biomaterialia*, 16, 2015, 126-135.

[27] Volkmer, E. *et al.* Hypoxia in static and dynamic 3D culture systems for tissue engineering of bone. *Tissue engineering. Part A*, 14, 8, 2008, 1331-1340.

[28] Fauriat, C., Long, E. O., Ljunggren, H. G. & Bryceson, Y. T. Regulation of human NK-cell cytokine and chemokine production by target cell recognition. *Blood*, 115, 11, 2010, 2167-2176.

[29] Almeida, C. R., Caires, H. R., Vasconcelos, D. P. & Barbosa, M. A. NAP-2 Secreted by Human NK Cells Can Stimulate Mesenchymal Stem/Stromal Cell Recruitment. *Stem cell reports*, 6, 4, 2016, 466-473.

[30] Mounayar, M. *et al.* PI3kalpha and STAT1 Interplay Regulates Human Mesenchymal Stem Cell Immune Polarization. *Stem cells*, 33, 6, 2015, 1892-1901.

[31] Honczarenko, M. *et al.* Human bone marrow stromal cells express a distinct set of biologically functional chemokine receptors. *Stem cells*, 24, 4, 2006, 1030-1041.

[32] Ponte, A. L. *et al.* The in vitro migration capacity of human bone marrow mesenchymal stem cells: comparison of chemokine and growth factor chemotactic activities. *Stem cells*, 25, 7, 2007, 1737-1745.

[33] Brodbeck, W. G. *et al.* Biomaterial adherent macrophage apoptosis is increased by hydrophilic and anionic substrates in vivo. *Proceedings of the National Academy of Sciences of the United States of America*, 99, 16, 2002, 10287-10292.

[34] Brodbeck, W. G. *et al.* Influence of biomaterial surface chemistry on the apoptosis of adherent cells. *Journal of biomedical materials research*, 55, 4, 2001, 661-668.

[35] Murray, P. J. *et al.* Macrophage activation and polarization: nomenclature and experimental guidelines. *Immunity*, 41, 1, 2014, 14-20.

[36] Rattigan, Y., Hsu, J. M., Mishra, P. J., Glod, J. & Banerjee, D. Interleukin 6 mediated recruitment of mesenchymal stem cells to the hypoxic tumor milieu. *Experimental cell research*, 316, 20, 2010, 3417-3424.

[37] Ringe, J. *et al.* Towards in situ tissue repair: human mesenchymal stem cells express chemokine receptors CXCR1, CXCR2 and CCR2, and migrate upon stimulation with CXCL8 but not CCL2. *Journal of cellular biochemistry*, 101, 1, 2007, 135-146.

[38] Schmal, H. *et al.* Comparison of cellular functionality of human mesenchymal stromal cells and PBMC. *Cytotherapy*, 9, 1, 2007, 69-79.

[39] Pattappa, G. *et al.* CCL5/RANTES is a key chemoattractant released by degenerative intervertebral discs in organ culture. *European cells & materials*, 27, 2014, 124-136; discussion 136.

[40] Ries, C. *et al.* MMP-2, MT1-MMP, and TIMP-2 are essential for the invasive capacity of human mesenchymal stem cells: differential regulation by inflammatory cytokines. *Blood*, 109, 9, 2007, 4055-4063.

[41] Oliveira, M. I., Santos, S. G., Oliveira, M. J., Torres, A. L. & Barbosa, M. A. Chitosan drives anti-inflammatory macrophage polarisation and pro-inflammatory dendritic cell stimulation. *European cells & materials*, 24, 2012, 136-152; discussion 152-133.

[42] Navarro, M., Ginebra, M. P., Planell, J. A., Barrias, C. C. & Barbosa, M. A. In vitro degradation behavior of a novel bioresorbable composite material based on PLA and a soluble CaP glass. *Acta biomaterialia*, 1, 4, 2005, 411-419.

[43] Antunes, J. C. *et al.* Layer-by-layer self-assembly of chitosan and poly(gamma-glutamic acid) into polyelectrolyte complexes. *Biomacromolecules*, 12, 12, 2011, 4183-4195.

[44] Nakagawa, Y. *et al.* Endotoxin contamination in wound dressings made of natural biomaterials. *Journal of biomedical materials research. Part B, Applied biomaterials*, 66, 1, 2003, 347-355.

[45] Bidarra, S. J. *et al.* Injectable in situ crosslinkable RGD-modified alginate matrix for endothelial cells delivery. *Biomaterials*, 32, 31, 2011, 7897-7904.

[46] Otsu, N. A Threshold Selection Method from Gray-Level Histograms. *Systems, Man and Cybernetics, IEEE Transactions on*, 9, 1, 1979, 62-66.

3.9 Supplementary Data

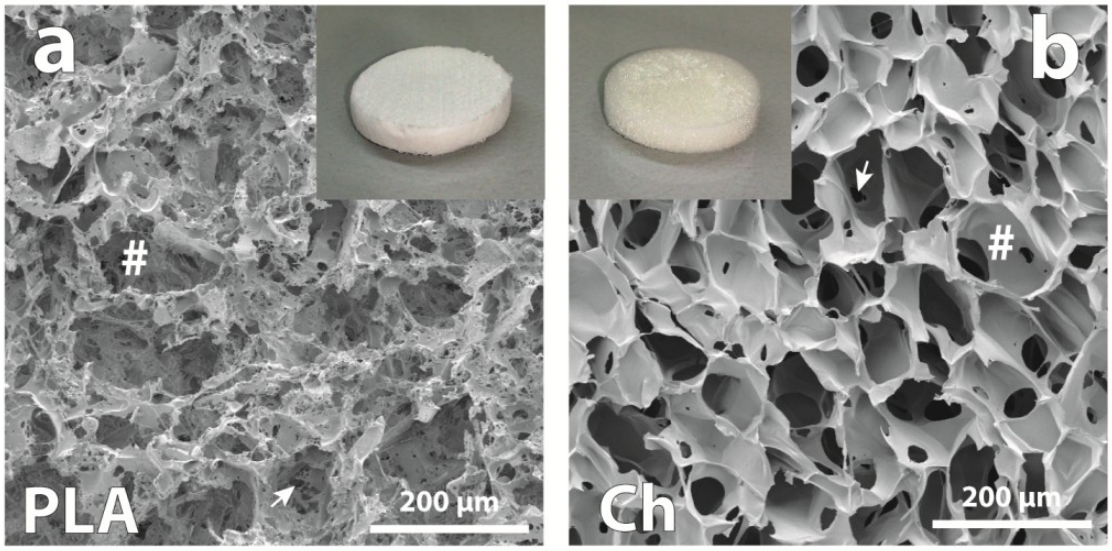

Supplementary Figure S1 - Structure of (a) PLA and (b) chitosan (Ch) scaffolds. Photographs and SEM (Scanning Electron Microscopy) images show the macroscopic and microscopic structure of the scaffolds. The presence of large (#) and small (arrows) interconnecting pores is visible.

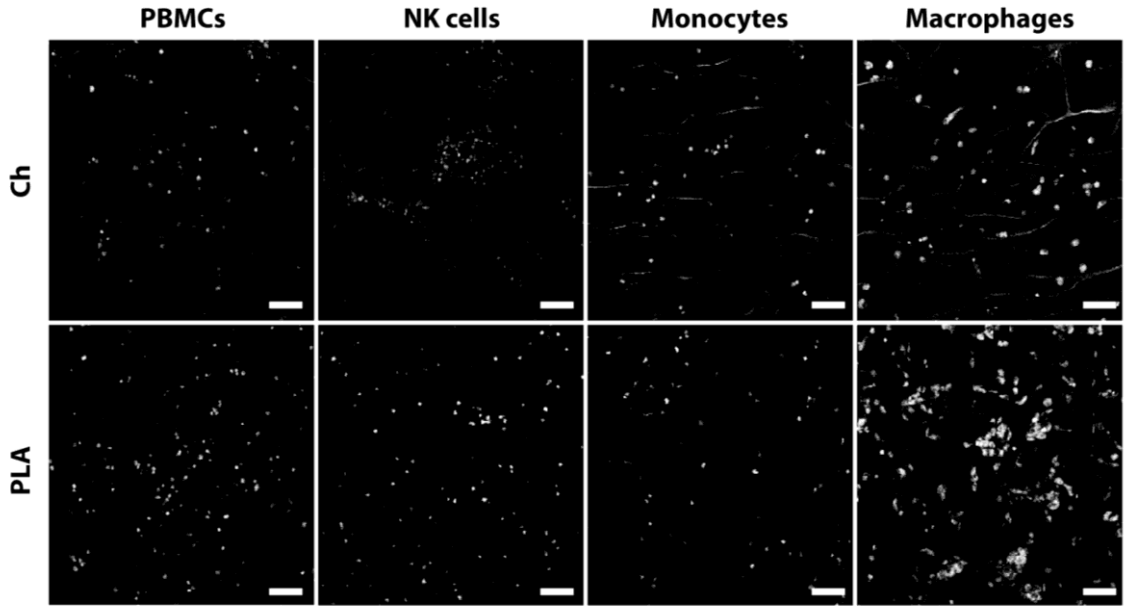

Supplementary Figure S2 - Immune cells are homogenously distributed throughout the scaffolds. Nuclei of cells within (Ch) chitosan (top) and PLA (bottom) scaffolds. Upon cell culture for 2 days (or 9 days for macrophages) in the indicated scaffolds, cells were fixed and stained for nuclei with propidium iodide before being visualized by laser

scanning confocal microscopy. The chitosan scaffolds can be observed due to their autofluorescence. Scale Bar, 100 μm. n=3

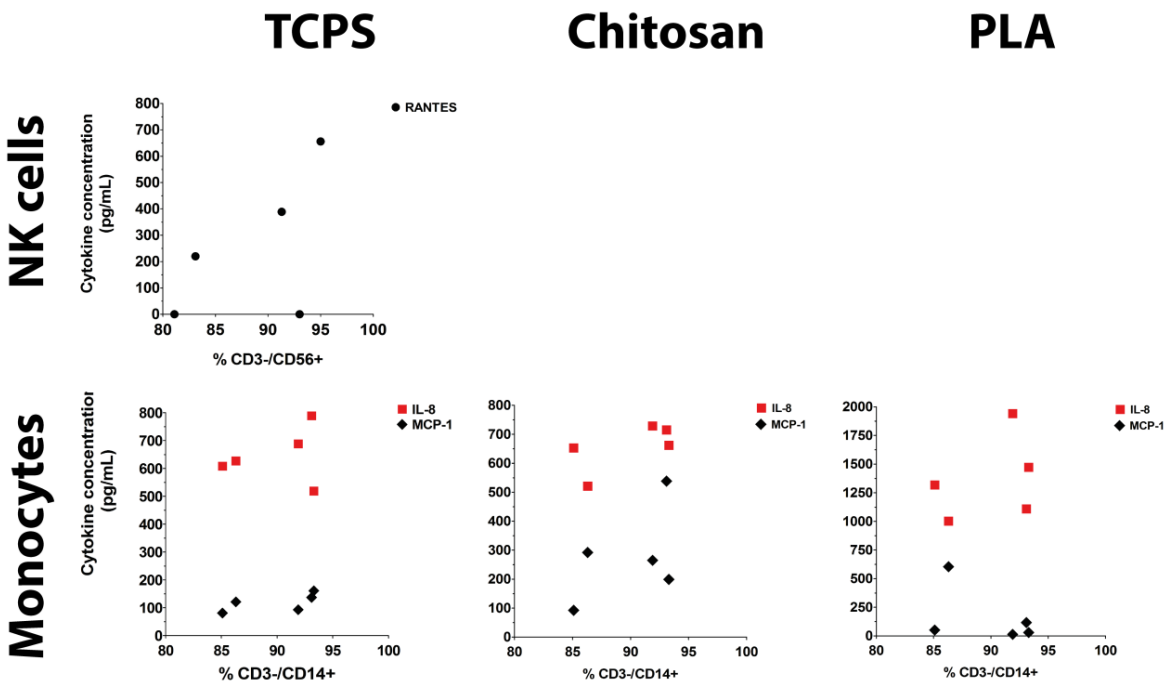

Supplementary Figure S3 - NK cell (top) and monocyte (bottom) purity impact on the production of selected cytokines. No correlation between cell purity and the concentration of cytokines has been found. RANTES: black circles; IL-8: red squares; MCP-1: black diamonds. n = 5 donors.

CHAPTER 4

“DO FUNDO DO FIM DO MUNDO

Do fundo do fim do mundo
Vieram me perguntar
Qual era o anseio fundo
Que me fazia chorar.
E eu disse: «É esse que os poetas
Têm tentado dizer
Em obras sempre incompletas
Em que puseram seu ser.»
E assim com um gesto nobre
Respondi a quem não sei
Se me houve por rico ou pobre.”

14-7-1934

Poesias Inéditas (1930-1935). Fernando Pessoa. Lisboa: Ática, 1955 (imp. 1990) -153.

The contents of this chapter are based on:

A CO-CULTURE SYSTEM WITH THREE DIFFERENT PRIMARY HUMAN CELL POPULATIONS REVEALS THAT MSC DIMINISH MACROPHAGE-DRIVEN FIBROBLAST RECRUITMENT

Hugo R. Caires [1,2,3]

Patrícia Silva [2,3]

Mário A. Barbosa [1,2,3]

Catarina R. Almeida [2,3,4]

[1] ICBAS - Instituto de Ciências Biomédicas Abel Salazar, Universidade do Porto, Rua Jorge Viterbo Ferreira, 228, 4050-313 Porto, Portugal

[2] i3S - Instituto de Investigação e Inovação em Saúde da Universidade do Porto, Rua Alfredo Allen, 208, 4200-135 Porto, Portugal Portugal

[3] INEB - Instituto de Engenharia Biomédica, Porto, Portugal

[4] Department of Medical Sciences and Institute for Biomedicine - iBiMED, University of Aveiro, 3810-193 Aveiro, Portugal (current address)

Manuscript in preparation, **(2016)**

4.1 Abstract

The biological response to implanted biomaterials is a complex and highly coordinated phenomenon involving many different cell types that interact within 3D microenvironments. Here, we increased the complexity of a 3D platform to include at least three cell types that play a role in the host response upon scaffold implantation. With this system it was possible to address how immune responses triggered by 3D biomaterials mediate recruitment of cells that promote tissue regeneration, MSC, or a foreign body response, fibroblasts. Primary human macrophages yielded the highest fibroblast recruitment when interacting with chitosan scaffolds but not PLA. Interestingly, when there were MSC and fibroblasts in the same environment, macrophages differentiated in chitosan scaffolds again promoted a significant increase on fibroblast recruitment, but not of MSC. However, macrophages that were firstly allowed to interact with MSC within the scaffolds were no longer able to recruit fibroblasts. Overall, this study strength the idea that *ex vivo* predictive systems need to consider the different players involved in the biological response to biomaterials and that timing of arrival of specific cell types will affect the outcome. This 3-cell-3D platform might be used as tool to predict the impact of novel immunomodulatory materials for tissue regeneration.

KEYWORDS: Inflammation; 3D Biomaterials; Macrophage; Fibroblasts; Mesenchymal stem cell; Recruitment; Primary Human Cells

4.2 Introduction

Implantation of regenerative biomaterials triggers two opposing types of host responses: an immune reaction against the foreign body material[1,2] and tissue repair/regeneration[3,4]. While the beneficial aspects of this immune reaction, such as debris clearance and progenitor cell recruitment, initiate healing[5], their potentially damaging effects, such as excessive inflammation followed by fibrotic encapsulation of a biomaterial should be minimized for scaffold-guided regeneration to succeed[6].

MSC display the ability to migrate to inflamed tissues, can secrete a plethora of bioactive molecules with immunomodulatory and pro-regenerative action, and can differentiate in different lineages to directly replace damaged cells[7]. Thus, MSC have become an attractive target in many regenerative strategies, including stem cell therapy, implantation of classically engineered cell-scaffold tissue constructs and lately for *in situ* tissue engineering[8]. While MSC have a pivotal role in supporting the regenerative process, fibroblasts are perceived as critical effector cells in foreign body response (FBR) through exacerbated production of extracellular matrix (ECM) components[9] and secretion of pro-inflammatory cytokines[10,11]. Importantly, colonization of an implanted scaffold by blood-derived immune cells is the main driver of the inflammatory response, which in turn can mediate recruitment of MSC and/or fibroblasts and heavily influence the healing outcome. Thus, in *in vivo* microenvironments the interactions between different cell types will dictate the regenerative outcome.

In the first 48 hrs upon biomaterial implantation, neutrophils[12], monocytes[13] and Natural Killer (NK) cells[14] are sequentially recruited to cleanse and coordinate the repair of the injured area but also to degrade the foreign material[15]. The recruited monocytes gradually differentiate into macrophages, which replace the exhausted neutrophils and NK cells[6]. Thereafter, macrophages become the dominant infiltrating cells that respond according to the biomaterial properties by secreting large amounts of bioactive mediators that can drive inflammation and tissue repair[6,16-18]. Mediators produced by immune cells can promote recruitment of MSC[19] or other cells such as fibroblasts[11]. Thus, biomaterial-evoked immune responses might control the type of stromal cells recruited and consequently the regenerative outcome.

Previous studies have been performed with co-cultures with only two cell types, investigating the outcome of immune cell – MSC interactions or immune cell – fibroblasts interactions[20-23]. However, there is an increasing demand for *ex vivo* strategies that predict the effect of biomaterials in more complex settings, closer to a physiological

scenario. Here we developed an *in vitro* platform to analyse the interactions between materials and three different types of primary human cells: immune cells, fibroblasts and MSC. As models for biomaterials with distinct physico-chemical properties, we used Poly-Lactic Acid (PLA), an FDA approved synthetic polymer used for bone repair or as internal fracture fixation device[24,25], and chitosan, which is a natural polysaccharide, currently explored for many applications, including wound dressings and bone regeneration[26-28]. Here, we characterized the ability of different human immune cell populations reacting to the different 3D scaffold models to promote fibroblast recruitment and explored how MSC impact on this mobilization.

4.3 Results

4.3.1 MSC-mediated fibroblast recruitment is highly dependent on the biomaterial properties

Many implanted engineered tissue-constructs rely on MSC as a cell source that decreases fibrous capsule thickness and consequently improves tissue integration[29-31]. Fibroblasts are major contributors for the fibrous capsule formation following host response to implanted biomaterials[6]. Thus, we firstly investigated whether MSC seeded within two different model scaffolds modulated recruitment of fibroblasts. For those experiments, a modified Boyden chamber model was used. Briefly, 3D PLA or chitosan scaffolds were placed on 24 well plates and primary human bone marrow MSC were seeded and cultured in DMEM without serum for 24 hrs to ensure production of paracrine factors. Then, primary human dermal fibroblasts (HDF) were added to Matrigel-coated transwells were inserted on top of the chamber and were allowed to migrate for 24 hrs. It was found that MSC seeded in chitosan scaffolds did not promote HDF recruitment (Figure 1a) while MSC in PLA induced a 1.6 fold increase in the number of recruited HDF (Figure 1b).

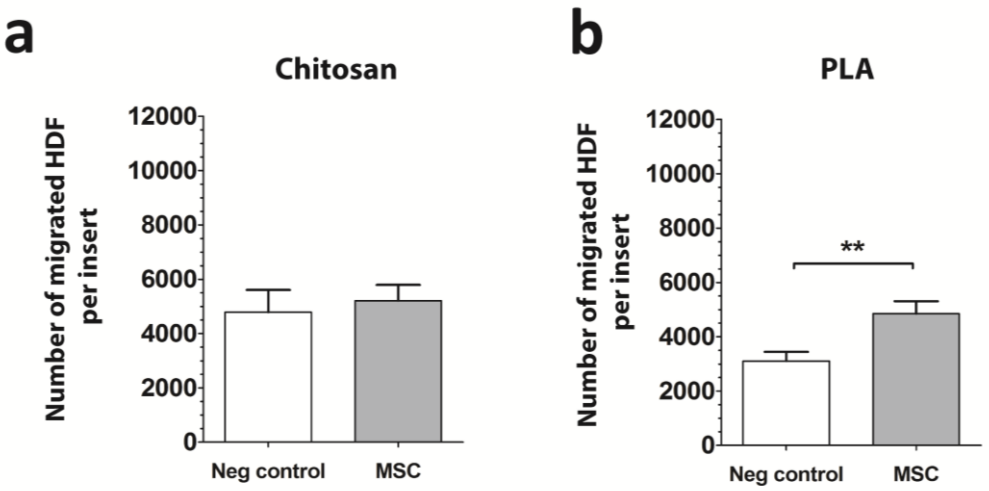

Figure 1 - Human dermal fibroblast (HDF) invasion is promoted by MSC seeded in 3D chitosan or PLA scaffolds. Invasion assays were performed with HDF placed on the top chamber of transwell system and allowed to invade for 24 hrs stimulated by MSC in (a) chitosan or (b) PLA scaffolds in the bottom chamber. Graph bars show mean ± SEM. n=5, $p < 0.01$ (**).

4.3.2 Fibroblast recruitment mediated by immune cells in distinct materials

Invasion assays were performed to clarify which type of immune responses, evoked by different immune cells interaction with PLA or chitosan 3D scaffolds or 2D TCPS, promoted the highest fibroblast recruitment. For that, the materials were seeded with different immune populations (peripheral blood mononuclear cells (PBMC), NK cells, monocytes or macrophages) and incubated in DMEM without serum for 24 hrs to ensure production of paracrine factors. To analyse the role of macrophages, monocytes were allowed to differentiate in the different materials for 7 days, before washing and also incubating in DMEM with no serum for 24 hrs. Then, invasion of HDF through Matrigel-coated transwells was analysed.

No statistical significance was achieved for HDF recruitment mediated by PBMC, NK cells and monocytes. However, when monocytes differentiated into macrophages the number of recruited HDF was markedly higher when in contact with chitosan scaffolds but not on 2D TCPS or in 3D PLA (Figure 2). Indeed, macrophages were able to recruit 2.7 times more HDF in chitosan matrices against 0.8 and 1.5 fold observed for 2D TCPS and PLA scaffolds, respectively.

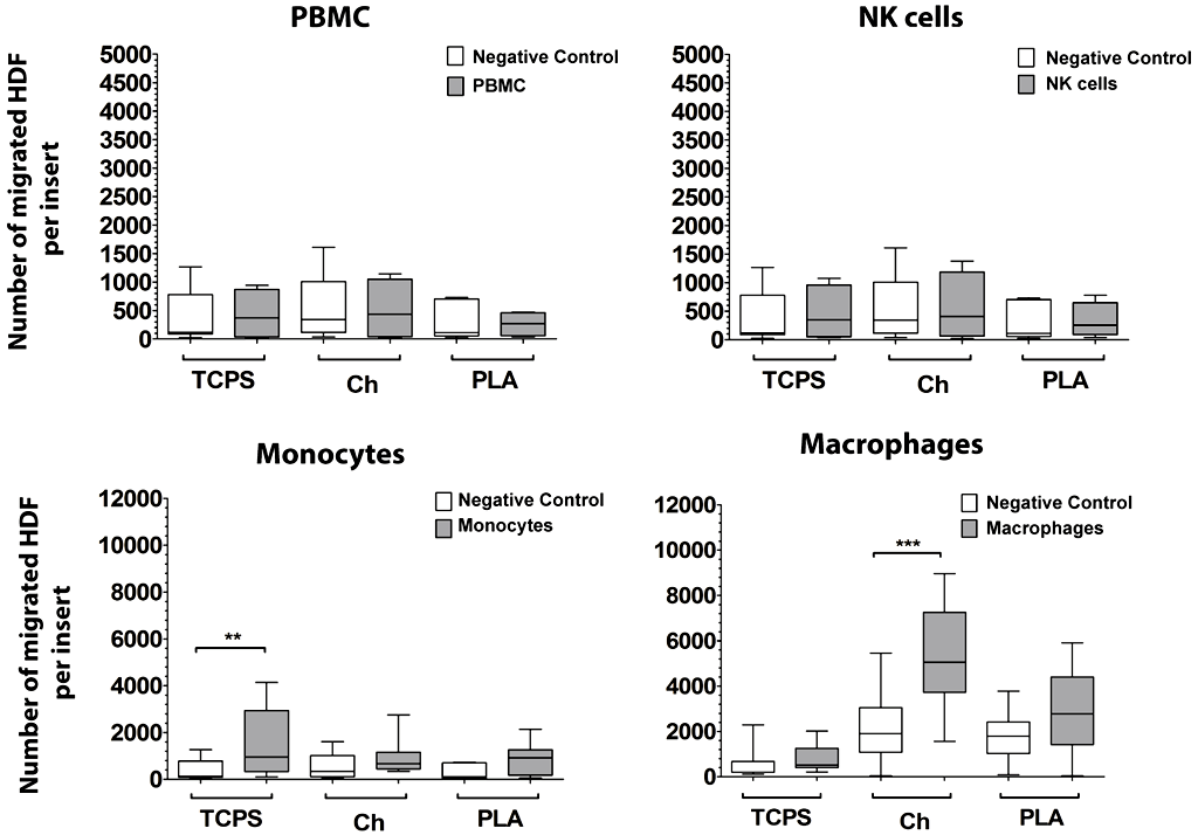

Figure 2 – Human dermal fibroblast (HDF) recruitment promoted by immune cells in different materials. Invasion assays were performed with HDF placed on the top chamber of a Matrigel-coated transwell system and allowed to invade for 24 hrs towards PBMCs, NK cells, monocytes or macrophages on 2D TCPS, or in chitosan or PLA scaffolds as stimuli. Graphs are box and whiskers plots with median ± maximum to minimum value. n=4-7, $p < 0.05$ (*).

4.3.3 Macrophages in chitosan scaffolds recruit more HDF in competition with MSC

In vivo it is expected that both fibroblasts and MSC will be present around an injury/implant area. Therefore, we investigated how the immune response triggered by macrophage-biomaterial interactions affects recruitment of these two stromal cell types in competition. To explore this, a modified Boyden chamber invasion assay was performed where HDF and MSC at a 1:1 ratio were allowed to migrate towards chitosan or PLA scaffolds seeded with macrophages. MSC vs HDF could be distinguished by staining for CD146[32] (Figure 3a).

It was found that Macrophages differentiated in the presence of chitosan induced a significant recruitment of fibroblasts in detriment of MSC towards the 3D scaffold (Figure 3b). However, the same outcome was not observed when macrophages were cultured in 3D PLA scaffolds or on 2D TCPS.

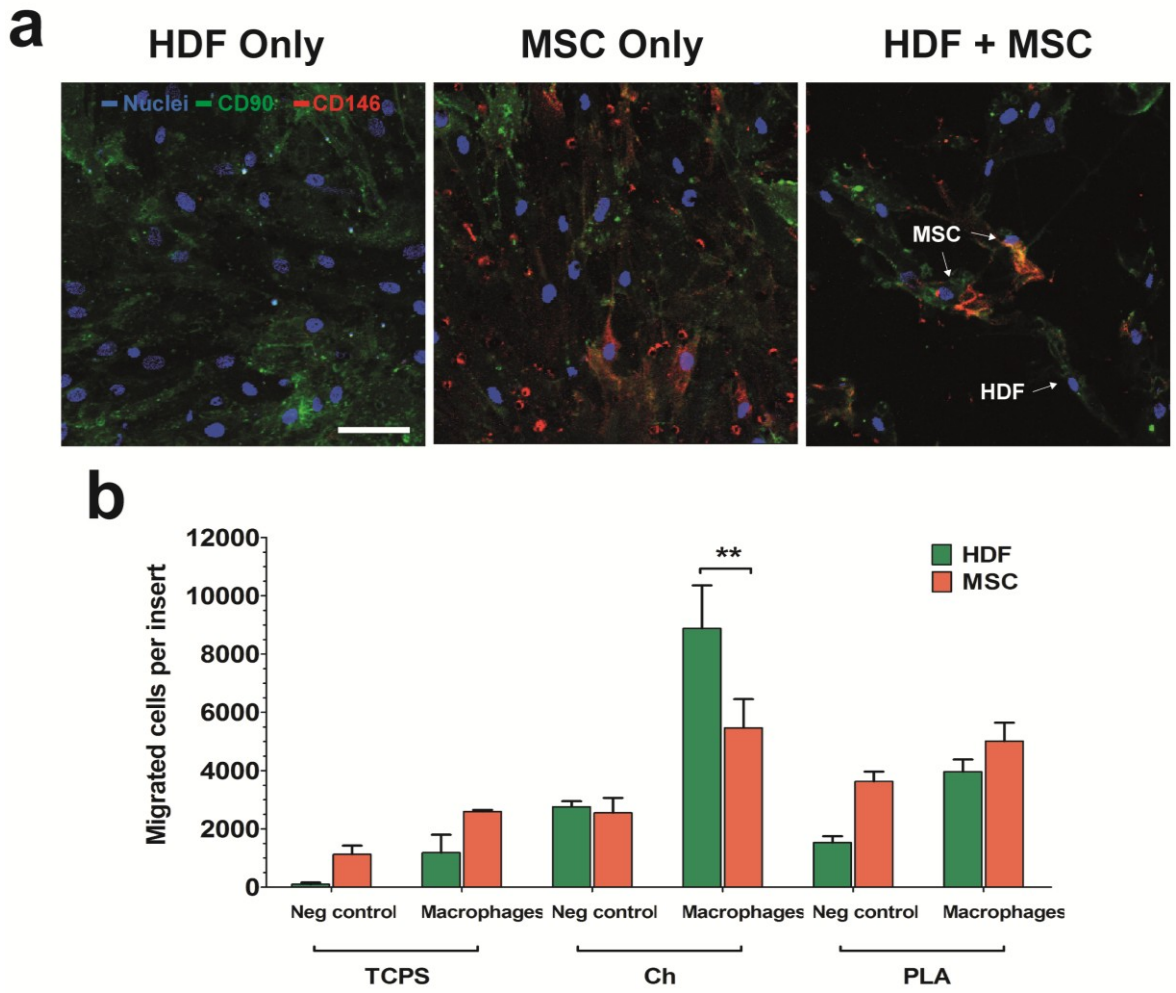

Figure 3 - MSC and HDF competitive recruitment promoted by macrophages in different materials. Invasion assays were performed in the presence of macrophages differentiated on 2D TCPS or in chitosan and PLA scaffolds for 7 days that were washed and pre-incubated for 24 hrs in DMEM serum free media before adding MSC and HDF (mixed at 1:1 ratio) to the top chamber. (a) Representative images upon CD90 (green) and CD146 (red) staining of migrated cells when only HDF (left), only MSC (middle) or HDF mixed with MSC (right) were allowed to invade. Differential cell identification was performed based on CD146 positive expression by MSC but not HDF (arrows). (b) Number of recruited MSC (red bar) and HDF (green bar) by macrophages differentiated in different materials. Graphs bars represent mean ± SEM. n=3 donors, $p < 0.01$ (**).

4.3.4 MSC interaction with macrophages within 3D scaffolds blocks fibroblast recruitment

From an *in situ* tissue engineering perspective, the arrival of endogenous MSC to the implant site is a key event for reduced FBR and improved regeneration[8,29]. Thus, we sought to understand whether MSC interaction with macrophages could regulate the subsequent mobilization of fibroblasts. For that, macrophages were allowed to differentiate in the scaffolds before adding the MSC. Then, cells were cultured in DMEM without serum for 24 hrs and invasion assays where then performed with HDF in the upper chamber. Macrophages alone in chitosan or PLA scaffolds were able to recruit 2.5 times more HDF compared with the negative controls but importantly, interaction with MSC either in chitosan or PLA scaffolds did not promote any fibroblast recruitment (Figure 4a, b). This was not due to a reduction in macrophages activity as resazurin assays suggest that MSC and macrophages remained metabolically active upon interaction (Supplementary Figure 1).

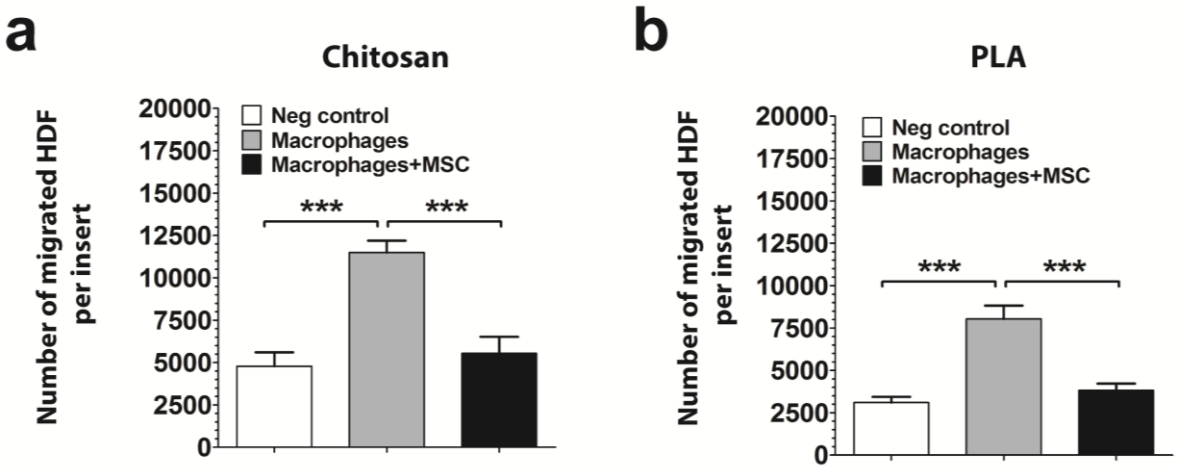

Figure 4 - HDF recruitment promoted in chitosan or PLA scaffolds by macrophages alone or co-cultured with MSC. Invasion assays were performed with HDF placed on the top chamber of transwell system and allowed to invade for 24 hrs stimulated by macrophages alone or co-cultured with MSC in (a) chitosan or (b) PLA scaffolds in the bottom chamber. Graphs are box and whiskers plots with median ± maximum to minimum value. n=5, $p < 0.001$ (***).

4.4 Discussion

Here, we report on a 3-cell platform to screen how the responses of different immune cell populations reacting with model 3D biomaterials affect recruitment of stromal cell types that can be found at an implant site. This system allowed us to investigate whether activation of immune cells by PLA or chitosan scaffolds would promote recruitment of fibroblasts and also whether MSC could regulate this process.

Macrophages differentiated in the presence of chitosan scaffolds were the most effective cells in recruiting fibroblasts. This correlates with the idea that macrophages are pivotal for the foreign body response through recruitment and activation of fibroblasts[33,34]. Most interestingly, using a competitive assay it was found that when MSC and HDF co-habited within the same environment (upper chamber) there are differences on preferential stromal cell type recruitment by macrophages. This implies that heterotypic cross-talk between these cells influence the cell dynamics towards the implant site. Under this environment, only the macrophages differentiated in chitosan scaffolds were able to promote a significant increase of fibroblast recruitment in detriment of MSC. This event could increase the likelihood of fibrotic ECM formation at the implant site for chitosan scaffolds. Indeed, higher numbers of fibroblasts near the implanted scaffold have been correlated with increased inflammation and fibrous capsule thickness[11]. The ratio of fibroblasts:MSC being recruited may play a role in determining the degree and extent of fibrosis since the presence of MSC has been associated with decreased thickness of the fibrous capsule that circumvents the implant[11,29]. Considering this, we sought to understand whether the arrival of MSC at the implant site and consequent interaction with the macrophages would interfere with the subsequent fibroblast recruitment profile. For that, macrophages were allowed to differentiate in the scaffolds before adding MSC to understand whether this interaction could regulate the recruitment of HDF. Interestingly, MSC interaction with differentiated macrophages resulted in impairment of fibroblast recruitment. Cells were metabolically active upon interaction, which excludes macrophage-mediated MSC apoptosis due to allogenic reaction as an explanation for this finding. This suggests the existence of an immunomodulatory mechanism to halts both macrophage and MSC ability to recruit fibroblasts towards the implant site.

In summary, this work provides a comprehensive analysis of the consequence of primary human responses triggered by different 3D biomaterials on recruitment of HDF. Moreover, it was found that interaction of MSC and HDF within the same environment can alter recruitment of each cell type by macrophages depending of the scaffold properties. Surprisingly, the macrophage-MSC interaction at both biomaterials interface did not

promote fibroblast recruitment. This finding suggests that stem cell arrival to the implanted scaffolds could provide the needed switch from inflammation and fibrosis towards constructive remodelling.

4.5 Materials & Methods

4.5.1 Scaffold Fabrication

PLA scaffolds: Poly-96L/4DL-lactic acid (from PURAC, Netherlands) was used. PLA scaffolds were fabricated by solvent casting and particle leaching as previously described[35]. A 5% (w/v%) PLA solution in chloroform was mixed with sieved sodium chloride (NaCl) measuring between 75 and 150 μm. The slurry was cast into 24 well Teflon moulds until complete chloroform evaporation. NaCl particles were dissolved by immersing the cylinders in distilled water.

Chitosan scaffolds: Chitosan (France-Chitine) was purified as described[36]. Chitosan sponges were prepared by freeze-drying using a 2% solution of chitosan (degree of acetylation: 12.00 ± 2.35%, molecular weight: 324 ± 27 x 10^3). Both PLA and chitosan scaffolds were cut into a cylinder shape of 11 mm diameter and 2 mm height (20.2 ± 0.5 mg and 5.8 ± 0.5 mg average weight for PLA and chitosan, respectively) and disinfected as previously described[28].

4.5.2 Measurement of endotoxin levels

PLA and chitosan extracts were prepared by chopping the scaffolds into small pieces that were suspended in 40 ml endotoxin-free water per gram of dry polymer, and incubated for 24 h at 50 ºC under continuous shaking (250 rpm), as described elsewhere[37]. Endotoxin detection was performed by Analytical Services Unit of iBET, Oeiras, Portugal using a Charles River endotoxin detection kit.

4.5.3 Cells

Human bone marrow MSC (Lonza) were cultured in MSC growth medium (DMEM with low glucose supplemented with Glutamax plus 10% MSC selected inactivated FBS and 1% penicillin/streptomycin (all from Invitrogen)). Adult human dermal fibroblasts (Invitrogen) were cultured in DMEM with high glucose supplemented with glutamine plus 10% inactivated FBS (all from Biowest) and 1% penicillin/streptomycin (Invitrogen). Cells were incubated at 37ºC/5% (V/V) CO_2 and medium was changed twice per week until cells reached approximately 80% confluence. For expansion, cells were detached by

treatment with 0.05% trypsin/EDTA (Invitrogen) and replaced in 150 cm^2 tissue culture flasks (BD Falcon). MSC and HDF were used at passages 5-8 and 3-7, respectively.

Peripheral blood mononuclear cells (PBMC), Natural Killer (NK) cells and monocytes were obtained from buffy coats of healthy human donors, kindly provided by Centro Hospitalar de São João. Briefly, a PBMC suspension was prepared by density gradient centrifugation and NK cells were purified by negative selection using the EasySep human NK cell enrichment kit (StemCell Technologies), as detailed elsewhere[38]. Human monocytes were isolated by negative selection using a RosetteSep human monocyte enrichment cocktail (StemCell Technologies), as previously described[39]. PBMC, NK cells and monocytes used in the following experiments were isolated from the same donor. The percentages of CD56+CD3- cells for the isolated NK cells and CD14+CD3- for monocytes were on average 89±6% and 87±8%, respectively, as confirmed by flow cytometry. Macrophages were differentiated from monocyte-enriched populations by culturing directly on 2D TCPS (Tissue Culture Polystyrene), in PLA or chitosan 3D scaffolds for 7 days in RPMI medium supplemented with 1% penicillin/streptomycin and 10% inactivated FBS.

4.5.4 Cell seeding

To understand how distinct materials affected immune cells, PBMC, NK cells or monocytes isolated from the same donor were seeded on 2D TCPS, in PLA or chitosan 3D scaffolds. For that, 25 µl of cell suspension was added to each side of the scaffold with a total of $6x10^4$ immune cells per scaffold. Then, the seeded scaffolds were incubated for 4 hrs at 37ºC/5% (V/V) CO_2 to promote cell adhesion before adding 750 µl of DMEM without serum. Cell culture proceeded for more 48 hrs. For macrophages, $6x10^4$ monocytes were seeded as described and allowed to differentiate in the materials for 7 days.

For invasion assays, immune cells were pre-cultured in DMEM without serum for 24 hrs. Then, the invasion assay was incubated for another 24 hrs. The total time of cell-material interaction was 48 hrs corresponding to the amount of time through which the initial acute inflammatory response is mounted upon biomaterial implantation. For macrophages, monocytes were allowed to differentiate in the materials for 7 days before washing and incubating the cells for 24 hrs with or without $6x10^4$ MSC in DMEM before performing the 24 hrs invasion assay.

4.5.5 Invasion assay

Studies on invasion of HDF were performed using a modified transwell chamber system. For the top compartment, membrane filters with a pore size of 8 µm that had been coated with Matrigel (BD Biosciences) were used. Matrigel mimics the extracellular matrix that cells need to invade through in order to arrive to the implant site. The lower compartments of the invasion chamber were filled with 750 µl DMEM medium, as a negative control, or serum-free DMEM with immune cells and/or MSC previously seeded on 2D TCPS or in 3D PLA and chitosan scaffolds. Custom spacer rings with 2 mm height were used to maintain the distance from the seeded scaffolds to the transwell insert. Then, Matrigel-coated inserts that had been pre-incubated for 1 hr with serum-free DMEM were placed in the wells, forming the upper compartment. HDF at $4x10^4$ cells in 500 µl serum-free DMEM medium were seeded into the upper compartment. The invasion chambers were incubated for 24 hrs at 37ºC/5% CO_2. After incubation, inserts were washed with PBS and cells were fixed in 4% paraformaldehyde for 20 min at room temperature (RT). Inserts were washed with PBS and kept at 4ºC until analysis. Cells on the top surfaces of filters were wiped off with cotton swabs and the membrane was carefully cut and mounted in a slide with Vectashield and DAPI. Cells that had migrated into the lower compartment and attached to the lower surface of the filter were counted in an inverted fluorescence microscope (ZeissAxiovert). Cell nuclei were counted in ten 200X fields of view for each membrane. The number of migrated cells was estimated by taking into account the area of a field of view and the total area of the membrane.

4.5.6 Competition assay

Studies on the invasion of MSC mixed with HDF were performed using a modified transwell chamber system as previously described. Then, $4x10^4$ MSC and HDF mixed at 1:1 ratio in 500 µl serum-free DMEM medium were seeded into the upper compartment. The invasion chambers were incubated for 24 hrs at 37ºC/5% CO_2. After incubation, inserts were washed with PBS and cells were stained with CD146 Alexa Fluor 647 (30 µl, AbD Serotec) in PBS (1:5) for 30 min. on ice and washed twice with PBS. Then cells were fixed in 4% paraformaldehyde for 30 min at 4ºC and counterstained with CD90 PE (30 µl, Immunotools) in PBS (1:5) for another 30 min. on ice and washed twice with PBS. Cells on the top surfaces of filters were wiped off with cotton swabs and the membrane was carefully cut and mounted in a slide with Vectashield and DAPI. Cells that had migrated into the lower compartment and attached to the lower surface of the filter were imaged and counted in a laser scanning confocal microscope (Leica TCS SP5 II, model DMI6000B-CS, Bioimaging Center for Biomaterials and Regenerative Therapies,

b.IMAGE, Porto). Cell nuclei with or without CD146 positive staining were counted in five 200X fields of view for each membrane. Negative (with HDF only) and positive (with MSC only) controls were used to establish the criteria for positive CD146 staining. CD90 was used to delineate both MSC and HDF cell cytoplasm while CD146 was used to identify MSC. The number of migrated MSC and HDF was estimated by taking into account the area of a field of view and the total area of the membrane.

4.5.7 Statistical analysis

Statistical analysis was performed using Prism5 software, v5.01. D'Agostino & Pearson omnibus normality test was used together with the analysis of Q-Q plots to understand whether the fibroblast invasion process followed normality. Upon normality of the data was confirmed, two tailed paired t-test was used to compare two samples. Repeated measures ANOVA test followed by Bonferroni post-test was used to compare more than two samples. For grouped samples, two-way ANOVA test was used followed by Bonferroni post-test. Data are mean ± Standard Error of the Mean (SEM) unless stated otherwise. Values of $p < 0.05$ (*), $p < 0.01$ (**) and $p < 0.001$ (***) were considered statistically significant.

4.6 Acknowledgements

The authors would like to thank Centro Hospitalar de São João for kindly donating the buffy coats. This work was financed by FEDER funds -Programa Operacional Factores de Competitividade – COMPETE and by Portuguese funds through FCT – Fundação para a Ciência e a Tecnologia in the framework of project EXPL/BIM-MED/0022/2013.

4.7 Competing financial interests

The authors declare no competing financial interests.

4.8 References

[1] Jones, K. S. Effects of biomaterial-induced inflammation on fibrosis and rejection. *Seminars in immunology*, 20, 2, 2008, 130-136.

[2] Veiseh, O. *et al.* Size- and shape-dependent foreign body immune response to materials implanted in rodents and non-human primates. *Nature materials*, 14, 6, 2015, 643-651.

[3] Thevenot, P. T. *et al.* The effect of incorporation of SDF-1alpha into PLGA scaffolds on stem cell recruitment and the inflammatory response. *Biomaterials*, 31, 14, 2010, 3997-4008.

[4] Ratanavaraporn, J., Furuya, H., Kohara, H. & Tabata, Y. Synergistic effects of the dual release of stromal cell-derived factor-1 and bone morphogenetic protein-2 from hydrogels on bone regeneration. *Biomaterials*, 32, 11, 2011, 2797-2811.

[5] Kyritsis, N. *et al.* Acute inflammation initiates the regenerative response in the adult zebrafish brain. *Science*, 338, 6112, 2012, 1353-1356.

[6] Anderson, J. M., Rodriguez, A. & Chang, D. T. Foreign body reaction to biomaterials. *Seminars in immunology*, 20, 2, 2008, 86-100.

[7] Caplan, A. I. & Correa, D. The MSC: an injury drugstore. *Cell stem cell*, 9, 1, 2011, 11-15.

[8] Chen, F. M., Wu, L. A., Zhang, M., Zhang, R. & Sun, H. H. Homing of endogenous stem/progenitor cells for in situ tissue regeneration: Promises, strategies, and translational perspectives. *Biomaterials*, 32, 12, 2011, 3189-3209.

[9] Darby, I. A., Laverdet, B., Bonte, F. & Desmouliere, A. Fibroblasts and myofibroblasts in wound healing. *Clinical, cosmetic and investigational dermatology*, 7, 2014, 301-311.

[10] Duffield, J. S., Lupher, M., Thannickal, V. J. & Wynn, T. A. Host responses in tissue repair and fibrosis. *Annual review of pathology*, 8, 2013, 241-276.

[11] Thevenot, P. T., Baker, D. W., Weng, H., Sun, M. W. & Tang, L. The pivotal role of fibrocytes and mast cells in mediating fibrotic reactions to biomaterials. *Biomaterials*, 32, 33, 2011, 8394-8403.

[12] Jhunjhunwala, S. *et al.* Neutrophil Responses to Sterile Implant Materials. *PloS one*, 10, 9, 2015, e0137550.

[13] Tsirogianni, A. K., Moutsopoulos, N. M. & Moutsopoulos, H. M. Wound healing: immunological aspects. *Injury*, 37 Suppl 1, 2006, S5-12.

[14] Agaiby, A. D. & Dyson, M. Immuno-inflammatory cell dynamics during cutaneous wound healing. *J Anat*, 195 (Pt 4), 1999, 531-542.

[15] Franz, S., Rammelt, S., Scharnweber, D. & Simon, J. C. Immune responses to implants - a review of the implications for the design of immunomodulatory biomaterials. *Biomaterials*, 32, 28, 2011, 6692-6709.

[16] Mantovani, A., Biswas, S. K., Galdiero, M. R., Sica, A. & Locati, M. Macrophage plasticity and polarization in tissue repair and remodelling. *The Journal of pathology*, 229, 2, 2013, 176-185.

[17] Anderson, J. M. & McNally, A. K. Biocompatibility of implants: lymphocyte/macrophage interactions. *Seminars in immunopathology*, 33, 3, 2011, 221-233.

[18] Shi, C. & Pamer, E. G. Monocyte recruitment during infection and inflammation. *Nature reviews. Immunology*, 11, 11, 2011, 762-774.

[19] Caires, H. R. *et al.* Macrophage interactions with PLA and chitosan scaffolds lead to improved recruitment of human MSC: a comprehensive study with different immune cells. *Journal of the Royal Society, Interface / the Royal Society*, *in press*, 2016.

[20] Grotenhuis, N., Bayon, Y., Lange, J. F., Van Osch, G. J. & Bastiaansen-Jenniskens, Y. M. A culture model to analyze the acute biomaterial-dependent reaction of human primary macrophages. *Biochemical and biophysical research communications*, 433, 1, 2013, 115-120.

[21] Damanik, F. F., Rothuizen, T. C., van Blitterswijk, C., Rotmans, J. I. & Moroni, L. Towards an in vitro model mimicking the foreign body response: tailoring the surface properties of biomaterials to modulate extracellular matrix. *Scientific reports*, 4, 2014, 6325.

[22] Hajkova, M. *et al.* A local application of mesenchymal stem cells and cyclosporine A attenuates immune response by a switch in macrophage phenotype. *Journal of tissue engineering and regenerative medicine*, 2015.

[23] Zhou, G., Loppnow, H. & Groth, T. A macrophage/fibroblast co-culture system using a cell migration chamber to study inflammatory effects of biomaterials. *Acta biomaterialia*, 26, 2015, 54-63.

[24] Suuronen, R., Pohjonen, T., Hietanen, J. & Lindqvist, C. A 5-year in vitro and in vivo study of the biodegradation of polylactide plates. *Journal of oral and maxillofacial surgery : official journal of the American Association of Oral and Maxillofacial Surgeons*, 56, 5, 1998, 604-614; discussion 614-605.

[25] Serra, T., Planell, J. A. & Navarro, M. High-resolution PLA-based composite scaffolds via 3-D printing technology. *Acta biomaterialia*, 9, 3, 2013, 5521-5530.

[26] Dai, T., Tanaka, M., Huang, Y. Y. & Hamblin, M. R. Chitosan preparations for wounds and burns: antimicrobial and wound-healing effects. *Expert review of anti-infective therapy*, 9, 7, 2011, 857-879.

[27] Oliveira, S. M. *et al.* Engineering endochondral bone: in vivo studies. *Tissue engineering. Part A*, 15, 3, 2009, 635-643.

[28] Santos, S. G. *et al.* Adsorbed fibrinogen leads to improved bone regeneration and correlates with differences in the systemic immune response. *Acta biomaterialia*, 9, 7, 2013, 7209-7217.

[29] Swartzlander, M. D. *et al.* Immunomodulation by mesenchymal stem cells combats the foreign body response to cell-laden synthetic hydrogels. *Biomaterials*, 41, 2015, 79-88.

[30] Liu, X. *et al.* Human embryonic stem cells and macroporous calcium phosphate construct for bone regeneration in cranial defects in rats. *Acta biomaterialia*, 10, 10, 2014, 4484-4493.

[31] Chen, W. *et al.* Umbilical cord and bone marrow mesenchymal stem cell seeding on macroporous calcium phosphate for bone regeneration in rat cranial defects. *Biomaterials*, 34, 38, 2013, 9917-9925.

[32] Halfon, S., Abramov, N., Grinblat, B. & Ginis, I. Markers distinguishing mesenchymal stem cells from fibroblasts are downregulated with passaging. *Stem cells and development*, 20, 1, 2011, 53-66.

[33] Xia, Z. & Triffitt, J. T. A review on macrophage responses to biomaterials. *Biomedical materials*, 1, 1, 2006, R1-9.

[34] Kobayashi, H. *et al.* Vascular-inducing poly(glycolic acid)-collagen nanocomposite-fiber scaffold. *Journal of biomedical nanotechnology*, 9, 8, 2013, 1318-1326.

[35] Navarro, M., Ginebra, M. P., Planell, J. A., Barrias, C. C. & Barbosa, M. A. In vitro degradation behavior of a novel bioresorbable composite material based on PLA and a soluble CaP glass. *Acta biomaterialia*, 1, 4, 2005, 411-419.

[36] Antunes, J. C. *et al.* Layer-by-layer self-assembly of chitosan and poly(gamma-glutamic acid) into polyelectrolyte complexes. *Biomacromolecules*, 12, 12, 2011, 4183-4195.

[37] Nakagawa, Y. *et al.* Endotoxin contamination in wound dressings made of natural biomaterials. *Journal of biomedical materials research. Part B, Applied biomaterials*, 66, 1, 2003, 347-355.

[38] Almeida, C. R., Vasconcelos, D. P., Goncalves, R. M. & Barbosa, M. A. Enhanced mesenchymal stromal cell recruitment via natural killer cells by incorporation of inflammatory signals in biomaterials. *Journal of the Royal Society, Interface / the Royal Society*, 9, 67, 2012, 261-271.

[39] Almeida, C. R. *et al.* Impact of 3-D printed PLA- and chitosan-based scaffolds on human monocyte/macrophage responses: unraveling the effect of 3-D structures on inflammation. *Acta biomaterialia*, 10, 2, 2014, 613-622.

4.9 Supplementary Data

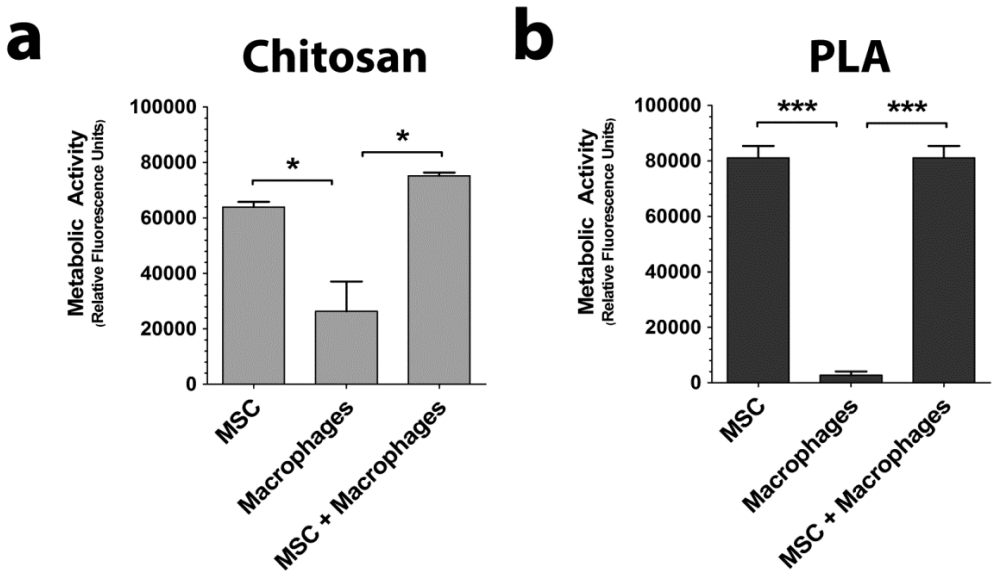

Supplementary Figure S1 - Metabolic activity of MSC and macrophages alone or co-cultured in (a) chitosan or (b) PLA scaffolds following invasion assays with HDF seeded in the upper chamber. Relative fluorescence unit (RFU) as a measure of metabolic activity determined by resazurin assays upon 48 hrs of cell culture in serum free media. Graphs bars represent mean ± SEM. n=3 donors, $p < 0.05$ (*) and $p < 0.001$ (***).

CHAPTER 5

“HÁ MUITO TEMPO QUE NÃO ESCREVO.

Há muito tempo que não escrevo. Têm passado meses sem que viva, e vou durando, entre o escritório e a fisiologia, numa estagnação íntima de pensar e de sentir. Isto, infelizmente, não repousa: no apodrecimento há fermentação.

Há muito tempo que não só não escrevo, mas nem sequer existo. Creio que mal sonho. As ruas são ruas para mim. Faço o trabalho do escritório com consciência só para ele, mas não direi bem sem me distrair: por detrás estou, em vez de meditando, dormindo, porém estou sempre outro por detrás do trabalho.

Há muito tempo que não existo. Estou sossegadíssimo. Ninguém me distingue de quem sou. Senti-me agora respirar como se houvesse praticado uma coisa nova, ou atrasada. Começo a ter consciência de ter consciência. Talvez amanhã desperte para mim mesmo, e reate o curso da minha existência própria.

Há muito tempo que não sou eu.”

Livro do Desassossego por Bernardo Soares. Vol.I. Fernando Pessoa. Lisboa: Ática, 1982. - 139.

GENERAL DISCUSSION & OUTLOOK

5.1 Main findings

Designing new biomaterials that can positively interact with the immune system instead of just attempting to avoid it constitutes a recent paradigm change in regenerative medicine[1]. Although inflammation has been increasingly recognized as a key component of the regenerative process, the role of immune cells and inflammatory mediators in scaffold-guided regeneration remains poorly understood. Thus, this thesis aims to understand how the primary human immune responses, evoked by distinct 3D scaffold models, modulate recruitment of primary human BM-MSC and fibroblasts, instrumental cell types to determine the healing outcome. Our hypothesis focus on exploiting the regenerative cell mobilization upon immune responses to implanted materials. Thus, in Chapter 2 an imaging platform was developed to follow human MSC dynamical behaviour within complex 3D microenvironments. It was shown that Dendra2 photoconversion can be efficiently used to monitor and compare changes in MSC motility and morphology within distinct engineered matrices throughout 7 days. In Chapter 3 it was shown that distinct materials trigger specific immune cell responses which consequently had a major impact on MSC recruitment towards the implant. Additionally, in Chapter 4 it was demonstrated that distinct biomaterials can also modulate the immune cells ability to mobilize fibroblasts towards the implant site, but that in more complex systems, with the presence of a third cell type, MSC, this recruitment can be modified. Taken together, the gathered knowledge represents an important leap forward in the characterization of human immune cells ability to mediate stromal cell recruitment upon scaffold implantation. And importantly, these results illustrate scaffold's potential to regulate the recruitment dynamics of pro-regenerative/fibrotic cell types through immune-modulation. This thesis work highlights a new concept for *in situ* tissue engineering scaffold development with potential for clinical translation.

5.2 Concepts of *in situ* tissue engineering: time for an integrated approach

The finding that many adult tissues contain stem cells that function to maintain and regenerate tissues upon injury paved the way to the idea that we could recruit these endogenous stem cells to enhance tissue regeneration[2]. Most excitingly, such strategies bypass the bottleneck issues of conventional tissue engineering and regenerative medicine related with *ex-vivo* expanded MSC. In line with this conceptual approach, Kitaori *et al.*[3] have shown that SDF-1 promotes bone regeneration by recruiting

systemically administered MSC to the fracture site. And importantly, inhibition of SDF-1 or blocking of its receptor, CXCR4, prevents MSC recruitment and results in impaired bone healing. The notion that stem cell recruitment by specific chemokine gradients is required for tissue regeneration, now supported by a number of *in vivo* studies[4-7], gave rise to *in situ* or scaffold-guided regenerative approaches. Such approaches aim to develop off-the-shelf biodegradable scaffolds that can therapeutically augment our otherwise rather limited regenerative potential upon severe injuries. Landmark studies of Ji *et al.*[8], have shown that biomaterial-mediated SDF-1 delivery can be efficiently used to recruit MSC to a cranial defect resulting in an astonishing six-fold increase in bone formation compared to biomaterial alone. This promising approach based on scaffold-mediated chemokine delivery for stem cell recruitment has been successfully demonstrated in a number of *in vivo* studies[9-15]. Nevertheless, several issues hamper the efficient usage of chemoattractants as a therapeutic approach. The most prominent ones include their high cost, short half-live, rapid diffusion, amenability to cleavage by proteases, controlled release under spatial defined gradients within a specific timeframe to promote chemotaxis of endogenous MSC and their largely uncharacterized inflammatory side effects[16]. Here it was shown that specific biomaterials can induce immune cells to produce high and sustainable amounts of well-known stem cell chemoattractants. And importantly, this event was followed by the recruitment of high numbers of MSC towards the implanted material. Thus, our findings highlight a potential new approach in which scaffolds are specifically designed to modulate the immune system to produce the required stem cell chemoattractants instead of acting as delivery systems for exogenous chemokines. Interestingly, this novel approach would circumvent many of aforementioned concerns that plague the efficient usage of exogenous chemoattractants for enhanced stem cell recruitment.

Despite the successful nature of such strategies, implantation of the so called “regenerative biomaterials” also triggers an opposing type of host response: an immune reaction against the implanted foreign material. This often culminates in biomaterials fibrotic encapsulation and it is one of the leading causes for implant failure. Therefore and as alternative, studies such as Lee *et al.*[17] attempt to improve scaffold-guided healing by targeting the biomaterial-induced FBR. These authors have shown that vanillin-incorporated PLGA modulate macrophage activation and consequently led to a less severe FBR. The identification of the host inflammatory response as a critical component on scaffold-guided regeneration prompted the development of novel immunomodulatory strategies to decrease the FBR and improve the healing outcome[18-24]. Here it was demonstrated that distinct biomaterials can also modulate the immune cells ability to

promote/avoid fibroblast recruitment. Importantly, our results suggested that although macrophages were a major player in mediating this recruitment other immune cells, as PBMC and monocytes, can also play a role depending on the biomaterial. Therefore, strategies to hamper these immune cells ability to promote fibroblast mobilization upon scaffold interaction could be of interest for ameliorating the FBR and their fibrotic encapsulation.

Despite these two strategies have been successfully used to enhance endogenous tissue regeneration evidences suggest that biomaterial-evoked inflammation, endogenous MSC recruitment and FBR can be intimately related. Importantly, pioneer studies by Thevenot *et al.*[25] in a mice model have shown that SDF-1 incorporation in PLGA scaffolds enhances the recruitment of endogenous stem cells which in turn ameliorate the FBR to biomaterial implant through modifying immune cell responses. This and others studies[26-30] highlight a complex interaction between the host immune response, stem cell recruitment and fibrotic encapsulation of implanted scaffolds with significant implications for the healing outcome. Within this context, our results suggested that immune cells can induce specific stromal cell recruitment profiles upon interaction with distinct biomaterials. And importantly, the preferential/premature mobilization of MSC by immune cell-biomaterial interaction might influence the subsequent fibroblast dynamics towards the implant site. This could imply that an early boost on MSC recruitment instead of a continuous one might be a more efficient strategy to diminish the FBR and improve healing.

In summary, most of these studies show that the scaffolds ability to promote progenitor cell recruitment and/or to modulate the immune response is pivotal to successfully augment endogenous tissue regeneration[25,31-39]. Even though *in situ* tissue engineering has made tremendous progress with these two independent approaches, the field is still at its infancy in understanding the interplay between scaffold-mediated inflammation, tissue fibrosis and regeneration. Considering the experimental evidences so far, we anticipate that the next generation of regenerative scaffolds will most likely be designed to integrate both *in situ* engineering conceptual approaches. For instance such biomaterials could be designed to hijack the host immune response to recruit specific stromal cell types to potentiate regeneration instead of fibrotic encapsulation of the implant. Within this context, deeper insights on the complex interaction between biomaterials, host immune response and stromal cell recruitment are required to translate forward into design rules for the next generation of *in situ* tissue engineering scaffolds.

5.3 Translating forward: deciphering host response in relevant models

Mechanistic studies in physiologically relevant *in vitro* models are critical to systematically gather and translate the needed knowledge into future clinical applications. Such models provide an important tool to unravel the complexity of biological systems in order to understand mechanisms of biomaterial-immune cells-stromal cells interactions. For instance, Damanik and colleagues[40] have recently developed an *in vitro* model to study how biomaterials surface modifications modulate rat-derived macrophage and/or fibroblast behaviour. It was possible to correlate specific surface modifications with cell adhesion, proliferation, secretion profile and collagen/elastin production. This and other studies[41] with rat cells shed some light on some of the factors that can be used to modulate the host response. Nevertheless, Chamberlain *et al.*[42] demonstrated that primary human macrophage cytokine production, phenotype and intrinsic activation state have limited correlation to immortalized cell lines and/or macrophages derived from other species. Thus, and although the aforementioned reports are important proof-of-concept studies their immediate translation into a human scenario is rather limited.

Considering this, McNally *et al.*[43] have recently developed a human model of IL-4-induced macrophage fusion and FBGC formation to study the effects of different 2D material surfaces on phenotypic expression in primary human macrophages. Similarly, a number of other 2D models with primary human immune cells are available to study/predict the human host response to implanted biomaterials[43-48]. Nevertheless, these models display two important intrinsic limitations if one wants to apply to *in situ* tissue engineering studies. Firstly, marked differences on immune cells responses when on 2D substrates *versus* their “native” 3D microenvironments have been reported[49-51]. And secondly, such models clearly focus on the contribution of one immune cell type (mostly macrophages) upon interaction with 2D surfaces for the biomaterials fibrotic encapsulation. In a physiologic scenario, scaffold-guided regeneration involves the coordinated movement of distinct cell types in close interaction with several immune cells. Thus, if one aspires to create design rules for immune-modulatory scaffolds with clinical translation, more sophisticated *in vitro* systems will be required. Considering the need for a more physiologically relevant model, we developed a modified 3D Boyden invasion system using distinct primary human immune cells in co-culture with other primary human cell types and biomaterials in a three-dimensional environment. Importantly it allowed us

to study how human immune responses, triggered by different 3D scaffolds, guided the recruitment of other cells to assist in the healing process.

In our quest to unveil the role of biomaterial-evoked immune responses on stromal cell recruitment we first sought to investigate whether the 3D scaffold models could distinctly modulate immune cell behaviour. To address this, PLA or chitosan 3D scaffolds were seeded with different immune populations from the same human blood donor (PBMC, NK cells, monocytes or macrophages) and cultured. The investigations carried out in this 3D model were performed in the absence of serum or with a pre-washing step to avoid interference of unknown molecules in the secretion profile and cell recruitment assays. This enabled a clearer analysis of the factors produced and their effect on cell recruitment. Arguably, this could also be a limitation of this work since immune responses can be influenced by the adsorbed proteins to the materials surface[52,53]. Battiston and colleagues[54-56] have shown that the variation in protein adsorption, which was a function of surface chemistry, led to the varied cytokine release profile of adhered monocytes on different surfaces. Thus it would be interesting to study whether specific surface modifications/adsorbed protein coatings could modulate immune cells ability to promote recruitment of regenerative cell types towards the implant. This would be an elegant alternative to the expensive delivery of a limited number of chemokines to induce endogenous progenitor cell recruitment for *in situ* regeneration.

Here it was shown that distinct materials induced specific secretion profiles by distinct immune cell populations. This was expected since PLA and chitosan scaffolds display many distinct features known to influence immune cell behaviour including surface chemistry[57], roughness[58] and stiffness[22]. Importantly, we have observed that several chemokines known to induce MSC and/or fibroblast recruitment were highly expressed by macrophages, particularly upon differentiation in the presence of 3D biomaterials. Thus we sought to understand the functional role of the immune cells secretome on mediating the stromal cell recruitment towards the distinct biomaterials. For that, a Matrigel-coated transwell chamber seeded with stromal cells (MSC and/or fibroblasts) was inserted on top of the mentioned 3D culture system, to mimic the extracellular matrix basement membrane that these stromal cells need to invade to arrive to the implant site. With this model several aspects of stromal cell mobilization towards the implant site could be studied, from the type of immune responses evoked by distinct 3D materials, their effect on mediating invasion of stromal cells towards the implanted scaffolds, to the impact of immune cell interaction with the recruited MSC at the scaffold interface. Importantly, data derived from primary human cells from several donors, was obtained. Moreover, this primary human 3D model fulfils the missing gap between the over simplistic 2D culture

systems and the *in vivo* animal models that despite physiologically relevant may not fully represent the human responses due to inter-species immunological discrepancies[59]. The development of such 3D models are not only instrumental to unveil mechanistic aspects of the human healing response upon scaffold implantation but can also have an important applicability in the field of personalized regenerative medicine as a predictive tool of hosts immune/healing response to a given implanted material.

5.4 A new perspective from within: Dendra2 imaging platform

For successful *in situ* tissue regeneration, endogenously recruited MSC must be able to colonize the engineered scaffold that gaps the wound limits. Colonization of the implanted scaffold by hosts cells, and therefore its *in vivo* performance, is highly dependent on the 3D architectural features of the porous scaffold[60]. Thus, there has been an increasing demand for imaging tools able to monitor and compare cell dynamics within 3D scaffolds with distinct properties. Indeed, the advance of live imaging methods is instrumental for tissue engineering scaffold development and has been identified as a strategic priority in the field[61].

Several studies illustrate confocal microscopy potential to interrogate how specific engineered matrix features can be optimized to facilitate MSC ingrown[62-65]. Nevertheless, most of these confocal imaging platforms fail to perform a longitudinal assessment of MSC dynamical behaviour within 3D scaffolds. This is important taking into account the physiologic timeframe and dynamics of the scaffold colonization process. As a result, other methods as photoacoustic[66,67] and optical coherence microscopy (OCT)[68-70] have been increasingly recognized as promising alternatives to characterize cell motility within tissue engineered constructs. Mostly because they far exceed the live cell imaging time allowed by confocal imaging techniques due to phototoxicity/photobleaching constrains, even that they do not match confocal spatial resolution. Longitudinal monitoring of MSC migration is possible with such alternative imaging modalities but intricate. Since cells would need to be permanently on the microscope over imaging time which usually is not feasible for long term experiments (e.g. more than one week). In addition, for OCT imaging the scaffold materials must be selected to have different scattering properties from the cells. Importantly, the ECM components that are gradually secreted by cultured cells has been reported to obscure the cell signal over time[69].

Within this framework, we have developed an efficient confocal imaging method for tissue engineering applications that takes advantage of the photoswitchable Dendra2 fluorescent protein. And importantly, a direct comparison of MSC migration within distinct 3D

engineered matrices with a longitudinal perspective is now possible using a confocal microscope. Apart from surpassing current long term imaging limitations, this Dendra2 imaging strategy could be used to simultaneously investigate intracellular protein dynamics during the 3D migration process by Dendra2 tagging or be even used as a reporter gene for MSC differentiation[71-73]. Moreover, our Dendra2 imaging principle could also be applied in wide-field mercury lamp fluorescence microscopes widely available in research institutions[72].

Despite the imaging functionality, our results suggest that the transfection process, but not the Dendra2 protein expression, hinders MSC proliferation. Nevertheless, others have reported that electroporation has no influence on MSC differentiation and proliferation[74]. Thus, several strategies could be employed to overcome this issue, including electroporation with different settings and MSC donors or even by using alternative transfection techniques such as viral transduction or lipofection[75-77].

Although this technique can be used to compare cell motility within distinct matrices we found that Dendra2 expression seems to slowdown MSC migration velocity by 43% on 2D. Therefore, no absolute measurements of cells velocity could be provided. However, it would be important to confirm whether this observation is maintained in a 3D environment where cells can rely on different migration processes. Alternatively, other photoconvertible proteins could be used to overcome these limitations[78]. Thus it would be possible to calculate the absolute values for Euclidean distance using the current imaging framework. This could be achieved by combining the centre-of-mass position of photoconverted population with specific landmarks on the scaffold itself to triangulate cells positions over the distinct time-points[79].

Importantly, MSC dynamical behaviour was characterized in matrices with distinct optical densities and properties. These included a Matrigel matrix that mimicked the basement membrane in the invasion assays. The slower migration in Matrigel compared with porous scaffolds could be explained by the increased steric hindrance of the matrix, due to a tighter mesh size combined moderate gel stiffness, which can limit cell spreading[80-83]. In such scenario MSC would need to use alternative migration modes to invade the matrix. Moreover, MSC invasion would be assisted by their proteolytic activity which is reported to be augmented under inflammatory settings[81,84-87].

Taken together, Dendra2 imaging it is a highly flexible and adaptable platform that allows coupling 3D cell morphology analysis and quantification of cell migration in real-time, studies on cell-ECM interactions in a range of bioengineered matrices with distinct optical properties, and reliable imaging for more than 7 days.

5.5 Biomaterial immune-modulation: Aiming for the strategic control of stromal cell recruitment

Biomaterial implantation unavoidably leads to tissue damage, immune cell recruitment, adhesion at the scaffolds interface and cell activation. This ultimately drives the inflammatory process whose role has been increasingly recognized as a key component of tissue repair and regeneration. Importantly, the scaffold features can influence many aspects of immune cells behaviour. These features are largely responsible for the type of infiltrating immune cells, activation state and secretion profile that mediate subsequent steps of the healing cascade, including the mobilization of distinct stromal cell types[29,39].

Here it was showed that marked differences on immune cells proliferation, metabolism and actin cytoskeleton morphology are induced by distinct 3D materials. Additionally, the responses of immune cells known to participate on early (NK cells, monocytes and PBMC) and/or late (predominantly macrophages but also PBMC at some extent) phases of host response to the implanted scaffolds were investigated to trace a putative profile of MSC and fibroblast recruitment over the inflammatory process.

Our results suggest that NK cells and PBMC proliferate at different extents depending on the biomaterial. Thus the proportion of each immune population at the implant site may be partially regulated by their selective recruitment from circulation but also by the biomaterial-induced proliferative state. Importantly, this could be targeted to enhance the number of specific “pro-regenerative” immune cells at the biomaterial interface. Despite the increased cell number of PBMC and NK cells in some materials both populations exhibited rather similar secretion amounts of key inflammatory mediators regardless of the 3D scaffold, suggesting a self-regulatory mechanism. This translated into a comparably low ability to mobilize MSC or fibroblasts which suggests that these cells role in host response is probably more related with avoiding biomaterial-derived infections and not mediating stromal cell recruitment. Nevertheless, we have recently shown that NK cells have the ability to induce MSC migration through production of RANTES and NAP-2 chemokines[88]. Moreover, blocking CXCR2 receptor, a receptor that recognizes both chemokines, abolished NK cell-mediated MSC recruitment. Although a similar outcome was observed here for NK cells on TCPS, RANTES expression was significantly down-regulated when NK cells interacted with the 3D biomaterials. Therefore it would be interesting to find immune-modulatory strategies to restore these early cells ability to mobilize endogenous MSC upon interaction with implanted biomaterials.

In our model, monocytes (whose accumulation *in vivo* peaks at around 72 hrs) do not seem to proliferate upon biomaterial interaction. Several reports state that distinct monocyte subsets are continuously recruited from the blood stream to the inflammation site throughout the healing process[89]. Contrary to the other immune cells, monocytes seem to slightly adjust the secreted cytokine levels depending on the biomaterial, at least for the analyzed markers. Thus, PLA scaffolds encouraged a significantly higher production of IL-8 compared to chitosan. Interestingly, this was followed by a trend for monocytes to recruit more fibroblasts (but not MSC) in PLA matrices which suggests some degree of decision making over the type of recruited stromal cell early on in the inflammatory phase.

Upon arrival to the implant site, monocytes gradually differentiate into macrophages representing the dominant immune cell type at later stages (days to weeks) of the host's healing response[90,91]. Macrophages differentiation is perceived as pivotal in orchestration of either tissue regeneration or foreign body response[92]. Indeed, their remarkable plasticity enables them to assume diverse and context-dependent polarization states which influence the healing outcome[93]. These are broadly categorized by their functional properties and patterns of cytokine secretion into M1 (pro-inflammatory), $M2_{wound\ healing}$ which are more amiable to promote fibrosis and $M2_{regulatory}$ which suppresses the immune responses to resolve inflammation and encourage functional tissue restoration. Nevertheless, Madden *et al.*[94] have shown that many macrophages that stained *in vivo* for specific cell surface markers of M1 also stained for M2, that is, in what appears to be a mixed M1–M2 phenotype. This was corroborated by Van Putten *et al.*[41] that also suggested that many macrophages in the FBR induced by hexamethylenediisocyanate cross-linked dermal sheep collagen (HDSC) did not fit into the classical M1 or M2 dichotomy. Thus, although the aforementioned classification system constitutes a practical framework, in reality a continuum of phenotypes with overlapping functions co-exist[95]. Regarding to the biomaterial models used in this thesis, our group has previously demonstrated that PLA and chitosan lead to production of a mixture of cytokines characteristic of both M1 and M2 macrophages[57]. Here, these 3D biomaterials also had a profound effect on macrophages secretion profile. Similarly to their precursor cells, macrophages tuned their secretion profile according to the type of biomaterial encountered. Interestingly, among the inflammatory mediators distinctly expressed were IL-6, IL-8, MIP-1α, MIP-1β, MCP-1 and RANTES. All these mediators have been implicated as potent chemoattractants for MSC and/or fibroblast recruitment[86,96-100]. Therefore, instead of classifying macrophage biomaterial-induced polarization markers for M1 or M2 we found it more meaningful to investigate their functional outcome on

mediating the late stromal cell mobilization[101]. Here we found that macrophages were the immune cell type specifically activated by 3D biomaterials to secrete large amounts of bioactive molecules that could strongly encourage MSC and fibroblast recruitment towards the implant site. Most interestingly, it was demonstrated that when these stromal cells co-exist within the same environment differences on preferential cell recruitment by macrophages arose and notably were scaffold-dependent: macrophages in chitosan scaffolds promoted a significant increase of fibroblast recruitment in detriment of MSC, contrarily to what was observed with PLA. Since higher numbers of fibroblasts near the implanted scaffold have been correlated with increased inflammation and fibrous capsule thickness[29] our results could suggest an increased likelihood that chitosan leads to a stronger FBR comparably to PLA scaffolds upon implantation. Nevertheless, additional *in vivo* studies comparing the host response to implanted PLA and chitosan scaffolds are required to further validate our 3D model and substantiate this claim. Considering our findings, chitosan scaffolds modified to ameliorate/modulate immune cell activation[23,24,102,103] or designed to recruit higher numbers of endogenous MSC to down-regulate excessive fibrosis[30,104] could greatly benefit their biocompatibility.

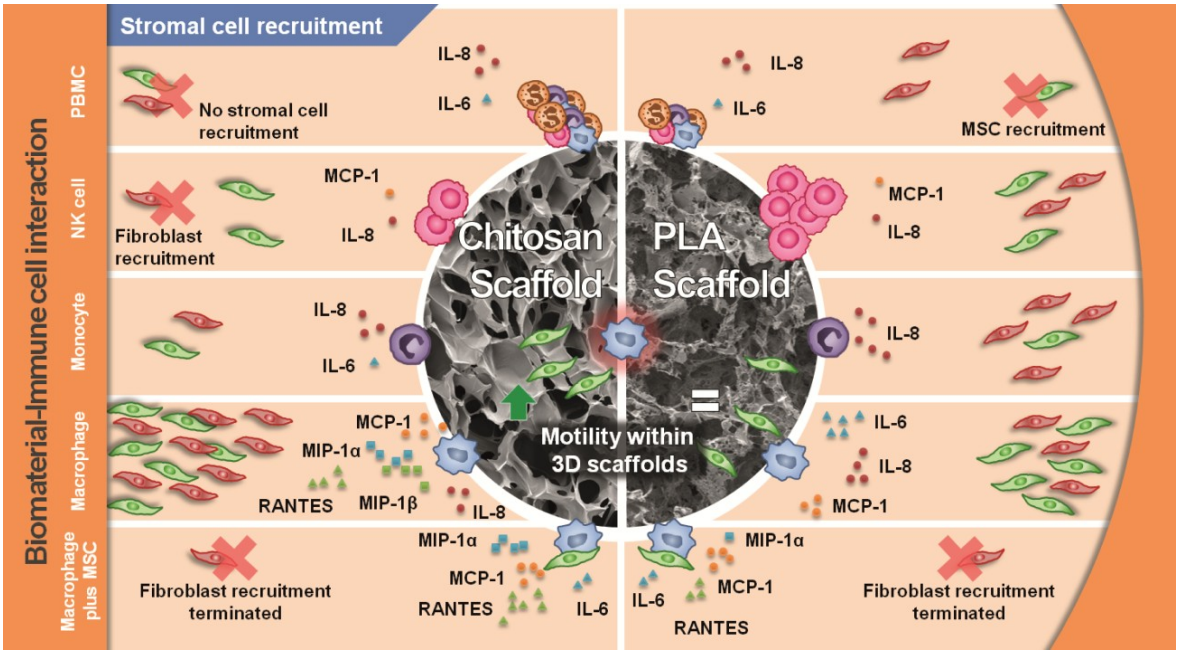

Figure 1 - Blueprint of primary human immune cells impact on stromal cell recruitment towards chitosan (right) or PLA (left) 3D scaffolds. Chitosan scaffolds: Upon implantation, PBMC, NK cells and monocytes are recruited to and activated at the implant interface to secrete several mediators including IL-6, IL-8 and MCP-1. PBMC and NK cells can proliferate upon contact with chitosan. In an early phase NK cells are

responsible for mobilization of MSC with few MSC and fibroblasts being recruited by monocytes. Upon monocyte-to-macrophage differentiation these cells secrete huge amounts of inflammatory mediators such as MCP-1, MIP-1α/β, and RANTES, and promotes preferential recruitment of fibroblast in detriment of MSC to the implant surroundings. Nevertheless, recruited MSC accumulate at the injury site and their interaction with macrophages at the scaffolds interface strongly accelerates the colonization rate. In turn, MSC interaction with macrophages at the scaffolds interface terminates subsequent fibroblast which can be a key event in shifting from fibrotic encapsulation towards tissue regeneration. PLA scaffolds: Upon interaction with PLA scaffolds, PBMC, NK cells and monocytes can secrete cytokines such as IL-6, IL-8 or MCP-1. NK cells greatly increase their numbers within the PLA scaffolds. During the early inflammatory phase, PBMC and monocytes are responsible for a higher fibroblast mobilization towards implanted PLA matrix. However, monocytes differentiation into mature macrophages is followed by the secretion of high amounts of inflammatory mediators as IL-6, IL-8 and MCP-1 which ultimately drives a preferential recruitment of MSC over fibroblast towards the implant. This environment has no effect of the scaffold repopulation rate by mobilized MSC. Similar to chitosan scaffolds, MSC interaction with macrophages at the implant interface represses further fibroblast recruitment towards the scaffold. PBMC: peripheral blood mononuclear cells; NK cells: natural killer cells; MSC: mesenchymal stromal/stem cells; Stromal green cells (MSC); Stromal red cells (Fibroblasts).

In order to validate our 3D model, the *in vivo* host response to implanted materials could be evaluated through several parameters at days 0, 1, 4 and 7 post-implantation in an air pouch model[24]. These would include the number of NK cells (CD3-/CD56+), monocytes/macrophages (CD14+/CD68+), cytotoxic T cells (CD3+/CD8+), regulatory T cells (CD3+/CD25+) and B cells (B220+). To compare the obtained results with the literature it would be also interesting to profile M1 (CCR7+/CD80+) and M2 (CD163+/CD206+) macrophage marker expression to trace a putative M2/M1 ratio. Additionally, it would be important to quantify the presence of inflammatory cytokines/chemokines in tissue exudates (IL-6, MIP-1, RANTES, MCP-1, TGF-β, IL-10, PGE2, etc.) by ELISA at the different time-points. To finalize, the number of recruited MSC (CD106+/CD146+) and fibroblasts (SMA-α) should be correlated with the scoring of histological images to include fibrous encapsulation thickness, number of blood vessels and extent of scaffold biodegradation. If a correlation were observed between ratio of fibrotic-to-progenitor cells mobilized to implant site and *in vivo* foreign body response

endpoint markers, our 3D *in vitro* model would be a valuable tool in scaffold biocompatibility testing for biomedical industry.

5.6 Beyond MSC mobilization:

Can macrophages modulate the scaffold colonization process?

Adding to the scaffolds features on defining MSC motility within 3D biomaterials, another equally important (yet often neglected) complexity factor emerges: the inflammatory milieu / immune cells already present at the scaffold interface. Shockingly, studies that address the inflammatory component on scaffold colonization rate by endogenous MSC are scarce to nonexistent. It was shown that the presence of macrophages in 3D scaffolds was pivotal to promote MSC recruitment. Thus we evaluated whether their interaction with these cells at the scaffold interface could also modulate the MSC migration within the 3D scaffolds and consequently the scaffolds colonization rate. Most interestingly, we demonstrate that although stem cell motility within PLA and chitosan 3D matrices was similar in the absence of immune cells their motility could be significantly altered by the presence of macrophages. Indeed, a significant increase in MSC motility within chitosan was observed with no effect on cells motility in PLA. This implies that macrophages promote a faster colonization of chitosan scaffolds by the recruited progenitor cells but not in PLA scaffolds. This detailed analysis of MSC motility within distinct 3D microenvironments and inflammatory settings revealed itself as an important leap forward for the longitudinal characterization of MSC dynamical behaviour under physiologically relevant inflammatory conditions. It would be interesting to investigate whether macrophages could selectively facilitate or hamper scaffold colonization by distinct cell types. To test this, analogous studies with macrophages and fibroblasts from the same donor could be performed in Dendra2 imaging platform. If a correlation were observed biomaterials designed to modulate this macrophage ability could be pursued as a novel strategy to improve healing outcome.

Thus, an improved understanding on how biomaterial physico-chemical features modulate immune cells to improve not only the recruitment but also scaffold's repopulation by the endogenous MSC is warranted for an integrated and smarter *in situ* engineering scaffold design.

5.7 MSC on the spot: resolving inflammation and fibrosis?

Upon arrival to the implant site, MSC are primed by high levels of TNF-α, IL-1β and IFN-γ already present in the pro-inflammatory environment. This drives MSC to secrete immunomodulatory and trophic factors, which suppress inflammation and fibrosis. Similarly, MSC secrete TNF-stimulated gene/protein-6 (TSG-6) which disrupts IL-8 binding site, downregulating the expression of adhesion molecules at the inflamed endothelium surface thus inhibit rolling and transendothelial migration of neutrophils. This strategy impairs neutrophils influx and ROS respiratory burst avoiding further tissue damage and inflammation[105]. IL-10 which can also be secreted by MSC have been reported to inhibit neutrophils recruitment[106].

MSC have been reported to mediate M1-to-M2 macrophage polarization by two main negative feedback loops: PGE2 and TSG-6[107-109]. Indeed, MSC seem to "educate" macrophages with a rather characteristic anti-inflammatory polarization profile (called M2m) which renders them to secrete high levels of IL-10 and IL-6 and low IL-12 and TNF-α[107,110]. Interestingly, Swartzlander el al.[30] reported that MSC encapsulated within poly(ethylene glycol) (PEG) hydrogels diminish the fibrous capsule thickness formed around the implant, suggesting some degree of immunomodulation over the FBR process. Since this interaction seems critical to meditate pro-inflammatory-to-regulatory environmental transition we investigated whether this putative cross-talk would impact subsequent fibroblast recruitment. Notably, macrophage-MSC interaction resulted in repression of fibroblast mobilization regardless of the scaffold material. This suggests a mechanism that halts both macrophage and MSC ability to recruit fibroblasts (and eventually other cell types) towards the implant site once stem cell recruitment is achieved. To this regard, future studies should be conducted to elucidate whether MSC co-culture is able to induce a specific macrophage polarization to assist in this repressive effect. Moreover, additional mechanistic studies should be performed to understand whether this process activation relies on a certain MSC:Macrophage threshold ratio. Likewise, the specific factors involved in MSC-mediated fibroblast blocking mechanism should be unravelled. This could be achieved by proteomic analysis of the distinct cell supernatants followed by inhibition studies with possible candidates.

Overall, these findings highlight the importance of the in-depth mechanistic understanding about interactions between macrophages, fibroblast and MSC to unravel new targets and strategies to regulate the endogenous stromal cell recruitment dynamics towards the implant site.

5.8 Healing response: more than stromal cell mobilization

The severity of inflammation is closely linked to the features of subsequent processes of repair/regeneration of tissues[92,111]. In this framework, mobilized fibroblasts have the ability to perpetuate the inflammatory response via expression of key chemokines[29,112]. One of such examples is their interaction with macrophages. (myo)fibroblasts activated by pro-inflammatory macrophages can secrete MCP-1, RANTES and IP-10 that exacerbates inflammation through recruitment of additional monocytes and other leukocytes[113]. Moreover, some of these cytokines, such as MCP-1 also act in an autocrine loop on fibroblasts through stimulation of collagen synthesis and up-regulation of TGF-β1, contributing to tissue fibrosis[114]. In the inflammatory milieu, IL-6 is another cytokine that could enhance collagen and elastin secretion by fibroblasts[115,116]. Interestingly, most of these cytokines were secreted in high amounts by the distinct immune cell upon interaction with 3D biomaterials.

Here we demonstrate that macrophages can recruit MSC and fibroblasts, at later stages of inflammation, and that preferential recruitment of one cell type in detriment of the other is biomaterial-dependent. Despite both of these stromal cell types share many features in common, including the similar expression of surface markers and chemokine receptors, they display marked differences on their immunomodulatory properties and function[117-120]. During prolonged foreign body stimuli (e.g. due to slow scaffold degradation), fibroblasts and leucocytes which exert pro-inflammatory and pro-fibrotic effects, act in concerted manner to promote fibrotic encapsulation of the biomaterial walling it from the organism. This process may severely compromise the functional healing of *in situ* engineered scaffold by impeding its colonization by host's cells. This stresses the need for tight regulatory mechanisms of immune cell/fibroblast pro-inflammatory and fibrotic phenotypes upon recruitment, which can be mediated by synchronized MSC mobilization[30]. Proper functionality of these safeguard mechanisms can rely on the proportion of MSC:fibroblast mobilization towards the implant (which can be deregulated in aged individuals[121-123]). Additionally, the timely degradation of the scaffold can also be decisive to direct successful tissue regeneration instead of fibrosis. In contrast to fibroblasts and leucocytes, recruited MSC2 (meanwhile polarized by inflammatory milieu[124]) secrete a plethora of bioactive factors with a strong immunomodulatory and anti-fibrotic action over these cell types to ameliorate inflammation and fibrotic encapsulation of the implanted scaffold[118,125-128]. Thus, timely regulation of the activation state of fibroblasts that were mobilized into the scaffold can also be pivotal to prevent excessive fibrosis.

5.9 Experimental pitfalls and other considerations

Although this thesis work is exclusively derived from primary human cells, which facilitates data translation towards the clinics, some potential drawbacks should be noted. When using primary human cell sources, there is significant donor-to-donor variability, and thus samples from multiple donors were used for each experiment to achieve more meaningful results. Nevertheless, this study was performed in a relatively small-scale and it would be beneficial to increase the number of donors. More importantly, future studies should also characterize biomaterial-evoked immune responses in patients with associated co-morbidities, who may be more likely to be the recipients of such *in situ* regenerative therapies. For instance, diabetic patients exhibit impaired/delayed wound healing responses as higher blood glucose levels affects leukocyte function[129]. Moreover the concentration of progenitor cells in human blood is significantly decreased in aged individuals[130]. Interestingly, both of the risk factors are associated with delayed or impaired wound healing through a reduced ability to shift from an M1 to an M2 macrophage phenotype[131]. Therefore, the development of such diseased 3D models would contribute to the understanding of the impact of classical risk factors for impaired healing, such as age, diabetes or obesity, on these patients regenerative potential[132]. Importantly, such knowledge would greatly benefit clinical decision between implantation of off-the-shelf regenerative scaffolds or traditionally engineered tissue constructs in those particular patient cohorts.

Another potential drawback of our model is the restricted temporal assessment of distinct immune responses and stromal cell trafficking towards the implant site. To this regard, future studies could employ cell replenishment strategies in the distinct chambers/reservoirs to allow for a more prolonged *in vitro* culture. Interestingly, this approach would also allow studying how cellular changes over the inflammatory/regenerative process in bone-marrow/blood stream/implant site compartments (mimicked by cell replenishment in different reservoirs) could influence the healing response. This would enable the study of cell trafficking events extending beyond the initial inflammatory phase and would greatly increase the 3D model complexity.

Despite MSC hypo-immunogenicity due to low expression levels of HLA class I, no expression of HLA class II and CD40, CD80, and CD86 co-stimulatory molecules, some clinical trials reported that allogeneic MSC can be recognized by the innate and adaptive immune system[133,134]. To this regard several studies state that this recognition could be minimized by inflammatory MSC priming prior to cell infusion. Therefore, another potential limitation of this study lies on the use of contact co-cultures between MSC and

macrophages from different donors. Nevertheless, inflammatory environments, as the ones generated during macrophage-biomaterial interaction, have been demonstrated to change immunomudulatory gene expression in MSC or promote the cell–cell contact suppressive effect. Indeed, several reports on culture systems state that cell–cell contact is a key factor involved in the immunomodulatory effects of MSC[135-137]. The net result is an enhanced immunosuppressive response by cultured MSC. Moreover, the concentration of MSC used in our co-culture experiments should be high enough to strongly influence the cell culture microenvironment and suppress an eventual macrophage-mediated allogeneic reaction. Consistent with this, we have observed that cells remained metabolically active upon interaction, which suggests that MSC immunosuppressive properties might prevail. Importantly, the obtained data can also provide important insights for tissue engineering and regenerative medicine therapies that rely on the use of allogeneic MSC.

With this limitation in mind, future studies should be performed with contact co-cultures of the three cell types (immune cells, MSC and fibroblasts) from the same human donor to exclude eventual allogeneic reactions. With this setting it would be interesting to investigate the impact of biomaterial-evoked immune responses over co-cultured fibroblasts ECM production (e.g. elastin and collagen I) in the distinct scaffolds. Similarly, it would be important to analyze whether MSC can also play a regulatory role over this potentially detrimental macrophage-fibroblast interaction.

5.10 CONCLUSIONS & OUTLOOK

The complexity of biomaterial-evoked immune responses poses a challenging environment for *in situ* tissue engineering strategies. Clearly, a better understanding of the underlying pathways that control the fate of implanted biomaterials is crucial to design novel immunomodulatory approaches that potentiate tissue regeneration and remodeling while preventing fibrosis.

In line with this, this thesis provided a comprehensive analysis of the primary human responses triggered by different 3D biomaterials and their functional consequence on the preferential recruitment of primary human MSC or fibroblasts. Contrary to MSC, fibroblast recruitment can be signalled early on in the host response and can be promoted by several immune cells depending on the biomaterial properties. Moreover, macrophages were the most effective cells to mediate stromal cell recruitment to the implant which should predominate at later stages of the host response. Importantly, the scaffold properties strongly influence the macrophage-mediated preferential stromal cell type recruitment which can be instrumental to predict/determine the healing outcome. Strikingly, MSC arrival to the implant site and consequent interaction with macrophages can modulate their phenotype and block subsequent fibroblast recruitment to the vicinity of the scaffold. Future work should determine whether a certain MSC:macrophage ratio threshold is required and which signalling molecules are involved in mediating this fibroblast influx blocking mechanism. Additionally, it would be interesting to characterize an eventual regulatory role by recruited MSC over the pro-fibrotic profile of the previously mobilized fibroblasts at the scaffold interface.

Regarding the outreach of the presented work, the system here developed should be further validated *in vivo* to be applied in the clinics as a predictive 3D model to calculate the likelihood of a given scaffold material to promote endogenous tissue regeneration when implanted in a given patient. The same principle applies to the development of novel immunomodulatory scaffolds for *in situ* regeneration. Normal biological patient-to-patient variation, as well as comorbidities will result in dissimilarities in the immunological and regenerative competence between patients. Thus and most interestingly, mapping of specific immune cell populations responsible for stromal cell recruitment, as the one here established (Figure 1), may be instrumental to enable patient-tailored regenerative treatment. Additionally, such knowledge could be integrated in clinical management to provide personalized pre-operative boosting and/or depletion of specific circulating immune cell populations to synergistically augment the likelihood of scaffold-guided tissue regeneration for a given patient.

In conclusion, immunomodulatory scaffold development for *in situ* regeneration holds great promise for future application and commercialization. However, the mechanistic understanding on how the biomaterials and immune cells interact to yield the proper regenerative response remains a jigsaw puzzle. Taken together, the data presented in this thesis provides one of the first steps towards a novel integrative concept in *in situ* tissue engineering which can assist future scaffold development.

5.11 References

[1] Vishwakarma, A. *et al.* Engineering Immunomodulatory Biomaterials To Tune the Inflammatory Response. *Trends in biotechnology*, 34, 6, 2016, 470-482.

[2] Rennert, R. C., Sorkin, M., Garg, R. K. & Gurtner, G. C. Stem cell recruitment after injury: lessons for regenerative medicine. *Regenerative medicine*, 7, 6, 2012, 833-850.

[3] Kitaori, T. *et al.* Stromal cell-derived factor 1/CXCR4 signaling is critical for the recruitment of mesenchymal stem cells to the fracture site during skeletal repair in a mouse model. *Arthritis and rheumatism*, 60, 3, 2009, 813-823.

[4] Otsuru, S., Tamai, K., Yamazaki, T., Yoshikawa, H. & Kaneda, Y. Circulating bone marrow-derived osteoblast progenitor cells are recruited to the bone-forming site by the CXCR4/stromal cell-derived factor-1 pathway. *Stem cells*, 26, 1, 2008, 223-234.

[5] Glass, G. E. *et al.* TNF-alpha promotes fracture repair by augmenting the recruitment and differentiation of muscle-derived stromal cells. *Proceedings of the National Academy of Sciences of the United States of America*, 108, 4, 2011, 1585-1590.

[6] Mathieu, M. *et al.* Decreased pool of mesenchymal stem cells is associated with altered chemokines serum levels in atrophic nonunion fractures. *Bone*, 53, 2, 2013, 391-398.

[7] Li, J. *et al.* Effect of SDF-1/CXCR4 axis on the migration of transplanted bone mesenchymal stem cells mobilized by erythropoietin toward lesion sites following spinal cord injury. *International journal of molecular medicine*, 36, 5, 2015, 1205-1214.

[8] Ji, W. *et al.* Incorporation of stromal cell-derived factor-1alpha in PCL/gelatin electrospun membranes for guided bone regeneration. *Biomaterials*, 34, 3, 2013, 735-745.

[9] Liu, H., Li, M., Du, L., Yang, P. & Ge, S. Local administration of stromal cell-derived factor-1 promotes stem cell recruitment and bone regeneration in a rat periodontal bone defect model. *Materials science & engineering. C, Materials for biological applications*, 53, 2015, 83-94.

[10] Liu, Y. S. *et al.* The effect of simvastatin on chemotactic capability of SDF-1alpha and the promotion of bone regeneration. *Biomaterials*, 35, 15, 2014, 4489-4498.

[11] Lee, C. H. *et al.* Harnessing endogenous stem/progenitor cells for tendon regeneration. *The Journal of clinical investigation*, 125, 7, 2015, 2690-2701.

[12] Jay, S. M. *et al.* Dual delivery of VEGF and MCP-1 to support endothelial cell transplantation for therapeutic vascularization. *Biomaterials*, 31, 11, 2010, 3054-3062.

[13] Kuraitis, D. *et al.* A stromal cell-derived factor-1 releasing matrix enhances the progenitor cell response and blood vessel growth in ischaemic skeletal muscle. *European cells & materials*, 22, 2011, 109-123.

[14] Purcell, B. P., Elser, J. A., Mu, A., Margulies, K. B. & Burdick, J. A. Synergistic effects of SDF-1alpha chemokine and hyaluronic acid release from degradable hydrogels on directing bone marrow derived cell homing to the myocardium. *Biomaterials*, 33, 31, 2012, 7849-7857.

[15] Yu, J. *et al.* The effect of stromal cell-derived factor-1alpha/heparin coating of biodegradable vascular grafts on the recruitment of both endothelial and smooth muscle progenitor cells for accelerated regeneration. *Biomaterials*, 33, 32, 2012, 8062-8074.

[16] Chen, F. M., Wu, L. A., Zhang, M., Zhang, R. & Sun, H. H. Homing of endogenous stem/progenitor cells for in situ tissue regeneration: Promises, strategies, and translational perspectives. *Biomaterials*, 32, 12, 2011, 3189-3209.

[17] Lee, Y., Kwon, J., Khang, G. & Lee, D. Reduction of inflammatory responses and enhancement of extracellular matrix formation by vanillin-incorporated poly(lactic-co-glycolic acid) scaffolds. *Tissue engineering. Part A*, 18, 19-20, 2012, 1967-1978.

[18] Taraballi, F. *et al.* Biomimetic collagenous scaffold to tune inflammation by targeting macrophages. *Journal of tissue engineering*, 7, 2016, 2041731415624667.

[19] Zhong, Y. & Bellamkonda, R. V. Dexamethasone-coated neural probes elicit attenuated inflammatory response and neuronal loss compared to uncoated neural probes. *Brain research*, 1148, 2007, 15-27.

[20] Browne, S. *et al.* Modulation of inflammation and angiogenesis and changes in ECM GAG-activity via dual delivery of nucleic acids. *Biomaterials*, 69, 2015, 133-147.

[21] Vegas, A. J. *et al.* Combinatorial hydrogel library enables identification of materials that mitigate the foreign body response in primates. *Nature biotechnology*, 34, 3, 2016, 345-352.

[22] Blakney, A. K., Swartzlander, M. D. & Bryant, S. J. The effects of substrate stiffness on the in vitro activation of macrophages and in vivo host response to poly(ethylene glycol)-based hydrogels. *Journal of biomedical materials research. Part A*, 100, 6, 2012, 1375-1386.

[23] Vasconcelos, D. P. *et al.* Development of an immunomodulatory biomaterial: using resolvin D1 to modulate inflammation. *Biomaterials*, 53, 2015, 566-573.

[24] Vasconcelos, D. P. *et al.* Modulation of the inflammatory response to chitosan through M2 macrophage polarization using pro-resolution mediators. *Biomaterials*, 37, 2015, 116-123.

[25] Thevenot, P. T. *et al.* The effect of incorporation of SDF-1alpha into PLGA scaffolds on stem cell recruitment and the inflammatory response. *Biomaterials*, 31, 14, 2010, 3997-4008.

[26] Holladay, C. *et al.* Functionalized scaffold-mediated interleukin 10 gene delivery significantly improves survival rates of stem cells in vivo. *Molecular therapy : the journal of the American Society of Gene Therapy*, 19, 5, 2011, 969-978.

[27] Holladay, C. A. *et al.* Recovery of cardiac function mediated by MSC and interleukin-10 plasmid functionalised scaffold. *Biomaterials*, 33, 5, 2012, 1303-1314.

[28] Zhu, H. *et al.* Mesenchymal stem cells attenuated PLGA-induced inflammatory responses by inhibiting host DC maturation and function. *Biomaterials*, 53, 2015, 688-698.

[29] Thevenot, P. T., Baker, D. W., Weng, H., Sun, M. W. & Tang, L. The pivotal role of fibrocytes and mast cells in mediating fibrotic reactions to biomaterials. *Biomaterials*, 32, 33, 2011, 8394-8403.

[30] Swartzlander, M. D. *et al.* Immunomodulation by mesenchymal stem cells combats the foreign body response to cell-laden synthetic hydrogels. *Biomaterials*, 41, 2015, 79-88.

[31] Segers, V. F. *et al.* Local delivery of protease-resistant stromal cell derived factor-1 for stem cell recruitment after myocardial infarction. *Circulation*, 116, 15, 2007, 1683-1692.

[32] Kim, K., Lee, C. H., Kim, B. K. & Mao, J. J. Anatomically shaped tooth and periodontal regeneration by cell homing. *Journal of dental research*, 89, 8, 2010, 842-847.

[33] Shen, W. *et al.* The effect of incorporation of exogenous stromal cell-derived factor-1 alpha within a knitted silk-collagen sponge scaffold on tendon regeneration. *Biomaterials*, 31, 28, 2010, 7239-7249.

[34] Ratanavaraporn, J., Furuya, H., Kohara, H. & Tabata, Y. Synergistic effects of the dual release of stromal cell-derived factor-1 and bone morphogenetic protein-2 from hydrogels on bone regeneration. *Biomaterials*, 32, 11, 2011, 2797-2811.

[35] Ko, I. K. *et al.* Combined systemic and local delivery of stem cell inducing/recruiting factors for in situ tissue regeneration. *FASEB journal : official publication of the Federation of American Societies for Experimental Biology*, 26, 1, 2012, 158-168.

[36] Anderson, E. M. *et al.* Local delivery of VEGF and SDF enhances endothelial progenitor cell recruitment and resultant recovery from ischemia. *Tissue engineering. Part A*, 21, 7-8, 2015, 1217-1227.

[37] Gower, R. M. *et al.* Modulation of leukocyte infiltration and phenotype in microporous tissue engineering scaffolds via vector induced IL-10 expression. *Biomaterials*, 35, 6, 2014, 2024-2031.

[38] Zachman, A. L. *et al.* Pro-angiogenic and anti-inflammatory regulation by functional peptides loaded in polymeric implants for soft tissue regeneration. *Tissue engineering. Part A*, 19, 3-4, 2013, 437-447.

[39] Nair, A. *et al.* Biomaterial implants mediate autologous stem cell recruitment in mice. *Acta biomaterialia*, 7, 11, 2011, 3887-3895.

[40] Damanik, F. F., Rothuizen, T. C., van Blitterswijk, C., Rotmans, J. I. & Moroni, L. Towards an in vitro model mimicking the foreign body response: tailoring the surface properties of biomaterials to modulate extracellular matrix. *Scientific reports*, 4, 2014, 6325.

[41] van Putten, S. M., Ploeger, D. T., Popa, E. R. & Bank, R. A. Macrophage phenotypes in the collagen-induced foreign body reaction in rats. *Acta biomaterialia*, 9, 5, 2013, 6502-6510.

[42] Chamberlain, L. M., Godek, M. L., Gonzalez-Juarrero, M. & Grainger, D. W. Phenotypic non-equivalence of murine (monocyte-) macrophage cells in biomaterial and inflammatory models. *Journal of biomedical materials research. Part A*, 88, 4, 2009, 858-871.

[43] McNally, A. K. & Anderson, J. M. Phenotypic expression in human monocyte-derived interleukin-4-induced foreign body giant cells and macrophages in vitro: dependence on material surface properties. *Journal of biomedical materials research. Part A*, 103, 4, 2015, 1380-1390.

[44] Brodbeck, W. G., Macewan, M., Colton, E., Meyerson, H. & Anderson, J. M. Lymphocytes and the foreign body response: lymphocyte enhancement of macrophage adhesion and fusion. *Journal of biomedical materials research. Part A*, 74, 2, 2005, 222-229.

[45] Grotenhuis, N., Bayon, Y., Lange, J. F., Van Osch, G. J. & Bastiaansen-Jenniskens, Y. M. A culture model to analyze the acute biomaterial-dependent reaction of human primary macrophages. *Biochemical and biophysical research communications*, 433, 1, 2013, 115-120.

[46] Kajahn, J. *et al.* Artificial extracellular matrices composed of collagen I and high sulfated hyaluronan modulate monocyte to macrophage differentiation under conditions of sterile inflammation. *Biomatter*, 2, 4, 2012, 226-236.

[47] Jones, J. A. *et al.* Proteomic analysis and quantification of cytokines and chemokines from biomaterial surface-adherent macrophages and foreign body giant cells. *Journal of biomedical materials research. Part A*, 83, 3, 2007, 585-596.

[48] Lee, H. S. *et al.* Correlating macrophage morphology and cytokine production resulting from biomaterial contact. *Journal of biomedical materials research. Part A*, 101, 1, 2013, 203-212.

[49] Stich, S. *et al.* Regenerative and immunogenic characteristics of cultured nucleus pulposus cells from human cervical intervertebral discs. *PloS one*, 10, 5, 2015, e0126954.

[50] Bartneck, M. *et al.* Inducing healing-like human primary macrophage phenotypes by 3D hydrogel coated nanofibres. *Biomaterials*, 33, 16, 2012, 4136-4146.

[51] Bartneck, M., Heffels, K. H., Bovi, M., Groll, J. & Zwadlo-Klarwasser, G. The role of substrate morphology for the cytokine release profile of immature human primary macrophages. *Materials science & engineering. C, Materials for biological applications*, 33, 8, 2013, 5109-5114.

[52] Backovic, A. *et al.* Identification and dynamics of proteins adhering to the surface of medical silicones in vivo and in vitro. *Journal of proteome research*, 6, 1, 2007, 376-381.

[53] Kim, Y. K., Que, R., Wang, S. W. & Liu, W. F. Modification of biomaterials with a self-protein inhibits the macrophage response. *Advanced healthcare materials*, 3, 7, 2014, 989-994.

[54] Battiston, K. G., Labow, R. S. & Santerre, J. P. Protein binding mediation of biomaterial-dependent monocyte activation on a degradable polar hydrophobic ionic polyurethane. *Biomaterials*, 33, 33, 2012, 8316-8328.

[55] McBane, J. E., Matheson, L. A., Sharifpoor, S., Santerre, J. P. & Labow, R. S. Effect of polyurethane chemistry and protein coating on monocyte differentiation towards a wound healing phenotype macrophage. *Biomaterials*, 30, 29, 2009, 5497-5504.

[56] Battiston, K. G., McBane, J. E., Labow, R. S. & Paul Santerre, J. Differences in protein binding and cytokine release from monocytes on commercially sourced tissue culture polystyrene. *Acta biomaterialia*, 8, 1, 2012, 89-98.

[57] Almeida, C. R. *et al.* Impact of 3-D printed PLA- and chitosan-based scaffolds on human monocyte/macrophage responses: unraveling the effect of 3-D structures on inflammation. *Acta biomaterialia*, 10, 2, 2014, 613-622.

[58] McWhorter, F. Y., Wang, T., Nguyen, P., Chung, T. & Liu, W. F. Modulation of macrophage phenotype by cell shape. *Proceedings of the National Academy of Sciences of the United States of America*, 110, 43, 2013, 17253-17258.

[59] Mestas, J. & Hughes, C. C. Of mice and not men: differences between mouse and human immunology. *Journal of immunology*, 172, 5, 2004, 2731-2738.

[60] Lawrence, B. J. & Madihally, S. V. Cell colonization in degradable 3D porous matrices. *Cell adhesion & migration*, 2, 1, 2008, 9-16.

[61] Nam, S. Y., Ricles, L. M., Suggs, L. J. & Emelianov, S. Y. Imaging strategies for tissue engineering applications. *Tissue engineering. Part B, Reviews*, 21, 1, 2015, 88-102.

[62] Mandal, B. B. & Kundu, S. C. Cell proliferation and migration in silk fibroin 3D scaffolds. *Biomaterials*, 30, 15, 2009, 2956-2965.

[63] Lei, Y., Gojgini, S., Lam, J. & Segura, T. The spreading, migration and proliferation of mouse mesenchymal stem cells cultured inside hyaluronic acid hydrogels. *Biomaterials*, 32, 1, 2011, 39-47.

[64] Peyton, S. R. *et al.* Marrow-derived stem cell motility in 3D synthetic scaffold is governed by geometry along with adhesivity and stiffness. *Biotechnology and bioengineering*, 108, 5, 2011, 1181-1193.

[65] Schultz, K. M., Kyburz, K. A. & Anseth, K. S. Measuring dynamic cell-material interactions and remodeling during 3D human mesenchymal stem cell migration in hydrogels. *Proceedings of the National Academy of Sciences of the United States of America*, 112, 29, 2015, E3757-3764.

[66] Zhang, Y. *et al.* Chronic label-free volumetric photoacoustic microscopy of melanoma cells in three-dimensional porous scaffolds. *Biomaterials*, 31, 33, 2010, 8651-8658.

[67] Cai, X., Paratala, B. S., Hu, S., Sitharaman, B. & Wang, L. V. Multiscale photoacoustic microscopy of single-walled carbon nanotube-incorporated tissue engineering scaffolds. *Tissue engineering. Part C, Methods*, 18, 4, 2012, 310-317.

[68] Yang, Y. *et al.* Investigation of optical coherence tomography as an imaging modality in tissue engineering. *Physics in medicine and biology*, 51, 7, 2006, 1649-1659.

[69] Tan, W., Oldenburg, A. L., Norman, J. J., Desai, T. A. & Boppart, S. A. Optical coherence tomography of cell dynamics in three-dimensional tissue models. *Optics express*, 14, 16, 2006, 7159-7171.

[70] Chen, C. W., Betz, M. W., Fisher, J. P., Paek, A. & Chen, Y. Macroporous hydrogel scaffolds and their characterization by optical coherence tomography. *Tissue engineering. Part C, Methods*, 17, 1, 2011, 101-112.

[71] Wu, S., Koizumi, K., Macrae-Crerar, A. & Gallagher, K. L. Assessing the utility of photoswitchable fluorescent proteins for tracking intercellular protein movement in the Arabidopsis root. *PloS one*, 6, 11, 2011, e27536.

[72] Baker, S. M., Buckheit, R. W., 3rd & Falk, M. M. Green-to-red photoconvertible fluorescent proteins: tracking cell and protein dynamics on standard wide-field mercury arc-based microscopes. *BMC cell biology*, 11, 2010, 15.

[73] Wu, B., Piatkevich, K. D., Lionnet, T., Singer, R. H. & Verkhusha, V. V. Modern fluorescent proteins and imaging technologies to study gene expression, nuclear localization, and dynamics. *Current opinion in cell biology*, 23, 3, 2011, 310-317.

[74] Helledie, T., Nurcombe, V. & Cool, S. M. A simple and reliable electroporation method for human bone marrow mesenchymal stem cells. *Stem cells and development*, 17, 4, 2008, 837-848.

[75] Lin, P. *et al.* Efficient lentiviral transduction of human mesenchymal stem cells that preserves proliferation and differentiation capabilities. *Stem cells translational medicine*, 1, 12, 2012, 886-897.

[76] Moon, H. H. *et al.* MSC-based VEGF gene therapy in rat myocardial infarction model using facial amphipathic bile acid-conjugated polyethyleneimine. *Biomaterials*, 35, 5, 2014, 1744-1754.

[77] Zhang, F., Jing, S., Ren, T. & Lin, J. MicroRNA-10b promotes the migration of mouse bone marrow-derived mesenchymal stem cells and downregulates the expression of E-cadherin. *Molecular medicine reports*, 8, 4, 2013, 1084-1088.

[78] Adam, V., Berardozzi, R., Byrdin, M. & Bourgeois, D. Phototransformable fluorescent proteins: Future challenges. *Current opinion in chemical biology*, 20, 2014, 92-102.

[79] Bins, A. D. *et al.* Intravital imaging of fluorescent markers and FRET probes by DNA tattooing. *BMC biotechnology*, 7, 2007, 2.

[80] Miron-Mendoza, M., Seemann, J. & Grinnell, F. The differential regulation of cell motile activity through matrix stiffness and porosity in three dimensional collagen matrices. *Biomaterials*, 31, 25, 2010, 6425-6435.

[81] Lautenschlager, F. *et al.* The regulatory role of cell mechanics for migration of differentiating myeloid cells. *Proceedings of the National Academy of Sciences of the United States of America*, 106, 37, 2009, 15696-15701.

[82] Brunner, C. A. *et al.* Cell migration through small gaps. *European biophysics journal : EBJ*, 35, 8, 2006, 713-719.

[83] Zaman, M. H. *et al.* Migration of tumor cells in 3D matrices is governed by matrix stiffness along with cell-matrix adhesion and proteolysis. *Proceedings of the National Academy of Sciences of the United States of America*, 103, 29, 2006, 10889-10894.

[84] Wolf, K. *et al.* Multi-step pericellular proteolysis controls the transition from individual to collective cancer cell invasion. *Nature cell biology*, 9, 8, 2007, 893-904.

[85] Ehrbar, M. *et al.* Elucidating the role of matrix stiffness in 3D cell migration and remodeling. *Biophysical journal*, 100, 2, 2011, 284-293.

[86] Ponte, A. L. *et al.* The in vitro migration capacity of human bone marrow mesenchymal stem cells: comparison of chemokine and growth factor chemotactic activities. *Stem cells*, 25, 7, 2007, 1737-1745.

[87] Ries, C. *et al.* MMP-2, MT1-MMP, and TIMP-2 are essential for the invasive capacity of human mesenchymal stem cells: differential regulation by inflammatory cytokines. *Blood*, 109, 9, 2007, 4055-4063.

[88] Almeida, C. R., Caires, H. R., Vasconcelos, D. P. & Barbosa, M. A. NAP-2 Secreted by Human NK Cells Can Stimulate Mesenchymal Stem/Stromal Cell Recruitment. *Stem cell reports*, 6, 4, 2016, 466-473.

[89] Italiani, P. & Boraschi, D. From Monocytes to M1/M2 Macrophages: Phenotypical vs. Functional Differentiation. *Frontiers in immunology*, 5, 2014, 514.

[90] Anderson, J. M. & McNally, A. K. Biocompatibility of implants: lymphocyte/macrophage interactions. *Seminars in immunopathology*, 33, 3, 2011, 221-233.

[91] Anderson, J. M., Rodriguez, A. & Chang, D. T. Foreign body reaction to biomaterials. *Seminars in immunology*, 20, 2, 2008, 86-100.

[92] Veiseh, O. *et al.* Size- and shape-dependent foreign body immune response to materials implanted in rodents and non-human primates. *Nature materials*, 14, 6, 2015, 643-651.

[93] Mantovani, A., Biswas, S. K., Galdiero, M. R., Sica, A. & Locati, M. Macrophage plasticity and polarization in tissue repair and remodelling. *The Journal of pathology*, 229, 2, 2013, 176-185.

[94] Madden, L. R. *et al.* Proangiogenic scaffolds as functional templates for cardiac tissue engineering. *Proceedings of the National Academy of Sciences of the United States of America*, 107, 34, 2010, 15211-15216.

[95] Sica, A. & Mantovani, A. Macrophage plasticity and polarization: in vivo veritas. *The Journal of clinical investigation*, 122, 3, 2012, 787-795.

[96] Rattigan, Y., Hsu, J. M., Mishra, P. J., Glod, J. & Banerjee, D. Interleukin 6 mediated recruitment of mesenchymal stem cells to the hypoxic tumor milieu. *Experimental cell research*, 316, 20, 2010, 3417-3424.

[97] Ringe, J. *et al.* Towards in situ tissue repair: human mesenchymal stem cells express chemokine receptors CXCR1, CXCR2 and CCR2, and migrate upon stimulation with CXCL8 but not CCL2. *Journal of cellular biochemistry*, 101, 1, 2007, 135-146.

[98] Takano, T. *et al.* Mesenchymal stem cells markedly suppress inflammatory bone destruction in rats with adjuvant-induced arthritis. *Laboratory investigation; a journal of technical methods and pathology*, 94, 3, 2014, 286-296.

[99] Schmal, H. *et al.* Comparison of cellular functionality of human mesenchymal stromal cells and PBMC. *Cytotherapy*, 9, 1, 2007, 69-79.

[100] Pattappa, G. *et al.* CCL5/RANTES is a key chemoattractant released by degenerative intervertebral discs in organ culture. *European cells & materials*, 27, 2014, 124-136; discussion 136.

[101] Murray, P. J. *et al.* Macrophage activation and polarization: nomenclature and experimental guidelines. *Immunity*, 41, 1, 2014, 14-20.

[102] Vasconcelos, D. P. *et al.* Macrophage polarization following chitosan implantation. *Biomaterials*, 34, 38, 2013, 9952-9959.

[103] Santos, S. G. *et al.* Adsorbed fibrinogen leads to improved bone regeneration and correlates with differences in the systemic immune response. *Acta biomaterialia*, 9, 7, 2013, 7209-7217.

[104] Lim, T. C. *et al.* Chemotactic recruitment of adult neural progenitor cells into multifunctional hydrogels providing sustained SDF-1alpha release and compatible structural support. *FASEB journal : official publication of the Federation of American Societies for Experimental Biology*, 27, 3, 2013, 1023-1033.

[105] Dyer, D. P. *et al.* TSG-6 inhibits neutrophil migration via direct interaction with the chemokine CXCL8. *Journal of immunology*, 192, 5, 2014, 2177-2185.

[106] Yang, Z., Zingarelli, B. & Szabo, C. Crucial role of endogenous interleukin-10 production in myocardial ischemia/reperfusion injury. *Circulation*, 101, 9, 2000, 1019-1026.

[107] Cho, D. I. *et al.* Mesenchymal stem cells reciprocally regulate the M1/M2 balance in mouse bone marrow-derived macrophages. *Experimental & molecular medicine*, 46, 2014, e70.

[108] Chiossone, L. *et al.* Mesenchymal stromal cells induce peculiar alternatively activated macrophages capable of dampening both innate and adaptive immune responses. *Stem cells*, 2016.

[109] Prockop, D. J. Concise review: two negative feedback loops place mesenchymal stem/stromal cells at the center of early regulators of inflammation. *Stem cells*, 31, 10, 2013, 2042-2046.

[110] Kim, J. & Hematti, P. Mesenchymal stem cell-educated macrophages: a novel type of alternatively activated macrophages. *Experimental hematology*, 37, 12, 2009, 1445-1453.

[111] Franz, S., Rammelt, S., Scharnweber, D. & Simon, J. C. Immune responses to implants - a review of the implications for the design of immunomodulatory biomaterials. *Biomaterials*, 32, 28, 2011, 6692-6709.

[112] Kendall, R. T. & Feghali-Bostwick, C. A. Fibroblasts in fibrosis: novel roles and mediators. *Frontiers in pharmacology*, 5, 2014, 123.

[113] Lukacs, N. W. *et al.* Stimulus and cell-specific expression of C-X-C and C-C chemokines by pulmonary stromal cell populations. *The American journal of physiology*, 268, 5 Pt 1, 1995, L856-861.

[114] Gharaee-Kermani, M., Denholm, E. M. & Phan, S. H. Costimulation of fibroblast collagen and transforming growth factor beta1 gene expression by monocyte chemoattractant protein-1 via specific receptors. *The Journal of biological chemistry*, 271, 30, 1996, 17779-17784.

[115] John, T. *et al.* Effect of pro-inflammatory and immunoregulatory cytokines on human tenocytes. *Journal of orthopaedic research : official publication of the Orthopaedic Research Society*, 28, 8, 2010, 1071-1077.

[116] Hong, H. H. & Trackman, P. C. Cytokine regulation of gingival fibroblast lysyl oxidase, collagen, and elastin. *Journal of periodontology*, 73, 2, 2002, 145-152.

[117] Sindberg, G. M. *et al.* Comparisons of phenotype and immunomodulatory capacity among rhesus bone-marrow-derived mesenchymal stem/stromal cells, multipotent adult progenitor cells, and dermal fibroblasts. *Journal of medical primatology*, 43, 4, 2014, 231-241.

[118] Savvatis, K. *et al.* Mesenchymal stromal cells but not cardiac fibroblasts exert beneficial systemic immunomodulatory effects in experimental myocarditis. *PloS one*, 7, 7, 2012, e41047.

[119] Hematti, P. Mesenchymal stromal cells and fibroblasts: a case of mistaken identity? *Cytotherapy*, 14, 5, 2012, 516-521.

[120] Halfon, S., Abramov, N., Grinblat, B. & Ginis, I. Markers distinguishing mesenchymal stem cells from fibroblasts are downregulated with passaging. *Stem cells and development*, 20, 1, 2011, 53-66.

[121] Sharpless, N. E. & DePinho, R. A. How stem cells age and why this makes us grow old. *Nat Rev Mol Cell Biol*, 8, 9, 2007, 703-713.

[122] Liu, L. & Rando, T. A. Manifestations and mechanisms of stem cell aging. *The Journal of cell biology*, 193, 2, 2011, 257-266.

[123] Pereira, C. L. *et al.* The effect of hyaluronan-based delivery of stromal cell-derived factor-1 on the recruitment of MSCs in degenerating intervertebral discs. *Biomaterials*, 35, 28, 2014, 8144-8153.

[124] Bernardo, M. E. & Fibbe, W. E. Mesenchymal stromal cells: sensors and switchers of inflammation. *Cell stem cell*, 13, 4, 2013, 392-402.

[125] Buckley, C. D. *et al.* Fibroblasts regulate the switch from acute resolving to chronic persistent inflammation. *Trends in immunology*, 22, 4, 2001, 199-204.

[126] Ren, G. *et al.* Mesenchymal stem cell-mediated immunosuppression occurs via concerted action of chemokines and nitric oxide. *Cell stem cell*, 2, 2, 2008, 141-150.

[127] Van Linthout, S. *et al.* Mesenchymal stem cells improve murine acute coxsackievirus B3-induced myocarditis. *European heart journal*, 32, 17, 2011, 2168-2178.

[128] Mias, C. *et al.* Mesenchymal stem cells promote matrix metalloproteinase secretion by cardiac fibroblasts and reduce cardiac ventricular fibrosis after myocardial infarction. *Stem cells*, 27, 11, 2009, 2734-2743.

[129] Young, A. & McNaught, C.-E. The physiology of wound healing. *Surgery - Oxford International Edition*, 29, 10, 475-479.

[130] Jie, K. E., Goossens, M. H., van Oostrom, O., Lilien, M. R. & Verhaar, M. C. Circulating endothelial progenitor cell levels are higher during childhood than in adult life. *Atherosclerosis*, 202, 2, 2009, 345-347.

[131] Brown, B. N. *et al.* Macrophage phenotype as a predictor of constructive remodeling following the implantation of biologically derived surgical mesh materials. *Acta biomaterialia*, 8, 3, 2012, 978-987.

[132] Shaw, S. Y. & Brettman, A. D. Phenotyping patient-derived cells for translational studies in cardiovascular disease. *Circulation*, 124, 22, 2011, 2444-2455.

[133] Griffin, M. D. *et al.* Anti-donor immune responses elicited by allogeneic mesenchymal stem cells: what have we learned so far? *Immunology and cell biology*, 91, 1, 2013, 40-51.

[134] Ankrum, J. A., Ong, J. F. & Karp, J. M. Mesenchymal stem cells: immune evasive, not immune privileged. *Nature biotechnology*, 32, 3, 2014, 252-260.

[135] Han, K. H. *et al.* Immunosuppressive mechanisms of embryonic stem cells and mesenchymal stem cells in alloimmune response. *Transplant immunology*, 25, 1, 2011, 7-15.

[136] English, K. *et al.* Cell contact, prostaglandin E(2) and transforming growth factor beta 1 play non-redundant roles in human mesenchymal stem cell induction of CD4+CD25(High) forkhead box P3+ regulatory T cells. *Clinical and experimental immunology*, 156, 1, 2009, 149-160.

[137] Gao, F. *et al.* Mesenchymal stem cells and immunomodulation: current status and future prospects. *Cell death & disease*, 7, 2016, e2062.

SHORT BIOGRAPHY

Hugo R. Caires was born in Madeira Island, Portugal, in 1988. He received his BSc. degree in Nuclear Medicine at ESTSP of the Polytechnic Institute of Porto, in 2010, where later he became an invited assistant professor in 2011. Then, he moved to ICBAS, University of Porto, to accomplish his PhD as part of Pathology and Molecular Genetics doctoral program. In September 2012, he started his PhD research mentored by Catarina R. Almeida at INEB in the Microenvironments for NEWTherapies group led by Professor Mário A. Barbosa.

Hugo's work explores the idea that biomaterials can modulate the immune response to control the recruitment and motility of specific stromal cell types, pivotal to determine the likelihood of tissue regeneration/fibrosis. To pursue this novel concept, Hugo has developed an innovative 3D imaging platform, based on the use of fluorescent photoconvertible proteins, to interrogate stem cell dynamical behaviour within distinct 3D microenvironments with a longitudinal perspective. Importantly, he applied this platform to understand how the inflammatory microenvironment modulates stem cell migration in distinct bioengineered matrices. Hugo is focused on understanding and modulating the interaction between the immune responses towards biomaterials and mesenchymal stem cell recruitment to develop smarter *in situ* tissue engineering approaches. For that he developed a physiologically relevant triple co-culture system which allows now a better understanding of the underlying pathways that control the fate of implanted biomaterials. Hugo's work provides one of the first steps towards a novel integrative concept in *in situ* tissue engineering which can assist future immunomodulatory scaffold development.

“PARA SER GRANDE, SÊ INTEIRO: NADA

Para ser grande, sê inteiro: nada
Teu exagera ou exclui.
Sê todo em cada coisa. Põe quanto és
No mínimo que fazes.
Assim em cada lago a lua toda
Brilha, porque alta vive.

14-2-1933

Odes de Ricardo Reis . Fernando Pessoa. Lisboa: Ática, 1946 (imp.1994). - 148.

Mesenchymal Stem / Stromal Cell Mobilization Following Immune Responses to 3D Biomaterials: A Road Towards in situ Regeneration

Hugo Ronaldo Freitas Caires

SEDE ADMINISTRATIVA

INSTITUTO DE CIÊNCIAS BIOMÉDICAS ABEL SALAZAR

FACULDADE DE MEDICINA